



<https://theses.gla.ac.uk/>

Theses Digitisation:

<https://www.gla.ac.uk/myglasgow/research/enlighten/theses/digitisation/>

This is a digitised version of the original print thesis.

Copyright and moral rights for this work are retained by the author

A copy can be downloaded for personal non-commercial research or study,  
without prior permission or charge

This work cannot be reproduced or quoted extensively from without first  
obtaining permission in writing from the author

The content must not be changed in any way or sold commercially in any  
format or medium without the formal permission of the author

When referring to this work, full bibliographic details including the author,  
title, awarding institution and date of the thesis must be given

Enlighten: Theses

<https://theses.gla.ac.uk/>  
[research-enlighten@glasgow.ac.uk](mailto:research-enlighten@glasgow.ac.uk)

**AN EVALUATION OF  
SURFACE-ENHANCED RAMAN SPECTROSCOPY (SERS)  
AS A CHEMICAL SENSING TECHNIQUE.**

A thesis submitted to the University of Glasgow  
in part fulfillment for the degree of

DOCTOR OF PHILOSOPHY

in the Faculty of Science

by

MARK JOHN EDMISTON.

Department of Chemistry  
University of Glasgow.

October 1991

© Mark J. Edmiston.

ProQuest Number: 11011409

All rights reserved

INFORMATION TO ALL USERS

The quality of this reproduction is dependent upon the quality of the copy submitted.

In the unlikely event that the author did not send a complete manuscript and there are missing pages, these will be noted. Also, if material had to be removed, a note will indicate the deletion.



ProQuest 11011409

Published by ProQuest LLC (2018). Copyright of the Dissertation is held by the Author.

All rights reserved.

This work is protected against unauthorized copying under Title 17, United States Code  
Microform Edition © ProQuest LLC.

ProQuest LLC.  
789 East Eisenhower Parkway  
P.O. Box 1346  
Ann Arbor, MI 48106 – 1346

To Mum and Dad.

"ULFHEJM: Yes; even stone's got something to fight for. It's  
dead and'll do everything it can to save itself from being  
chiselled into life."

From *When we dead awaken* by Henrik Johan Ibsen (1828 - 1906).

"Then at the balance let's be mute,  
We never can adjust it;  
What's *done* we partly may compute,  
But know not what's *resisted*."

From *Address to the Unco Guid* by Robert Burns (1759 - 1796)

## ACKNOWLEDGEMENTS.

I would like to thank my supervisor, Dr. R.D. Peacock, for his guidance and encouragement throughout the course of this work.

Thanks are also due to Mr. D. Thom for scanning electron microscopy and assistance with the vapour-deposition of silver, Mr. G. McCulloch for infra-red spectra, Mrs K. Wilson for microanalyses, Dr. J-I. Song for the translation of reference no. 200, Dr. J. Adams for advice on the preparation of silica spheres and Mr. J. McIver for n.m.r. spectra and general technical assistance.

I must also take this opportunity to thank all my colleagues and friends in the department for making my time there more enjoyable.

I acknowledge the award of a maintenance grant from the SERC.

**CONTENTS**

Title page.	(i)
Dedication.	(ii)
Quotation.	(iii)
Acknowledgements.	(iv)
Contents.	(v)
Summary	(xix)
<b><u>CHAPTER ONE: GENERAL BACKGROUND TOPICS</u></b>	<b>1</b>
<b><u>A. Raman Spectroscopy.</u></b>	
1.1 Introduction.	1
1.2 Vibrational Raman effect.	4
1.3 Quantum selection rules.	6
1.4 Raman polarisation measurements.	7
1.4.1 Depolarisation ratios.	9
1.5 Resonance Raman Spectroscopy.	9
<b><u>B. Lasers.</u></b>	
1.1 Radiative processes.	11
(a) Absorption.	11
(b) Resonance fluorescence and fluorescence.	12
(c) Phosphorescence.	12
1.2 Lasing action: emission and absorption processes.	13

1.3	Examples of laser systems.	16
1.3.1	Rare gas discharge lasers.	16
1.3.2	Dye lasers .	18
1.3.3	Neodymium YAG lasers.	19

## CHAPTER TWO: SURFACE-ENHANCED RAMAN SPECTROSCOPY.

2.1	History.	20
2.2	SERS-active systems.	
2.2.1	Electrochemical systems.	22
2.2.1.1	The silver/pyridine/halide ion system.	22
2.2.1.2	Other electrochemical systems.	28
(a)	Roughening procedure: surface morphology.	28
(b)	Large scale and atomic scale roughness features.	29
(c)	Molecular interactions with electrode surfaces.	30
(d)	Potential and pH dependence.	32
(e)	Electrodeposition of other metals.	33
(f)	Role of surface carbon.	36
2.2.2	Vapour-deposited surfaces.	36

2.2.2.1	Categories of vapour-deposited surfaces.	37
(a)	Island films	37
(b)	Cold-deposited films.	38
(c)	Assemblies of metal spheroids.	38
(d)	Coated microspheres.	38
2.2.2.2	Studies with vapour-deposited surfaces.	39
2.2.2.3	Adsorption of gases.	41
2.2.2.4	Theoretical aspects.	42
(a)	Electromagnetic mechanisms.	42
(b)	Chemical Mechanisms.	43
2.2.2.5	Metal overlayers.	44
2.2.3	Metal colloids (sols).	45
2.2.3.1	Preparations of colloids.	45
(a)	Gold colloids.	45
(b)	Silver colloids.	46
2.2.3.2	The nature of colloids.	46
2.2.3.3	Colloidal particle size.	47
2.2.3.4	Aggregation studies.	48
2.2.3.5	The orientation of adsorbates at colloid surfaces.	49

(a)	Organic adsorbates.	50
(b)	Inorganic adsorbates.	53
2.2.3.6	Biologically active molecules: SERRS.	56
2.2.3.7	Theoretical aspects.	57
2.2.3.8	Related SERS-active substrates.	58
(a)	Supported colloids.	58
(b)	Mobile metal films.	59
(c)	Chemically prepared films.	60
2.2.4	Other SERS-active substrates.	60
2.2.4.1	Silver powder.	60
2.2.4.2	Rough silver surfaces.	61
2.3	Theory of SERS.	62
2.3.1	Background.	62
2.3.2	Factors influencing SERS.	62
(a)	Dielectric properties of the surface metal.	63
(b)	Morphology and dimensions of roughness species on the surface.	"
(c)	Molecule-surface separation.	"
(d)	Orientation of the molecule with respect to the surface.	"
(e)	Chemical nature of the adsorbed molecule.	"

2.3.3	Electromagnetic theory.	64
2.3.3.1	The image field model.	64
2.3.3.2	The electromagnetic mechanism.	67
2.3.3.3	Models of surface roughness.	69
(a)	Spherical particles.	70
(b)	Spheroidal particles.	72
2.3.3.4	Calculations and experiment.	74
2.3.3.5	Excitation profiles.	75
2.3.3.6	Coupling between particles.	75
2.3.3.7	Criticisms of the electromagnetic theory.	76
2.3.4	Chemical theory.	77
2.3.4.1	Evidence for chemical contributions to SERS enhancement.	77
2.3.4.2	Surface features.	79
2.3.4.3	Early adatom theory.	79
2.3.4.4	The chemical theory.	80
2.3.4.5	Magnitude of contribution of the chemical effect.	82
2.3.5	Other theoretical models.	84
2.3.5.1	Variations on the chemical model.	"
(a)	Modulated reflectivity model.	"

(b)	Inelastic Mie scattering.	84
2.3.5.2	Parametric excitation model.	85
2.3.5.3	Super radiance model.	85
2.3.5.4	Microensemble model.	86
2.4	Applications of SERS.	86
2.4.1	Chemical reactions at surfaces.	"
2.4.2	Behaviour of molecules adsorbed on metal surfaces.	87
2.4.3	Analytical chemistry.	88
2.4.3.1	Electrode surfaces.	88
2.4.3.2	Vapour-deposited surfaces.	89
2.4.3.3	Colloids.	91
2.5	Recent developments in SERS	94
2.5.1	Langmuir-Blodgett mololayers.	94
2.5.2	Fibre-optic sensors.	95
2.5.3	Flow-injection systems.	95
2.5.4	Surface-Enhanced Hyper Raman Spectroscopy (SEHRS).	
2.5.4.1	Hyper-Raman Scattering (HRS)	96
2.5.4.2	Applications of SEHRS.	97
<b><u>CHAPTER THREE: OBJECTIVES.</u></b>		<b>99</b>

<u>CHAPTER FOUR;</u>	<u>EXPERIMENTAL.</u>	101
4.1	Preparation of bipyridyl ligands and their ruthenium complexes.	"
4.1.1	2,2'-bipyridine.	"
(a)	Tris(2,2'-bipyridine) ruthenium(II) diiodide, $\text{Ru}(\text{bipy})_3\text{I}_2$ .	"
(b)	Tris(2,2'-bipyridine) ruthenium(II) dichloride, $\text{Ru}(\text{bipy})_3\text{Cl}_2$ .	"
(c)	Bis(2,2'-bipyridine) ruthenium(II) dithiocyanide, $\text{Ru}(\text{bipy})_2(\text{NCS})_2$ .	102
(d)	Bis(2,2'-bipyridine) ruthenium(II) dichloride dihydrate, $\text{Ru}(\text{bipy})_2\text{Cl}_2 \cdot 2\text{H}_2\text{O}$	"
(e)	Bis(2,2'-bipyridine) 1,10-phenanthroline ruthenium(II) dichloride, $[\text{Ru}(\text{bipy})_2(\text{phen})]\text{Cl}_2$ .	103
4.1.2	2,2'-bipyridine-4,4'-dicarboxylic acid.	104
(a)	Ruthenium(II) complex of 2,2'-bipyridine-4,4'-carboxylic acid.	"
4.1.3	Diethyl 2,2'-bipyridine-4,4'-dicarboxylate.	"
4.1.4	4,4'-diamino-2,2'-bipyridine.	107

	(a) Tris(4,4'-diamino-2,2'-bipyridine)	
	ruthenium(II) dichloride.	109
4.1.5	4,4'-dimethyl- and 4,4'-diphenyl-2,2'-bipyridine.	111
	(a) Tris(4,4'-diphenyl-2,2'-bipyridine)	
	ruthenium(II) dichloride.	"
	(b) Tris(4,4'-dimethyl-2,2'-bipyridine)	
	ruthenium(II) dichloride.	112
4.2	Column chromatography.	114
4.3	Preparation of SERS-active substrates.	115
4.3.1	Colloids.	"
4.3.2(a)	Chemically produced films.	"
	(b) Production of gold and copper active films.	116
4.3.3	Supported silver colloids.	117
4.3.4(a)	Silica spheres.	"
	(b) Chemically coated silver silica spheres.	118
4.3.5	Vapour-deposited surfaces.	119
4.4	Spectroscopy.	122
4.4.1	Raman spectroscopy.	"
4.4.2	Electronic absorption spectroscopy.	127
4.4.3	Nuclear magnetic resonance (n.m.r.)	
	spectroscopy.	"

4.4.4	Infra-red spectroscopy.	127
4.4.5	Scanning electron microscopy (SEM).	"
	(a) Preparation of samples.	"
	(b) SEM experiments.	128

## CHAPTER FIVE: STUDIES OF DISUBSTITUTED 2,2'-BIPYRIDINES

### AND TRIS-BIPYRIDYL RUTHENIUM(II)

### COMPLEXES.

5.1	Characterisation of bipyridyl ligands.	129
5.1.1	2,2'-bipyridine-4,4'-dicarboxylic acid (diacbipy).	"
5.1.2	Diethyl 2,2'-bipyridine-4,4'-dicarboxylate (diesbipy).	130
5.1.3	4,4'-diamino-2,2'-bipyridine (diambipy).	132
	(a) 2,2'-bipyridine-1,1'-dioxide	"
	(b) 4,4'-dinitro-2,2'-bipyridine-1,1'-dioxide	"
	(c) 4,4'-diamino-2,2'-bipyridine.	133
5.2	Absorption spectroscopy of ruthenium(II) complexes of substituted 2,2'-bipyridyl ligands	134
5.2.1	$\text{Ru}(\text{bipy})_3\text{Cl}_2$ and $\text{Ru}(\text{bipy})_3\text{I}_2$ .	"

5.2.2	Tris(diethyl-2,2'-bipyridine-4,4'-dicarboxylate) ruthenium(II) ditetrafluoroborate, Ru(diesbipy) <sub>3</sub> [BF <sub>4</sub> ].	138
5.2.3	Tris-(4,4'-diamino-2,2'-bipyridine) ruthenium(II) dichloride, Ru(diambipy) <sub>3</sub> Cl <sub>2</sub> .	140
5.2.4	Tris(4,4'-diphenyl-2,2'-bipyridine) ruthenium(II) dichloride, Ru(diphbipy) <sub>3</sub> Cl <sub>2</sub> .	148
5.2.5	Tris(4,4'-dimethyl-2,2'-bipyridine) ruthenium(II) dichloride, Ru(dimebipy) <sub>3</sub> Cl <sub>2</sub> .	151

**CHAPTER SIX: SPECTROSCOPIC INVESTIGATIONS OF POTENTIALLY  
SERS-ACTIVE SUBSTRATES.**

		153
6.1	Introduction.	"
6.2	Colloids.	154
6.2.1	Silver colloids/Ru(bipy) <sub>3</sub> I <sub>2</sub> .	155
6.3	Chemically prepared films.	159
6.3.1	Silver-coated microscope slides.	"
	(a) Characterisation of the surface.	"
	(b) SERRS with Ru(bipy) <sub>3</sub> I <sub>2</sub> and Ru(bipy) <sub>3</sub> Cl <sub>2</sub> .	163

(c)	Optimisation of surface preparation procedures.	165
(d)	Other aspects of the SERR spectrum of $[\text{Ru}(\text{bipy})_3]^{2+}$ .	167
(i)	Dependence on time.	"
(ii)	Dependence on adsorbate concentration.	169
(iii)	Enhancement: effect of charge.	172
(e)	SERRS with other 2,2'-bipyridyl and 1,10-phenanthroline complexes.	"
(f)	SERS-activity of silver-coated slides with organic and gaseous adsorbate species.	177
(i)	2,2'-bipyridine	"
(ii)	Pyridine.	180
(iii)	Benzoic acid.	182
(iv)	Benzene.	"
(v)	Gases.	185
6.3.2	Gold and copper-coated microscope slides.	186
6.3.3	General discussion.	"
6.4	Supported silver colloids.	189
6.4.1	Filter paper-supported colloids.	"
6.4.2	TLC plate-supported silver colloids.	193
6.4.3	Discussion.	"

6.5	Silica spheres: chemical methods.	195
6.5.1	Filter paper-supported silica spheres.	"
6.5.2	Glass-supported silica spheres.	196
6.5.3	Modification of a method of production of silver-coated latex spheres.	"
6.5.4	Discussion.	197
6.6	Vapour-deposited surfaces.	198
6.6.1	Polycarbonate surface.	"
	(a) Electron microscopy.	"
	(b) Absorption spectroscopy.	201
	(c) SERRS of Ru(bipy) <sub>3</sub> I <sub>2</sub> .	"
	(d) Other adsorbates.	209
6.6.2	Silica spheres.	"
6.6.3	Discussion	214
6.7	General comments.	216

**CHAPTER SEVEN: SERRS OF TRIS(2,2-BIPYRIDINE) RUTHENIUM(II)**  
**AND MODIFIED COMPLEXES ON**  
**CHEMICALLY-PREPARED AND VAPOUR-**  
**DEPOSITED SURFACES**

7.1	Introduction.	217
7.2	Chemically-prepared silver-coated slides.	218

7.2.1	Ru(bipy) <sub>3</sub> I <sub>2</sub> : assignment of RRS and SERRS.	218
7.2.2	RRS and SERRS with Tris (diethyl-2,2'- bipyridine-4,4'-dicarboxylate) ruthenium(II).	224
	(a) Resonance Raman spectrum.	"
	(b) Comparison of the RRS and SERRS of the diester complex.	228
7.2.3	Tris(4,4'-diamino-2,2'-bipyridine) ruthenium (II).	"
	(a) Resonance Raman spectrum.	231
	(b) Comparison of the RR and SERR spectra of the diamino complex.	232
	(c) Effect of protonation.	"
7.2.4	Tris(4,4'-diphenyl-2,2'-bipyridine) ruthenium(II).	233
	(a) Resonance Raman spectrum.	"
	(b) Comparison of the RR and SERR spectra of the diphenyl complex.	236
7.2.5	Tris(4,4'-dimethyl-2,2'-bipyridine) ruthenium (II).	237
	(a) Resonance Raman spectrum.	"
	(b) Comparison of the RR and SERR spectra of the dimethyl complex.	240

7.2.6	Discussion.	240
7.3	Vapour silver-coated polycarbonate.	243
7.3.1	Tris(2,2'-bipyridyl) ruthenium(II).	"
	(a) Note on the presentation of spectra.	"
	(b) Raman spectrum of the polycarbonate substrate.	"
	(c) SERR spectrum of Ru(bipy) <sub>3</sub> I <sub>2</sub> .	244
7.3.2	Tris(4,4'-diethoxycarbonyl-2,2'-bipyridine) ruthenium(II).	249
7.3.3	Tris(4,4'-diamino-2,2'-bipyridine) ruthenium(II).	254
7.3.4	Tris(4,4'-diphenyl-2,2'-bipyridine) ruthenium(II).	258
7.3.5	Tris(4,4'-dimethyl-2,2'-bipyridine) ruthenium(II).	262
7.3.6	Discussion.	265
	<b><u>CHAPTER EIGHT: CONCLUSIONS.</u></b>	268
	<b>REFERENCES.</b>	274

## SUMMARY.

The basic aim of this work was to explore ways of applying the technique of Surface-enhanced Raman spectroscopy (SERS) to the routine analysis of organic and inorganic compounds. Intensive study of the activity of a series of modified tris(2,2'-bipyridyl) ruthenium(II) complexes was designed to address the question of the nature of the surface/adsorbate molecule bond. The research was divided into three main areas.

(1) The preparation of disubstituted analogues of the complex tris(2,2'-bipyridyl) ruthenium(II) diiodide,  $\text{Ru}(\text{bipy})_3\text{I}_2$ . Four complexes, in addition to the parent complex, were prepared, each incorporating three 2,2'-bipyridyl ligands substituted in the  $\text{C}_4$  and  $\text{C}_4'$  positions. These complexes were tris(4,4'- diethoxycarbonyl, -diamino, -diphenyl and -dimethyl-2,2'-bipyridine) ruthenium(II). The 4,4'-diethoxycarbonyl and 4,4'-diamino ligands were prepared from literature procedures and the 4,4'-diphenyl and 4,4'-dimethyl ligands were used as received. Each of the complexes was purified by column chromatography and characterised, primarily, by electronic absorption spectroscopy.

(2) A study of SERS-active substrates. The analytical potential of several categories of surfaces was probed with organic molecules and  $\text{Ru}(\text{bipy})_3\text{I}_2$  and other complexes. The results showed that silver-coated

microscope slides, prepared through the reduction of ammonical silver nitrate solution, exhibited appreciable activity with a range of adsorbate species and particularly strong enhancement with  $\text{Ru}(\text{bipy})_3\text{I}_2$ . It was found that the molecules physisorbed on the metal surface.

Vapour-deposited silver-coated polycarbonate substrates also displayed SERRS-activity with  $\text{Ru}(\text{bipy})_3\text{I}_2$ . The resultant spectra were considerably less enhanced but showed evidence of chemisorption of the adsorbate.

These findings are discussed in relation to current theories of SERS enhancement.

(3) A comparative study of the SERRS of  $[\text{Ru}(\text{bipy})_3]^{2+}$  and disubstituted analogues with silver slides and silver polycarbonate. The effect of substitution of the 2,2'-bipyridyl ligands incorporated into the complexes was studied.

These results and the assignment of the SERR spectra showed that disubstitution does not affect the adsorption of the complex on silver slides, but does have a limited effect on the adsorption on silver polycarbonate.

All the findings of the work are summarised and discussed with regard to the analytical applications of the technique. It is proposed that SERS has only limited applicability in the area of chemical sensing

and that there is no ideal SERS-active substrate due to the large number of variables operating in any SERS analysis.

**CHAPTER ONE.**

**GENERAL BACKGROUND TOPICS.**

## **1. GENERAL BACKGROUND TOPICS.**

### **A. RAMAN SPECTROSCOPY.**

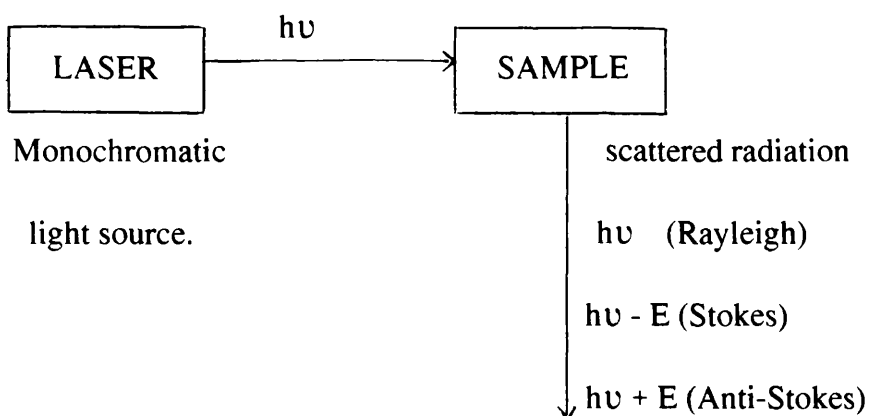
#### **1.1 Introduction.**

Raman spectroscopy provides rotational and vibrational (and sometimes electronic) spectra through inelastic scattering of visible light. This differs from absorption spectroscopy where transmitted radiation is examined.

If a substance is irradiated with an intense beam of monochromatic light (provided by a laser) then a small proportion of the radiation is scattered. Most of this scattered energy has the same frequency as the incident radiation: this is termed Rayleigh scattering. A small proportion of the radiation, however, will have a frequency other than the incident radiation. This is referred to as Raman scattering.

Scattered radiation of lower frequency than that of the incident beam is termed Stokes radiation, while radiation of higher frequency is termed Anti-Stokes radiation.

Figure 1.1 : Raman scattering.



Rayleigh and Raman scattering proceed through virtual excited states with no measurable lifetimes. These processes differ from fluorescence where the emitted frequency corresponds to molecular electronic (vibronic) transitions and is independent of the exciting frequency. Fluorescence proceeds through real excited states with measurable lifetimes.

Figure 1.2 displays an energy level diagram illustrating the types of scattering which takes place when a molecule is irradiated.

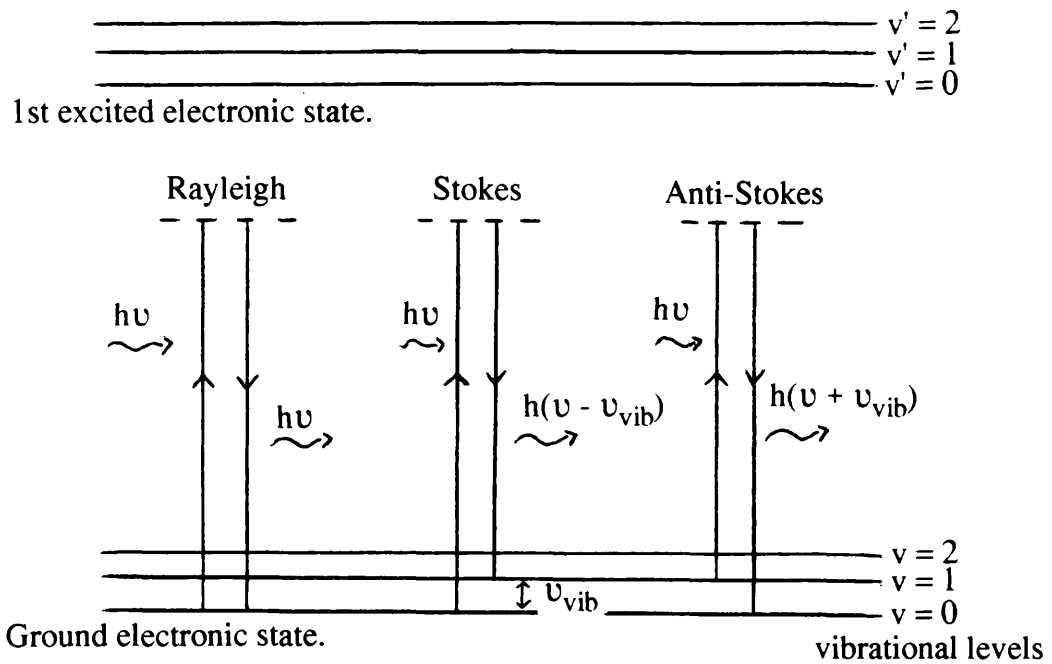


Figure 1.2: Raman scattering processes.

Anti-Stokes band intensities drop off rapidly with frequency in accordance with the Boltzmann distribution of molecules in excited vibrational states, given by equation 1.1.

$$\frac{N_{v+1}}{N_v} = e^{-(E_{v+1} - E_v)/kT} \quad , \quad (1.1)$$

where  $N_{v+1}$  and  $N_v$  are the numbers of molecules in the upper and lower vibrational states respectively,  $(E_{v+1} - E_v)$  is the difference in energy of the two vibrational states,  $T$  is the temperature in Kelvin and  $k$  is the Boltzmann constant.

Unlike anti-Stokes bands, Stokes bands maintain their intensities throughout the spectrum.

Raman spectroscopy represents a method of obtaining a complete vibrational spectrum from  $10 \text{ cm}^{-1}$  (far infra-red) to approximately

5000  $\text{cm}^{-1}$  in a single run and on a simple spectrometer. It can also yield a complete rotational spectrum from 10 to 500  $\text{cm}^{-1}$ .

A typical Raman spectrum is displayed in figure 1.3.

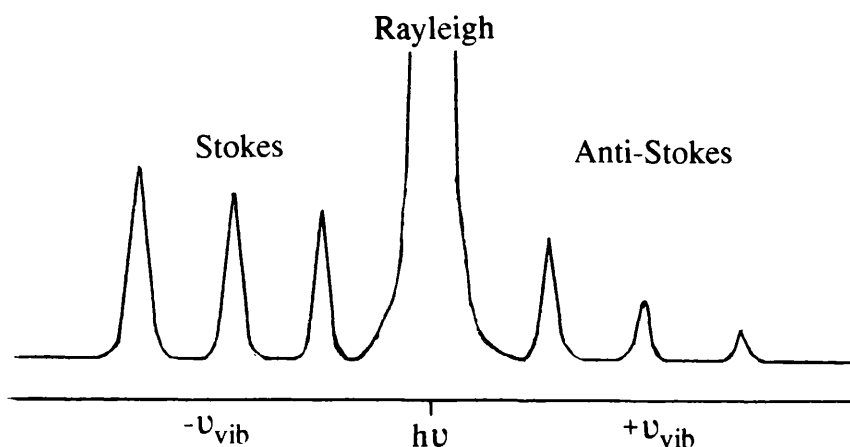


Figure 1.3: Typical Raman spectrum.

## 1.2 Vibrational Raman effect.

A molecule in an electric field is distorted due to the attraction of the nuclei to the negative pole of the field and the converse attraction of the electrons to the positive pole. This separation of the charges induces an electric dipole moment,  $\underline{\mu}$ , in the polarised molecule. The magnitude of the field-induced dipole depends on the magnitude of the electric field vector,  $\underline{E}$ , and the ease with which the molecule is distorted (polarisability) (equation 1.2).

$$\underline{\mu} = \underline{\alpha} \underline{E} \quad , \quad (1.2)$$

where  $\underline{\alpha}$  is the dynamic polarisability tensor of the molecule.

The polarisability tensor is anisotropic since an electric field applied

along a bond axis displaces an electron in the bond more easily than a field applied across the bond. It is a second-rank (polar) tensor with nine components and, for non-spherical molecules, equation 1.2 actually represents three equations (1.3a-c).

$$\mu_x = \alpha_{xx}E_x + \alpha_{xy}E_y + \alpha_{xz}E_z \quad (1.3a)$$

$$\mu_y = \alpha_{yx}E_x + \alpha_{yy}E_y + \alpha_{yz}E_z \quad b$$

$$\mu_z = \alpha_{zx}E_x + \alpha_{zy}E_y + \alpha_{zz}E_z \quad c$$

The origin of scattered light is in the characteristic electromagnetic fields radiated by an oscillating electric dipole moment,  $\underline{\mu}$ , induced in the molecule by the electric field vector of the incident electromagnetic radiation.

A light wave with electric field vector  $\underline{E}$  obeys expression 1.4.

$$\underline{E} = \underline{E}^0 \cos 2\pi \nu t \quad , \quad (1.4)$$

where  $\underline{E}^0$  is the maximum electric field,  $\nu$  is the frequency and  $t$  is the time.

The electric field vector induces an oscillating dipole moment given by equation 1.5.

$$\underline{\mu} = \underline{\alpha} \underline{E}^0 \cos 2\pi \nu t \quad (1.5)$$

When the oscillating dipole emits radiation of the same frequency as the applied field, Rayleigh scattering is observed. If the polarisation is modulated by molecular vibrations, the oscillating dipole will have vibrational oscillations superimposed on it. Equation 1.6 holds for small

displacements.

$$\underline{\alpha} = \underline{\alpha}_0 + (d\underline{\alpha}/dQ_v)_0 Q_v^0 \cos 2\pi\nu_{\text{vib}}t \quad , \quad (1.6)$$

where  $\underline{\alpha}_0$  = equilibrium polarisability,

$Q_v$  = normal co-ordinate of vibration,

$$[ Q_v = Q_v^0 \cos 2\pi\nu_{\text{vib}}t ]$$

$(d\underline{\alpha}/dQ_v)_0$  = rate of change of  $\underline{\alpha}$  with vibration.

Substitution of 1.6 into equation 1.5 gives the following expression:

$$\underline{\mu} = \{ \underline{\alpha}_0 + (d\underline{\alpha}/dQ_v)_0 Q_v^0 \cos 2\pi\nu_{\text{vib}}t \} \underline{E}^0 \cos 2\pi\nu t \quad (1.7)$$

$$\Rightarrow \underline{\mu} = \underline{\alpha}_0 \underline{E}^0 \cos 2\pi\nu t + \{ (d\underline{\alpha}/dQ_v)_0 Q_v^0 \underline{E}^0 \cos 2\pi\nu_{\text{vib}}t \cos 2\pi\nu t \} \quad (1.8)$$

Since  $2\cos A \cos B = \cos(A+B) + \cos(A-B)$ , equation 1.8 becomes:

$$\underline{\mu} = [ \underline{\alpha}_0 \underline{E}^0 \cos 2\pi\nu t ] + [ 1/2 (d\underline{\alpha}/dQ_v)_0 Q_v^0 \underline{E}^0 \{ \cos 2\pi(\nu + \nu_{\text{vib}})t \quad (1.9)$$

$$+ \cos 2\pi(\nu - \nu_{\text{vib}})t ]$$

Thus, the frequency spectrum of the scattered light contains small components,  $\nu \pm \nu_{\text{vib}}$  (Stokes and anti-Stokes), in addition to the dominant component,  $\nu$  (Rayleigh). All these components make up the Raman spectrum. The amplitude of the Raman wave is proportional to  $(d\underline{\alpha}/dQ_v)_0$ .

### 1.3 Quantum selection rules.

The polarisability tensor,  $\underline{\alpha}$ , is regarded as an operator bringing

about transitions between vibrational quantum states.

The transition polarisability is defined as follows:

$$(\underline{\alpha}_{\alpha\beta})_{fi} = \langle \nu_f | \alpha_{\alpha\beta} | \nu_i \rangle \quad , \quad (1.10)$$

where i and f represent the initial and final Raman states.

The vibrational Raman selection rules are the following:

$$(d\underline{\alpha}/dQ_v)_0 \neq 0 \quad ; \quad \Delta\nu_v = \pm 1 \quad (1.11)$$

Hence, the selection rule that "to be Raman active, a molecular vibration must cause a change in a component of the polarisability".

#### 1.4 Raman polarisation measurements.

In light scattering at  $90^\circ$ , two distinct polarisation components can be measured,  $I_{||}$  (parallel intensity) and  $I_{\perp}$  (intensity at  $90^\circ$ ) as shown in figure 1.4.

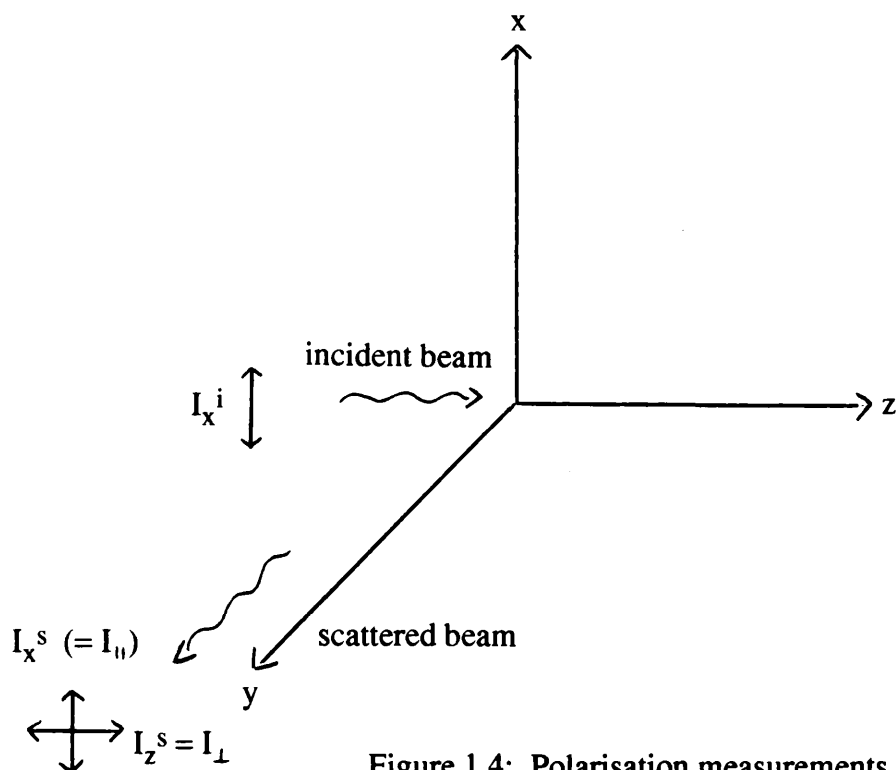


Figure 1.4: Polarisation measurements.

The intensities of  $I_{\parallel}$  and  $I_{\perp}$  can be measured through an oriented polaroid sheet.

The Raman depolarisation ratio is defined in equation 1.12.

$$\rho = I_{\perp} / I_{\parallel} \quad (1.12)$$

If the incident laser beam is linearly polarised along x,

$$\begin{aligned} \mu_x &= \alpha_{xx} E_x \\ \mu_y &= \alpha_{yx} E_x \\ \mu_z &= \alpha_{zx} E_x \end{aligned} \quad , \quad (1.13)$$

and hence, 
$$\rho = \alpha_{zx}^2 / \alpha_{xx}^2 \quad (1.14)$$

For an isotropic sample, this must be averaged over all orientations of the molecule.

Equation 1.15 can be obtained.

$$\rho = \frac{3\beta^2}{45\alpha^2 + 4\beta^2} \quad , \quad (1.15)$$

where  $\alpha$  is the mean polarisability and  $\beta^2$  is the polarisability anisotropy.

The mean polarisability can never vanish as all molecules have intrinsic polarisability. The polarisability anisotropy,  $\beta^2$ , can vanish in the case of electrically isotropic molecules such as carbon tetrachloride.

In general, from equation 1.15:

$$3/4 > \rho > 0 \quad (1.16)$$

#### 1.4.1 Depolarisation ratios.

Raman depolarisation ratios can assist vibrational band assignments.

The quantities  $\underline{\alpha}$  and  $\beta^2$ , from equation 1.15, are re-interpreted as transition polarisability components.

The mean polarisability,  $\underline{\alpha}$ , spans only the totally symmetric irreducible representation. Parts of  $\beta^2$  can span both totally symmetric and non-totally symmetric irreducible representations. Therefore,  $\rho = 3/4$  for a non-totally symmetric vibration and  $3/4 > \rho > 0$  for a totally symmetric vibration. Any deviation from complete depolarisation, therefore, indicates a totally symmetric vibration.

#### 1.5 Resonance Raman spectroscopy.

In conventional Raman spectroscopy, the sample is completely transparent (the laser frequency is well removed from any allowed electronic absorption). If, however, the exciting frequency is in the region of an electronic absorption, there can be tremendous enhancement of the Raman intensity.

The Raman transition polarisability,  $\underline{\alpha}_{\alpha\beta}$ , induced in a molecule due to the oscillating electric field vector of the light source, can be re-defined quantum mechanically:

$$(\alpha_{\alpha\beta})_{fi} = \sum_{m \neq i,f} \frac{\langle f | \underline{\mu}_{\alpha} | m \rangle \langle m | \underline{\mu}_{\beta} | i \rangle}{(E_m - E_i) - h\nu} + \frac{\langle f | \underline{\mu}_{\beta} | m \rangle \langle m | \underline{\mu}_{\alpha} | i \rangle}{(E_m - E_i) + h\nu} \quad (1.17)$$

where  $|i\rangle$ ,  $|m\rangle$  and  $|f\rangle$  are initial, intermediate and final Raman states. The energy of the states is represented by  $E$ ,  $\underline{\mu}$  is the electric dipole operator and  $h\nu$  is the excitation energy of the laser.

The fundamental processes involved in resonance Raman spectroscopy are displayed in figure 1.5.

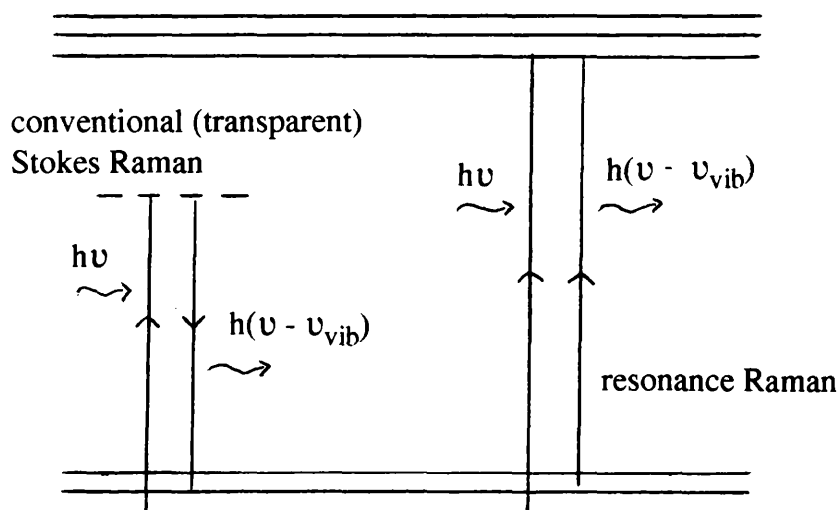


Figure 1.5: Resonance Raman scattering processes.

At resonance,  $h\nu$  is approximately equal to  $(E_m - E_i)$  and, consequently, the denominator of the first term of equation 1.17 tends to zero. Since scattered intensity depends on the square of the transition polarisability, large enhancement results.

Resonance enhancement enables vibrational spectra to be obtained

in unfavourable situations such as very dilute solutions, matrix isolated species and local sites in large biological molecules. Indeed, the study of biological molecules by resonance Raman methods has become extremely widespread. Fundamental chemically-based biological functions have been studied through the selective enhancement of active chromophores.

## **B. LASERS.**

### **1.1 Radiative processes.**

Figure 1.6 shows common absorption and emission processes for a typical organic molecule.

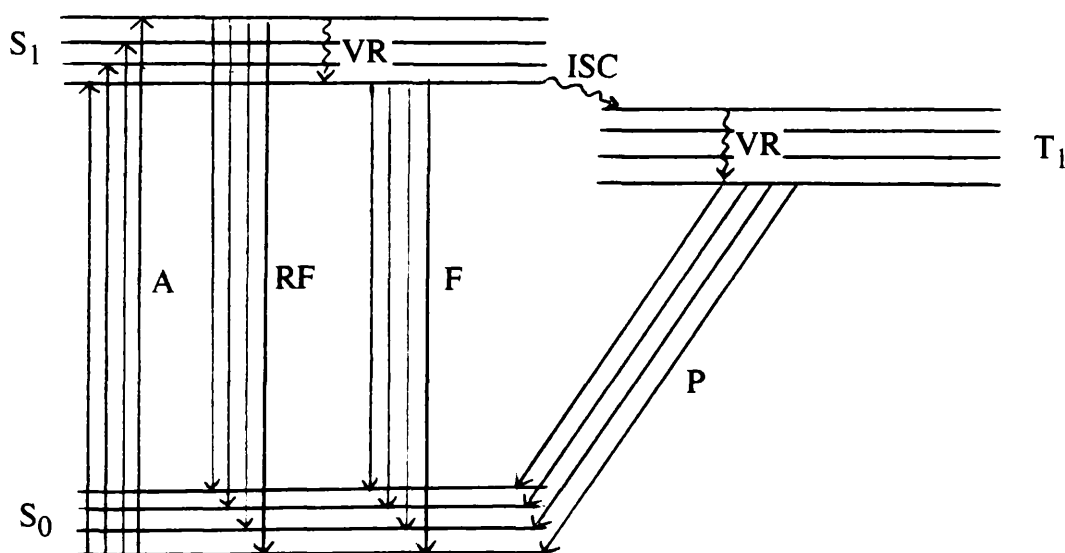


**Figure 1.6: Absorption and emission processes.**

#### **(a) Absorption (A).**

The room temperature absorption spectrum is dominated by

transitions from singlet ground vibrational states to upper vibrational states in the excited singlet electronic state. The absorption spectrum generally gives details of the upper vibrational states.

(b) Resonance fluorescence (RF) and fluorescence (F).

Resonance fluorescence is not always the favoured process.

Vibrational relaxation (VR) (energy degradation) to the lowest available vibrational level in the upper singlet electronic state can occur.

Fluorescence then proceeds from the lowest vibrational state. RF and F give details of the vibrational levels of the ground electronic state.

Resonance fluorescence is favoured by isolated conditions.

(c) Phosphorescence (P).

Inter system crossing (ISC) from the upper singlet state to the triplet state,  $T_1$ , followed by vibrational relaxation leads to phosphorescence. This process is formally spin-forbidden and the radiative lifetimes can be very long.

When the vibrational levels of the upper and lower singlet states overlap, energy can be dissipated through non-radiative processes such as ISC, internal energy conversion (IEC) and VR. These three processes compete with the radiative processes: under certain circumstances they may quench fluorescence and phosphorescence.

## 1.2 Lasing action: emission and absorption processes.

In a two-level system, several absorption and emission processes can take place. Figure 1.7 illustrates these.

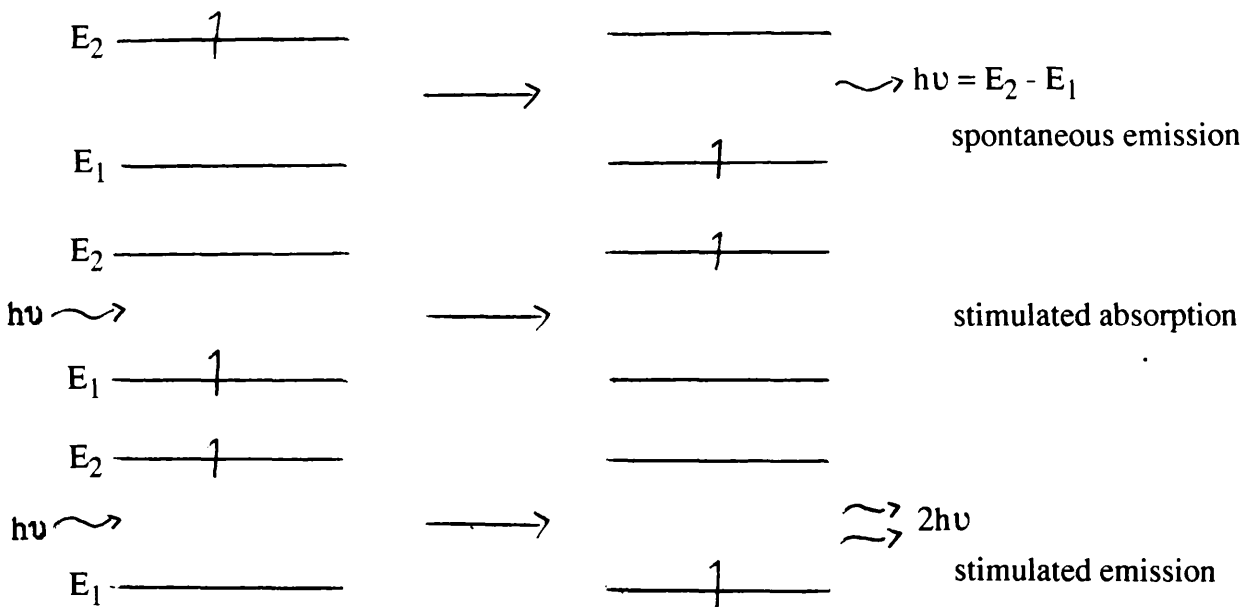


Figure 1.7: Absorption and emission processes in a two-level system.

Spontaneous emission always occurs in an excited system. It is frequency dependent, being of high probability at high frequencies. Stimulated absorption has a probability which depends on the density of radiation and the nature of the transition. Stimulated emission results in light amplification and is the basis of laser action: the production of coherent, monochromatic light.

The probabilities of each of the above three processes occurring can

be expressed as follows:

Spontaneous emission:  $A_{21}$ .

Stimulated absorption:  $B_{12}\rho(\nu)$ , where  $\rho(\nu)$  is the energy density.

Stimulated emission:  $B_{21}\rho(\nu)$ .

A and B are Einstein's "A and B" coefficients of spontaneous and stimulated emission, respectively.

If an equilibrium exists where  $n_1$  molecules are in  $E_1$  and  $n_2$  in  $E_2$  at temperature T, with radiation density  $\rho(\nu)$ , the total emission rate is equal to the total absorption rate:

$$n_2(A_{21} + B_{21}\rho(\nu)) = n_1 B_{12}\rho(\nu) \quad , \quad (1.18)$$

and hence:

$$\rho(\nu) = \frac{A_{21}/B_{21}}{[(n_1/n_2)(B_{12}/B_{21}) - 1]} \quad (1.19)$$

At thermal equilibrium, the Boltzmann distribution applies (equation 1.1). Substituting this expression into 1.19 gives:

$$\rho(\nu) = \frac{A_{21}/B_{21}}{[(B_{12}/B_{21}) e^{h\nu/kT} - 1]} \quad (1.20)$$

This expression is similar to Planck's radiation law which states:

$$\rho(\nu) = \frac{8\pi h\nu^3}{c^3} \left[ \frac{1}{e^{h\nu/kT} - 1} \right] \quad (1.21)$$

Equations 1.21 and 1.20 are only consistent if:

$$\frac{A_{21}}{B_{21}} = \frac{8\pi h \nu^3}{c^3} \quad \text{and} \quad \frac{B_{12}}{B_{21}} = 1 \quad (1.22)$$

At high frequencies, spontaneous processes dominate stimulated processes. Lower frequency spectroscopies are therefore dominated by induced processes.

The ratio of probabilities is given by equation 1.23:

$$\frac{\text{Probability (spontaneous emission)}}{\text{Probability (stimulated emission)}} = \frac{A_{21}}{B_{21}\rho(\nu)} = e^{h\nu/kT} - 1 \quad (1.23)$$

From this equation, it is clear that the spontaneous process is more probable when  $h\nu > kT$  and the stimulated process is more probable when  $h\nu < kT$ .

Therefore,

$$\frac{\text{Rate of emission}}{\text{Rate of absorption}} = \left[ \frac{A_{21} + B_{21}\rho(\nu)}{B_{12}\rho(\nu)} \right] \frac{n_2}{n_1} \quad (1.24)$$

$$= \left[ 1 + \frac{A_{21}}{B_{12}\rho(\nu)} \right] \frac{n_2}{n_1} \quad (1.25)$$

Expression 1.25 is approximately equal to  $(n_2/n_1)$  if  $h\nu \ll kT$ . Under the conditions of thermal equilibrium,  $n_2 < n_1$ . For laser action, however, population inversion ( $n_2 > n_1$ ) is required.

Population inversion was first described with a microwave system: the ammonia maser. This was a physical method of population inversion.

The first laser (1960) used ruby ( $\text{Cr}^{3+}$  doped alumina) as an active medium. The requirements for laser action are described as follows:

- (a) An optical medium with optical gain (population inversion).
- (b) A means of trapping light spontaneously emitted, leading to feedback. This is generally achieved through the use of a cavity.

The first ruby laser employed two exactly parallel mirrors (Fabry-Perot cavity), allowing standing waves to interfere.

When the lower lasing energy state is the ground state (which is repopulated as emission proceeds), only pulsed operation is possible. Lasing action is not possible while pumping (excitation) is occurring.

### 1.3 Examples of laser systems.

#### 1.3.1 Rare gas discharge lasers.

The first example of this type of laser employed a mixture of helium and neon and was the first laser which was able to be operated in a continuous wave (cw) mode. Helium acts as an energy store and transfer medium. Lasing action occurs in the neon. Figure 1.8 shows an energy level diagram of the processes involved.

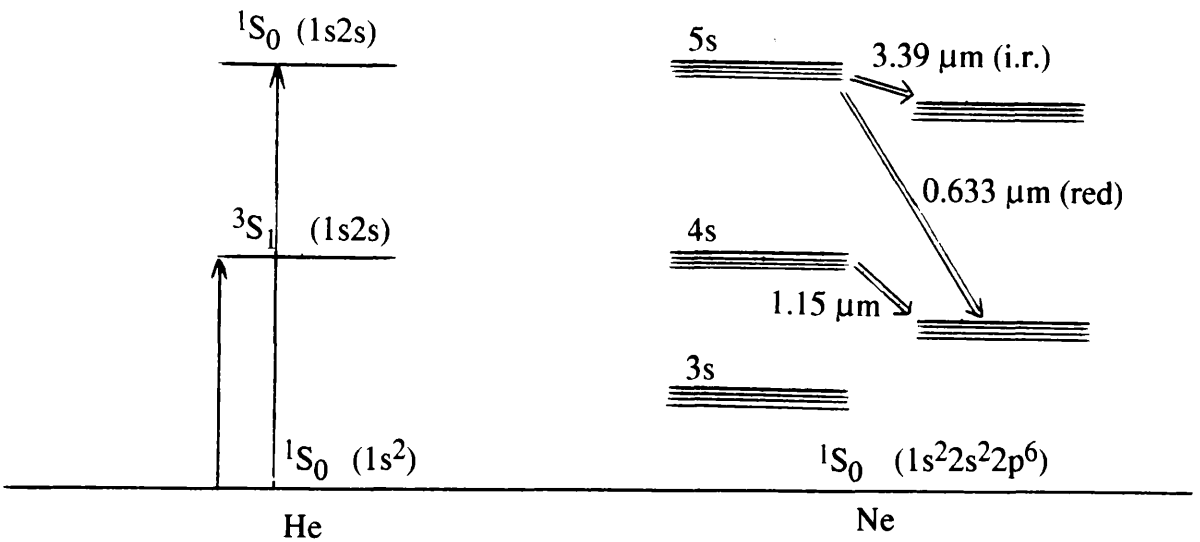


Figure 1.8: Helium/neon laser: energy processes.

The  $1S_0$  and  $3S_1$  levels of helium are forbidden and, therefore, metastable. Three laser lines are produced; the most frequently used being the red  $0.633 \mu\text{m}$  line. Pumping is achieved through electrical discharge and the lower lasing (Ne) levels can decay to the ground state allowing continuous wave operation.

All rare gas discharge lasers operate on the basis of these principles. All have a discharge tube and two Fabry-Perot mirrors, one semi-reflecting. Table 1.1 details the main laser lines available from rare gas discharge lasers.

The power output from these lasers ranges from 1 mW to 100 W.

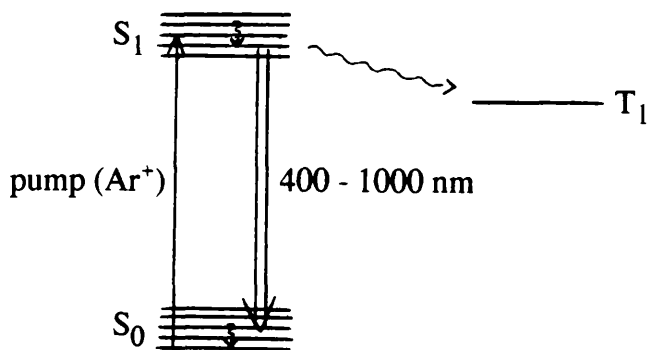
Table 1.1: Rare gas discharge lasers: output wavelengths.

Helium/Neon	632.8	1150.0	3390.0	(nm)
Argon ion	488.0	514.5		
Krypton ion	520.8	530.8	568.2	647.1
Cadmium/helium	325.0	441.7		

1.3.2 Dye lasers.

The active media present in these lasers are solutions of organic dyes. Dye lasers can be smoothly tuned over various wavelength ranges, depending on the particular active dye used. They can be pumped by flashes, pulsed lasers or, more commonly, by sufficiently powerful cw rare gas discharge lasers.

Dye lasers operate through fully allowed transitions with no intervening metastable state, as shown in figure 1.9.

Figure 1.9: Dye laser: energy processes.

Any one dyestuff can lase over a  $> 50$  nm region. Rhodamine 6G, for example, can be continuously tuned from 569.3 to 609.1 nm.

Dye lasers are extremely useful in the field of resonance Raman spectroscopy and in the study of the dependence of scattered intensity of a Raman-active vibration on excitation wavelength (excitation profiles).

### 1.3.3 Neodymium YAG lasers.

These solid state lasers use the active medium  $\text{Nd}^{3+}$  in yttrium aluminium garnet (YAG). Lasing action is displayed in figure 1.10.

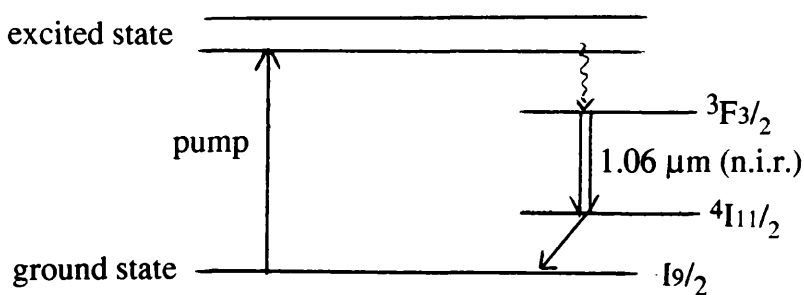


Figure 1.10: Neodymium YAG laser: energy processes.

As is evident from figure 1.10, continuous wave operation is possible. The lasing transition is 1060.0 nm (in the near infra-red).

The technique of Q-switching is normally employed. This involves rotating one cavity mirror and pumping, causing the population of the metastable level to build up. When the mirrors align, the energy is released in a single, short pulse (of picosecond duration). Output power levels of  $10^{12}$  W have been achieved with Q-switched  $\text{Nd}^{3+}$  YAG lasers in conjunction with several amplifiers.

CHAPTER TWO.

SURFACE-ENHANCED RAMAN SPECTROSCOPY.

## 2. SURFACE-ENHANCED RAMAN SPECTROSCOPY.

### 2.1 History.

In 1974, Fleischmann *et al.* (1) reported anomalously large Raman intensities from studies of pyridine adsorbed on silver electrodes which had been subjected to successive oxidation-reduction cycles (orc). They explained these mysterious inordinate signal strengths in terms of a large increase in the surface area of the electrode, due to the roughening procedure, and, therefore, in the number of adsorbate molecules sampled.

The next significant studies were made in 1977 by Albrecht and Creighton (2) and, independently, by Jeanmaire and Van Duyne (3). These investigations were also on the adsorption of pyridine on roughened silver electrodes. Both sets of results displayed a Raman signal intensity enhancement of approximately  $10^5$ . These groups were the first to recognise that the large increase in Raman-scattered intensity could not be accounted for by the increase in surface area alone. This was proven by showing that equally intense signals could be obtained with silver electrode surfaces roughened only slightly (the increase in surface area not exceeding a factor of ten). Their conclusion (2) was that the anomalous increase in signal intensity was caused by a surface effect which greatly increased the molecular Raman scattering

cross-section.

The nature of this "surface effect" was probed in subsequent years and two main theoretical models emerged : electromagnetic and chemical (discussed in section 2.3). As the subject grew, it was christened "surface-enhanced Raman scattering or spectroscopy" (SERS).

All of the early studies were of pyridine adsorbed on silver electrode surfaces and, indeed, electrodes were almost exclusively studied in the early years of the development of the field. Colloids and vapour-deposited surfaces, however, were found to be SERS-active and to give intensities comparable to those with electrode surfaces.

SERS has proved to be a very widely applicable technique: over one hundred different types of adsorbate molecules have been studied. The appreciation of the theoretical aspects of SERS led to the successful use of metals other than silver such as gold, copper, indium, aluminium, lead, platinum, rhodium and alkali metals.

In addition to having stimulated something of a renaissance in classical electrostatic and electromagnetic theory and related theoretical fields, SERS has, in recent years, been applied with some success to several chemical areas including the trace analysis of pollutants and contaminants.

## **2.2 SERS-ACTIVE SYSTEMS.**

"SERS-active systems" can be thought of as being surfaces with many, usually coupled, microscopic metal domains. The factors of surface roughness and surface morphology have been shown to be critical with respect to SERS enhancement. Surfaces which display adequate SERS-activity usually have roughness features in the range 10 to 500 nm. Common categories of roughness are metal spheres and ellipsoids, ridges and metal clusters. The type of surface upon which SERS is observed falls into three main areas :  
electrochemical, vapour-deposited and chemical.

### **2.2.1 Electrochemical systems.**

On electrode surfaces subjected to one or more oxidation-reduction cycles rough metal features form. During the oxidation half-cycle a metal salt is produced at the electrode surface and when reduced, the liberated metal does not re-deposit itself uniformly over the surface but, instead, forms clusters (4) of metal.

As described previously, SERS was first observed from electrodes and, as a result, the majority of studies have been with electrochemical systems.

#### **2.2.1.1 The silver/pyridine/halide ion system.**

This has been the most extensively studied electrochemical area.

Early experiments revealed a high degree of SERS enhancement and that pyridine could be adsorbed on the electrode surface either via Lewis base co-ordination through nitrogen (chemisorption) or by physisorption through water (5) as shown in figure 2.1.

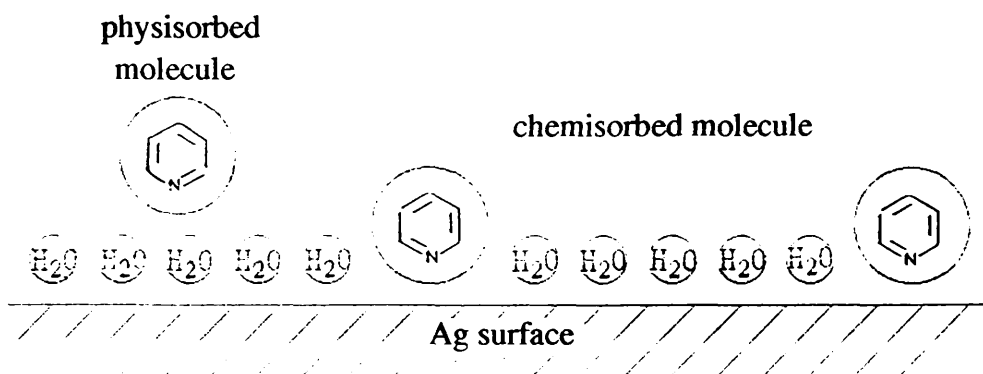


**Figure 2.1: Bonding modes of pyridine on a silver electrode.**

Later results demonstrated that prolonged oxidation-reduction cycles reduced SER intensity and that highly enhanced spectra resulted from electrodes exposed to only one roughening cycle (5)(6).

It has been shown that the effect of the adsorption of halide ions (from the supporting electrolyte) on the pyridine/silver system is crucial.

Fleischmann *et al.* (1) observed that over the potential range 0.0 to -0.6 volts there was a remarkable change in the relative intensities of the 1008 and 1036  $\text{cm}^{-1}$  bands of pyridine. This evidence suggested the presence of interactions, probably involving the  $\pi$ -electrons of the pyridine ring, between the adsorbed molecules and the halide ions in

the electrochemical double layer as shown in figure 2.2.

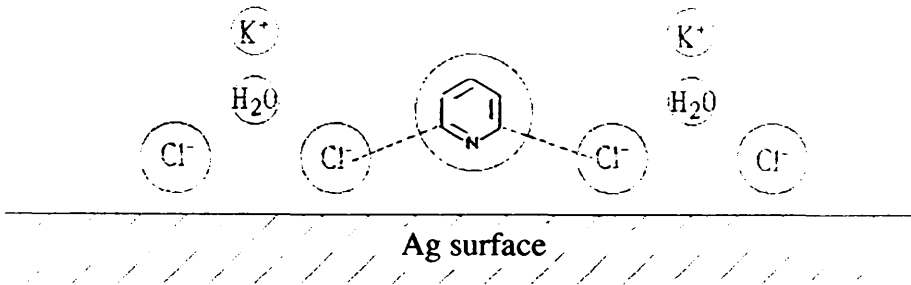


**Figure 2.2: Influence of chloride ions on the adsorption of pyridine on a silver electrode surface.**

### Potential dependence.

The factor of applied potential has been proven to be the most influential parameter controlling adsorption in the electrochemical environment.

Marinyuk *et al.* (6) observed a progressive increase in the Raman intensities of the ring modes of adsorbed pyridine between -0.3 and -0.8 volts, indicating re-orientation of the adsorbed molecules from end-on perpendicular co-ordination through nitrogen to flat co-ordination via the  $\pi$ - system of the pyridine ring. Such an increase in band intensities occurs due to the overlap of wave functions between electrons in the metal and the ring  $\pi$ - electrons.

Many other interesting phenomena have been discovered by varying the applied potential.

Furtak and Roy (7) have shown that surface coverage of halide ions is the factor most dominant over the potential dependence of these systems and that the Stark effect and bond perturbation play only minor roles (8). They argued that the variation in intensity and frequency of the spectra could be explained in terms of changes in surface coverage together with mutual depolarisation ratios. In addition, active sites on the surface were identified as silver clusters stabilised by co-adsorbed halide ions.

Further study (9) showed that the active clusters were  $[\text{Ag}_4]^+$  species, exhibiting electronic resonance through HOMO - LUMO transitions. It has also been proven that species adsorbed on and adjacent to the clusters demonstrate preferential scattering (10) (11).

#### Polycrystalline silver electrodes.

The measurement of the differential capacitance of electro-polished [100], [110] and [111] silver single crystal faces and of polycrystalline silver has been found to be highly dependent on the nature of the surface in addition to the composition of the solution. Such measurement has yielded important results.

By following capacitance/voltage curves, Fleischmann *et al.* (12)

showed that roughened electrodes consist of an ensemble of faceted microcrystals. The same group (13), by exciting an electrode surface with laser light during roughening, observed that sites where Lewis acid co-ordination took place were possibly formed by photolysis of silver chloride and that the adsorbed species were stabilised in the presence of chloride ions.

#### Surface species.

Although the predominant type of adsorption in the silver/pyridine/halide system had been thought to be well established, Regis and Corset (14) showed that the interactions of the species at the surface are considerably more complicated than had previously been thought. They discovered that the pyridinium ion, instead of pyridine itself, was preferentially adsorbed at the electrode surface in the presence of specifically adsorbed chloride.

#### Other effects.

The pyridine/chloride/silver electrode system has revealed many other important phenomena.

Sobocinski and Pemberton (15) probed silver active sites by studying the loss of SERS intensity from the system due to laser-induced heating. The induced desorption of pyridine and chloride from the active sites was found to be a first order reaction.

Competitive adsorption (16) has been observed at silver electrodes by varying the concentration of bulk pyridine and mono-substituted pyridines. The co-adsorption behaviour was well approximated by Langmuir isotherms; an area which has been gaining much momentum in recent years (183).

In their initial studies, Jeanmaire and Van Duyne (3) extended the applicability of the system to other nitrogen heterocycles and amines in addition to verifying the remarkable sensitivity of SERS for the study of pyridine adsorbed on silver electrode surfaces.

#### General discussion.

It is clear that for this system, SERS studies have given a far more detailed picture of the species present at electrode surfaces than could be derived from electrochemical measurements alone.

The experiments previously described, along with other studies involving cyanide adsorption (17) (18), indicate the formation of surface complexes associated with adatoms of silver (19) produced during the roughening procedures. The predominant type of surface complex in the pyridine/chloride/silver electrode system involves a Lewis acid-base interaction between the adsorbate and the metal surface.

All of the spectroscopic evidence put forward points to the formation of a distinct adsorbate-surface chemical bond, mediated by

halide ion adsorption, rather than simply electrostatic forces.

Physisorption, mediated by water molecules, occurs to a far lesser extent.

#### 2.2.1.2 Other electrochemical systems.

The early SERS electrochemical studies on the pyridine/halide/silver electrode system served to highlight a number of effects which in subsequent years became identified with other electrochemical systems. Many of these effects have been shown to have important consequences in relation to SERS theory and for the broader application of the technique. The experiments involved have extended SERS to other types of metal electrodes and have encompassed the use of a variety of organic and inorganic species. An account is now given of some of the important observations which have been made.

##### (a) Roughening procedure : surface morphology.

It has been demonstrated that the factors involved in the roughening procedure affect the subsequent SERS intensity.

Gao *et al.* (20) explored this dependence using benzonitrile and thiocyanate as model adsorbates on gold electrodes. They found that SERS intensities were maximised with roughening conditions yielding gold particles of approximately 100 nm diameter.

Practical considerations, however, need not only concern surface

morphology effects. Beer *et al.* (21) studied the effect of *ex. situ.* and *in. situ.* roughening procedures on the SERS intensities of pyridine, 4-ethyl pyridine and 4-cyano pyridine adsorbed on silver and gold electrodes. Roughening in the presence of the adsorbate (*in. situ.*) gave rise to new spectral features attributed to the trapping of adsorbate molecules in the surface and the subsequent complexation with metal atoms. It was concluded that the *ex. situ.* procedure was preferable when effects such as the orientation or the adsorption isotherm was of interest.

#### (b) Large scale and atomic scale roughness features.

Over a number of years, many experiments (22) (23) have been carried out in order to gauge the relative importance of both large scale roughness (having dimensions of the order of 5 to 10 nm) and atomic scale roughness in SERS electrochemical systems.

These experiments have included the variation of roughening procedures (24) (25), scanning electron microscopy studies (26) (27), study of the laser-induced thermal decay of SERS intensity as a probe of atomic scale roughness (28 - 30) and the determination of the electronic properties of roughened silver electrodes by differential reflectivity (31) (32). Control of large scale roughness was possible by regulating the roughening cycle. Atomic scale roughness, however, proved

considerably more difficult to characterise and control. The results of all these studies have shed new light on the complex roles of surface roughness in SERS. It has been shown that both categories of surface morphology have important and distinct contributions to the SERS enhancement mechanism.

### (c) Molecular interactions with electrode surfaces.

Many SERS studies with electrode systems have given rise to interesting vibrational information on the orientation of adsorbate molecules.

Loo *et al.* (33) investigated the co-ordination chemistry of malononitrile,  $(\text{CN})\text{CH}_2(\text{CN})$ . It was found that the degeneracy of the doubly degenerate cyanide stretching mode at  $2263\text{ cm}^{-1}$  in the normal Raman spectrum was removed when the molecule adsorbed on a copper electrode surface. Two distinct cyanide stretching bands were observed at  $2096$  and  $2204\text{ cm}^{-1}$ , indicating that only one  $\text{C}\equiv\text{N}$  was  $\pi$ -coordinated to the copper surface.

Gao and Weaver (34) attempted to probe the nature of adsorbate-surface bonding for simple aromatic molecules by studying the SERS of benzene and eight mono-substituted benzenes at gold electrode surfaces. They discovered that benzene itself adsorbed flat via the ring

$\pi$ -electron system. Mono-alkyl, benzoate and aldehyde substituted benzenes showed decreases in ring mode energies along with band broadening, suggesting some type of attachment via the benzene ring. For halogen-substituted benzene molecules, characteristic low-frequency halogen-surface vibrations were clearly visible, indicating the substituents had a role in the adsorption to the surface.

Other examples include Holze's (35) study of the adsorption of aniline on gold electrodes, where the observation of a gold-nitrogen vibrational mode indicated perpendicular edge-on adsorption.

The experiments of Bukowska *et al.* (36) on the adsorption of pyrrole (figure 2.3) on a roughened polycrystalline silver electrode confirmed the parallel orientation of the molecule on the surface and revealed other phenomena such as the competitive adsorption of chloride anions (from the supporting electrolyte).



Figure 2.3: Structure of pyrrole.

Sato *et al.* (37) also observed competitive adsorption with pyridine and 2- and 4-methyl pyridine on silver electrodes. Their results, combined with those of Lombardi *et al.* (38) and Furtak and Macomber (39)

highlighted the contribution of two effects, electronic and steric, to the competitive adsorption process. It was found that the steric factor rendered the adsorption of 2-methyl pyridine unfavourable. This was confirmed by Ikezawa *et al.* (16). The electronic effect of each methyl group was also found to be extremely important. Both factors have important implications with respect to the chemical (charge-transfer) mechanism of SERS enhancement.

#### (d) Potential and pH dependence.

The effect of applied potential on SERS, which has been amply displayed with the pyridine/halide/silver electrode system, has been proven to be as important a factor in other systems along with the effect of pH environment (40).

Lippert and Brandt (41) observed potential dependence with a macromolecular system; an area where, previously, SERS had not been widely applied (42). Their studies of poly(2-vinyl pyridine) showed that the species on the surface was predominantly the pyridinium ion when the electrode potential was positive and predominantly neutral pyridine around zero electrode charge. Orientation changes involving the polymer chain were observed in the fingerprint region of the SER spectra. It was found that the presence of the macromolecule improved the stability of the SERS active sites.

The potential and pH-dependent adsorption of aniline on silver electrodes was investigated by Holze (43). He found that, in neutral solution, aniline adsorbed *via* nitrogen co-ordination in a perpendicular orientation at positive relative potentials. In acidic solution, the predominant species was the anilinium cation which adsorbed flat through the interaction of the aromatic  $\pi$ -electron system.

The effect of pH and applied potential in conjunction with the influence of the supporting electrolyte anion was demonstrated by Kellogg and Pemberton (44) in their studies on the adsorption of cyanide on silver electrodes. Whereas the potential at which SERS intensity maximised was only slightly dependent on the nature of the supporting electrolyte anion in basic media, in acidic media the nature of the anion was critical. They found that, in acidic solution, end-bonded and side-bonded HCN were both present and that different anions had differing abilities to influence the association of HCN with the surface. In basic media, end-bonded cyanide ( $\text{CN}^-$ ) predominated.

This last example demonstrates the complexity of SERS electrochemical systems and how various solution effects (pH, potential and nature of supporting anion) influence SERS-activity.

#### (e) Electrodeposition of other metals.

The development of this area arose from the desire to extend the

applicability of SERS to metal surfaces other than silver, gold and copper. Experimentally, it involves coating SERS-active electrode surfaces with thin transition metal overlayers (liberated from their salts) in order that the chemical properties of the modified surface reflect mainly those of the overlaid film whilst maintaining SERS-activity due to the proximity of the underlying substrate.

In essence, it is a means of extending SERS to metals that, in themselves, do not exhibit appreciable Raman scattering enhancement.

Leung and Weaver (45) reported SERS enhancement from underpotential deposited monolayers of mercury, thallium and lead on roughened gold electrodes with adsorbed halides, thiocyanate and pyridine. Although the observed intensities were comparable to those obtained on an unmodified gold electrode, SERS intensity with pyridine was found to decrease slightly upon overlayer formation.

The same workers (46) also studied the SERS of carbon monoxide adsorbed on roughened gold electrodes modified by electrodeposition of thin films of platinum and palladium. Terminal and bridging carbon monoxide were found to be present, adsorbed to the transition metal overlayers rather than residual gold.

Fleischmann and Tian (47) reported the startling fact that the underpotential deposition of nickel and cobalt films induced SERS on a smooth silver electrode with pyridine as adsorbate.

Transition metal overlayers have also been used to study the morphology of electrode surfaces and the role the morphology plays in SERS enhancement.

Guy and Pemberton (48) analysed the quenching of the SERS of 3,6-dihydroxypyridazine (figure 2.4) adsorbed on lead-modified silver electrodes. Their observations of the loss of atomic scale roughness features during electroplating could not fully account for the extent of SERS quenching.

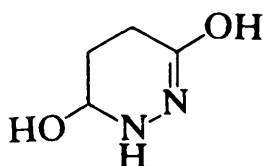


Figure 2.4: Structure of 3,6-dihydroxypyridazine.

The experiments of Fleischmann *et al.* (49) and Kellogg and Pemberton (50) on the adsorption of cyanide at modified silver electrodes showed the occurrence of preferential displacement of HCN from active sites by underpotential deposited lead and confirmed previous findings that both large and atomic scale roughness features contribute significantly to SERS in electrochemical systems.

Studies such as those previously described, along with

spectroelectrochemical experiments (51), have shown that the underpotential deposition of foreign metals gives rise to systematic variations in the electronic structure of the underlying metal and, therefore, in the optical properties of the electrode surface. This has been extremely useful for studying the properties of electrode surfaces since pure metals offer only a discrete set of surface electronic properties for study.

#### (f) Role of surface carbon.

Some researchers (52) (53) have argued that SERS enhancement for pyridine on silver electrode surfaces arises primarily from adsorption of the molecules on or in carbon overlayers on the metal surface. A more detailed study by Cooney *et al.* (54) suggests that the presence of ultra-high surface area carbon overlayers is essential to the observation of SERS from benzene, carbon dioxide and a range of alkenes.

Relatively few workers, however, have argued a convincing case for the participation of surface carbon in SERS at electrode surfaces. The majority view is still that atomic and large-scale metal roughness features are the important factors governing adsorption.

#### 2.2.2 Vapour-deposited surfaces.

The early results with electrochemical SERS-active systems shed a great deal of light on some of the mysteries of SERS but also threw up

many unresolved questions with respect to the theoretical aspects. In the early 1980s, many workers realised that in order to gain further understanding of SERS theory it was necessary to utilise systems wherein the morphology could be controlled more stringently. As the early theoretical studies used simple models of surface roughness, it seemed advantageous to duplicate these computational approximations experimentally. This reasoning, in part, led to the interest in the area of vapour-deposited SERS-active surfaces.

#### 2.2.2.1 Categories of vapour-deposited surfaces.

Variation of the experimental conditions of metal evaporation can produce rough surfaces with a range of morphologies.

##### (a) Island films.

This technique leads to the production of small metal particles of around 5 to 20 nm in diameter on polished glass, quartz or copper substrates. The metal surface is prepared by vapour-deposition of a small quantity of metal (5 to 15 nm mass-thickness) in ultra-high vacuum (approximately  $10^{-6}$  Torr) onto the substrate, which is held at elevated temperature. The heat of the substrate increases metal atom mobility causing the evaporated metal nuclei to grow into approximately spherical "islands".

(b) Cold-deposited films.

The ultra-high vacuum deposition of a small amount of metal onto a cold (between 30 and 120 K), polished substrate gives a rough film. Islands do not form due to the lack of mobility of the metal atoms. Monte Carlo techniques (55) have shown that the roughness of these films consists of closely packed, sharp surface features separated by equally sharp pores. The surface resonances (discussed in section 2.3.3) are delocalised over many peaks and troughs.

(c) Assemblies of metal spheroids.

The first step in the production of spheroid assemblies is the preparation, by lithographic methods, of a two-dimensional array of conical silica posts (56). Vacuum evaporation of silver at a glancing angle gives isolated silver particles of ellipsoidal shape on top of each silica post.

(d) Coated microspheres.

This method involves the vapour deposition of an even film of metal on plastic spheres (commonly teflon or polystyrene) fixed on support material (57). The substrate is not held at extreme temperatures as an even film is required. Uniform coverage of plastic spheres is essential. This is achieved through the use of spin-coating devices. One clear advantage of this type of surface is that the required surface roughness dimensions can be designed simply by selecting commercially available

plastic spheres of appropriate diameter and uniform size distribution.

Moody *et al.* (58) have shown, however, that the experimental parameters for the production of coated microspheres must be chosen carefully in order to maximise SERS enhancement.

This category of SERS-active surface has been used extensively in the field of chemical sensing (discussed in Section 2.4.3).

#### 2.2.2.2 Studies with vapour-deposited surfaces.

Yamada *et al.* (32) (59) examined the adsorption of pyridine on homogeneous silver island films, consisting of equal-sized silver spheres of approximately 20 nm diameter. Strong SER spectra were observed indicating nitrogen-bonded pyridine molecules and thus mirroring results with silver electrodes.

Albano *et al.* (60) studied the loss of signal intensity due to pyridine decomposition on annealed cold-deposited copper films. They found that the rate of decomposition of pyridine, which was monitored by detecting hydrogen desorption, increased as the annealing temperature increased. These results were interpreted in relation to the reaction of pyridine molecules inside pores on the cold-deposited surface. Other results (61) (62) have shown that, in these systems, pyridine molecules inside the cavities on the surface are the major source of Raman signals.

Other studies of pyridine adsorption include those of Erturk *et al.*

(63) who observed induced chemical and vibrational specificity of SERS by the postdeposition of silver in ultra-high vacuum at 40 K onto smooth silver already covered by a monolayer of adsorbate. They postulated a role for the postdeposited silver specific to chemical enhancement.

Otto's (64) experiments on the adsorption of pyridine, benzene, cyclohexane and pyrazine on cold-deposited silver films revealed some interesting experimental and theoretical aspects including the selective enhancement of one vibrational mode of pyridine caused by the presence of atomic scale roughness features.

Island films have also shown interesting effects. Venkatachalan *et al.* (65) observed laser induced conversion of adsorbed p-amino benzoic acid to p,p'-azo dibenzoate (figure 2.5). Their findings suggested a two-step conversion: hydrolysis of amine followed by dimerisation during exposure to the laser beam.

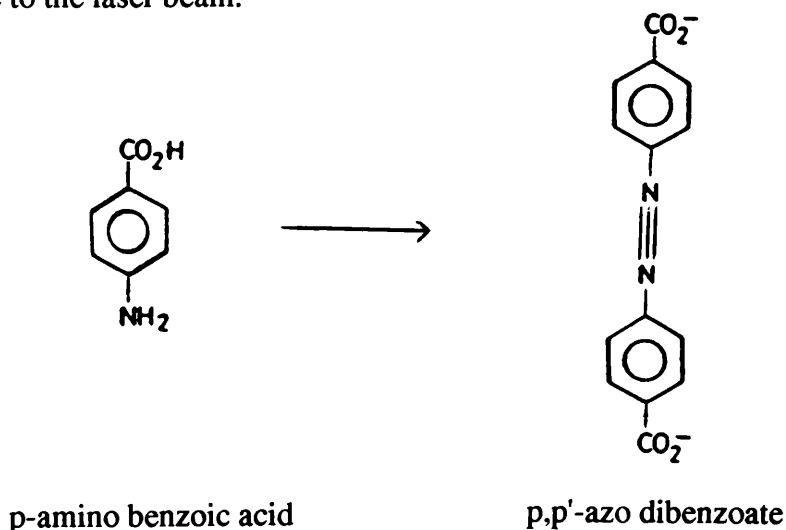


**Figure 2.5: Dimerisation of p-amino benzoic acid on a silver island film.**

### 2.2.2.3 Adsorption of gases.

The high vacuum conditions used in the preparation of these SERS-active systems has led to the extensive study of adsorbed gases (66). In particular, much attention has been focussed on the behaviour of olefins adsorbed on silver surfaces: this has given some clues to elucidate various heterogeneously catalysed reactions of industrial importance (67).

Studies of the adsorption of 1-butene and 1,3-butadiene on cold-deposited silver films by Itoh *et al.* (68) yielded interesting results on the orientation of the respective adsorbates. It was shown that 1-butene was weakly  $\pi$ -bonded and fixed in the *cis* conformation. They discovered three distinct types of adsorption state with 1,3-butadiene involving the adsorption of either one double bond or both.

The study of adsorbed gases has not been confined exclusively to olefins. Carbon monoxide adsorption has also yielded interesting vibrational information. Wood *et al.* (69) observed spectra from carbon monoxide adsorbed on silver and gold cold-deposited films strong enough to allow adsorbate detection at less than 1% of monolayer coverage. The spectra displayed internal CO stretch and CO-Ag stretch. The internal CO stretching frequency was found to be dependent on extent of coverage.

#### 2.2.2.4 Theoretical aspects.

As stated previously, the major use of vapour-deposited SERS-active systems has been in modelling simple rough surfaces experimentally in order to glean more knowledge of SERS theory. Some of the evidence obtained from these systems is presented at this point and discussed further in section 2.3.

##### (a) Electromagnetic mechanisms.

The results of Wood *et al.* (70) indicated that the nature of the surface was all important in determining SERS enhancement, thus suggesting a theoretical model based on the electromagnetic field density present near the metal surface. Evaporated surfaces exhibited larger, though shorter ranged, enhancements compared to roughened single-crystal silver surfaces.

Wang and Lee (71) probed further the nature of this "electromagnetic density" effect and, through the adsorption of crystal violet on silver island films, found that there was a linear correlation between surface plasmon resonance and SERS enhancement. Surface plasmon resonance is discussed more fully in section 2.3.3.2.

Osawa *et al.* (72) also found a linear correlation between electric field strength within the metal surface and SERS intensity from studies of p-nitrobenzoic acid adsorption on evaporated silver surfaces.

In Otto's (64) extensive study of cold-deposited silver films, discussed previously, he tested the electromagnetic model by measuring excitation profiles of various bands. It was found that the profiles did not exhibit any special chemical specificity but corresponded to the optical absorption of the silver surface, thus indicating purely electromagnetic surface-bound enhancement. These findings were mirrored by those of Pockrand (73).

All of these representative examples indicated a purely electromagnetic SERS mechanism. Other workers, however, proposed the existence of a second mechanism, closely related to the chemical nature of the adsorbate species.

#### (b) Chemical mechanisms.

The observations of Erturk *et al.* (74) of the quenching of the SERS-activity of ethylene and ethane on cold-deposited silver and copper films could not be explained by an electromagnetic enhancement mechanism. Other evidence (75) pointed to the existence of a resonance Raman effect operating via charge-transfer transitions involving the adsorbate species and the metal surface.

From comparative studies of pyridine exposed to silver, copper and gold films in ultra-high vacuum, Pockrand (76) concluded that SERS enhancement results from a combination of the electromagnetic (surface

plasmon) mechanism and an adatom-adsorbate induced resonance process. It was further postulated that only surface-bound molecules contribute to the chemical effect. The silver/copper/gold comparative results, however, also confirmed the crucial factor of surface optical properties: strong signals resulted from copper and gold surfaces only when exposed to red laser light.

Giergel *et al.* (11) also proposed a combination of both theoretical models and attempted to estimate the relative Raman scattering cross-sections for chemisorbed and physisorbed pyridine molecules on silver films in high vacuum. They proposed that greater enhancement results from chemisorbed molecules.

#### 2.2.2.5 Metal Overlayers.

As with electrochemical systems, the post-deposition of foreign metals in ultra-high vacuum has provided important clues to the nature of the SERS effect.

The results of Gao and López-Ríos (77), from the post-deposition of palladium on silver island films, along with other data (78), have clearly demonstrated the effect on SERS of changes in the electronic structure of the metal surface induced by the deposition of foreign metals. This work has further highlighted the important role played in SERS by the optical properties of the metal substrate and has led to the postulation

that the electromagnetic mechanism is the major effect giving rise to SERS enhancement.

### 2.2.3 Metal colloids (sols).

Although randomly rough electrode surfaces were found to be ideal for the study of the adsorption chemistry involved in SERS processes, they were not ideally suited for investigating the physical phenomena associated with SERS. The measurement of various optical properties, such as absorption spectra, was found to be extremely problematic. Since the determination of such properties was vital to the improvement in understanding of SERS, attention began to be focussed on more regular, finely divided metal surfaces such as colloids.

#### 2.2.3.1 Preparation of colloids.

##### (a) Gold colloids.

Gold colloids are generally prepared by the reduction of the tetrachloroaurate (III) ion,  $[\text{AuCl}_4]^-$ . The most frequently used reducing agent has been sodium citrate (79).

The typical experimental procedure involves the heating of a solution of tetrachloroaurate (III) followed by the addition, with stirring, of sodium citrate solution. After approximately thirty minutes, a deep red colloid results. The average diameter of gold particles produced in this manner is approximately 20 nm and of uniform size

distribution. Frens (80), however, has shown that, through the careful monitoring of the preparation procedure and the quantities involved, gold particles of controlled, uniform size can be produced within the range 12 to 150 nm.

An unaggregated gold colloid with particle diameters around 20 nm shows an absorption maximum at 520 nm, corresponding to the excitation of surface plasmons.

#### (b) Silver colloids.

The production of silver colloids of uniform particle shape and size has proved more testing.

The general method, of Creighton *et al.* (79), involves the reduction of silver nitrate,  $\text{AgNO}_3$ , by sodium tetrahydroborate,  $\text{NaBH}_4$ . Small volumes of each reactant are stirred constantly at  $0^\circ\text{C}$  for several minutes to produce the yellow colloid (absorption maximum at 385 nm). Electron microscopy studies (81) have shown that silver colloids are generally of irregular particle shape. Excessive aggregation was found to be a major problem associated with SERS experiments.

#### 2.2.3.2 The nature of colloids.

A colloidal suspension is preserved due to the negative charges on the metal particles resulting from adsorbed anions. The consequent electrostatic repulsion between the particles preserves the overall

dispersion and prevents aggregation. Addition of a neutral adsorbate species such as pyridine, as in SERS experiments, results in displacement of the adsorbed ions and a reduction in the charge of the metal particles. Collisions occur, leading to aggregation due to the presence of short-range attractive forces between the particles. At high concentrations of adsorbate species, the process of aggregation can be extremely rapid and result in precipitation of the metal. When the concentration of adsorbate is low, however, small dispersed aggregates form. The process of partial aggregation can be monitored by following the change in absorption maximum.

Partial aggregation seems, in many cases, to be a necessary factor in obtaining appreciable SER spectra. In colloid SERS experiments, control and monitoring of adsorbate concentration is essential in order to induce partial aggregation, but to prevent complete precipitation of metal.

### 2.2.3.3 Colloidal particle size.

A theoretical understanding of the fundamental processes associated with the SERS effect in colloidal metal systems required knowledge of colloidal particle size. Common methods of ascertaining particle sizes have included light absorption measurements and transmission electron microscopy (TEM) studies (82) of particle residues

after solvent evaporation.

Notholt and Gottmann (83), however, developed a method using photon correlation spectroscopy which gave particle size data to within 10% accuracy.

#### 2.2.3.4 Aggregation studies.

Siiman and Feilchenfeld (84) (85) have studied, in great detail, the process of silver colloidal aggregation. They induced aggregation with oxoanions such as chromate and tungstate. The kinetics of aggregation, as measured by SERS and TEM, were interpreted in terms of a fractal rate law and fractal structure of colloidal particle aggregates (figure 2.6).



Figure 2.6: Transmission Electron Micrographs of silver colloidal aggregates.

The study of colloidal aggregation has also had important consequences in regard to SERS electromagnetic theory. In particular,

the coupling of electromagnetic resonances as in colloidal suspensions is highly dependent on the process of particle association.

The studies of Weitz *et al.* (86) on gold colloidal aggregation also revealed fractal structures and led to new insights into the nature of gold colloids. The existence of heterogeneous colloidal gold surfaces with donor and acceptor sites Au(0) and Au(I), respectively, was proposed.

#### 2.2.3.5 The orientation of adsorbates at colloid surfaces.

Although electrode surfaces and colloidal suspensions have considerably different surface morphologies, their respective SERS results have broadly agreed with respect to the orientation of adsorbate species.

Muniz-Miranda *et al.* (87) demonstrated the equivalence of experiments carried out with colloids and electrodes using the three diazines pyrazine, pyrimidine (figure 2.7) and pyridazine adsorbed on silver sols. Only pyrazine failed to exhibit nitrogen-co-ordinative chemisorption in its SER spectrum on silver colloid. They proposed that this was due to co-adsorbed reduction products on the silver surface.

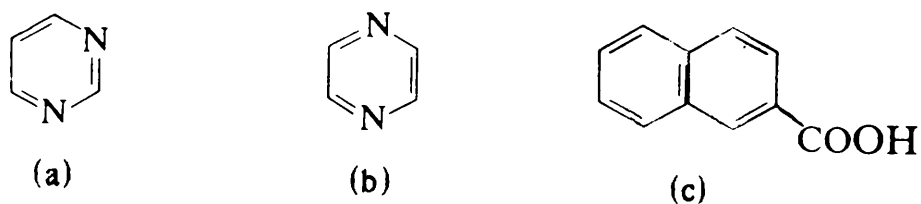


Figure 2.7: Structure of (a) pyrimidine, (b) pyrazine and (c) 2-naphthoic acid.

(a) Organic adsorbates.

Moskovits and Suh (88) studied the surface geometry of pyridine, quinoline and 2-naphthoic acid (figure 2.7) adsorbed on silver colloids. They found that whereas quinoline and pyridine were chemisorbed perpendicular to the surface via their respective nitrogen lone pairs, 2-naphthoic acid adsorbed in two very different fashions, perpendicular and flat, depending upon the concentration of the adsorbate species. These conclusions were evidenced by observing C-H stretching and bending modes in the SER spectra and applying a simple selection rule (89) (90) which states that vibrations deriving their intensities from a large value of  $\alpha_{zz}$  (where  $\alpha_{zz}$  = z-polarisability, z being the local surface normal direction) have the most intense SERS. The two possible orientations for 2-naphthoic acid are shown in figure 2.8.

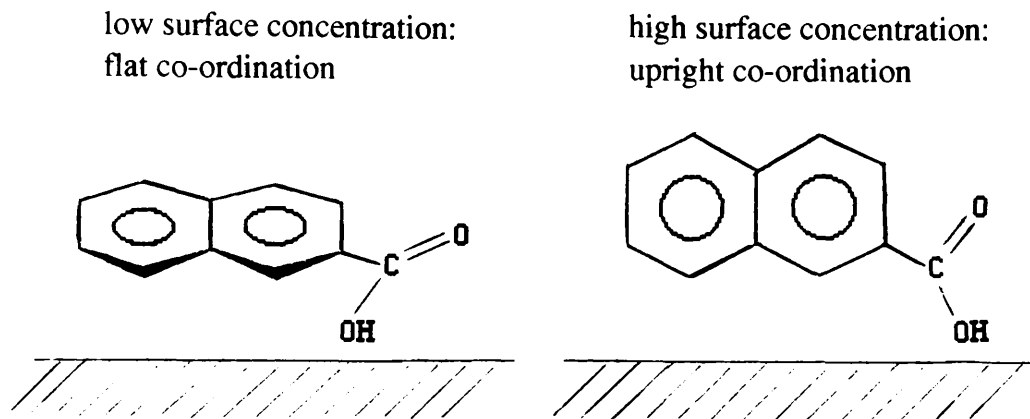


Figure 2.8: Orientations of 2-naphthoic acid on a silver colloid.

This selection rule, which has proved extremely useful in determining the orientation of organic molecules at colloidal surfaces, arose from SERS studies of molecular ions. Moskovits and Suh (90) observed SERS of the dianions of carboxylic acids such as phthalic, maleic and fumaric acids, using Raman depolarisation ratios to determine the orientation of adsorbate molecules.

Kim and Itoh (91) observed surface geometry changes of 2,2'-bipyridine adsorbed on a silver colloid. The behaviour of this system in the pH range 8.5 to 2.8 was compared with an electrochemical study by the same workers (92) involving 2,2'-bipyridine, chloride ions and silver electrodes. In the latter study, four different types of surface species were formed with variation in applied potential. In the silver colloid study, two types of surface species predominated at pH 8.5

and 2.8 respectively: one involving co-planar *cis* chemisorption and the other involving strong Lewis acid/base co-ordination through one bipyridyl nitrogen. Both of these categories of surface species were found to exist in the electrochemical system.

These studies confirmed the equivalence of colloidal and electrochemical SERS systems. Indeed, further investigation by the same group revealed that the second, Lewis acid/base colloidal surface complex involved co-adsorbed chloride ions (from HCl, used to induce pH changes).

Hildebrandt and Stockburger (93) used chloride and other anions to "activate" silver colloids. Other workers (94) noted that this activation procedure induced adsorption sites highly specific to certain adsorbates.

Studies with organic acids have also proved fruitful. Pagganone *et al.* (95) studied the molecular structure and orientation of benzoic acid adsorbed on silver colloids. Their findings, realised through a complete assignment of the SER spectrum of benzoic acid, indicated the chemisorption of the molecule as the benzoate ion in a bidentate fashion.

Wan *et al.* (96) studied the SERS of substituted benzoic acids. While it was noted that, at room temperature, each of the substituted benzoic acids displayed distinct spectra, at high temperature their SER

spectra were all very similar. These findings were ascribed to room temperature bidentate carboxylate co-ordination and high temperature monodentate bonding. They postulated that a monodentate bonding scheme would, according to Moskovits' (89) selection rule, result in carboxylate bands swamping the SER spectra and therefore lead to them all appearing similar.

Similar bonding modes were observed by Kai *et al.* (97) in the SER spectra of carbonate, hydrocarbonate and substituted acetic acids on silver sols. Their observation of highly enhanced spectra for carbonate indicated end-on adsorption through oxygen. Once again, the selection rule of Moscovits (89) ruled out flat orientation. The substituted acetic acids were found to be, initially, in a single bonding state through the carboxyl group. Changes in their SER spectra over a period of time, however, showed that a bidentate bridging adsorbed state was eventually reached.

#### (b) Inorganic adsorbates.

In the early years of SERS, studies with inorganic species were relatively few. Since the advent of colloids as SERS-active substrates, however, inorganic adsorbates have been increasingly used.

One particular area of interest has been that of oxo-complexes. Feilchenfeld and Siiman (85) observed SERS from  $[\text{MO}_4]^{2-}$  ions, where

M= Cr, Mo, W, on silver sols. Recently, Greaves and Griffith (98) reported appreciable SER spectra from vanadate,  $[\text{HVO}_4]^{2-}$ , and also phosphate and arsenate between pH 3 and 12 on silver colloids. Their results indicated that the oxo-molecules were chemisorbed to the silver surface in the manner shown in figure 2.9.

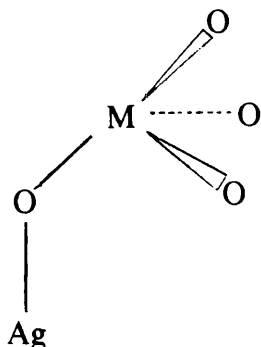


Figure 2.9: Bonding mode of the  $[\text{MO}_4]^{2-}$  ion on a silver colloid.

More complex inorganic molecules have been studied in recent years.

Dines and Peacock (99) observed the Surface-Enhanced Resonance Raman Spectroscopy (SERRS) of a series of iron (II) and ruthenium (II) complexes of 2,2'-bipyridine. They noted very intense spectra (figure 2.10) that displayed no evidence of chemical bond formation between the adsorbates and the silver colloid surface. This was evidenced by the lack of wavenumber shifts between the resonance Raman (RR) spectra and corresponding SERR spectra. SERRS is discussed in section 2.2.3.6.

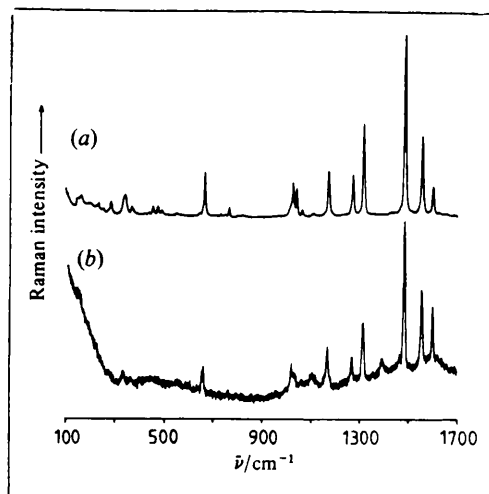
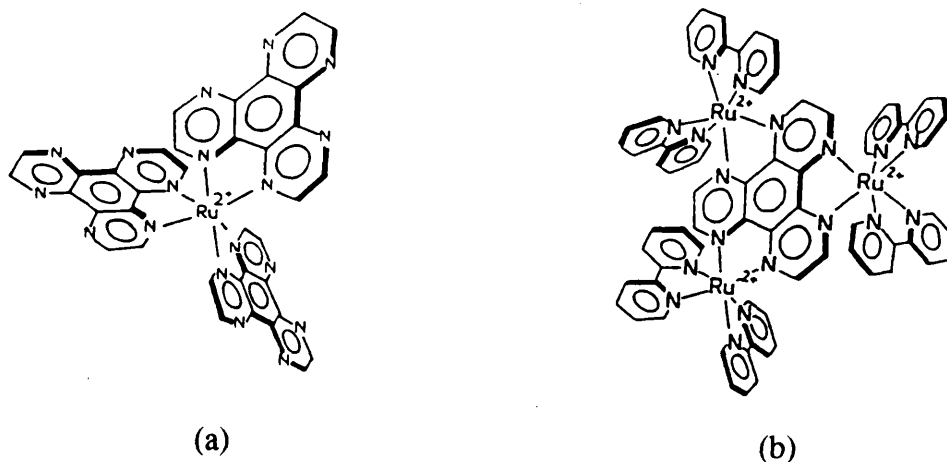


Figure 2.10: SERR spectra of  $[\text{Ru}(\text{bipy})_3]^{2+}$  under  $\text{Ar}^+$  excitation (488.0 nm). (a)  $4.2 \times 10^{-7}$  moles  $\text{l}^{-1}$ ; (b)  $2.9 \times 10^{-12}$  mol  $\text{l}^{-1}$ .

Vanhecke *et al.* (100) observed essentially identical RR and SERR spectra with ruthenium (II) tris-bipyridyl, but postulated that the nitrogen atoms of the ligand were co-ordinated to the ruthenium and silver in a similar mode. This is highly unlikely as such a bonding scheme, apart from being chemically unfavourable, would lead to wavenumber shifts in the SERR spectra. They extended their study to the ruthenium (II) tris-complex of 1,4,5,8,9,12-hexaazatriphenylene (HAT) (figure 2.11) and heteroleptic ruthenium (II) complexes of 2,2'-bipyridine and HAT in order to investigate the question of which ligand predominated in the adsorption mechanism. The use of the ligand HAT also permitted the study of novel polymetallic complexes (101) (figure 2.11). The results of these experiments demonstrated the

influence of the charge-transfer (chemical) mechanism in SERS.



**Figure 2.11: Structure of (a) Tris(1,4,5,8,9,12-hexaazatriphenylene) ruthenium(II) and (b) a triruthenium(II) hexa(2,2'-bipyridine) HAT complex.**

#### 2.2.3.6 Biologically active molecules: SERRS.

SERS-active colloid systems have recently been used to great effect in the analysis and vibrational study of biologically active molecules. This has led to the increasing use of Surface-Enhanced Resonance Raman Spectroscopy (SERRS). The SER effect combines with resonance Raman to give SERRS. SERRS is, in essence, identical to SERS but with the additional factor of the laser excitation being near an allowed absorption maximum of the adsorbate species under investigation. Chromophoric molecules such as haemoglobin (102) have been of

particular interest. The use of the technique has allowed the investigation of the nature of bonding of complex molecules and the detection of changes in conformation or molecular structure at the surface.

Unlike SERS, SERRS has shown wide and even conflicting variations in enhancement factors (103) (104) with adsorbate and with environment, leading to equally wide variations in theoretical models.

Colloid SERS systems have been applied to the trace analysis of drugs and other biological molecules. The possibility of applying colloid systems to the detection of complex molecular structures without their destruction has been clearly demonstrated. This aspect is further discussed in section 2.4.3.

### 2.3.7 Theoretical aspects.

As with island films, unaggregated colloids have provided valuable simple model systems for the study of SERS theory. The additional possibility of choosing particle sizes by careful control of practical procedures has also proved invaluable.

A great many of the theoretical studies with colloids have been concerned with gauging the relative contribution of the electromagnetic effect to overall SERS enhancement (79)(105)(106).

### 2.2.3.8 Related SERS-active substrates.

#### (a) Supported colloids.

Laserna *et al.* (107) reported the simple, one-stage preparation of silver coated filter paper. The preparation was based on the method of Creighton *et al.* (79), being the reduction of filter paper-supported silver nitrate with sodium tetrahydroborate applied evenly over the filter paper by means of a spraying device. SEM study revealed the presence of porous silver cluster formations with individual particle size around 100nm (figure 2.12).

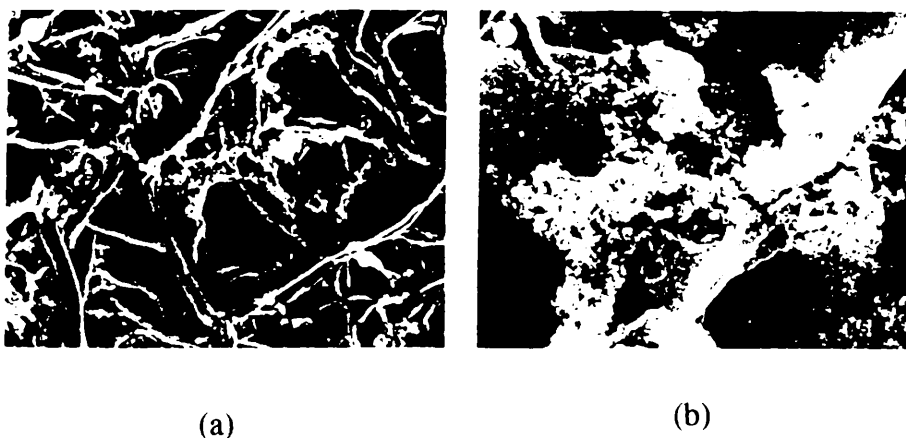


Figure 2.12: Scanning electron micrographs of silver-coated filter paper.  
(a) magnification x 220; bar length 100  $\mu\text{m}$ ;  
(b) magnification x 2200; bar length 10  $\mu\text{m}$ .

Simple organic test molecules (107-109) adsorbed on this type of surface have displayed intense, reproducible spectra. Although filter paper-supported silver colloids have no inherent aggregation problems, they have the disadvantage of low stability.

Séquaris and Koglin (110) supported silver colloid on TLC silica gel plates, obtaining highly intense SER spectra from 9-methyl guanine (figure 2.13).

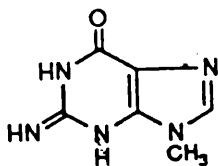


Figure 2.13: Structure of 9-methyl guanine.

#### (b) Mobile metal films.

Reports of the production of metal liquid-like films via the reduction of silver nitrate have recently appeared (111). Gordon *et al.* (112) developed a method of production of mobile silver films at the interface between an aqueous sol and the solution of a transition metal complex in an organic solvent. With several inorganic complexes, significant enhancement was observed similar to their SERR spectra with silver colloids.

An important practical consequence of these studies was that they represented a means of obtaining appreciable SERR spectra of water-

insoluble or sparingly soluble complexes normally unsuitable for SERR study with aqueous silver colloids.

### (c) Chemically prepared films.

A method for the production of this convenient and inexpensive type of substrate was reported by Ni and Cotton (113). Essentially a simple procedure, it involves the production of Tollen's reagent (ammonical silver nitrate) and its subsequent reduction to give a suspension of silver. The silver particles then form an active film on frosted microscope slides. The surface displayed appreciable SERS-activity with adsorbates such as 4,4'-bipyridine but it was noted that the resultant magnitude of enhancement was highly dependent on the preparative conditions.

## 2.2.4 Other SERS-active substrates.

### 2.2.4.1 Silver powder.

There have been a number of studies of the SERS of aggregated, precipitated silver powders (114) (115).

SERS with silver powder was used recently by Matsuta and Hirokawa (116) in an attempt to study the adsorption of the atmospheric pollutant gas sulphur dioxide at real environmental conditions (not under high vacuum: at one atmosphere). As would be expected, they found that oxygen and water vapour had significant

roles in the adsorption of the gas.

Dorain and Boggio (117) investigated the possibility of using the silver powder technique to study surface chemical reactions using nitrogen dioxide gas as a model adsorbate. Their results identified the major nitrate species present on silver microstructures during the surface reaction. This highlighted the potential of the technique for the study of *in situ* heterogeneous catalysis of gases on silver metal surfaces. The same workers also demonstrated the replacement reaction of adsorbed nitrate on silver powder surfaces with sulphur dioxide.

#### 2.2.4.2 Rough silver surfaces.

The production of rough silver was achieved by pre-depositing calcium fluoride (118) on a substrate followed by the deposition of an even silver film: the roughness of the resultant silver surface corresponded to the roughness of the pre-deposited calcium fluoride film.

Mechanical polishing (25) and ion-bombardment in high vacuum (119) also produce suitably rough surfaces.

Rowe *et al.* (120) reported the novel preparation of SERS-active substrates when silver halide films were exposed to ultra-violet radiation *in vacuo*, releasing halogen vapour and leaving a randomly

rough silver surface.

## **2.3. THEORY OF SERS.**

### **2.3.1 Background.**

The question of the nature of the enhancement mechanism of SERS has been the subject of a great body of work (121-124), both experimental and theoretical, over the last twelve years. This interest has been fuelled, primarily, in order to apply the technique in specific chemical areas. Many workers, however, have studied the enhancement mechanism from a purely theoretical viewpoint.

There has been and, indeed, still is a great deal of controversy over the enhancement mechanism although it is now widely accepted that two main mechanisms contribute, either independently or in tandem, to SERS enhancement. These mechanisms are electromagnetic and chemical (charge-transfer). The controversy chiefly lies in the relative contributions of the two main mechanisms to the overall enhancement factor.

### **2.3.2 Factors influencing SERS.**

Clues to the nature of the enhancement mechanism, some of which have been indicated previously, can be drawn from observations of some of the main factors that influence SERS. A summary of the most significant factors is now given.

(a) Dielectric properties of the surface metal.

The excitation wavelength used in SERS experiments has been shown to be critical. Studies with transition metal overlayers on silver electrode surfaces, as discussed previously, have confirmed that the electronic properties of the metal surface are of paramount importance in determining the extent of SERS enhancement.

(b) Morphology and dimensions of roughness species on the surface.

Flat surfaces do not produce appreciable SERS enhancement: some degree of roughness, whether random or uniform-sized spheres, seems to be necessary in order to observe SERS-activity at a metal surface. As the electrochemical studies showed, however, there is debate over the roles of large and atomic-scale roughness in producing enhanced spectra.

(c) Molecule-surface separation.

As will be discussed, a consequence of the electromagnetic effect is that SERS intensity falls off with distance from the surface. The chemical mechanism is a shorter-range effect.

(d) Orientation of the molecule with respect to the surface.

(e) Chemical nature of the adsorbed molecule.

This factor explains the molecular selectivity of SERS.

## Discussion.

Factor (a) is a purely electromagnetic effect, depending solely on the nature of the metal surface, whereas factor (e) is only dependent on the structure of the adsorbate molecule and is therefore a purely chemical effect.

For a given metal/molecule system, however, factors (b), (c) and (d) are considerably more difficult to justify. Macroscopically, the SERS effect is polydirectional: there is little dependence of the enhancement upon geometrical factors. Some degree of microdirectionality seems to be necessary, however, to explain why certain vibrational modes are enhanced preferentially to others in certain systems. Microscopic positioning of the molecule relative to the surface justifies a certain degree of bonding in the surface-molecule complex and, consequently, the dependence of the enhancement on both the distance and orientation factors.

## Theories of enhancement.

### 2.3.3 Electromagnetic theory.

#### 2.3.3.1 The image field model.

Although it is now known that surface roughness is a vital factor with respect to SERS, many early theoretical workers studied possible enhancement mechanisms arising from the electromagnetic interactions

between adsorbate molecules and a flat metal surface.

The basic tenets of the image field model, as proposed by King *et al.* (125) and Efrima and Metiu (126), are that SERS enhancement derives from the large polarisability when the Raman emitting system is taken to be composed of the adsorbate molecule and its conjugate-charge image in the metal.

King *et al.* (125) assumed a diagonal Raman polarisability tensor and a field polarised in the direction normal to the flat surface (z-axis). The dipole moment induced in the adsorbate molecule by the image field in addition to the incident field is given by equation 2.1.

$$\underline{\mu} = \alpha(\underline{E} + \underline{E}_{im}) \quad , \quad (2.1)$$

where  $\underline{E}$  = incident electric field,

$\underline{E}_{im}$  = image electric field,

$\alpha$  = zz component of the molecular polarisability and

$\underline{\mu}$  = field-induced dipole moment.

The image field is given by equation 2.2.

$$\underline{E}_{im} = \frac{[(\epsilon - \epsilon_0)/(\epsilon + \epsilon_0)]\underline{\mu}}{4r^3} \quad (2.2)$$

where  $r$  = distance between the point dipole and the surface,

$\epsilon$  = dielectric function of the metal surface

and  $\epsilon_0$  = dielectric function of the ambient.

King *et al.* found  $r$  very difficult to define, for real molecules and surfaces.

Substituting equation 2.2 into equation 2.1 and subsequent rearrangement gives the following expression.

$$\underline{\mu} = \underline{\alpha} [1 - (\underline{\alpha}/4r^3)(\epsilon - \epsilon_0/\epsilon + \epsilon_0)]^{-1} \underline{E} \quad (2.3)$$

In this form, equation 2.3 resembles the normal Raman expression for field-induced dipole moment,  $\underline{\mu} = \underline{\alpha} \underline{E}$  (1.2), with the normal polarisability,  $\underline{\alpha}$ , replaced by an effective polarisability,  $\underline{\alpha}_{\text{eff}}$ , given by equation 2.4.

$$\underline{\alpha}_{\text{eff}} = \frac{\underline{\alpha}}{1 - [(\underline{\alpha}/4r^3)(\epsilon - \epsilon_0/\epsilon + \epsilon_0)]} \quad (2.4)$$

Appreciable enhancement is only achieved if the quantity  $\underline{\alpha}_{\text{eff}}/\underline{\alpha}$  exceeds unity to any great extent. The magnitude of  $\underline{\alpha}_{\text{eff}}$  depends critically on  $r$ : it is only at very small values of  $r$  that the factor  $\underline{\alpha}_{\text{eff}}/\underline{\alpha}$  is significantly large.

Although some have tried to refine (127) (128) the image field model, many workers have found no evidence to support the existence of image field enhancement (129) (130). The majority view is that the image field effect makes only a minor contribution to SERS

enhancement.

### 2.3.3.2 The electromagnetic mechanism.

The surface of a good electric conductor (in the case of SERS, rough metal) has an electromagnetic resonance called the surface plasmon (131). Incident light on the metal surface can produce collective electron resonance phenomena creating oscillations in the charge density formed by the conduction electrons of the surface metal. The quanta associated with these oscillations are plasmons. For a plane wave incident from the ambient medium to excite the plasmon, both frequency and parallel momentum must be conserved. With air or vacuum as the medium, this condition cannot normally be achieved and hence a surface plasmon does not radiate but is surface-bound with its energy dissipated as heat over the metal surface. Ruling the surface with a grating, however, can allow the plasmon to radiate as, in this case, a new parallel momentum conservation rule applies.

A randomly rough surface, common to many categories of SERS-active systems, is essentially equivalent to a surface with a two-dimensional Fourier superposition of gratings. A portion of the energy of the plasmon is therefore radiated.

Small particles possess electromagnetic resonances which are similar to the surface plasmon. When a particle is small with respect to

the wavelength of incident radiation, a plasmon can be excited which has the symmetry of a time-varying dipole. The dipolar plasmon can then radiate. For a spherical metal particle, this resonance occurs at the frequency  $\omega_R$ , for which equation (2.5) holds.

$$\text{Re}[\epsilon(\omega_R)] = -2\epsilon_0 \quad (2.5)$$

The SERS effect has been observed in systems, such as small metal features and gratings, that can couple plasmon-like electromagnetic resonances to electromagnetic waves.

The assessment of Metiu and Das (132) is that surfaces absorb the incoming photon and store its electromagnetic energy into the surface plasmon, the energy being delocalised in the direction parallel to the surface but localised in the perpendicular direction. This results in a considerable increase in the density of electromagnetic energy near the metal surface. They argue that metal spheres, such as in aggregated colloids, localise photons, by plasmon excitation, in all directions resulting in a large concentration of electromagnetic energy. This energy is concentrated further by the gaps between the metal features.

In summary, the electromagnetic effect occurs due to the resonance excitation of specific modes of the metal surface arising from surface morphologies (133). It is related to the increase in electric field strength of the incident electromagnetic radiation (laser light) near the

metal surface due to the excitation and radiation of surface plasmon oscillations.

### 2.3.3.3 Models of surface roughness.

The calculations (134) (135) which elucidated the electromagnetic mechanism required certain approximations and assumptions to be made. It was assumed that SERS-active substrates were covered with submicroscopic surface roughness features which could be regarded as small metal ellipsoids with respect to their response to electromagnetic radiation. These assumptions were most accordant with unaggregated colloidal particles and island films.

### Field concentration effect.

An adsorbed metal placed near a surface consisting of metal ellipsoids will have an induced dipole moment due to the contributions of both the incident field and the field elastically scattered by the ellipsoid. When the metal features are small in relation to the wavelength of excitation, the scattered field increases greatly in magnitude compared to the incident field when the excitation frequency is in resonance with the surface plasmon frequency. The Raman-scattered field, under these conditions and for small Raman shifts, will also be in resonance with the surface plasmon of the metal feature, giving rise to highly enhanced scattered fields.

### 2.3.3.3 (a) Spherical particles (134) (136).

If a molecule is considered to be a classical electric dipole and placed at a position  $r'$  outside a spherical metal particle, upon irradiation with an electromagnetic plane wave of frequency  $\omega_0$ , the molecular dipole will radiate at the Raman frequency  $\omega$  with dipole moment given by equation 2.6.

$$\underline{\mu}(r',\omega) = \underline{\alpha}' \underline{E}(r',\omega_0) \quad , \quad (2.6)$$

where  $\underline{\alpha}' =$  Raman polarisability

$$\text{and } \underline{E}_{\underline{\mu}}(r',\omega) = \underline{E}_i(r',\omega_0) + \underline{E}_{LM}(r',\omega_0) \quad , \quad (2.7)$$

where  $\underline{E}_i =$  incident field and

$\underline{E}_{LM} =$  scattered field.

The electric field associated with the Raman radiation at a point of observation  $r$  is given by equation 2.8.

$$\underline{E}_R(r,\omega) = \underline{E}_{dip}(r,\omega) + \underline{E}_{sc}(r,\omega) \quad , \quad (2.8)$$

where  $\underline{E}_{dip} =$  field which would be present at  $r$  due to

the oscillating dipole,  $\underline{\mu}$ , had the sphere

been absent

and  $\underline{E}_{sc} =$  field scattered by the sphere that must be

calculated by solving the appropriate

boundary-value problem at the frequency  $\omega$ .

All four fields involved can be expressed as linear combinations of vector spherical harmonics. The values of the coefficients pertinent to the field  $\underline{E}_\mu$  can be obtained directly from Lorenz-Mie theory (137).

The Raman-scattered intensity, which is the square of the far-field amplitude of  $\underline{E}_R$ , is given by equation 2.9.

$$I_R = \lim_{kr \rightarrow \infty} [ \underline{E}_R (r, \omega) \{ \exp(ikr)/r \} ]^2 \quad (2.9)$$

The quantity  $\{ \exp(ikr)/r \}$  is the space-dependent part of a spherical wave.

The electromagnetic enhancement factor  $G$  can therefore be defined as  $G = I_R/I_R^0$ , where  $I_R^0$  is the Raman intensity in the absence of the metal sphere (normal Raman intensity). If the metal sphere was absent, the induced dipole moment would be given by  $(\underline{\alpha}E_i)$  and  $\underline{E}_R$  would be equivalent to  $\underline{E}_{dip}$ .

The expected enhancement for a sphere placed arbitrarily above a sphere of any size and with any polarisation of the incident and scattered fields can thus be determined.

#### Effect of particle size.

Metal particles that are close in size to the laser excitation wavelength display less enhancement. The dependence of the enhancement upon excitation frequency also depends on particle size.

Small particles display a sharp resonance caused by the excitation of dipolar surface plasmons, whereas larger particles show much broader excitation spectra due to the excitation of higher multipole plasmons.

In summary, the electromagnetic model for SERS from molecules adsorbed on spherical metal particles predicts that a high degree of enhancement will result from systems which fall into the following three categories.

- (i) The molecule is not too distant from the metal surface.
- (ii) The particle size is smaller than the wavelength of excitation.
- (iii) The frequency of excitation or scatter is near the surface plasmon resonance.

#### 2.3.3.3 (b) Spheroidal particles.

Although the physics of the electromagnetic effect are similar when a spherical particle is replaced by a non-spherical particle (138), the new geometry does give rise to some modifications. An account of these changes is now given.

- (i) The surface plasmon resonance shifts towards the red end of the spectrum.
- (ii) The SERS of adsorbates near the tip of prolate or the waist of oblate ellipsoids is enhanced, whereas that of molecules near the sides of prolate and the top of oblate ellipsoids (figure 2.14) is reduced with respect to the SERS of molecules near a regular sphere.

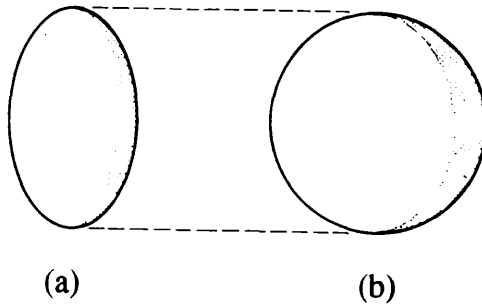


Figure 2.14: (a) prolate and (b) oblate ellipsoid.

High enhancement has been shown to derive from molecules near areas of high curvature (139).

(iii) The enhanced spectrum has two peaks, one due to the enhancement of the incident field and one due to the scattered field, separated by an energy gap corresponding to the frequency of the vibration causing the scattering.

(iv) If a metal surface is modelled in terms of an assembly of hemispherical or hemispheroidal bumps on a metal plane, the enhancement can increase greatly (122) compared with that of a free spheroid. This additional enhancement arises from the image of the metal spheroidal dipole in the underlying perfect mirror. If the rough surface consists of a large number of ellipsoids of differing size packed closely, a progressive red-shift in the plasmon resonance frequency occurs concurrently with increasing packing density.

An analogy of this process is colloidal aggregation, as similar red-shifts in the plasmon resonance maximum can occur upon particle association.

Several workers (140) have calculated expressions for the electromagnetic enhancement of molecules near spheroidal particles. The effect of other pertinent factors, such as molecular orientation, on the spheroidal model has also been estimated.

#### 2.3.3.4 Calculations and experiment.

As discussed previously, SERS-active systems whose geometry and morphology are well understood, including island films and microlithographically produced particles, have played an important role in testing the calculations on the electromagnetic model in an experimental environment. Indeed, quantitative agreement between observations and calculations has been noted in many cases.

Good agreement was found, by Liao *et al.* (56), between calculated and observed SERS enhancement of cyanide adsorbed on microlithographically produced ellipsoids.

Studies of the equivalence of calculated and observed SERS with electrode surfaces and colloidal suspensions have been few due to the more complex nature of the morphologies involved. The studies that have been undertaken, however, have shown appreciable quantitative or semi-quantitative agreement.

#### 2.3.3.5 Excitation profiles.

The measurement of excitation profiles of SERS systems provides a means of confirming that enhancement is caused by the electromagnetic mechanism. SERS excitation spectra peaks coincide with surface plasmon resonance maxima for most metal surfaces. Studies with cold-deposited films showed that, for silver, the excitation maximum (64) is in the red, with copper, gold and lithium in the far red and platinum (141) and indium (121) in the blue. These results are exactly as predicted on the basis of optical constants of the metals.

#### 2.3.3.6 Coupling between particles.

Models based on the electrostatics of isolated metal spheroids fail to account for several significant features of substrates with coupled metal particles such as cold-deposited films, electrodes and aggregated colloids. In each case, the surface plasmon absorption maximum lies to the red with respect to the corresponding maximum of isolated spheroids. This has been displayed clearly by metal colloid systems (99).

Maxwell-Garnett theory (142) has been applied to this problem in an attempt to take account of the coupling involved, with some success.

The effect of the coupling of metal particles leads to the question of the precise locations on the surface where the enhancement would be

expected to be at a maximum. As discussed previously, for spheroid models, these would be at the tips of prolate and the waists of oblate spheroids. Calculations on coupled features (143-145), however, have revealed that the voids between metal features exhibit the highest field densities and, therefore, enhancements.

#### 2.3.3.7 Criticisms of the electromagnetic theory.

General criticisms of the electromagnetic mechanism have been made in terms of the electrostatics of metal ellipsoids. Controversy has raged over the best method of interpreting certain experimental observations.

The assumptions made in electromagnetic theoretical calculations have proved slightly tenuous. One particular assumption is that the dielectric function is local (146) and therefore independent of the electromagnetic wave vector.

Some workers (121) have criticised the validity of applying classical electromagnetic theory to the study of SERS-active surfaces since the application of classical theory assumes continuous media. The particulate nature of the species involved in SERS-active systems has therefore caused problems.

### 2.3.4 Chemical theory.

It is logical to argue that, on the basis of the factors that influence SERS, the enhancement mechanism cannot be solely dependent on the nature of the active surface: the chemical structure and the bonding of the adsorbate to the surface must play an important part in the overall mechanism.

The evidence outlined below has led to the development of the chemical (charge-transfer) or adatom-complex model of enhancement.

#### 2.3.4.1 Evidence for chemical contributions to SERS enhancement.

(a) A purely electromagnetic theory of enhancement would result in SER spectra being simply enhanced duplicates of the corresponding normal Raman spectra. There are many examples, however, of SER spectra differing in relation to normal Raman spectra in terms of relative intensities and wavenumbers of bands.

This phenomenon was noted amongst the earliest SERS electrochemical studies. As discussed previously, pyridine commonly bonds to electrode surfaces via Lewis acid/base nitrogen-mediated adsorption (2). SER spectra of pyridine on electrode surfaces show changes in wavenumbers and relative intensities when compared to the Raman spectrum of neat pyridine. These observations can be understood in terms of the adsorbate forming a surface complex, with

the bulk adsorbate being the "ligands". Such a change inevitably alters the SER spectrum.

(b) Carbon monoxide and nitrogen, co-adsorbed in equal quantities onto cold-deposited silver films, display disparate enhancements (147).

Furthermore, the SER spectra show unique wavenumber shifts with respect to normal Raman spectra. The authors of this report overruled the possibility of displacement by one of the gases and postulated different bonding orientations for each: CO bonding end-on and N<sub>2</sub> oriented in a side-bonded mode. The different orientations cannot account for the extremely disparate SERS enhancements of the molecules, whose Raman scattering cross-sections are almost identical.

(c) In aqueous systems, such as the electrochemical environment, there has been little or no observation of SER scattering from water (148), which is an appreciable Raman scatterer. A solely surface-bound electromagnetic enhancement mechanism would not discriminate between adsorbate molecules and would therefore cause the spectrum of water to be enhanced.

(d) It has been noted that, in many cases, SERS excitation profiles obtained from colloidal silver do not correspond well with respective absorption maxima (79)(82)(149).

Although aggregation of colloids produces a red-shifted absorption maximum, as previously discussed, there is considerable evidence for

the presence of an adsorbate-metal charge-transfer absorption corresponding to the excitation maximum which is normally too weak to be detected in the optical absorption spectrum.

(e) The electromagnetic model predicts that enhancement would gradually tail off with distance from the metal surface. There is considerable evidence, however, for saturation of the effect at monolayer level (150) (151) with subsequent layers of adsorbate effectively exhibiting no enhancement. This is clearly indicative of an additional enhancement mechanism intrinsically linked with the chemical bonding of adsorbate molecules at the metal surface.

#### 2.3.4.2 Surface features.

It has been noted by many workers that small metal features, of 2 nm and smaller, do not contribute significantly to the electromagnetic mechanism. Such metal features are involved with the adsorption of molecules at the active surface and have the general term "atomic-scale roughness".

Otto (23) postulated that strong Raman enhancement is only observed when the adsorbate molecule is chemically bound to an atomic scale roughness feature (adatom).

#### 2.3.4.3 Early adatom theory.

It was initially thought that the adatom mechanism enhanced

Raman spectra by increasing the magnitude of the scattering cross-section of the adsorbed molecule. It was also believed that the scattering of electron-hole pairs at atomic-scale roughness played a large role in enhancement.

The manner in which the admolecule was involved in these processes was not clear, but the most likely explanation was the existence of Coulombic coupling between the admolecule and the electromagnetic fields associated with electron-pair excitation.

The original adatom model was a resonance Raman model with a transparent adsorbate and the production of new states on the surface in resonance with the exciting radiation.

#### 2.3.4.4 The chemical theory.

Avouris and Demuth (152) discovered a weak absorption in the electron energy loss spectrum (EELS) of several adsorbate species on silver close to, but not coincident with, the surface plasmon maximum. They interpreted the absorption as a charge-transfer band, either metal-adsorbate or adsorbate-metal.

This study turned the focus on the role of adatoms in the chemical model from electron-hole excitations to charge-transfer sites. Chemisorption and the formation of a charge-transfer complex are intrinsic factors in SERS chemical theory.

The chemical mechanism is defined as the enhancement of the Raman scattering cross-section of a chemisorbed molecule due to a resonance Raman process associated with a charge-transfer transition.

In this mechanism, it is clear that an accessible surface absorption develops (153) due to the broadening and shifting in energy of the free molecular states upon adsorption. This is caused by the formation of a surface energy band (molecule-molecule interaction) and by interactions with the metal energy states. The magnitude of HOMO-LUMO transitions in the free adsorbate molecule is too great for excitation by a conventional laser source, but once the molecule is bound to a surface the transitions are in resonance or approaching resonance with the laser excitation.

The involvement of this charge-transfer process in the SERS mechanism explains many of the experimental observations detailed previously that are irreconcilable with purely electromagnetic enhancement. The lack of enhancement with adsorbates such as nitrogen and methane can be interpreted in terms of the lack of a chemical bond and therefore of a charge-transfer complex.

Complex formation also explains observed differences in relative intensities and shifts in wavenumber in SER spectra compared to corresponding spontaneous spectra. One reviewer (121), however, believes this evidence does not necessarily discount the electromagnetic

mechanism as the main enhancement effect. He argues that bonding to the metal surface may alter the frequencies and relative intensities of the Raman bands without necessarily being involved in the actual enhancement. According to this view, the electromagnetic mechanism would be responsible for the enhancement of all SER spectra whether the adsorbate was surface-bound or not.

#### 2.3.4.5 Magnitude of contribution of the chemical effect.

Although the electromagnetic models are concerned essentially with physisorbed molecules, the basic equations defining electromagnetic enhancement can be altered slightly to encompass the polarisability of the metal-molecule complex rather than that of the molecule itself. In many cases, therefore, observations that are at odds with electromagnetic theory and apparently only explicable in relation to the chemical mechanism can be re-interpreted successfully.

The extent of contribution to overall enhancement of the chemical effect and, likewise, the electromagnetic mechanism varies greatly depending upon the adsorbate species and SERS-active systems involved.

The experiments of Murray and Bodoff (154) on the coverage of silver island films with  $^{14}\text{N}$ -radiolabelled potassium cyanide indicated that the chemical effect played a minor role in the enhancement

process, amounting to a factor of six against electromagnetic enhancement of  $10^4$ . In contrast, Yamada *et al.* (59) estimated a charge-transfer enhancement factor of  $10^3$  against an electromagnetic factor of 10, from studies of pyridine adsorbed on silver island films. They observed a clear charge-transfer band in the absorption spectrum at 600 nm which overlapped well with excitation profile measurements.

The uncertainty over the chemical mechanism is reflected in the indecisiveness over the role of adatoms (155) in the mechanism. The chemical model does not intrinsically require adatoms: only sites where chemisorption can take place.

### General discussion.

Although in many studies the question of the enhancement mechanism has been treated as either electromagnetic or chemical, in most cases there are contributions from both effects.

Campion and Mullins (156) observed unenhanced Raman spectra from pyridine adsorbed on various faces of single-crystal silver. Those who vigorously supported the chemical model postulated that there was no enhancement in this system due to the absence of chemisorption, whereas the supporters of the electromagnetic model argued that the lack of appropriate roughness features led to the absence of enhancement.

In more recent SERS studies, many workers have attempted to rationalise enhancement on the basis of both theories. Notholt and Ludwig (157), from studies of pyridine on silver electrodes, postulated a total enhancement factor, being the product of the enhancement factors from both effects and a constant.

The controversy that the SERS enhancement mechanism has aroused still persists to this day. Although there have been countless studies and elegant and comprehensive explanations of both main enhancement mechanisms, the central question of the extent to which the chemical mechanism contributes to SERS, if at all, still seems insoluble.

### **2.3.5 Other theoretical models.**

#### **2.3.5.1 Variations on the chemical model.**

##### **(a) Modulated reflectivity model (158).**

This model involves the modulation of the susceptibility of the metal surface, by injection and withdrawal of electrons, co-incident with the vibration of the adsorbate molecule and its effect on the Raman scattering cross-section.

##### **(b) Inelastic Mie scattering(159).**

This model, related to the above, considers the effect of charge injection and withdrawal on colloidal metal spheres (79). It was postulated that the charge injection-withdrawal process modulates the

polarisability of the metal sphere by shifting its surface plasmon resonance synchronously with vibration of the adsorbate, thus creating sum and difference side bands on the Mie-scattered light corresponding to the Raman effect.

It has also been proposed that inelastic Mie scattering explains the disparate enhancements associated with different bands in SER spectra. This, it is proposed, reflects the different charge injection-withdrawal abilities of different vibrational modes.

#### 2.3.5.2 Parametric excitation model (160).

In this model of enhancement, it is proposed that SERS is due to the instability of the Raman mode of the molecular dipole, caused by the coherent superposition of the laser excitation field and the surface field induced by the light scattered by the molecule. The scattered field further induces motion of the molecular dipole and, consequently, an unstable feedback is established; the SERS intensity increasing with time. The time taken to achieve maximum intensity depends upon the separation of the adsorbate molecule from the surface.

#### 2.3.5.3 Super radiance model (161).

This, somewhat speculative model, is involved with the possibility of several adsorbed molecules emitting in phase and the subsequent increase in Raman scattering cross-section.

#### 2.3.5.4 Microensemble model (162).

In this model, the adsorbed molecule and its surrounding media, including the metal surface, are considered to form a microensemble. The model is essentially charge-transfer based, but does take into account the role of surface roughness. It is proposed that the presence of roughness breaks the surface up into microdomains in which the electrons move freely, but with boundaries to motion between the domains.

### 2.4 APPLICATIONS OF SERS.

#### 2.4.1 Chemical reactions at surfaces.

The extraordinary sensitivity of SERS has led to the technique being used to study the progress of certain surface chemical reactions. This is possible through the detection of adsorbed reactants and reaction intermediates and products.

In Suh and Michaelen's (163) studies of the polymerisation of acrylic acid on silver electrodes, chemical changes in the polymer backbone were reflected in the SER spectra.

SERS has also been used to monitor redox processes at electrode surfaces (164). The influence of surface interaction effects on the SERS of adsorbed redox couples has been studied in relation to the frequency-potential dependence of oxidation state-sensitive vibrational modes.

### 2.4.2 Behaviour of molecules adsorbed on metal surfaces.

SERS is potentially a very sensitive tool for studying surface chemical properties such as the geometry and orientation of adsorbate species and changes in orientation induced by external variables. SERS has also proved effective in the study of the nature of the surface bonding site and the nature of the chemisorptive bond. The studies of Siiman *et al.* (165) illustrate this well. They observed SERS from nicotinamide adenine dinucleotide (NAD) and NADH (figure 2.15) adsorbed on silver colloids. The orientation and conformation of the bases adenine and nicotinamide in the surface-adsorbed forms of the coenzyme were inferred from the relative intensities of the SERS bands. It was found that these modes dominated the spectra and the alcohol and ring modes of the ribose and pyrophosphate groups were enhanced to a much lesser degree.

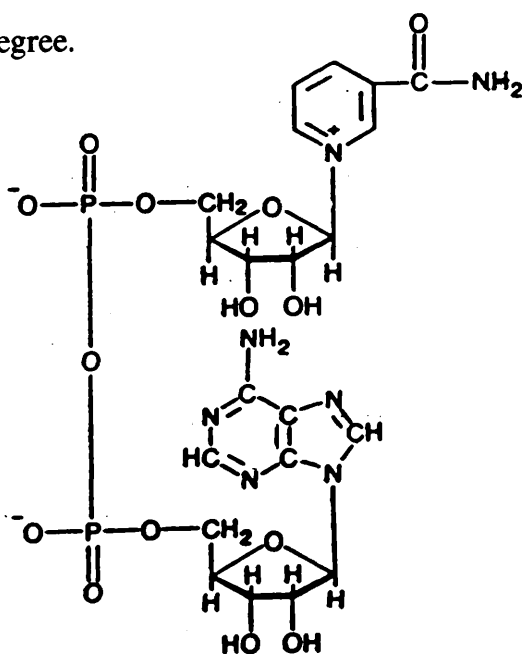


Figure 2.15: Structure of the coenzyme nicotinamide adenine dinucleotide(NAD) (unreduced form).

Other examples include the surface geometry changes of 2-naphthoic acid adsorbed on silver colloids (88).

### 2.4.3 Analytical chemistry.

This area of application of SERS has been gaining considerable momentum in recent years. The extreme sensitivity of SERS, which has led to many applications involving adsorption behaviour at metal surfaces, inevitably lends itself to the analysis of trace quantities of material.

Several categories of SERS-active substrates have been used. Surfaces which have exhibited the greatest analytical potential have been those of reproducible morphology. The control of roughness dimensions has also been an important factor.

#### 2.4.3.1 Electrode surfaces.

Although electrodes subjected to oxidation-reduction cycles have a randomly rough surface morphology and control of the size of roughness protusions is not simple, they have shown considerable potential in the area of chemical sensing.

Carraba *et al.* (166) carried out feasibility studies on the use of SERS on electrodes for the detection of organic water contaminants. This involved the analysis of a wide range of common families of organic contaminants found in surface and sub-surface water. With some

adsorbates, extremely low limits of detection were observed (pyridine at 8.5 pg) and the variation of electrode potential and excitation wavelength permitted the qualitative detection of a two-component mixture of contaminants. It was concluded that SERS on silver electrodes had potential applications in chemical sensing and also in the determination of hydrological transport and rates of movement in sub-surface systems.

#### 2.4.3.2 Vapour-deposited surfaces.

The production of vapour coated microspheres was reported by Goudonnet *et al.* (57). Their initial aim was to use the substrate as a test surface for SERS theoretical models. More recent application of the substrate in the field of analytical chemistry, however, has overshadowed this.

Coated microspheres have many important advantages as analytical SERS-active substrates. Firstly, the preparation procedure, although employing high vacuum coating apparatus, is fairly standard and requires no extremes of temperature as with other vapour-deposited surfaces. The second and most important advantage is that the dimensions of the metal spheres can be chosen whereas with island films and cold-deposited surfaces, the active dimensions depend on careful control of the preparation procedure. This makes coated

microspheres ideal for analytical applications where maximisation of signal strength is critical (58).

The initial studies of Goudonnet *et al.* employed phthalic (figure 2.16), benzoic and nitrobenzoic acids as model adsorbates, all showing intense, reproducible SER spectra with excitation wavelength appropriate to the size of the silver structures.

Vo-Dinh *et al.* (167) investigated more closely the potential analytical applications of the technique. With various organic compounds such as carbazole, 1-amino pyrene (figure 2.16) and benzoic acid, detection limits were found to be between 0.2 and 1.4 ng, with good reproducibility. The same group carried on this work into the area of organophosphorus chemical agents (168), again obtaining clear, reproducible SER spectra down to nanogram levels.

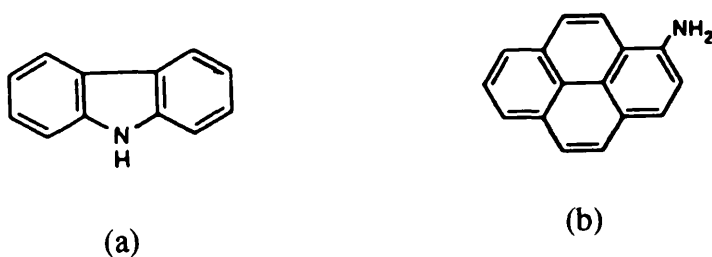


Figure 2.16: Structure of (a) carbazole and (b) 1-amino pyrene.

A variation of the microlithography method of producing silver particles on prolate silica posts, developed by Enlow *et al.* (169), has also displayed analytical SERS-activity. Intense spectra were observed from various nitro-polynuclear aromatic compounds. 1-nitropyrene was detected by SERS in nanogram quantities. This important class of pollutant compounds (170) has been analysed using various techniques, with SERS increasingly coming into the foreground.

#### 2.4.3.3 Colloids.

As already stated, SERS-active colloid systems have been used extensively for the chemical sensing of biologically-active molecules, often encompassing the utilisation of surface-enhanced resonance Raman spectroscopy (SERRS). SERS and SERRS as techniques have the important advantage of yielding complete vibrational spectra of active molecules without their destruction. The types of biological molecules studied have included nucleic acids (171)(172), eye lens pigments (173), haemoglobin (102), cytochromes (174) and other proteins.

Kniepp and Fleming (172) reported the observation of intense SERS spectra from deoxyribonucleic acid (DNA) and thermally denatured DNA (figure 2.17) adsorbed on silver sol particles. In addition to showing a detection limit of 10  $\mu\text{g}$  per ml, the study of this system also provided

valuable information on the behaviour of DNA at the metal surface. It was inferred that, on adsorption, DNA retained its double-stranded  $\alpha$ -helical geometry and that the SER spectra were enhanced via the electromagnetic mechanism.

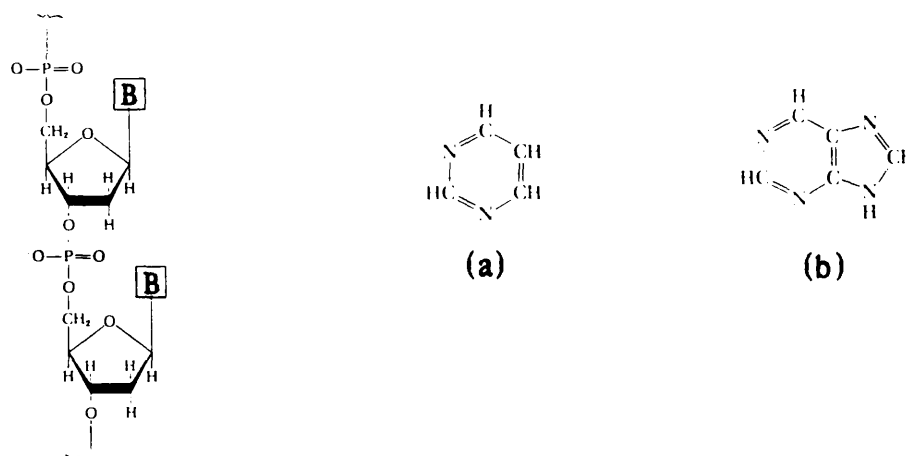


**Figure 2.17: Structure of deoxyribonucleic acid (DNA).  
B = pyrimidine (a) or purine (b) base unit.**

Nabiev *et al.* (94) also observed SERS from DNA molecules. The adsorption of nucleotides, calf thymus DNA and plasmid DNA, in the supercoiled and relaxed conformations, on silver colloids was studied. Activation (93) of the colloids with chloride ions induced adsorption sites highly specific to adenine nucleotides. This permitted the selective detection of the sites of destabilisation of double-stranded DNA helices and identification of the nucleotides at these sites. The detection limit for these systems was found to be approximately  $10^{-3}$  g.

A study by Nie *et al.* (173) on the SERS of some eye lens pigments of certain diurnally active animals on silver colloids displayed the significant potential of the technique. Lenticular pigments such as kynurenine, N-formyl kynurenine,  $\beta$ -carboline and bityrosine (figure 2.18) were used in the analysis. All showed distinct, highly-enhanced spectra. The findings of this group were shown to be very significant with respect to the metabolic and photochemical generation of lens pigments.

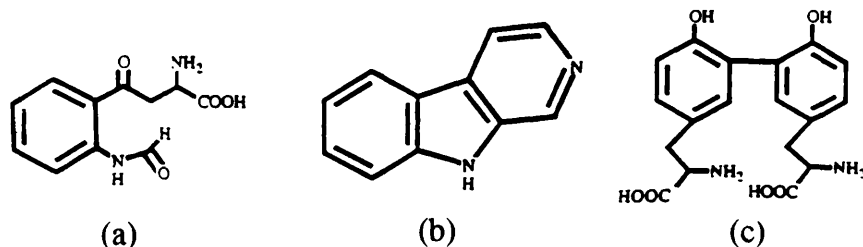


**Figure 2.18: Structure of the lenticular pigments (a) N-formyl kynurenine, (b)  $\beta$ -carboline and (c) bityrosine.**

The exhaustive studies of Chimanov, Efremov and Nabiev (175) (176) on a variety of biomolecules adsorbed on silver colloids (and also electrodes) yielded important results. Their analysis of the water-soluble proteins lysozyme and bovine serum albumin, various dipeptides and amino acids gave highly enhanced spectra. It was found that amino acids such as tryptophan (figure 2.19) were chemisorbed via

the aromatic side chain.

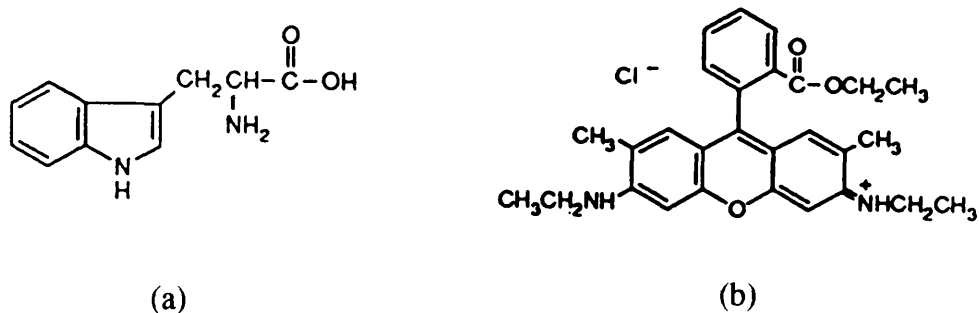


Figure 2.19: Structure of (a) tryptophan and (b) rhodamine 6G.

Silver colloids have also proved effective in the trace determination of nitrogen-containing drugs (177) and dyes (178). Many studies, for example, of the dye molecule rhodamine 6G (figure 2.19) have been undertaken. Through adsorption isotherms from SERRS of rhodamine 6G, Hildebrandt and Stockburger (179) identified two types of adsorption sites on activated silver colloid surfaces: one involved with physisorption and the other in chemisorption of the dye molecule. Distinct and highly enhanced SERR spectra were observed, indicating the power of the technique as an analytical tool for dye molecules.

## 2.5 RECENT DEVELOPMENTS IN SERS.

### 2.5.1 Langmuir-Blodgett monolayers.

SERS has proved a sensitive technique for the characterisation of monolayers and interfaces consisting of Langmuir-Blodgett films (180) (181). Indeed, Langmuir-Blodgett monolayers have provided an

elegant way of studying properties of SERS such as physisorption, chemisorption, distance dependence and coverage dependence.

Depolarisation ratios and excitation profiles have been studied under qualitative control of adsorbate molecular monolayers on SERS-active surfaces.

### 2.5.2 Fibre-optic sensors.

Bello and Vo-Dinh (182) recently developed a fibre-optic system able to excite and collect SER spectra routinely. The SERS signals were generated from a sensing plate tip, having silver-coated microparticles deposited on a glass support. The SERS-active substrate was produced by, firstly, depositing a small volume of a 5% aqueous solution of 100 nm diameter commercially available alumina particles on a clean microscope slide, followed by vacuum evaporation of a thin layer of silver. The substrate, under optimum experimental conditions, yielded reproducible, highly enhanced spectra with organic adsorbates.

### 2.5.3 Flow-injection systems.

Many workers (183)(184) have demonstrated the effectiveness of flow-injection sampling systems for real-time quantitative analysis of aqueous solutions of adsorbates by SERS.

Taylor *et al.* (185) studied the SERRS of crystal violet with a unique flow-injection system (figure 2.20). This optimised system was able to

deliver within five minutes, with the aid of an optical multichannel analyser for detection, quantitative and structural information on extremely dilute adsorbate solutions. With crystal violet, high-quality, reproducible spectra were obtained down to approximately  $10^{-19}$  grammes of material, thus demonstrating the potential of the technique for routine, rapid SERS analyses.

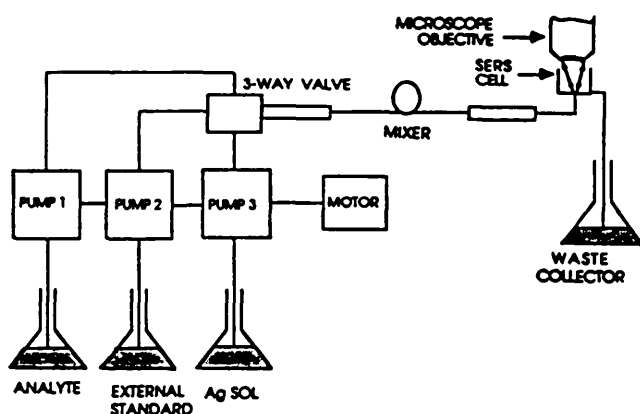


Figure 2.20: Schematic diagram of a SERS flow-injection system.

#### 2.5.4 Surface-Enhanced Hyper Raman Spectroscopy (SEHRS) (186).

##### 2.5.4.1 Hyper-Raman Scattering (HRS).

Hyper-Raman scattering, a non-linear process, was first observed in 1965 (187).

When monochromatic radiation is focussed on a material, inelastically scattered light displaced from the incident frequency is found (Raman scattering). Very weak inelastically scattered radiation displaced from double the incident frequency can also be detected. This is termed hyper-Raman scattering (HRS), a three-photon process with

extremely small cross-sections. The HRS selection rules permit the observation of nuclear motions and the study of low frequency vibrational modes due to the weakness of the hyper-Rayleigh line.

SEHRS offers the possibility of boosting the inherently small HR cross-sections, due to surface effects, and therefore increase non-linear scattered intensities. Picosecond neodymium YAG lasers are commonly used as the excitation source.

#### 2.5.4.2 Applications of SEHRS.

The studies of Golab *et al.* (188) on pyridine adsorbed on silver electrodes excited by cw mode-locked Nd YAG laser techniques realised spectra similar to those obtained with conventional SERS, with some slight differences in relative intensities of bands, but of far greater enhancement. The overall enhancement of SEHRS over bulk HRS was estimated to be approximately  $10^{13}$ , a factor of  $10^7$  greater than the typical SERS enhancement with pyridine on silver electrodes.

Johnson and Soper (189) observed conventional enhancements of  $10^3$  to  $10^6$ , however, in the SEHRS of pyridine adsorbed on silver colloids. Changes were also noted in the relative intensities of SEHRS with respect to HRS, indicating the influence of surface morphology effects.

It was concluded from these two studies that SEHRS is considerably

more sensitive to orientation effects than SERS.

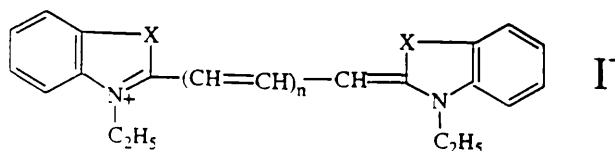


**Figure 2.21: Structure of 3,3'-diethyloxa(thia)carbocyanine dyes.**  
X = O, S; n = 1, 2, 3.

The recent study of Yu *et al.* (190) on the picosecond SEHRS spectra of several non-centrosymmetric oxa- and thia-carbocyanine dye molecules (figure 2.21) adsorbed on pre-aggregated silver colloid yielded important new vibrational information. The SEHRS spectra obtained displayed dramatic changes compared to their respective FT-Raman and SERS spectra, including some bands only detectable through SEHRS. It was noted that the SEHRS spectra consisted of mainly central  $\pi$ - conjugated chain vibrational modes, instead of end-chromophore vibrations which were predominant in the corresponding Raman spectra.

These studies have shown that the technique of SEHRS, in addition to producing high quality, highly enhanced surface Raman spectra, is capable of yielding important vibrational data that is unable to be obtained through Raman, i.r. and surface-enhanced Raman methods.

**CHAPTER THREE.**

**OBJECTIVES.**

### **3. OBJECTIVES.**

The overall objective of this study was to explore ways of applying SERS to the analysis of a variety of organic and inorganic species. It is clear from the volume of SERS analytical literature that, with certain adsorbate species on appropriate surfaces and under the right conditions, SERS is extremely sensitive to low concentrations of adsorbate species. In order to utilise SERS as an analytical technique in a rational way, the precise nature of the surface/adsorbate molecule interaction (which is not properly understood) must be probed. To this end, a systematic investigation of a range of different SERS-active substrates, coupled with different types of adsorbate molecules, was undertaken.

The initial aim was to find SERS-active surfaces suitable for intensive study.

SERS-active surfaces include:

- (a) Colloids.
- (b) Vapour-deposited surfaces.
- (c) Chemically-produced active films.

Potential variable molecular parameters include the following:

- (a) The charge of the adsorbate.
- (b) The overall shape of the molecule.
- (c) The hydrophobic or hydrophilic nature of the molecule.

(d) The influence of co-ordinating groups in the molecule.

The conclusions drawn from these systematic studies should lead to a better understanding of the adsorption of different molecules at SERS-active surfaces. Tris(2,2-bipyridyl) ruthenium(II) and modified analogues were chosen as appropriate test molecules.

The programme of work was divided into three parts:

(1) The preparation of modified 2,2'-bipyridyl ligands and subsequent tris-ligand ruthenium (II) complexes.

Characterisation of ligands and complexes. Extensive study of the absorption spectroscopy of the tris-ligand complexes.

(2) SERS feasibility studies of a variety of active surfaces with inorganic and organic molecules.  $[\text{Ru}(\text{bipy})_3]^{2+}$  was the main test molecule.

(3) Comparative studies of  $[\text{Ru}(\text{bipy})_3]^{2+}$  and disubstituted analogues with chemically prepared and vapour-deposited silver surfaces.

CHAPTER FOUR.

EXPERIMENTAL.

## 4. EXPERIMENTAL.

### 4.1 Preparation of bipyridyl ligands and their ruthenium complexes.

#### 4.1.1 2,2'-bipyridine.

This ligand was used as received (99%, Aldrich).

#### (a) Tris(2,2'-bipyridine) ruthenium(II) diiodide, Ru(bipy)<sub>3</sub>I<sub>2</sub>.

The method of Palmer and Piper (191) was used to prepare this complex.

Ruthenium trichloride trihydrate (RuCl<sub>3</sub>·3H<sub>2</sub>O) (0.25 g, 0.956 mmoles), 2,2'-bipyridine (0.45 g, 2.88 mmoles) and Analar ethanol (20 ml) were placed in a round-bottom flask and refluxed for 72 hours. At the end of this period, half the volume of solvent was removed (rotary evaporator). Following the addition of excess potassium iodide, Ru(bipy)<sub>3</sub>I<sub>2</sub> precipitated out. Subsequent filtration afforded 0.49 g (80.1%) of complex.

#### (b) Tris(2,2'-bipyridine) ruthenium(II) dichloride, Ru(bipy)<sub>3</sub>Cl<sub>2</sub>.

An alternative method, that of Braddock and Meyer (192), was used to prepare this complex.

Ruthenium trichloride trihydrate (0.20 g, 0.765 mmoles), 2,2'-bipyridine (0.36 g, 2.31 mmoles) and reagent grade N,N- dimethyl formamide (15 ml) were placed in a round-bottom flask and refluxed for 3 hours. At the end of this period, the solution was concentrated to

approximately 5 ml and added, dropwise, to a saturated solution of tetra-n-butyl ammonium chloride in Analar acetone. This resulted in the precipitation of 0.47 g (74.7%) of the complex.

(c) Bis(2,2'-bipyridine) ruthenium(II) dithiocyanide, Ru(bipy)<sub>2</sub>(NCS)<sub>2</sub>.

The method used was that of Wajda and Rachlewicz (193).

Ruthenium trichloride trihydrate (0.25 g, 0.692 mmoles) was dissolved in 65 ml of absolute ethanol. A further solution of 0.30 g (1.92 mmoles) of 2,2'-bipyridine in 30 ml of ethanol was prepared.

Upon mixing the solutions, a brown precipitate formed immediately.

The mixture was refluxed for a total of 15 hours (isomantle).

After filtering the residue, 0.45 g (5.56 mmoles) of sodium thiocyanate was added to the filtrate and the resulting solution was refluxed for 6 hours. Dark brown/violet crystals precipitated. Filtering and subsequent washing with distilled water and ethanol gave 0.25 g (61% yield) of product.

(d) Bis(2,2'-bipyridine) ruthenium (II) dichloride dihydrate,

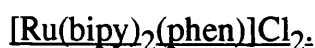


The procedure used was based on the method of Meyer (194).

RuCl<sub>3</sub>.3H<sub>2</sub>O (0.42 g, 1.61 mmoles), 2,2'-bipyridine (0.50 g, 3.21 mmoles) and lithium chloride (0.46 g, 0.0108 moles) were dissolved in purified DMF (40 ml) contained in a 100 ml round-bottom flask fitted with reflux condenser apparatus. The mixture was refluxed for 8 hours

whilst being constantly stirred magnetically. After cooling to room temperature, the solution was poured into rapidly stirred Analar acetone (200 ml). The round bottom flask was washed with more acetone (2 x 50 ml) and the combined mixtures allowed to stand at 0°C overnight. The resultant dark green microcrystalline material was collected on a medium porosity sintered-glass filter funnel and washed with water (75 ml) and diethyl-ether (75 ml). The total yield of complex was 0.57 g (68%).

(e) Bis(2,2'-bipyridine) 1,10-phenanthroline ruthenium(II) dichloride.



The method used to prepare this complex was based on the method described by Crosby and Elfring (195). A similar method, that of Bosnich (196), was not attempted.

A suspension of  $\text{Ru(bipy)}_2\text{Cl}_2$  (0.61 g, 1.17 mmoles) in distilled water (200 ml) and Analar methanol (100 ml) was heated until dissolution was complete. 1,10-phenanthroline monohydrate (0.25 g, 1.39 mmoles) was added.

The resultant solution was refluxed for one hour. The bright orange solution produced at the end of the heating period was filtered and evaporated to dryness on a steam bath. The solid was immediately recrystallised from hot methanol. After collection on a sintered-glass filter funnel, 0.54 g (69.5% yield) of product was obtained.

#### 4.1.2 2,2'-bipyridine-4,4'-dicarboxylic acid.

The scheme for this reaction is shown in figure 4.1.

The ligand was prepared by the method of Case (197). Potassium permanganate (22 g, 0.1392 moles) and 4,4'-dimethyl-2,2'-bipyridine (99%, Aldrich, 4 g (0.0217 moles)) in distilled water (380 ml) were heated (isomantle) to discolourisation of the permanganate. The precipitated manganese dioxide was removed by filtration and the colourless filtrate extracted with Analar diethyl ether to remove unchanged reactant. The filtrate was then acidified with concentrated hydrochloric acid and the resultant precipitated crude acid collected by filtration, yielding 1.15 g (21.7%) of product.

#### (a) Ruthenium(II) complex of 2,2'-bipyridine-4,4'-carboxylic acid.

In an attempt to prepare the ruthenium tris-ligand complex, the ligand was reacted with  $\text{RuCl}_3 \cdot 3\text{H}_2\text{O}$  according to the method of Braddock and Meyer (192). When the reacted solution was added dropwise to a saturated solution of tetra-N-butyl ammonium bromide in acetone, no complex precipitated. The DMF/acetone was distilled off to produce a large mass of deep purple material (approximately 8 g, >100% based on the formation of the tris-ligand complex).

#### 4.1.3 Diethyl 2,2'-bipyridine-4,4'-dicarboxylate (scheme : fig 4.1).

The procedure reported by Maerker and Case (198) was employed

in the preparation of this ligand.

2,2'-bipyridine-4,4'-dicarboxylic acid (1.15 g, 4.7 mmol) in a mixture of 13 ml of concentrated (98%) sulphuric acid and 27.5 ml of absolute ethanol was refluxed for 10 hours, cooled to room temperature and poured on ice. Neutralisation with 25% aqueous sodium hydroxide afforded a grey-white solid. The latter was collected by filtration and recrystallised twice from absolute ethanol, yielding 0.90 g (38.4%) of white crystals.

(a) Tris (diethyl 2,2'-bipyridine-4,4'-dicarboxylate) ruthenium (II) ditetrafluoroborate.

A method suggested by Cook *et al* (199) was utilised in the preparation of the tris-ligand ruthenium (II) complex.

Ethenediol (85 ml) was placed in a round bottom flask. To this was added 0.285 g (0.95 mmol) of diethyl 2,2'-bipyridine-4,4'-dicarboxylate and 0.12 g (0.32 mmol) of dipotassium aquapentachloro ruthenate (III),  $K_2[RuCl_5(H_2O)]$ . The mixture was refluxed for 72 hours (isomantle) and filtered hot. The filtrate had approximately half its volume of ethenediol removed. Distilled water (20 ml) was added and the solution extracted with toluene to remove excess unreacted ligand. Addition of 2 ml of a saturated solution of sodium tetrafluoroborate did not result in precipitation of the complex. Removal of further solvent only resulted in precipitation of excess  $NaBF_4$ .

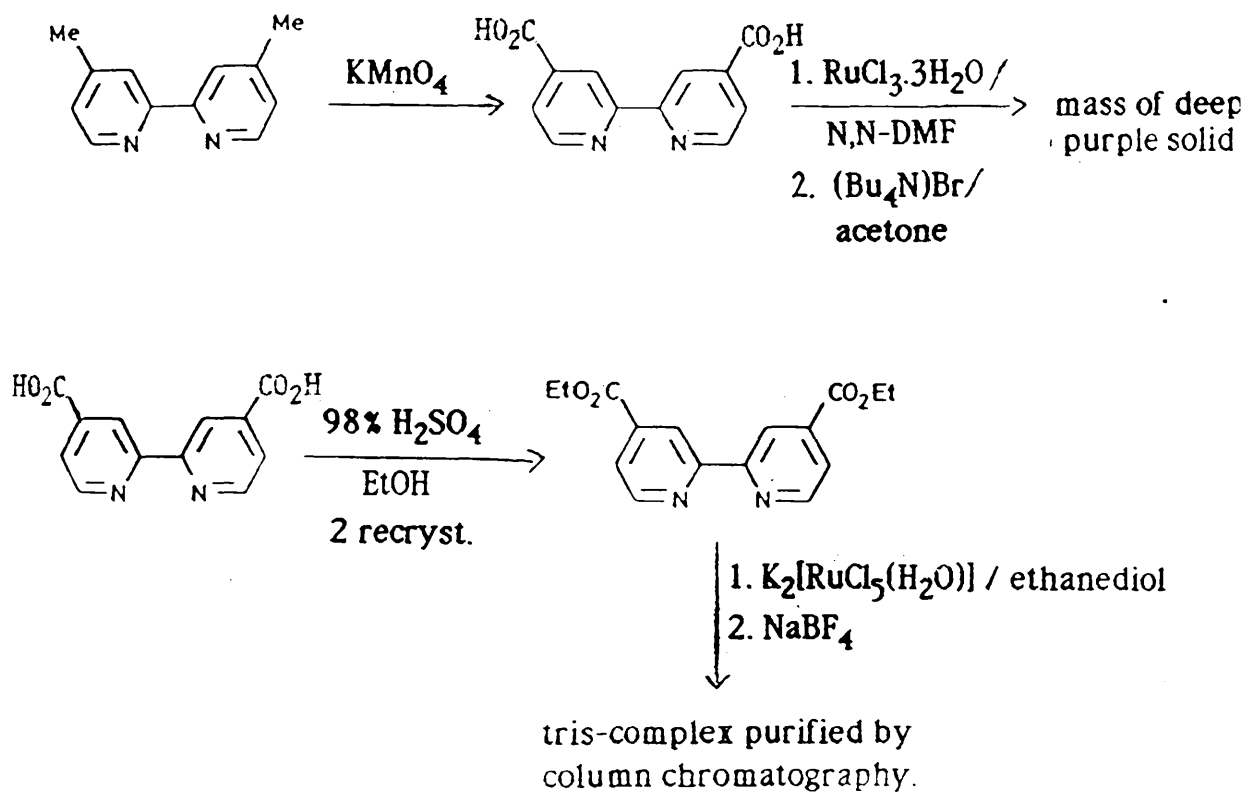


**Figure 4.1: Preparative routes to 2,2'-bipyridine-4,4'-dicarboxylic acid and diethyl 2,2'-bipyridine-4,4'-dicarboxylate and their ruthenium(II) complexes.**

#### 4.1.4 4,4'-diamino-2,2'-bipyridine (scheme: figure 4.2).

There are various synthetic routes to this ligand. The one which was chosen was *via* the preparation of 2,2'-bipyridine-1,1'-dioxide and, subsequently, 4,4'-dinitro-2,2'-bipyridine-1,1'-dioxide(200).

##### Oxidation step.

2,2'-bipyridine (5 g, 0.032 moles), glacial acetic acid (25 ml) and 30% hydrogen peroxide (5 ml) were heated in a water bath for 4 hours. A further 5 ml of peroxide were added and the mixture heated for an additional 8 hours. After cooling to 0°C, the solution was made alkaline with a concentrated solution of potassium hydroxide to give a white material which was recrystallised from water and dried with Analar chloroform. The yield of N,N-dioxide was 5.1 g (84.8%).

This reaction was repeated many times and on each occasion the yield was greater than 80%.

##### Nitration step.

2,2'-bipyridine-1,1'-dioxide (10 g, 0.053 moles) was added to a mixture of 26 ml of fuming nitric acid (95%, specific gravity 1.5) and 30 ml of concentrated (98%) sulphuric acid. The acid/N,N-dioxide mixture was heated in a water bath for 4 hours. At the end of this period, the mixture was poured into ice to form a green solution. After a few minutes, yellow solid began to form near the top of the iced solution. Once all the ice had melted, the yellow material was collected by

filtration. Recrystallisation from distilled water yielded 4.23 g (28.5%) of 4,4'-dinitro-2,2'-bipyridine- 1,1'-dioxide.

#### Amination step.

Amination of the nitro-N,N-dioxide compound was effected by using the procedure of Maerker and Case(198).

Iron powder (8.5 g, 0.152 moles) was added to 3.8 g (0.0137 moles) of the nitro-N,N-dioxide in 150 ml of glacial acetic acid at 100°C, with stirring. The temperature of the mixture was maintained at 114°C for 70 minutes. After cooling to room temperature, 100 ml of water was added. The solution was made alkaline with 25% sodium hydroxide solution and brought to a volume of 600 ml with water. Filtration afforded a black, tarry precipitate which was dried in an oven for 30 minutes. The dried solid was extracted with 95% (bulk) ethanol until further extraction no longer gave a purple alcohol solution. The combined extracts were filtered and then acidified, with cooling to 0°C, with concentrated hydrochloric acid. The resulting suspension was filtered, the white precipitate washed with 95% ethanol and discarded and the alcoholic wash solution combined with the filtrate. The solution was then concentrated to a volume of 250 ml .

On standing for 24 hours, orange/brown needles deposited in the concentrate and were collected by filtration (0.95 g). The filtrate, after further concentration, yielded a second crop of crystals (0.25 g). The

solids were combined and recrystallised from aqueous ethanol (50 ml 95% ethanol/8 ml water) to give 0.54 g of the hydrochloride of the product. The latter material was dissolved in water and the free base precipitated after the addition of dilute sodium hydroxide solution. The white precipitate, after three recrystallisations, weighed 0.18 g (6.7% yield). Two further attempts at this preparation did not improve the yield of diamine.

(a) Tris(4,4'-diamino-2,2'-bipyridine) ruthenium (II) dichloride.

The method of Cook *et al* (199) was used for this preparation.

Dipotassium aquapentachlororuthenate(III),  $K_2[RuCl_5(H_2O)]$  (0.08 g, 0.21 mmoles), in 10 ml of hot distilled water containing one drop of 6M hydrochloric acid was added to a solution of 4,4'-diamino bipyridine in 8 ml of DMF. The resulting mixture was refluxed for 15 minutes. Phosphinic acid,  $H_3PO_2$  (30%, 1.95 ml), was then added followed by neutralisation with 0.52 ml of 2M sodium hydroxide solution. The solution was refluxed for a further 30 minutes after which it was filtered hot and 1.73 ml of 6M hydrochloric acid was added. At this stage, approximately half the solvent was removed and the solution was allowed to cool in ice overnight.

Crystallisation did not result, even after further solvent removal.

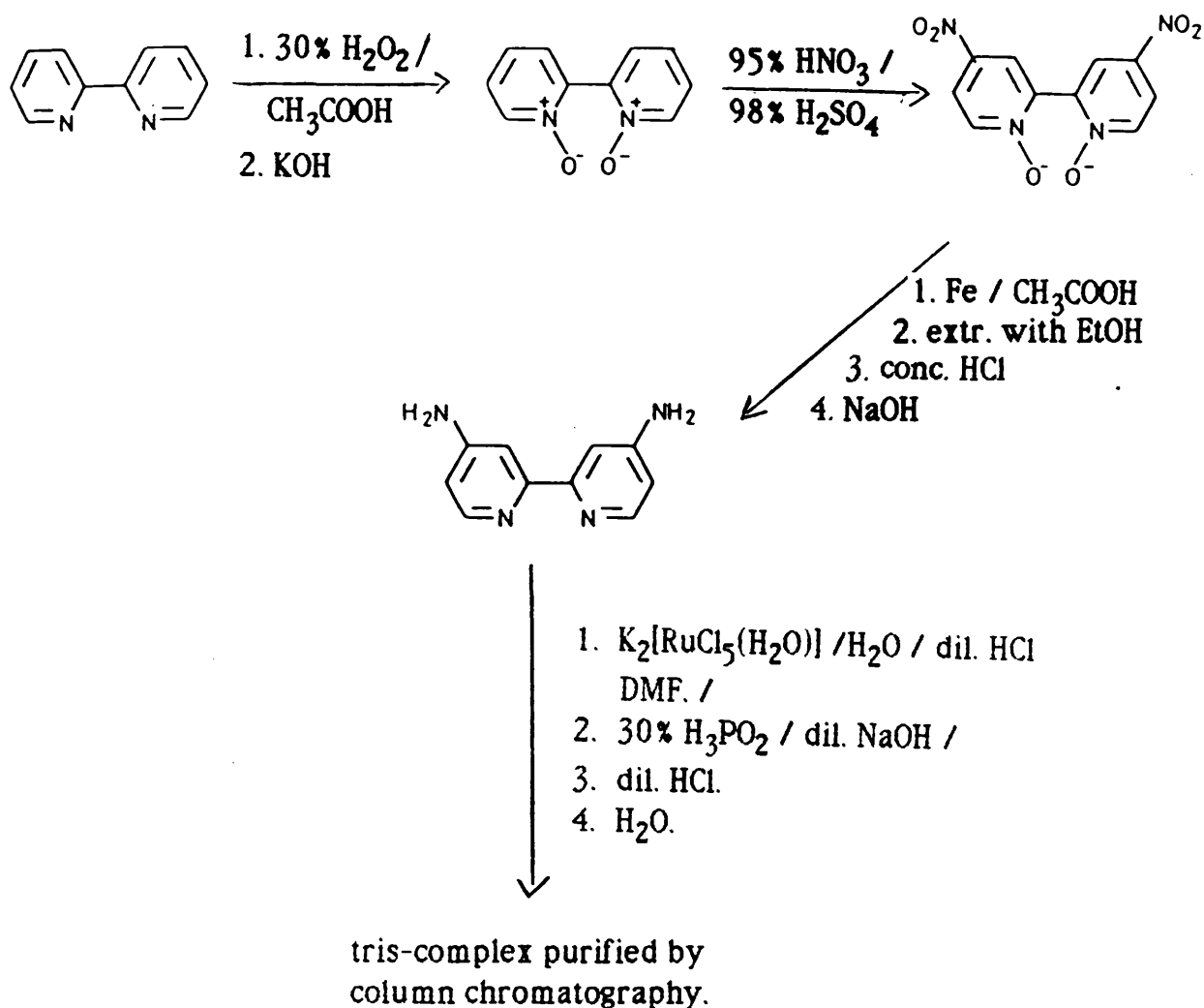


**Figure 4.2: Preparative route to 4,4'-diamino-2,2'-bipyridine and its ruthenium(II) complex.**

#### 4.1.5 4,4'-diphenyl- and 4,4'-dimethyl-2,2'-bipyridine.

The ligands 4,4'-diphenyl and 4,4'-dimethyl-2,2'-bipyridine were used as received (99%, Aldrich).

##### (a) Tris(4,4'-diphenyl-2,2'-bipyridine) ruthenium(II) dichloride.

The preparation of this complex was a two-step process (scheme: figure 4.3). An attempt was made to prepare the complex *via* a facial DMSO-ruthenium (III) complex.

##### Attempted preparation of *fac* -[RuCl<sub>3</sub>(DMSO)<sub>3</sub>] (201).

Concentrated hydrochloric acid (5 ml) was added to a solution of hydrated ruthenium trichloride (0.2498 g, 0.955 mmoles) in dimethyl sulphoxide (1.5 ml). The mixture was heated at 85 °C for approximately 30 minutes, concentrated to 2 ml and cooled overnight at 10°C. Instead of yellow needle-like crystals of the facial isomer separating out, dark orange *mer* product was formed.

The *mer* isomer was used in the second stage of the reaction.

##### Preparation of [Ru(diphbipy)<sub>3</sub>Cl<sub>2</sub>].H<sub>2</sub>O (202).

To a solution of *mer* -[RuCl<sub>3</sub>(DMSO)<sub>3</sub>] (0.1017 g, 0.230 mmoles) in absolute ethanol (15 ml), 4,4'-diphenyl-2,2'-bipyridine (0.2136 g, 0.694 mmoles) (1 : 3 molar ratio) was added. The mixture was refluxed for 2 hours whence a dark brown solution was obtained. The solution was concentrated to 5 ml, cooled to room temperature and diethyl ether added. Fine brown product precipitated and was filtered, washed with

diethyl ether and dried in vacuo, yielding 0.1573 g (61.4%).

(b) Tris(4,4'-dimethyl-2,2'-bipyridine) ruthenium(II) dichloride.

The route to the tris-ligand complex was *via* two steps (scheme: figure 4.3). The first step was the preparation an octahedral *mer*-trichloride tri(DMSO) ruthenium(III) complex (201). This complex was then reacted, in the appropriate proportions, with the modified bipyridyl ligand (202).

Preparation of *mer*-[RuCl<sub>3</sub>(DMSO)<sub>3</sub>] (201).

Concentrated hydrochloric acid (36%, 5 ml) was added to a solution of hydrated ruthenium trichloride (0.2512 g, 0.961 mmoles) in dimethyl sulphoxide (DMSO) (1.5 ml). The mixture was maintained at reflux, in an oil bath at 135<sup>0</sup>C, for 1.5 hours and then cooled to room temperature. The compound separated out and was filtered and carefully washed twice with small portions of ice-cold acetone. Subsequent drying gave 0.2841 g (67.0%) of product.

Preparation of [Ru(dimebipy)<sub>3</sub>Cl<sub>2</sub>].H<sub>2</sub>O (202).

To a solution of *mer*-[RuCl<sub>3</sub>(DMSO)<sub>3</sub>] (0.2053 g, 0.465 mmoles) in absolute ethanol (20 ml), 4,4'-dimethyl-2,2'-bipyridine (0.2598 g, 1.41 mmoles) (1 : 3 molar ratio) was added and the resultant mixture refluxed for 2 hours whence a dark solution was obtained. The solution was concentrated to 5 ml, cooled to room temperature and reagent grade diethyl ether (3 ml) was added to precipitate the complex. The

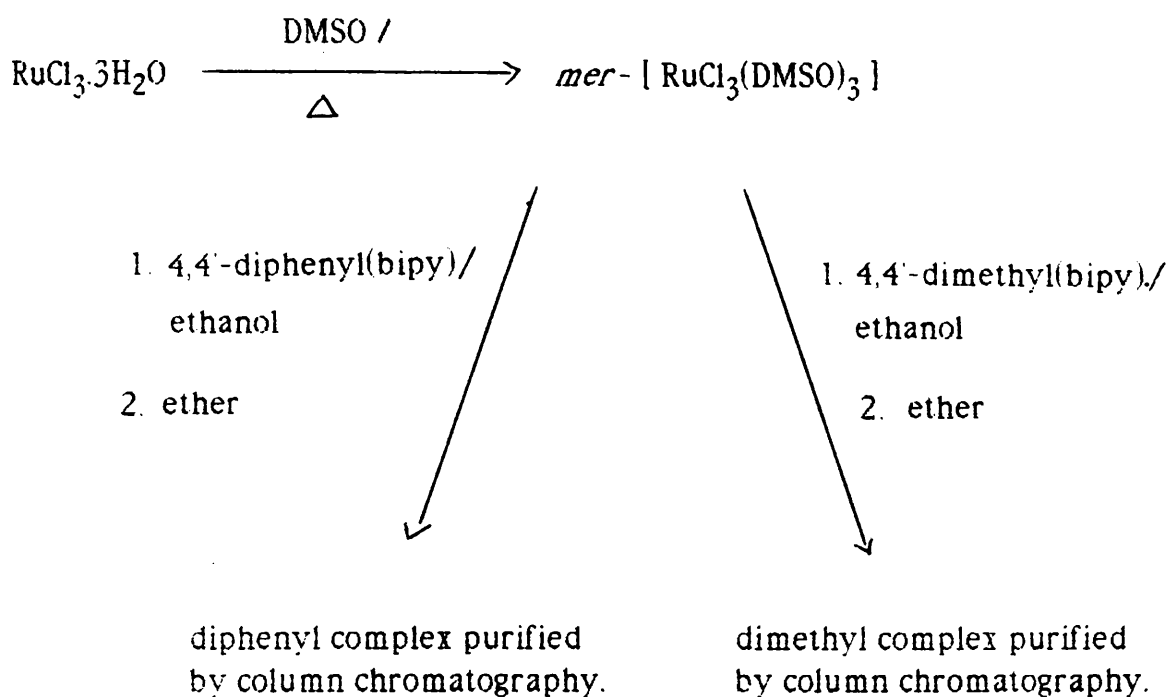


**Figure 4.3: Preparative routes to the tris-ligand ruthenium(II) complexes of 4,4'-diphenyl and 4,4'-dimethyl-2,2'-bipyridine.**

product was filtered, washed with diethyl ether and dried *in vacuo*.

The yield was 0.2004 g (58.1%), assuming one water of crystallisation in the formulation.

#### 4.2 Column chromatography.

Several ruthenium(II) tris-bipyridyl complexes were purified by column chromatography. In all cases, a 0.5 m long, 1 cm diameter glass column with porous frit was used. The support used was sephadex LH20 (Pharmacia). The general procedure followed is now described.

Sufficient sephadex to fill the column was mixed thoroughly with the solvent (in most cases, reagent grade ethanol). Whilst mobile, the resultant slurry was poured into the column and allowed to settle. This normally took two or three attempts as excess solvent had to be drained away. When the solvent had drained to the head of the sephadex support, an ethanolic solution of the impure complex was poured into the column and allowed to migrate. Once all the sample had migrated onto the column, a large volume of solvent was poured into the column. Care was taken to ensure that the solvent reservoir was constantly replenished. The normal time taken for complete separation and collection of the fractions was between 1.5 and 2 hours. Adequate separation of the fractions was achieved with all the samples of ruthenium complexes purified.

The sephadex could be re-used by slushing the full quantity of support out of the column and extracting any material which had remained with the appropriate solvent. Highly polar or completely non-polar solvents had to be used in some cases.

### 4.3 Preparation of SERS-active substrates.

#### 4.3.1 Colloids.

Silver colloids were prepared according to the method of Creighton *et al.* (79). The following solutions were prepared : sodium tetrahydroborate,  $\text{NaBH}_4$ , ( $10^{-3}\text{mol l}^{-1}$ ) and silver nitrate,  $\text{AgNO}_3$ , ( $2 \times 10^{-3}\text{mol l}^{-1}$ ).

Both solutions were pre-cooled in ice and 3 ml of  $\text{NaBH}_4$  were added dropwise to 1 ml of  $\text{AgNO}_3$  with stirring to give yellow silver colloidal solution. The reaction was scaled-up successfully.

#### 4.3.2 (a) Chemically produced films.

The procedure used to produce silver active films was a modification of the method reported by Ni and Cotton (113).

Frosted microscope slides were cleaned in concentrated nitric acid and washed in distilled water. Solutions of sodium hydroxide (5% w/v), glucose (10% w/v) and silver nitrate (2% w/v) were prepared.

Ten drops of the sodium hydroxide solution were added to 10 ml of the silver nitrate solution in a 150 ml beaker. This resulted in the formation of a dark brown precipitate (silver hydroxide). Ammonia

(s.g. 0.88) was added dropwise with stirring until the precipitate redissolved. Dry frosted microscope slides were placed round the circumference of the beaker and 3 ml of the glucose solution were added. The solution was then mixed thoroughly. The beaker containing the microscope slides was placed in a near-boiling water bath for approximately 30 seconds. The slides were inspected constantly throughout this operation and the beaker was removed from the water bath when a light yellow coating of silver had formed on the frosted part of the slide. The beaker was placed in an ultra-sound bath for 1 minute to encourage the formation of an even silver layer. Prolonged exposure of the slides/silver solution to heat produced white silver films.

Once produced, the silver coated slides were stored under distilled water until required. The slides were found to be stable under distilled water for several weeks.

#### (b) Production of gold and copper active films.

Various attempts were made to produce gold and copper coated slides in the same manner as above. The relevant metal salts used were hydrogen tetrachloroaurate(III),  $\text{HCl}_4\text{Au}$ , and cupric chloride,  $\text{CuCl}_2$ .

Reducing agents used were glucose for gold slides and a glucose/sodium citrate mixture for copper slides.

### 4.3.3 Supported silver colloids.

Silver-coated filter-paper substrates were prepared according to the method of Laserna *et al* (107).

A petri-dish was half-filled with an 0.1 molar solution of silver nitrate. An appropriately sized piece of filter-paper (Whatman No.1) was placed in the dish and, therefore, saturated with silver nitrate. After a few minutes, the saturated filter-paper was removed from the petri-dish and allowed to dry briefly on a larger piece of filter-paper. A previously prepared solution of sodium tetrahydroborate (0.2 molar) was sprayed onto the saturated filter-paper in a vertical fashion from approximately 20 cm distance (a TLC spray was used for this purpose).

The freshly prepared silver-coated filter-paper was grey/green in colour: after a few hours it became brown.

Silver-coated TLC silica-gel plates were prepared in an identical manner (110).

### 4.3.4 (a) Silica spheres.

The controlled growth of monodisperse silica spheres was first reported by Stober *et al* in 1968 (203). The procedure has been developed in recent years by Adams *et al* (204).

The reaction is straightforward, being essentially the alkaline hydrolysis of tetraethylorthosilicate. A typical example is repeated

here.

A brown, wide-necked bottle was washed with detergent, rinsed thoroughly with distilled water followed by ethanol and diethyl ether and dried in an oven for 30 minutes. Distilled water (6.7 ml), laboratory grade ethanol (28.9 ml) and ammonia (s.g. 0.88, 1 ml) were added to the bottle and mixed thoroughly. Tetraethylorthosilicate (TEOS) (10 ml) was added to the mixture, the bottle sealed and the contents mixed thoroughly by shaking. The reaction mixture was then left for three days. During this period, a milky suspension formed. The silica was dried down using a rotary evaporator.

According to Adams *et al*, these proportions of reactants should give silica particles of approximately 140 nm diameter.

Reactions were carried out with different proportions of reactants as detailed in table 4.1.

Table 4.1: Preparation of silica spheres: proportions of reactants.

Volume of: (ml)	<u>TEOS</u>	<u>water</u>	<u>ammonia</u>	<u>ethanol</u>	<u>(sphere size)</u>
	10	13.2	2	68	(390 nm)
	5	10.2	5.9	73	(230 nm)
	10	13.1	1	28.9	(195 nm)

(b) Chemically coated silver silica spheres.

Attempts were made to chemically coat silica spheres of an

appropriate size with silver based on a method developed for latex spheres (205).

A quantity of silica spheres (140 nm) was mixed thoroughly in 20 ml of distilled water to give a grey suspension and the excess was filtered off. Acetaldehyde (2 ml) was added to 8 ml of the silica suspension in a small beaker. The beaker was placed in an ultra-sound bath and 4 ml of a previously prepared Tollens reagent solution (5 ml of 5%  $\text{AgNO}_3$ /5 ml of 2M (3.5%)  $\text{NH}_3$ ) was added. The mixture was then sonicated for approximately 2 hours. At the end of this period, a brown suspension had formed.

#### 4.3.5 Vapour-deposited surfaces.

Vapour-deposition of silver onto various substrates was effected by using a circular silver metal target in conjunction with a Polaron E5000 sputter-coater. A diagram of the coating unit is displayed in figure 4.4.

##### Operating procedure.

Once the silver target and samples had been loaded into the unit, the sample stage was cooled for 30 minutes.

The vacuum chamber was evacuated to 0.08 torr ('PUMP' operation). Argon gas was then admitted *via* the argon inlet valve followed by almost immediate re-evacuation of the chamber. This argon flush/evacuation procedure was repeated twice. Heating of the

target was begun ('SET HT') and a potential of 0.75 kV applied across it.

The argon inlet valve was opened slowly until a current of 25 mA was displayed on the ammeter. This operation was accompanied by the gradual appearance of purple silver plasma at the target. The current was maintained at 25 mA until the desired thickness of silver had coated onto the sample. This was calculated by using the following formula:

$$d = I V t G \quad , \quad (4.1)$$

where  $d$  = thickness of coating ( $\text{\AA}$ ),

$I$  = current (mA),

$V$  = voltage (kV),

$t$  = time (minutes) and

$G$  = gap factor. For this unit = 5.

Therefore, for  $I = 25$  mA,  $V = 0.75$  kV,  $t = 10$  mins,  $G = 5$  ;

$$\underline{d = 937.5 \text{ \AA} \text{ i.e. } 93.75 \text{ nm.}}$$

A coating time of 10 minutes would, therefore, give a film of approximately 100 nm thickness.

Once the coating part of the operation had been completed, all three dials were switched off and air admitted to the system through the air bleed valve.

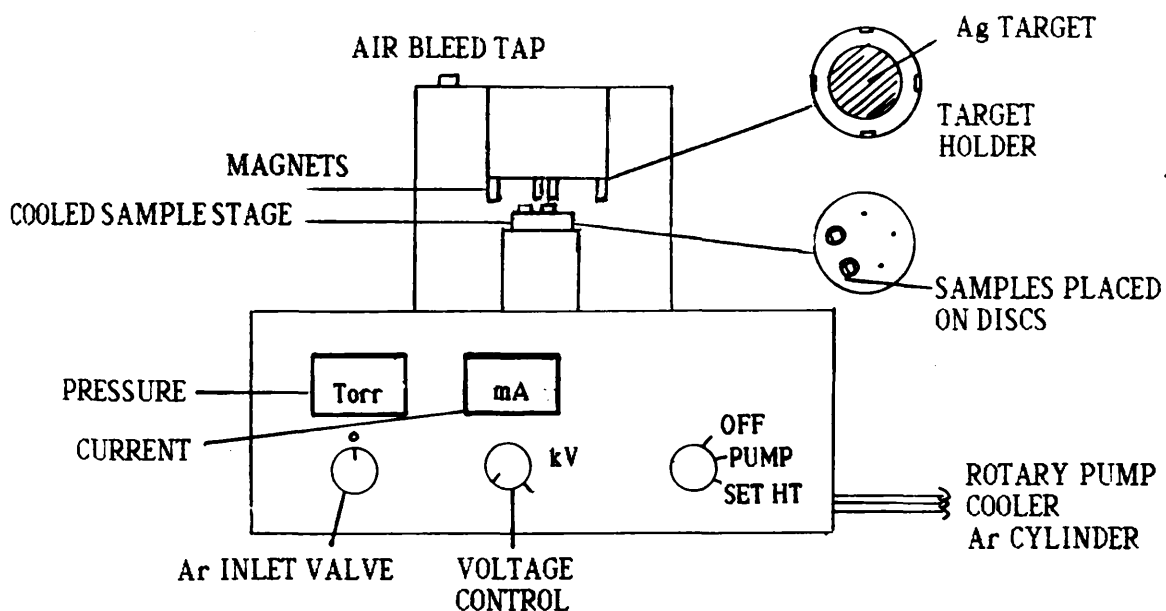


Figure 4.4: Sputter-coating unit.

## Substrates.

### (a) Polycarbonate.

Pieces of this new type of substrate were prepared for coating by rinsing in laboratory grade ethanol and air-drying. Due to the nature of these substrates, they had to be coated with silver on both sides.

### (b) Silica spheres.

Silica sphere substrates were prepared for coating in the following ways :

- (i) A silica suspension was allowed to dry slowly in air to give plates of semi-transparent or opaque silica. The plates were then stuck onto glass with adhesive and coated with the required thickness of silver.
- (ii) Silica spheres dried by rotary evaporation were ground thoroughly (mortar/pestle) and applied on a piece of glass which had been coated with an even layer of adhesive (araldite or 3M spray-glue). Excess silica was removed and another piece of glass was placed over the spheres and subjected to pressure (bulldog clip) for 24 hours. This produced a fairly even layer of silica which could be silver coated.

## 4.4 Spectroscopy.

### 4.4.1 Raman spectroscopy.

A schematic diagram of the laser Raman system used is displayed in figure 4.5.

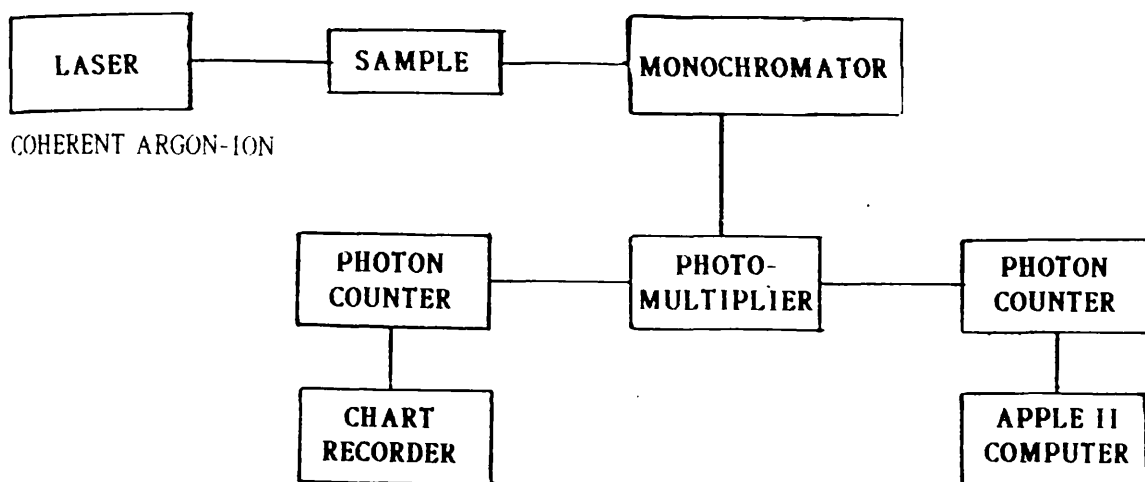


Figure 4.5: Laser Raman system.

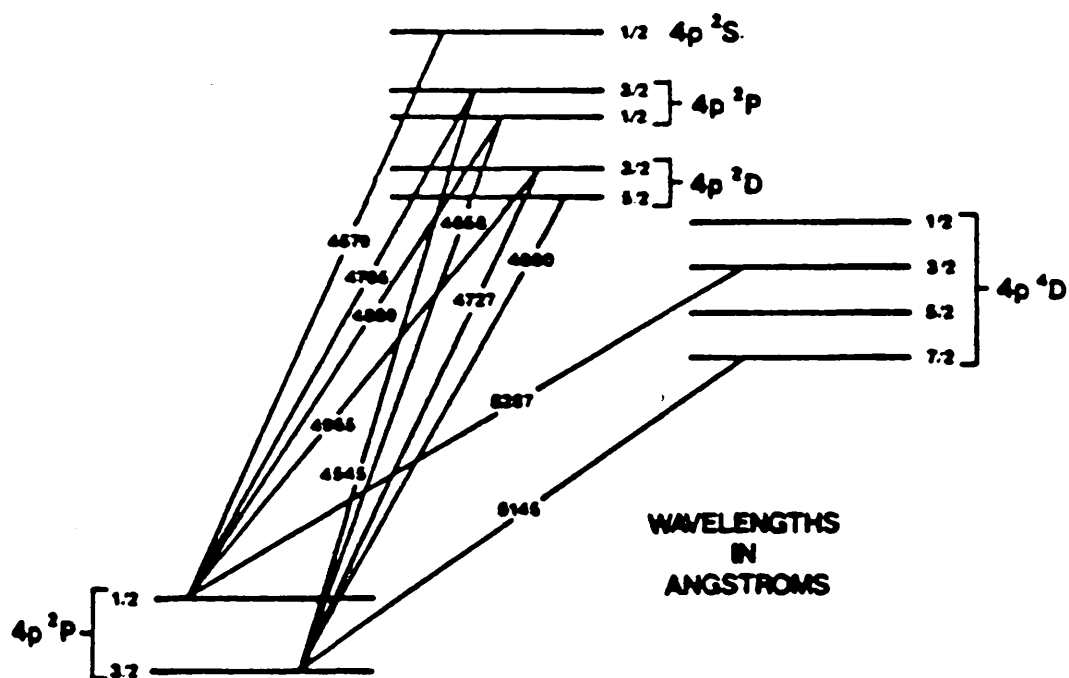


Figure 4.6: Lasing transitions in an argon-ion laser.

All Raman experiments were carried out with the following apparatus :

LASER: Coherent Innova 70 Argon-ion laser. Exciting lines 457.5 - 514.5 nm. Figure 4.6 shows an energy level diagram of the lasing transitions.

SPECTROMETER: Spex Ramalog IV spectrometer.

PHOTOMULTIPLIER TUBE: RCA.

PHOTON COUNTING SYSTEM: Spex.

RECORDER: Servoscribe chart recorder.

Typical operating conditions.

Laser power : 100 mW at sample.

Scan speed :  $1000 \text{ cm}^{-1} \text{ min}^{-1} / 30 \text{ steps s}^{-1}$ .

SERS experiments (figure 4.7).

In each case, SERS substrates were immersed in the appropriate adsorbate solution for at least two minutes prior to use. Adsorbate solutions were normally contained in small petri-dishes, except in the case of vapour-deposited surfaces where the substrate was either placed on a drop of adsorbate solution or spotted with a small amount of solution and dried.

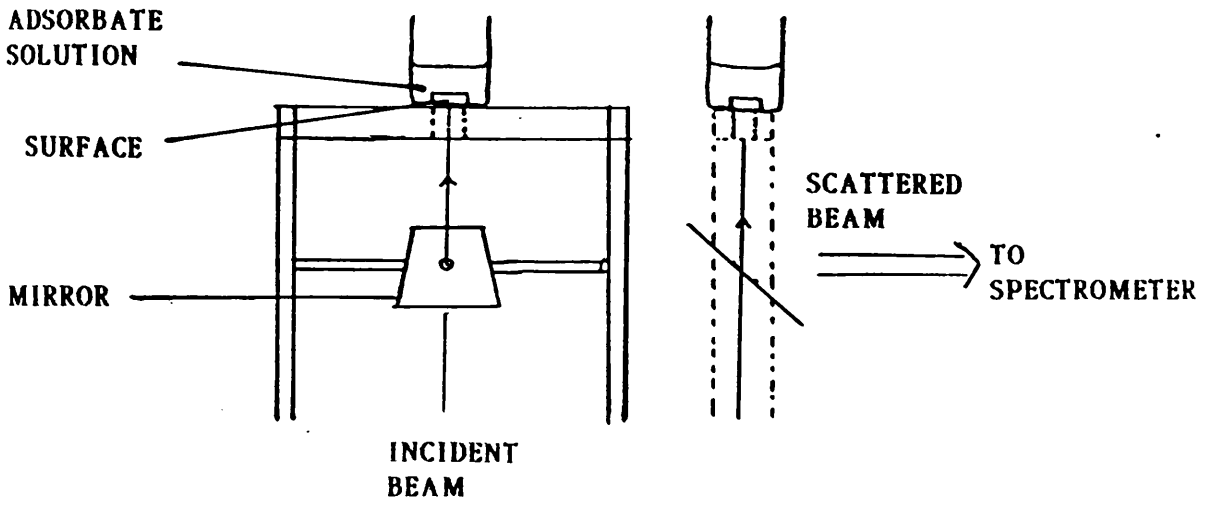


Figure 4.7: SERS experiments.

SERS experiments with gases: use of a vacuum line.

(a) Hydrogen sulphide gas/silver slides.

A lecture-bottle of H<sub>2</sub>S was used.

A dry ice/chloroform slush bath (-75°C) was prepared in a Dewar flask. An empty vessel fitted with a Rotaflo tap and quickfit connections was placed in the slush bath. Hydrogen sulphide was admitted into the vessel *via* a pasteur pipette/teflon tube from the gas cylinder. The H<sub>2</sub>S liquefied and collected at the bottom of the vessel.

Several pieces of silver coated microscope slides were placed in a second vessel, equipped with a side-arm and 10 mm<sup>2</sup> quartz cell in addition to a Rotaflo tap and quickfit connections. This vessel was attached to a vacuum line along with the vessel containing H<sub>2</sub>S. A Dewar flask, filled with liquid nitrogen, was placed round the vessel containing H<sub>2</sub>S liquid. The vessel containing the silver slides was evacuated to 10<sup>-6</sup> Torr and H<sub>2</sub>S was allowed to diffuse into this vessel by removing the liquid nitrogen from around the other vessel and allowing it to warm up gradually.

(b) Benzene/pyridine vapour/silver slides.

Several pieces of silver slides were placed in the quartz cell part of a vacuum/u.v. vessel (described above). One drop of benzene or pyridine was placed in the other half of the vessel. This part of the

vessel was cooled in liquid nitrogen, solidifying the liquid. The vessel was then evacuated to  $10^{-5}$  Torr and isolated from the vacuum line.

The liquid warmed up, liquefied and vapourised.

The main problems associated with this method resulted from the condensation of the benzene/pyridine in the vessel.

#### 4.4.2 Electronic absorption spectroscopy.

All absorption spectra were obtained from a Perkin-Elmer Lambda 9 U.V./vis./n.i.r. spectrometer. Dilute solutions of species under investigation were placed in 10 mm<sup>2</sup> quartz cells.

#### 4.4.3 Nuclear magnetic resonance (n.m.r.) spectroscopy.

<sup>1</sup>H n.m.r. spectra were obtained from a 200 MHz Bruker n.m.r. spectrometer.

#### 4.4.4 Infra-red spectroscopy.

Infra-red spectra were obtained from 8 mm diameter KBr discs of samples on a Perkin-Elmer PE 93 infra-red spectrometer. A Philips P9800 FT-ir spectrometer was used for some samples.

#### 4.4.5 Scanning electron microscopy (SEM).

##### (a) Preparation of samples.

Samples were cut to approximately 10 mm square. They were mounted on small stainless steel stubs which were covered with a thin

layer of silver paint. Once the silver paint had dried completely, the samples were ready for SEM study.

In order to give acceptable images, SEM samples must be conductive. This normally entails coating samples with a thin, even layer of gold/palladium. As all the samples which required SEM analysis were already coated with silver of some kind, this initial step was unnecessary.

(b) SEM experiments.

A Philips scanning electron microscope was used. The maximum possible magnification was x 100,000.

CHAPTER FIVE.

STUDIES OF DISUBSTITUTED 2,2'-BIPYRIDINES AND  
TRIS-BIPYRIDYL RUTHENIUM(II) COMPLEXES.

## 5. STUDIES OF DISUBSTITUTED 2,2'-BIPYRIDINES AND TRIS-BIPYRIDYL RUTHENIUM (II) COMPLEXES.

### 5.1 Characterisation of bipyridyl ligands.

As detailed in chapter 4, three substituted 2,2'-bipyridine ligands were prepared. A brief account of the spectroscopic and analytical evidence obtained is now presented.

#### 5.1.1 2,2'-bipyridine-4,4'-dicarboxylic acid (diacbipy).

The infra-red spectrum of this ligand displayed characteristic hydroxyl stretching at  $3400\text{ cm}^{-1}$  and carbonyl stretching at  $1700\text{ cm}^{-1}$ . Heteroaromatic C—H stretching modes were observed at 3000-3100  $\text{cm}^{-1}$ .

Microanalysis gave the following results:

Found: C: 49.95%; H: 2.70%; N: 9.83%.

Requires: C: 59.00%; H: 3.30%; N 11.50%.

Although, superficially, these results appear extremely inaccurate, it should be noted that the product was extremely impure and recrystallisation proved impossible. Interpretation of the results on the basis of C/H/N ratios gave the following:

Found: C: 5.92; H: 3.85; N: 1.00.

Requires: C: 6.00; H: 4.00; N: 1.00.

Taking into account the purity of the product, it is clear that

2,2-bipyridine-4,4'-dicarboxylic acid was formed.

### 5.1.2 Diethyl 2,2'-bipyridine-4,4'-dicarboxylate (diesbipy).

The final product obtained was fairly pure and crystalline. The infra-red spectrum of the product displayed a clear aryl-substituted ester carbonyl stretching mode at  $1730\text{ cm}^{-1}$ . The melting point of the product ( $159\text{-}160^{\circ}\text{C}$ ) was within one degree of the value quoted in the literature (198).

The analytical data obtained was as follows:

Found: C: 54.93; H: 4.47; N: 7.97.

Requires: C: 64.00; H: 5.33; N: 9.33.

C/H/N ratios were as follows:

Found: C: 16.10; H: 15.72; N: 2.00.

Requires: C: 16.00; H: 16.00; N: 2.00.

The most conclusive proof of the identity of the product came from the  $^1\text{H}$  n.m.r. spectrum (figure 5.1).

The assignment of the spectrum is indicated overpage (labelling: figure 5.1).

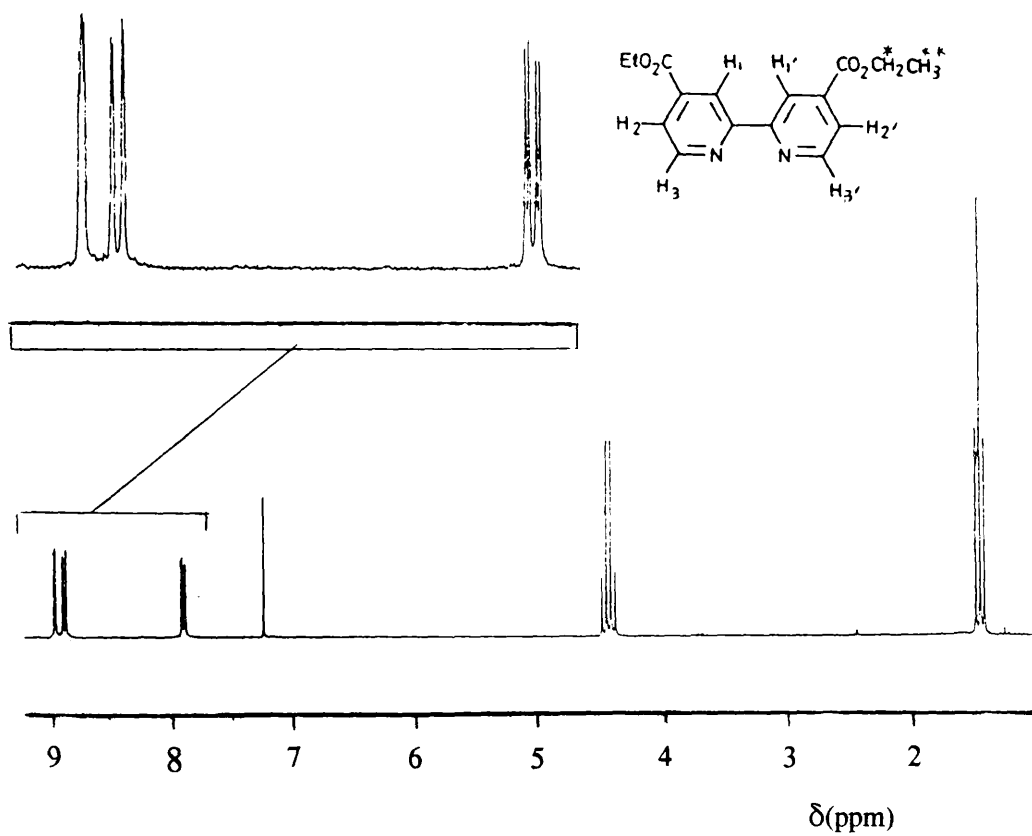


**Figure 5.1:**  $^1\text{H}$  n.m.r. spectrum of diethyl 2,2'-bipyridine-4,4'-dicarboxylate. Solvent:  $\text{CDCl}_3$ .

<u>Chemical shift</u>		<u>assignment</u>	<u>coupling</u>
1.44 ppm	triplet ; integral 6	2 methyls	$J_{H^{**}H^*}$
4.44 ppm	quartet ; integral 4	2 methylene	$J_{H^*H^{**}}$
7.89- 7.92 ppm	2 doublets ; int. 1,1	H3 H3'	$J_{H_3H_2}$ $J_{H_3'H_2'}$
8.84 ppm	2 doublets ; int. 1,1	H2 H2'	$J_{H_2H_3}$ $J_{H_2'H_3'}$
8.94 ppm	quartet ; int. 2	H1 H1'	$J_{H_{1,1'}H^{**}}$

### 5.1.3 4,4'-diamino-2,2'-bipyridine (diambipy).

#### (a) 2,2'-bipyridine-1,1'-dioxide.

The infra-red spectrum of this compound showed nitrosyl stretching at  $1250\text{ cm}^{-1}$  in addition to characteristic heteroaromatic C—H stretching and breathing modes.

Microanalysis gave the following data:

Found: C: 63.93; H: 4.20; N: 14.94.

Requires: C: 63.83; H: 4.26; N: 14.89.

All these results are consistent with the formation of the N,N-dioxide compound.

#### (b) 4,4'-dinitro-2,2'-bipyridine-1,1'-dioxide.

The i.r. spectrum of this product showed a band at  $1290\text{ cm}^{-1}$ , ascribed to the nitrosyl stretching mode. Bands were also observed at

1340 and 1520  $\text{cm}^{-1}$  due to C—NO<sub>2</sub> (conjugated) stretch (symmetric and asymmetric).

Analytical data:

Found: C: 40.49; H: 1.88; N: 19.00.

Requires: C: 43.17; H: 2.16; N: 20.14.

Corresponding C/H/N ratios:

Found: C: 2.46; H: 1.38; N: 1.00.

Requires: C: 2.50; H: 1.50; N: 1.00.

Considering the impurity of the yellow material obtained, these results correlate fairly well.

(c) 4,4'-diamino-2,2'-bipyridine.

Infra-red analysis of the recrystallised product revealed N—H bend at 1600  $\text{cm}^{-1}$  and N—H stretch (symmetric and asymmetric) at 3410 and 3300  $\text{cm}^{-1}$ , respectively.

Analytical data:

Found: C: 63.77; H: 5.42; N: 28.93.

Requires: C: 64.52; H: 5.38; N: 30.11.

C/H/N ratios:

Found: C: 2.57; H: 2.62; N: 1.00.

Requires: C: 2.50; H: 2.50; N: 1.00.

These analyses agree fairly well with the theoretical data. Even after several recrystallisations, the product still appeared impure.

Mass spectrometry was employed in an attempt to confirm the identity of the product. The parent molecular ion peak was at 186 g (molecular weight of 4,4'-diamino-2,2'-bipyridine) and peaks were observed at 170 and 154 g, indicating the loss of each amino substituent.

## 5.2 Absorption spectroscopy of ruthenium(II) complexes of substituted 2,2'-bipyridyl ligands.

### 5.2.1 Ru(bipy)<sub>3</sub>Cl<sub>2</sub> and Ru(bipy)<sub>3</sub>I<sub>2</sub>.

The chemistry of the tris(2,2'-bipyridyl) ruthenium(II) ion has been known for many years (206) (207). The attention paid to [Ru(bipy)<sub>3</sub>]<sup>2+</sup> and related complexes in the fields of photochemistry and electrochemistry is, in part, due to the chemical stability of the species. These complexes, in addition to analogous 1,10-phenanthroline complexes, have been used as dyes in luminescent solar collectors (199). The complex, as produced by the method previously described, is a racemic mixture of (+) and (-) enantiomers. The chirality of the species is not relevant to this study as conventional Raman techniques are insensitive to optical activity.

Pure Ru(bipy)<sub>3</sub>Cl<sub>2</sub> and Ru(bipy)<sub>3</sub>I<sub>2</sub> were produced, showing no evidence of the formation of any by-products. The characteristic electronic absorption spectra of these complexes (199) afforded a

simple method of characterisation.

Figure 5.2 shows the absorption spectrum of a  $1.2 \times 10^{-4} \text{ mol l}^{-1}$  solution of  $\text{Ru}(\text{bipy})_3\text{I}_2$  compared with the spectrum of a dilute solution of  $\text{RuCl}_3 \cdot 3\text{H}_2\text{O}$ . An intense maximum is observed at 451 nm. In addition, there is a shoulder present at approximately 415 nm. The absorption maximum is assigned as a metal (d)  $\rightarrow$  ligand ( $\pi^*$ ) charge-transfer transition. Two one-electron transitions lie within the main absorption band. These involve transitions from the d orbitals of e symmetry, under the  $D_3$  point group, to the  $a_2$  and e components of the  $\pi^*$  ligand orbitals (206)(208). Figure 5.3 illustrates these transitions.

The other ruthenium(II) complexes produced were also characterised by absorption spectroscopy. Table 5.1 summarises known (199) absorption maxima and extinction coefficient data for each of the other complexes prepared.

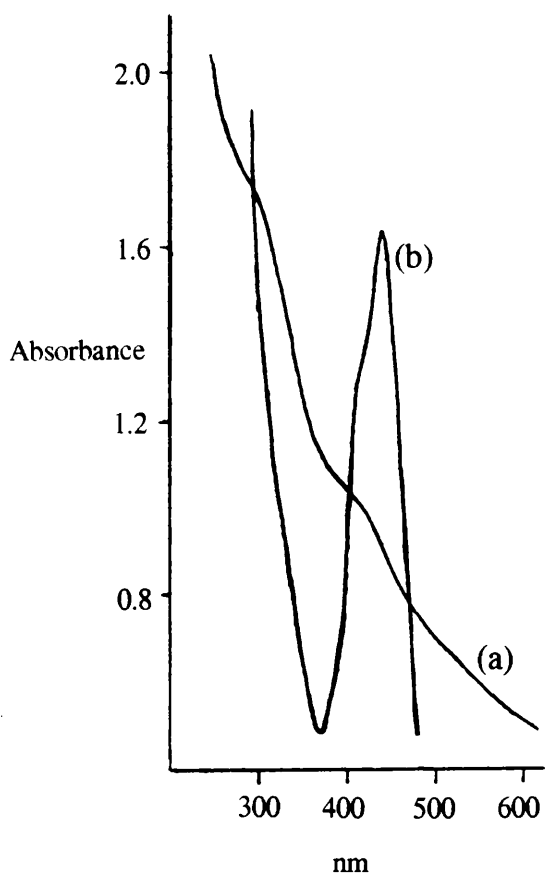
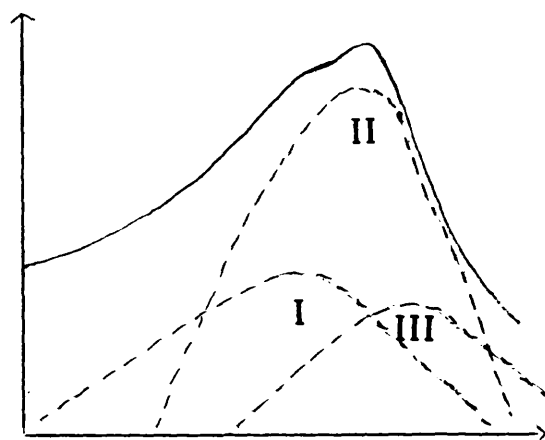
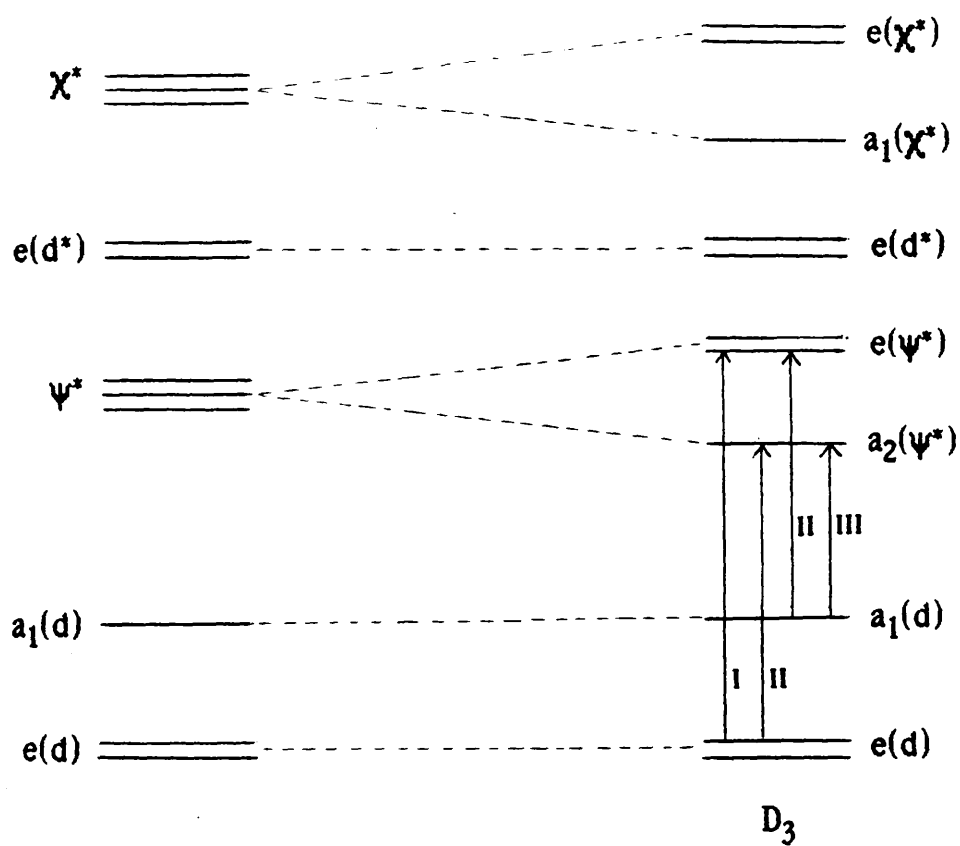


Figure 5.2: Electronic absorption spectra of (a) a dilute aqueous solution of  $\text{RuCl}_3 \cdot 3\text{H}_2\text{O}$  and (b) a  $1.2 \times 10^{-4} \text{ mol l}^{-1}$  aqueous solution of  $\text{Ru}(\text{bipy})_3\text{I}_2$ .



**Figure 5.3: Electronic transitions of the  $\text{Ru}(\text{bipy})_3^{2+}$  molecule (208).**

Table 5.1: Spectroscopic properties of tris(2,2'-bipyridyl)-  
ruthenium(II) complexes (reference (199): solvent: ethanol/  
methanol (4:1 v/v)).

<u>Complex.</u>	<u><math>\lambda_{\text{max}}</math> (abs.) (nm)</u>	<u>extinction coefficient, <math>\epsilon_s \times 10^4</math></u>
Tris-(2,2'-bipyridine) ruthenium(II)	450	1.43
------(4,4'-bisethoxycarbonyl)-----	464	2.33
------(4,4'-diamino)-----	504	1.05
------(4,4'-diphenyl)-----	473	2.80
------(4,4'-dimethyl)-----	455	1.70

5.2.2 Tris(diethyl-2,2'-bipyridine-4,4'-dicarboxylate) ruthenium(II)  
ditetrafluoroborate, Ru(diesbipy)<sub>3</sub>[BF<sub>4</sub>].

As discussed in section 4.1.3 (a), crystallisation of the complex did not occur. In order to characterise the product, a quantity of the reaction mixture concentrate was diluted in distilled water (1:100) to give a bright orange solution. Two portions were diluted in this manner. The absorption spectrum of one of the solutions is displayed in figure 5.4. The two solutions display intense metal (d)  $\rightarrow$  ligand ( $\pi^*$ ) charge-transfer maxima at 466 and 465 nm, corresponding well to the expected maxima as detailed in table 5.1. The spectra did not indicate the presence of any by-products or impurities, although NaBH<sub>4</sub> is

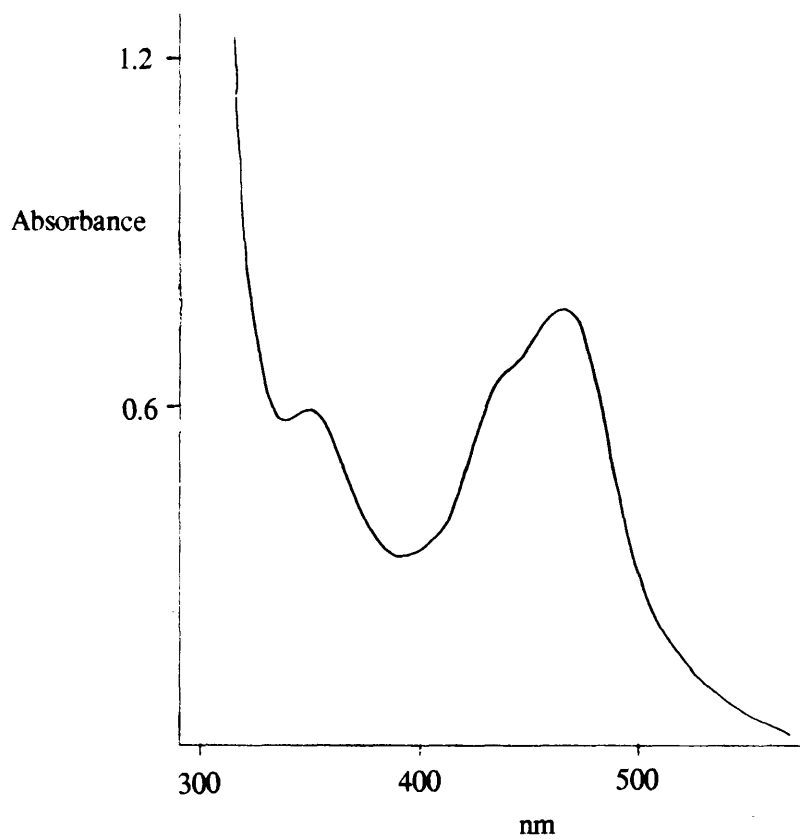


Figure 5.4: Electronic absorption spectrum of an  $8.9 \times 10^{-4} \text{ mol l}^{-1}$  aqueous solution of  $\text{Ru}(\text{diesbipy})_3[\text{BF}_4]_2$ .

certainly present as a result of the preparative procedure. The concentrations of the solutions, determined from the Beer-Lambert law and extinction coefficient data (table 5.1), were  $8.9 \times 10^{-4}$  and  $9.3 \times 10^{-4}$  mol l<sup>-1</sup>, respectively. The shift in the absorption maxima to longer wavelength, with substitution in the C<sub>4</sub> and C<sub>4'</sub> positions, is as expected on the basis of molecular orbital calculations (209).

### 5.2.3 Tris(4,4'-diamino-2,2'-bipyridine) ruthenium(II) dichloride,

#### Ru(diambipy)<sub>3</sub>Cl<sub>2</sub>.

As with the diester species, this complex did not crystallise. A 1:20 dilution in distilled water of the dark red reaction concentrate was prepared. Initially this diluted solution was red. After approximately one week, however, it had become deep blue.

In order to obtain an absorption spectrum of the blue solution, a small volume was forced through glass microfibre paper (to filter some material which had deposited in the solution). The filtered solution was light red in colour. The absorption spectra of each of these solutions is displayed in figure 5.5. The blue solution has maxima at 650.8 and 514.4 nm and the light red solution has an intense maximum at 503.4 nm. It is clear that the light red solution contains the 4,4-diamino substituted complex since the absorption maximum corresponds well with the value from table 5.1.

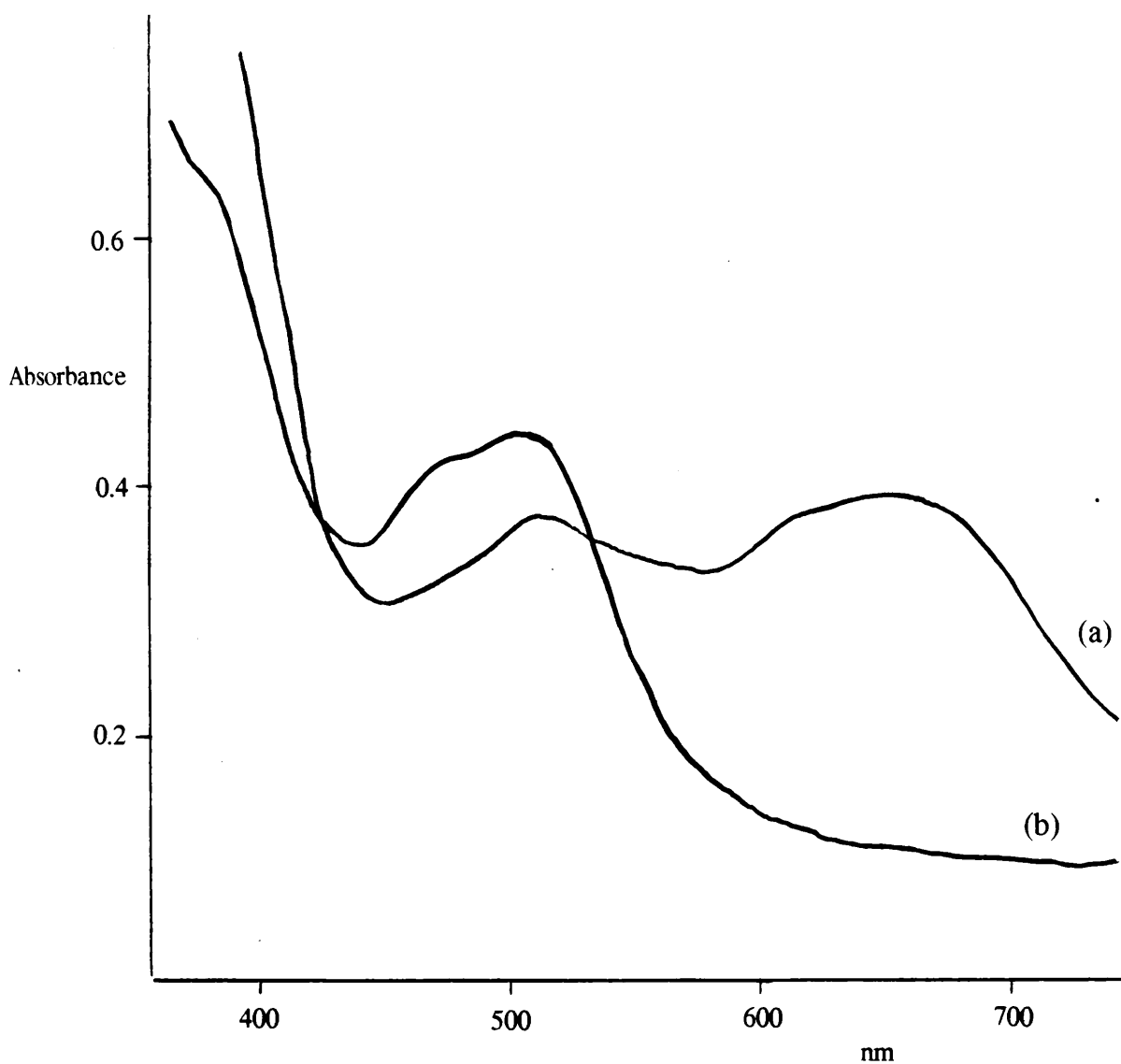


**Figure 5.5:** Electronic absorption spectra of (a) Ru(diambipy)<sub>3</sub>Cl<sub>2</sub> reaction concentrate in distilled water after one week (blue) and (b) the same solution after draining through glass microfibre paper (light red).

Dilution of the reaction concentrate in ethanol (1:20) gave a wine coloured solution. This solution was stable: no colour change was observed.

#### Purification by column chromatography.

##### (a) Blue solution (reaction concentrate in water).

Although the blue solution adsorbed onto the sephadex column, it did not travel. More polar solvents such as ethanol and methanol and non-polar solvents such as carbon tetrachloride did not elute the blue material.

##### (b) Wine solution (Reaction concentrate in ethanol).

This solution adsorbed onto the sephadex column and migrated. Two fractions were obtained and the absorption spectra of each was obtained (figure 5.6). Fraction 1 was green and showed a maximum at 631.6 nm. Fraction 2 was red and showed a maximum at 504 nm. Clearly, fraction 2 is the tris-ligand complex. A possible identity of fraction 1 is the bis-ligand neutral complex,  $\text{Ru}(\text{diambipy})_2\text{Cl}_2$ . The formation of impurities such as this, in this category of reaction, is well known (206). The absorption spectrum of  $\text{Ru}(\text{bipy})_2\text{Cl}_2$ , however, has a maximum at 525 nm: such a large shift (525  $\rightarrow$  631.6 nm), on substitution of the 2,2'-bipyridyl ligands, is unlikely. Fraction 1 may, therefore, be the tris-ligand ruthenium(III) complex.

The purified ethanolic solution of  $\text{Ru}(\text{diambipy})_3\text{Cl}_2$  was suitable for

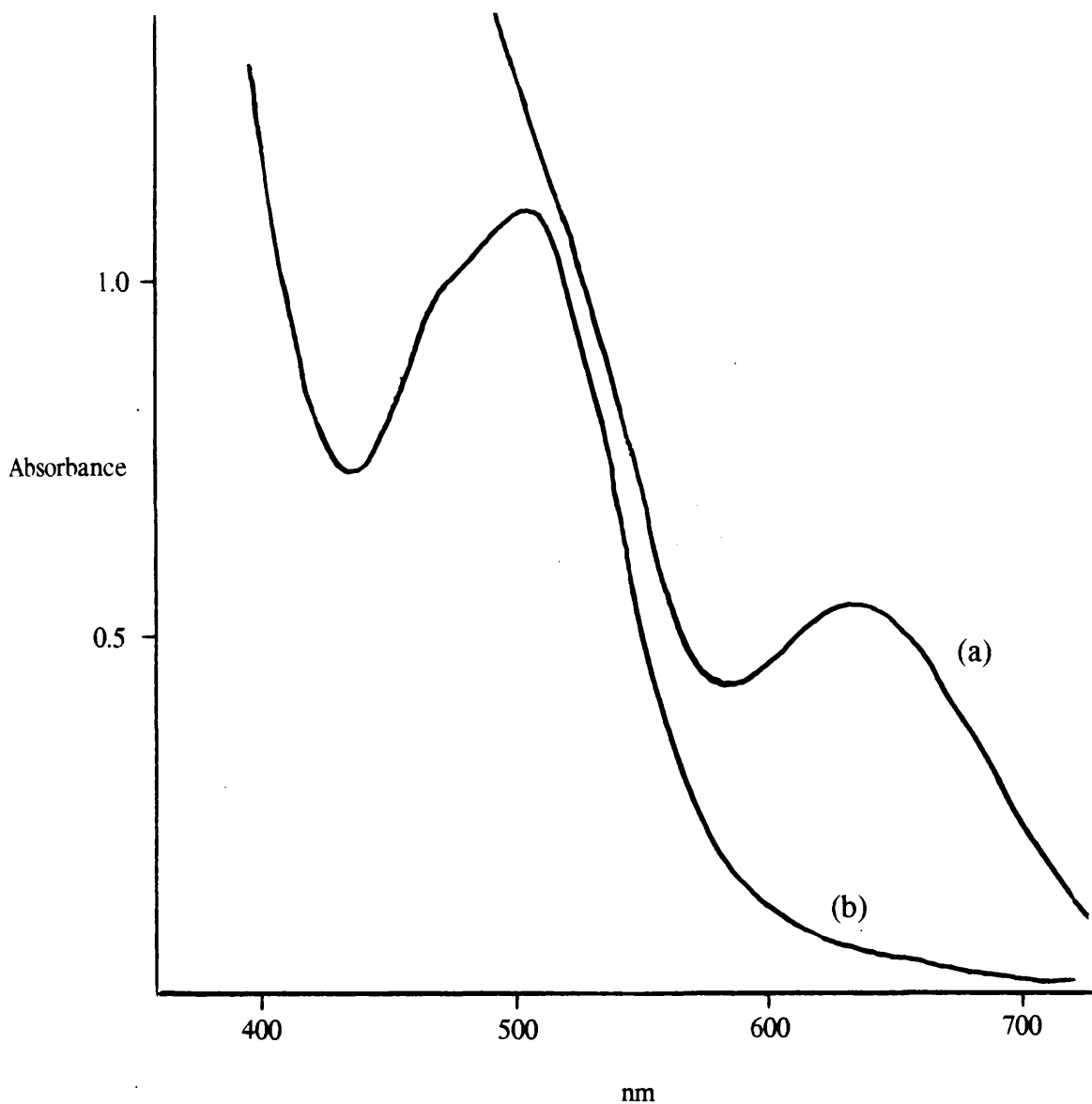


**Figure 5.6: Electronic absorption spectra of fractions obtained from the column chromatography of a solution of the Ru(diambipy)<sub>3</sub>Cl<sub>2</sub> reaction concentrate in ethanol. (a) Fraction 1 (green); (b) fraction 2 (red).**

use in SERS experiments.

### Reaction of $[\text{Ru}(\text{diambipy})_3]^{2+}$ with acid.

The SERS of the protonated diamine complex was of interest. To this end, a 5 ml sample of the complex in ethanol was treated with 1 ml of approximately  $4 \text{ mol l}^{-1}$  hydrochloric acid. It was observed that, after several hours, the initially red solution had become deep blue (in an identical manner to the reaction concentrate/water solution).

Absorption spectra of the solution, at several intervals, were obtained.

The spectrum of the solution after treatment with concentrated aqueous sodium hydroxide was also obtained. Figure 5.7 displays all these spectra and the spectrum of a solution of the complex in ethanol with 2 ml of water added. The spectra of the complex after treatment with acid show the progressive appearance and strengthening of a maximum at approximately 650 nm which eventually becomes the dominant absorption in the visible region. After neutralisation with sodium hydroxide, the blue solution once again became red and the 504 nm absorption was observed. The spectrum of the complex/ethanol/water mixture shows a small absorption around 650 nm.

Clearly, a new species is forming on addition of acid and also water (at a considerably slower rate), but not with ethanol.

The progress of the complex/ethanol/acid reaction was followed more accurately (figures 5.8 and 5.9). The reaction exhibited a half-

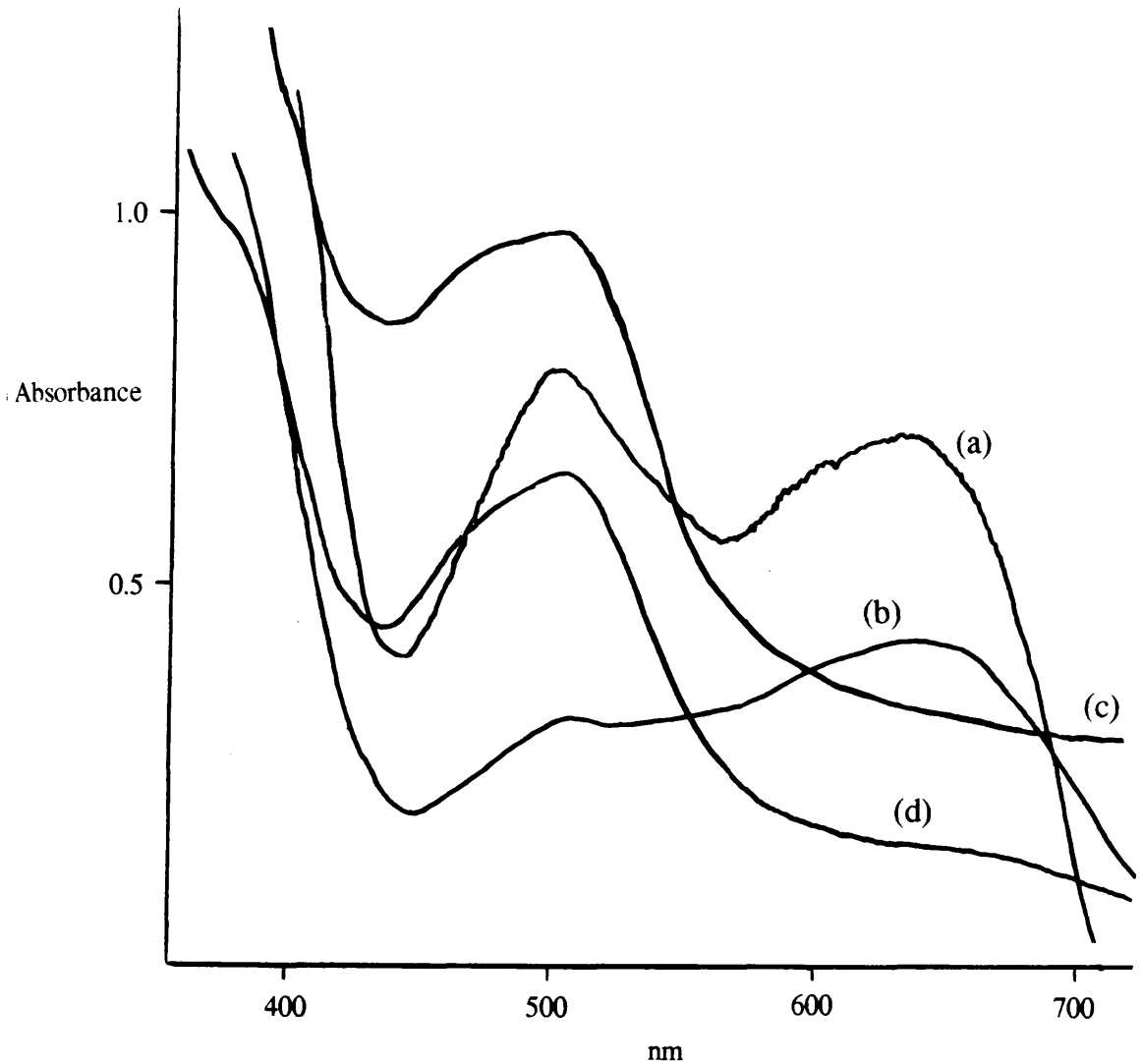


**Figure 5.7:** Electronic absorption spectra of a 5 ml sample of  $\text{Ru}(\text{diambipy})_3\text{Cl}_2$  in ethanol (a) treated with 1 ml of 4 molar HCl, after 5 hours, (b) the same solution after 16 hours, (c) the same solution after the addition of 2 ml of dilute aqueous NaOH and (d) the original solution, after treatment with 2 ml of distilled  $\text{H}_2\text{O}$ , after 19 hours.

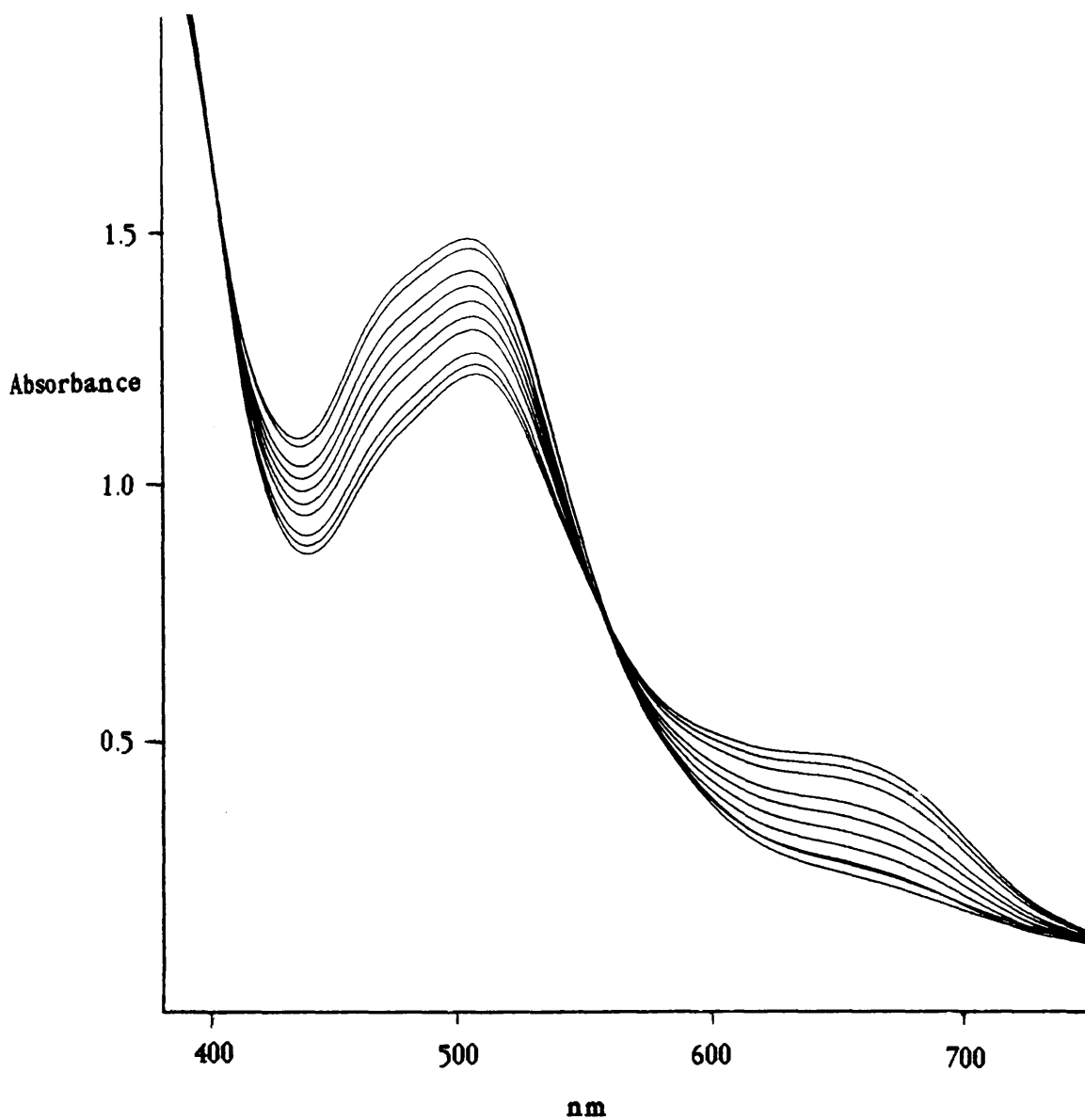
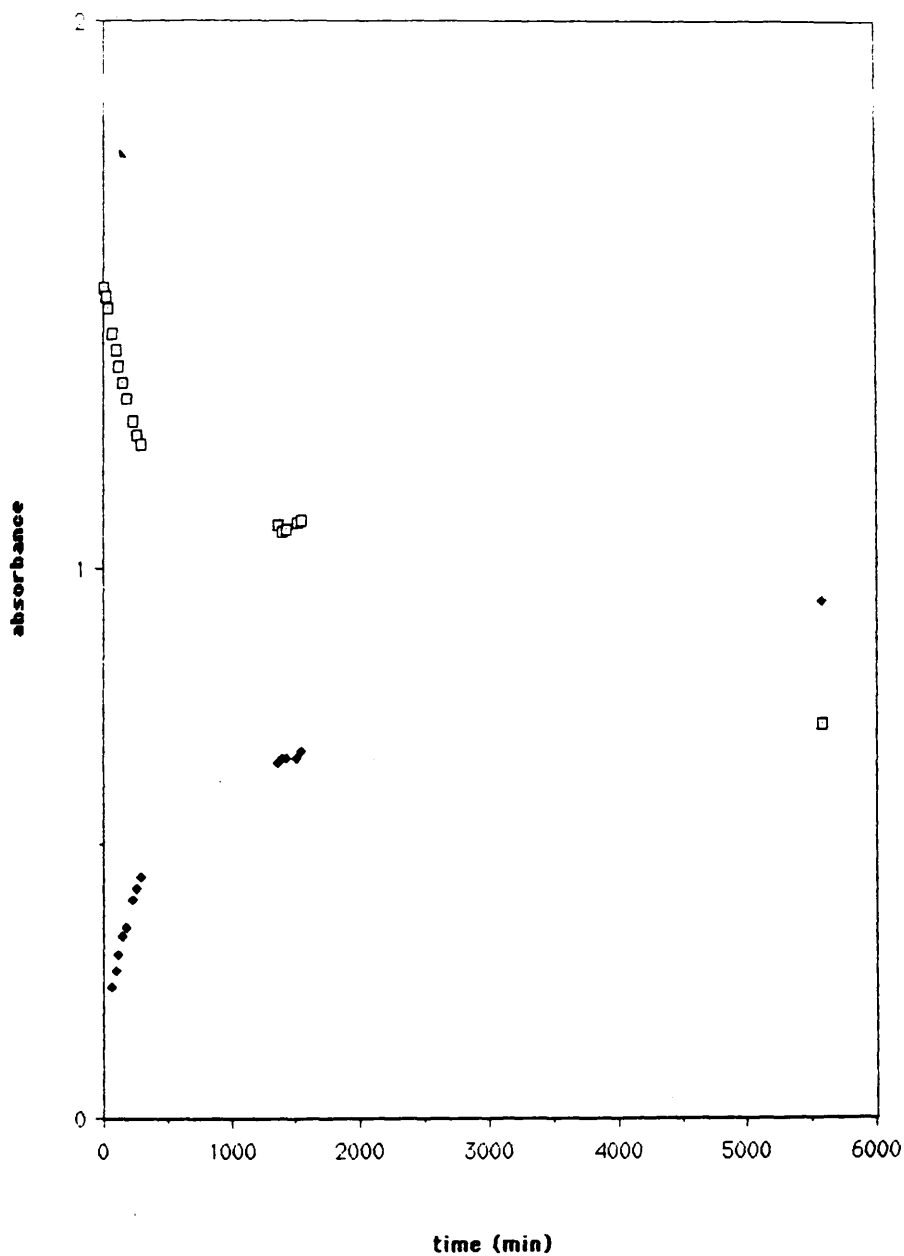


Figure 5.8: Electronic absorption spectra, at various intervals, of a 10 ml sample of Ru(diambipy)<sub>3</sub>Cl<sub>2</sub> in ethanol with 1 ml of 4 molar HCl added.



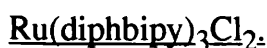
**Figure 5.9:** Graph of the reaction of Ru(diambipy)<sub>3</sub>Cl<sub>2</sub> with HCl with time. □ indicates the absorbance of the 504 nm band and ◆ indicates the absorbance of the 650 nm band.

life of approximately 100 hours, with the blue absorption becoming dominant beyond this point.

The identity of the blue species is probably the tris-ligand ruthenium(III) ion. It is highly unlikely that the protonation of the 4,4'-diamino substituents of the 2,2'-bipyridyl ligand would cause such drastic changes in the absorption spectrum of the complex. Oxidation of  $[\text{Ru}(\text{bipy})_3]^{2+}$  in acidic media is known (206), but, normally, an oxidising agent such as cerium(IV) or lead(IV) oxide is required. It is possible that the substitution of the 2,2'-bipyridyl ligands makes the ruthenium(II) complex more susceptible to slow oxidation in the acidic environment. This explains the slower rate of oxidation in water and the stability of the ruthenium(II) complex in ethanol, since alcohols do not promote oxidation.

The absorption maximum of the blue ruthenium(III) complex is primarily a ligand( $\pi$ )  $\rightarrow$  metal( $t_{2g}$ ) charge-transfer transition (206).

#### 5.2.4 Tris(4,4'-diphenyl-2,2'-bipyridine) ruthenium(II) dichloride,



A small amount of the solid product was dissolved in absolute ethanol to give a dark red solution. The absorption spectrum of this solution (figure 5.10) displayed several broad maxima, indicating the presence of by-products.

Several samples of the solution were subjected to column chromatography. In each case, three fractions were eluted. The absorption spectra of each of these fractions are shown in figure 5.10.

The main features of the spectra were as follows:

Fraction 1: orange; absorption maximum at 474 nm.

Fraction 2: pink; maxima at 525 and 390 nm.

Fraction 3: yellow; maxima at 525 (weak) and 390 nm.

Fractions 2 and 3 were very close together on the column, but well separated from fraction 1.

Fraction 1 is clearly the  $[\text{Ru}(\text{diphbipy})_3]^{2+}$  complex. The shape and value of the absorption maximum are as expected (table 5.1). Fraction 2 is almost certainly the neutral bis-ligand ruthenium(II) complex.

The absorption spectrum of fraction 3 was similar to that of fraction 2, but with the absorption at 525 nm much reduced in intensity. Since fraction 3 was so close to fraction 2 on the sephadex column, it is likely that the former is  $\text{Ru}(\text{diphbipy})_2\text{Cl}_2$  which, for some reason, travelled at a slower rate through the support.

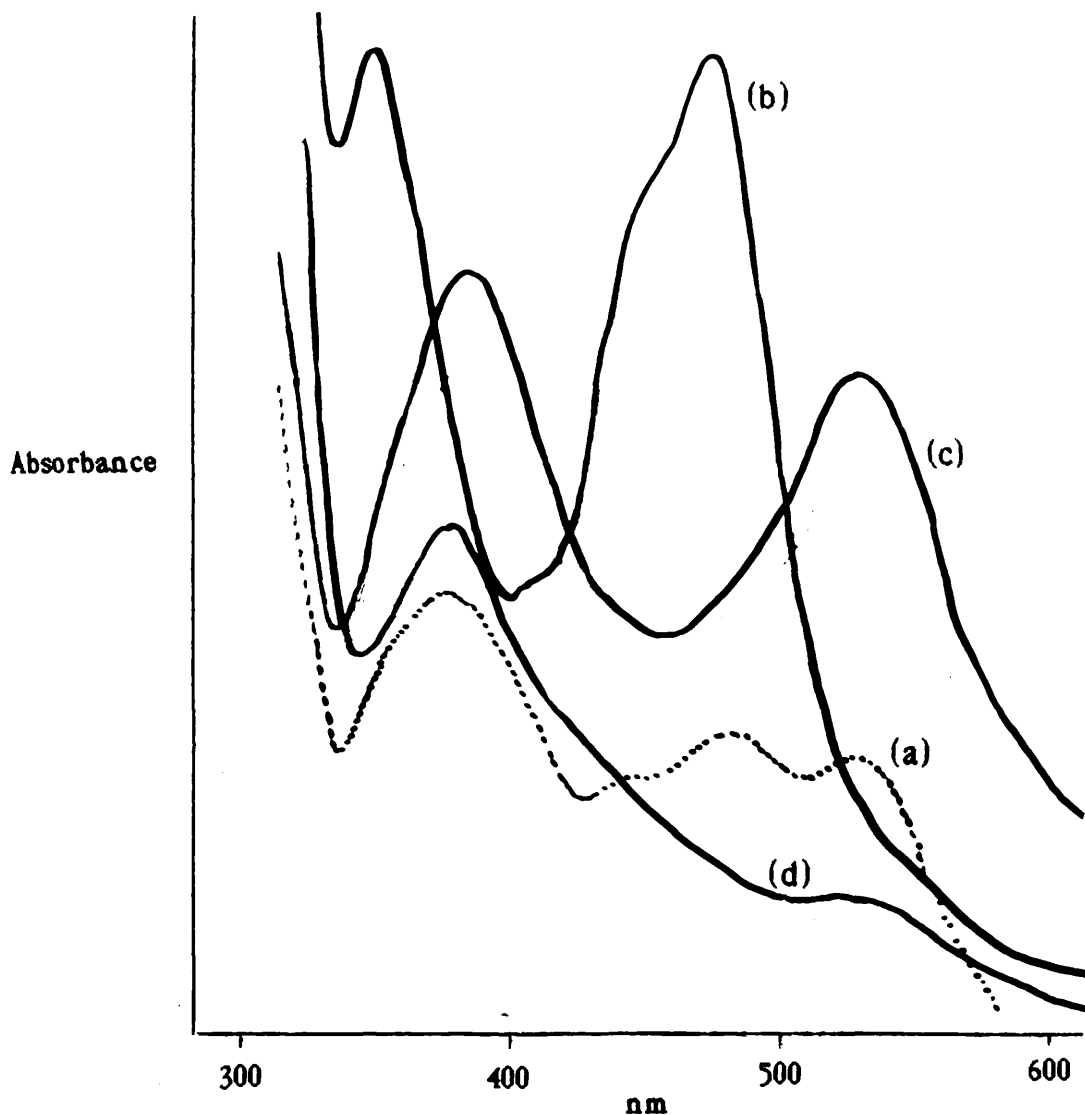


**Figure 5.10:** Electronic absorption spectra of Ru(diphbipy)<sub>3</sub>Cl<sub>2</sub> in ethanol. (a) reaction product (mixture); (b) fraction 1 (orange) from column chromatography of the reaction product; (c) fraction 2 (pink); (d) fraction 3 (yellow). Absorbance data are not indicated as the spectra are presented for comparison of absorption maxima only.

### 5.2.5 Tris(4,4'-dimethyl-2,2'-bipyridine) ruthenium(II) dichloride,



A small amount of the orange product, dissolved in absolute ethanol, gave a very clean absorption spectrum (figure 5.11), with an intense maximum observed at 454.5 nm. This is clearly the metal(d)  $\rightarrow$  ligand ( $\pi^*$ ) transition of the complex, as detailed in table 5.1. Column chromatography yielded only one fraction, indicating the complex, as prepared, was pure.

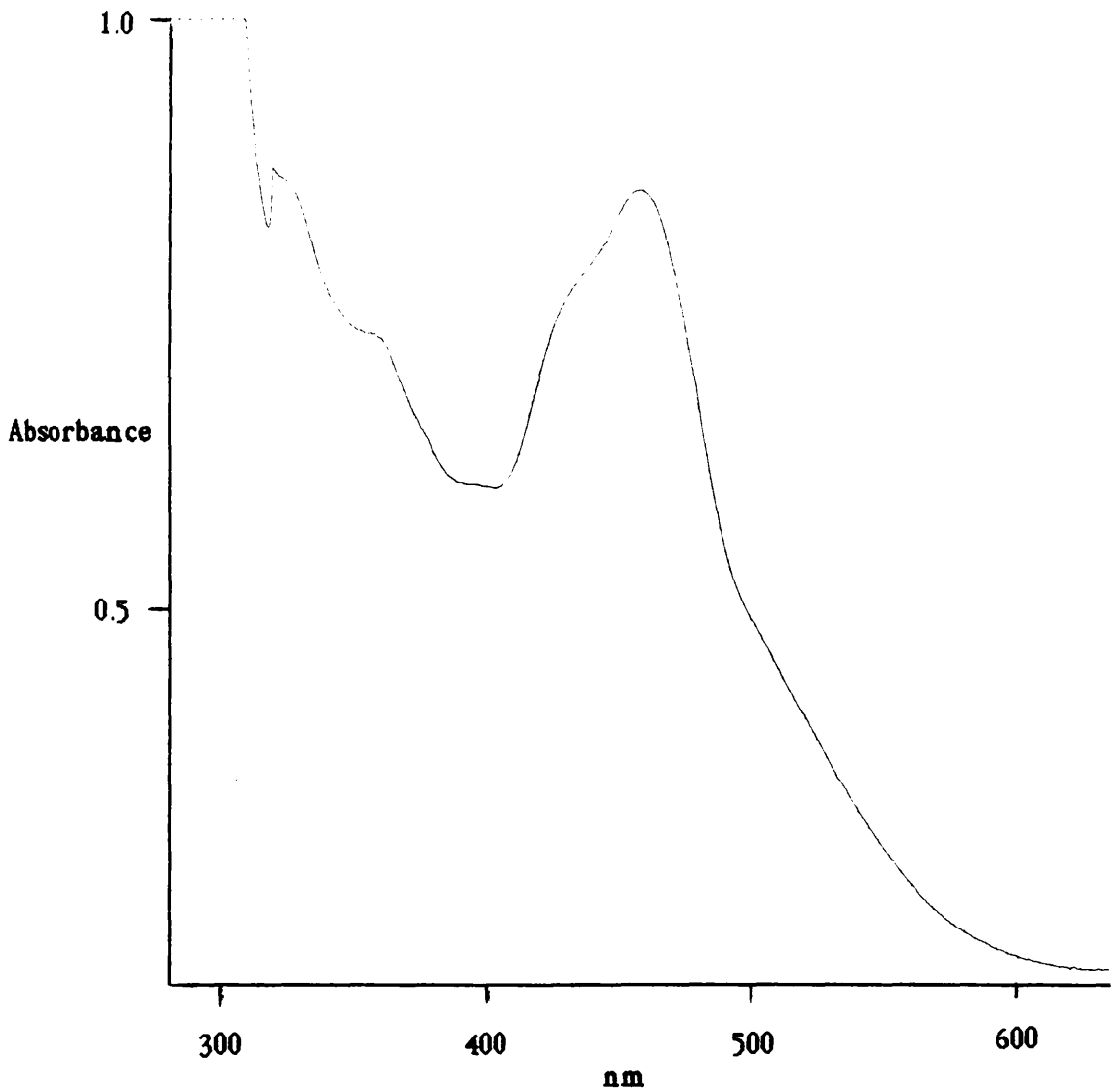


Figure 5.11: Electronic absorption spectrum of a dilute ethanolic solution of Ru(dimebipy)<sub>3</sub>Cl<sub>2</sub>.

**CHAPTER SIX.**

**SPECTROSCOPIC INVESTIGATIONS OF**

**POTENTIALLY SERS-ACTIVE SUBSTRATES.**

## **6. SPECTROSCOPIC INVESTIGATIONS OF POTENTIALLY SERS-ACTIVE SUBSTRATES.**

### **6.1 Introduction.**

As discussed in chapter 3, the overall objective of these studies was to probe the nature of the surface/adsorbate molecule interaction. The primary aim was to find a suitable surface for intensive SERS study. A summary of the most important requirements for a probe surface, specific to these studies, is given at this point.

#### **(a) Range.**

With respect to SERS, it would be advantageous if the surface was able to sense a wide range of adsorbate molecules. In particular, the surface must be active with  $[\text{Ru}(\text{bipy})_3]^{2+}$  and modified analogues.

#### **(b) Reproducibility.**

The surface must be highly reproducible in order that meaningful comparisons can be made of SER spectra of different adsorbate molecules adsorbed on the same type of surface. A surface with a simple, regular morphology would be advantageous.

#### **(c) Ease of production.**

A surface to be subjected to intensive SERS study would, ideally, have a simple and inexpensive preparative procedure.

$[\text{Ru}(\text{bipy})_3]^{2+}$  and analogues were chosen as initial test molecules

since the SER spectrum of  $\text{Ru}(\text{bipy})_3\text{Cl}_2$  has been studied (99) and has shown a high degree of enhancement. The reason for studying disubstituted analogues of  $[\text{Ru}(\text{bipy})_3]^{2+}$  was to address, in part, the question of the influence of co-ordinating groups in adsorbate molecules on SERS enhancement.

Inorganic complexes are advantageous for SERS investigation as they are generally of high symmetry. This gives the possibility of different selection rules for the Raman spectra of free and adsorbed molecules. The  $[\text{Ru}(\text{bipy})_3]^{2+}$  ion is of  $D_3$  symmetry (figure 6.1).

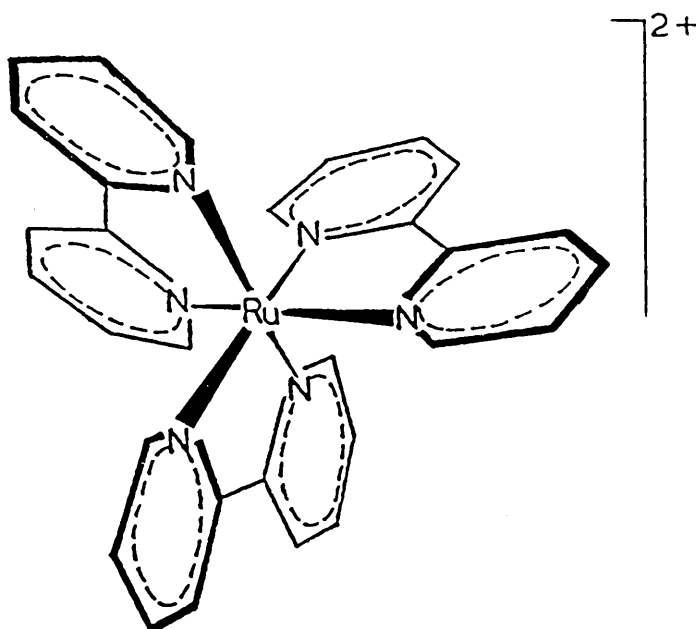


Figure 6.1: Structure of the (+)- $[\text{Ru}(\text{bipy})_3]^{2+}$  cation.

## 6.2 Colloids.

Colloids are potentially useful in the context of this body of work as they provide an ideal control system on account of the vast amount of

work which has already been published. The literature has shown that colloidal SERS-active systems can detect a large variety of chemical species.

### 6.2.1 Silver colloids/Ru(bipy)<sub>3</sub>I<sub>2</sub>.

Figure 6.2 shows the electronic absorption spectrum of a freshly prepared silver colloid sample. The colloid is yellow in colour and displays a strong absorption maximum at 390 nm. This maximum represents the surface plasmon resonance peak and, in this case, is characteristic of roughly spherical metal particles with diameters in the region 5 to 50 nm (79). Figure 6.2 also shows the absorption spectrum obtained when 2 ml of the silver colloid sample was mixed with 2 ml of a  $1 \times 10^{-4}$  mol l<sup>-1</sup> aqueous solution of Ru(bipy)<sub>3</sub>I<sub>2</sub>. It can be seen that the addition of the adsorbate solution induced a red-shift in the surface plasmon maximum: in this case to 500 nm. This was reflected in the colour change of the complex/colloid mixture which became orange. It has been suggested that such a shift is due to the formation of colloidal aggregates. Indeed, it was observed that, after some time, the complex/colloid solution became green and large metal particles were visible in the cell. This process illustrates the disadvantage of colloids in SERS experiments: the precipitation of metal. The maximum that develops at 500 nm, however, renders this system, in the partially

aggregated state, suitable for SERS study with an argon-ion laser since the new surface plasmon resonance falls within the range of  $\text{Ar}^+$  exciting lines, 457.1 to 514.5 nm.

There was no evidence of the formation of a charge-transfer band in the absorption spectrum.

The SERR spectrum of colloidal silver after exposure to  $\text{Ru}(\text{bipy})_3\text{I}_2$  is shown in figure 6.3 ( $\text{Ar}^+$  laser, 488.0 nm excitation). It should be noted that the enhanced spectrum of this system is SERRS as the excitation wavelength is close to both the surface plasmon resonance of the colloidal surface and the metal(d)  $\rightarrow$  ligand( $\pi^*$ ) charge-transfer absorption of the bulk adsorbate. In the region 1000 to 1750  $\text{cm}^{-1}$ , highly intense Raman bands were observed, most ascribed to 2,2'-bipyridyl ring modes. The resonance Raman spectrum of  $\text{Ru}(\text{bipy})_3\text{I}_2$  is also shown in figure 6.3. The enhancement of SERRS over RRS is approximately  $10^6$ . It is also clear that the relative intensities and wavenumbers of the Raman bands in the SERR spectrum compared to those in the RRS, indicating the absence of a chemical bond between the adsorbate molecules and the colloidal surface. The absence of any obvious charge-transfer band in the absorption spectrum of the complex/colloid mixture further confirmed this. SERS enhancement in this system is *via* the electromagnetic (surface plasmon excitation) mechanism.

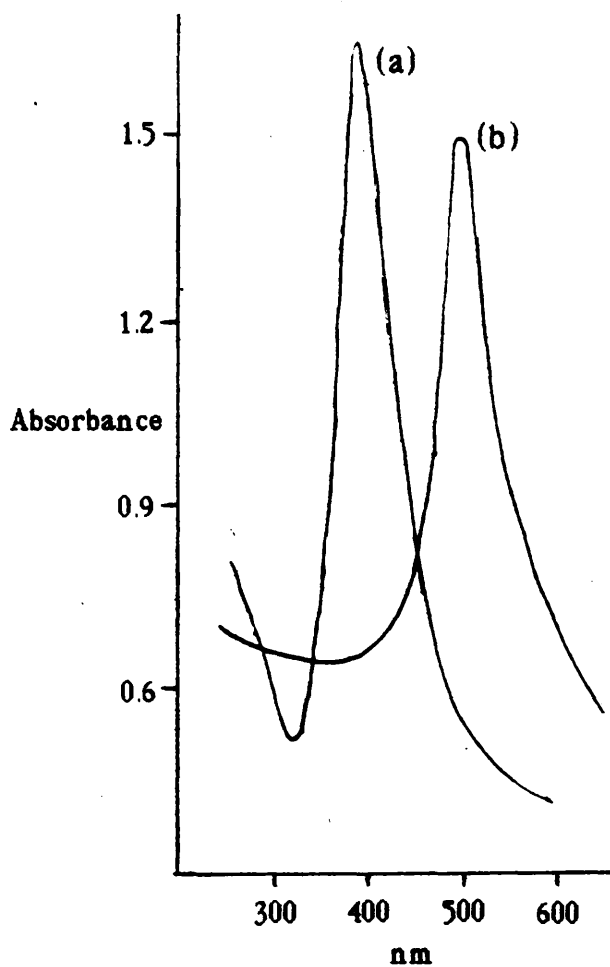
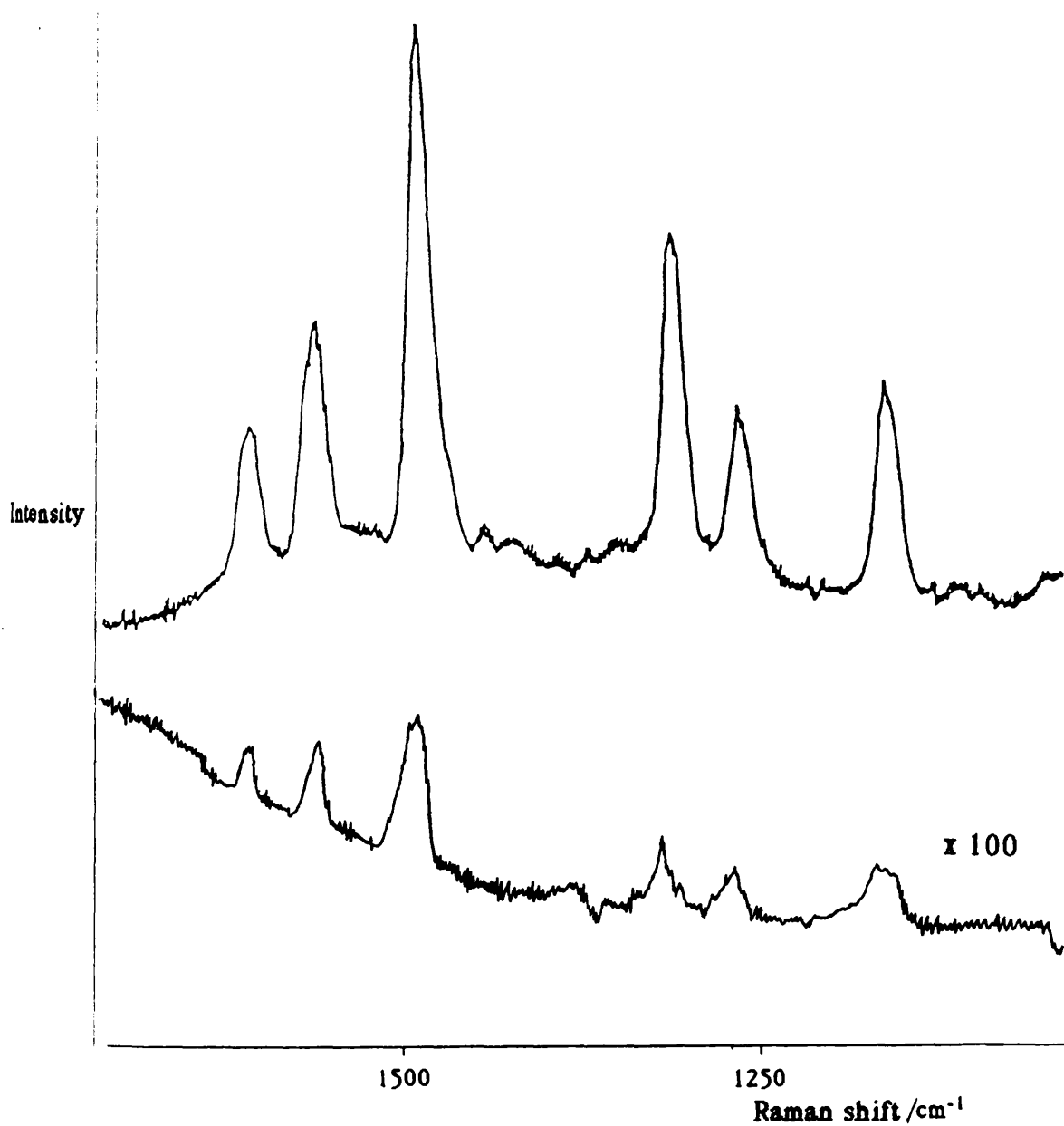


Figure 6.2: Electronic absorption spectra of (a) a freshly-prepared silver colloid sample and (b) 2 ml of the colloid mixed with 2 ml of an aqueous solution of Ru(bipy)<sub>3</sub>I<sub>2</sub> (1 x 10<sup>-4</sup> mol l<sup>-1</sup>)



**Figure 6.3:** (a) SERR and (b) RR spectra of the silver colloid/Ru(bipy)<sub>3</sub>I<sub>2</sub> system (10<sup>-4</sup> mol l<sup>-1</sup>). [Ar<sup>+</sup> laser, 488.0 nm excitation].

### 6.3 Chemically prepared films

#### 6.3.1 Silver-coated microscope slides.

The initial studies of Ni and Cotton (113) with silver-coated slides indicated that they had some potential in the field of chemical sensing.

##### (a) Characterisation of the surface.

###### Absorption spectrum.

Figure 6.4 displays the electronic absorption spectra of a piece of silver-coated slide before and after exposure to a solution of  $\text{Ru}(\text{bipy})_3\text{I}_2$ . Before exposure, the silver slide displays an absorption maximum at 410 nm. The position of this surface plasmon maximum, being close to the maximum for silver colloids, is not surprising as the preparative methods for both substrates are very similar. The shift to longer wavelength, with silver slides, is consistent with a "partially aggregated" silver film. The absorption spectrum after exposure shows a peak at approximately 450 nm, with the feature at 410 nm still visible. The maximum at 450 nm simply corresponds to the addition of the  $\text{Ru}(\text{bipy})_3\text{I}_2$  solution and the resultant metal(d)  $\rightarrow$  ligand( $\pi^*$ ) transition.

###### Electron microscopy.

Scanning electron microscopy (SEM) was used to study a frosted microscope slide surface before and after coating with silver and after exposure to a solution of 2,2'-bipyridine (figure 6.5).

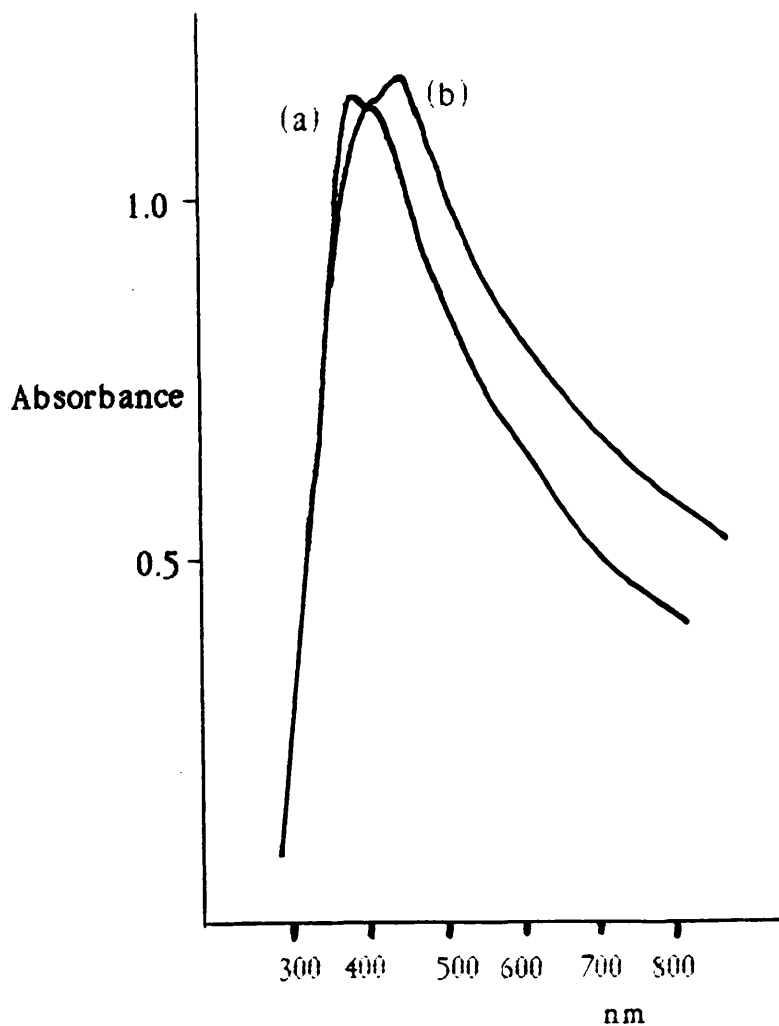
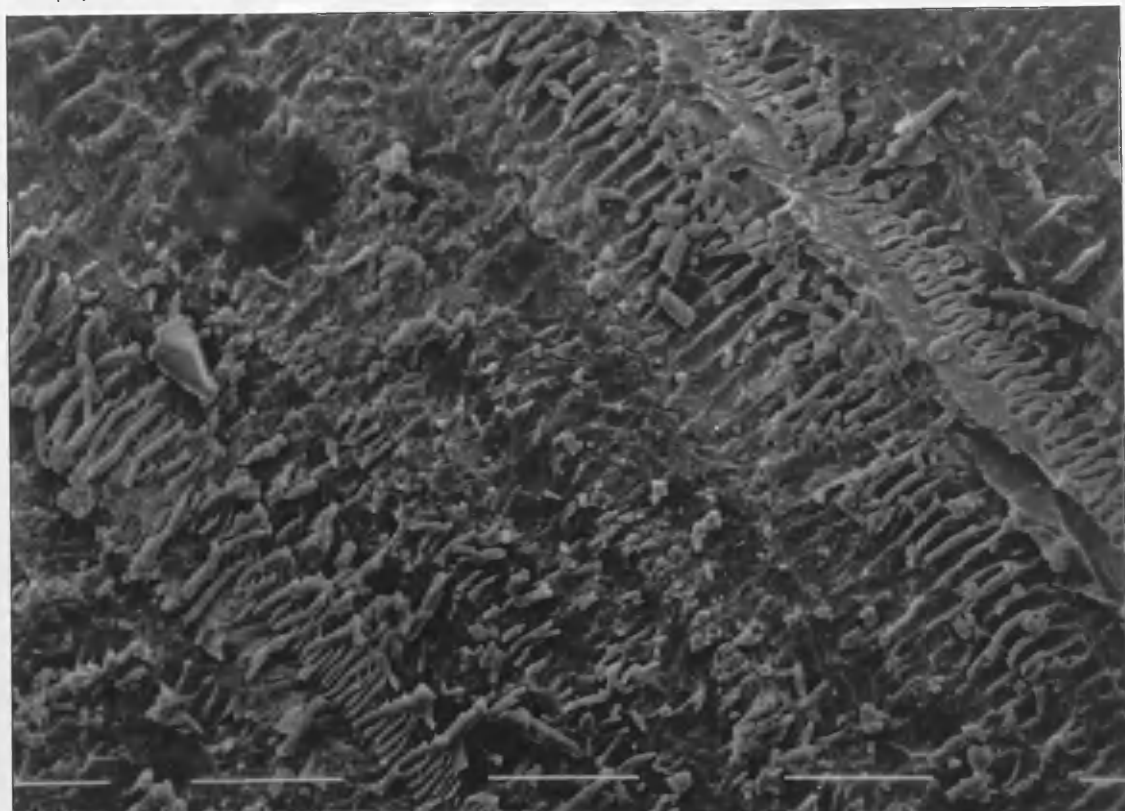


**Figure 6.4:** Electronic absorption spectra of a piece of chemically silver-coated slide (a) before and (b) after exposure to a  $10^{-3} \text{ mol l}^{-1}$  aqueous solution of  $\text{Ru}(\text{bipy})_3\text{I}_2$ .

(a)



(b)

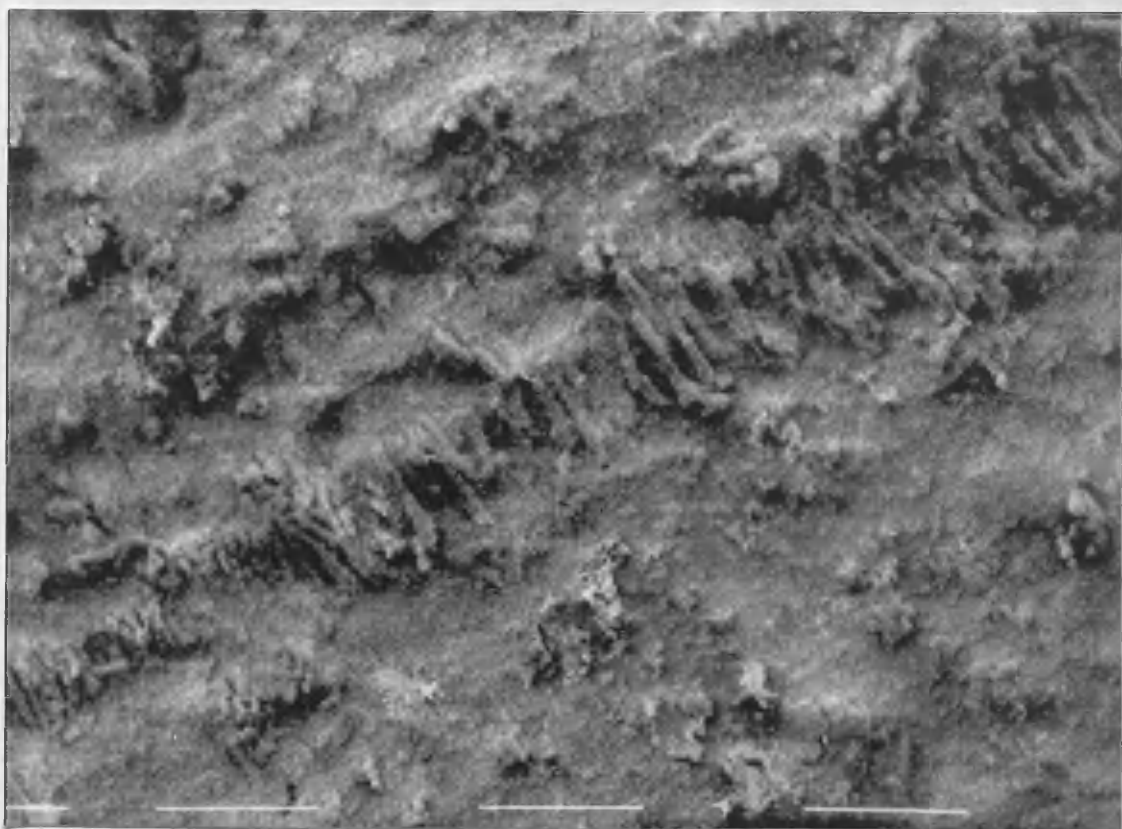
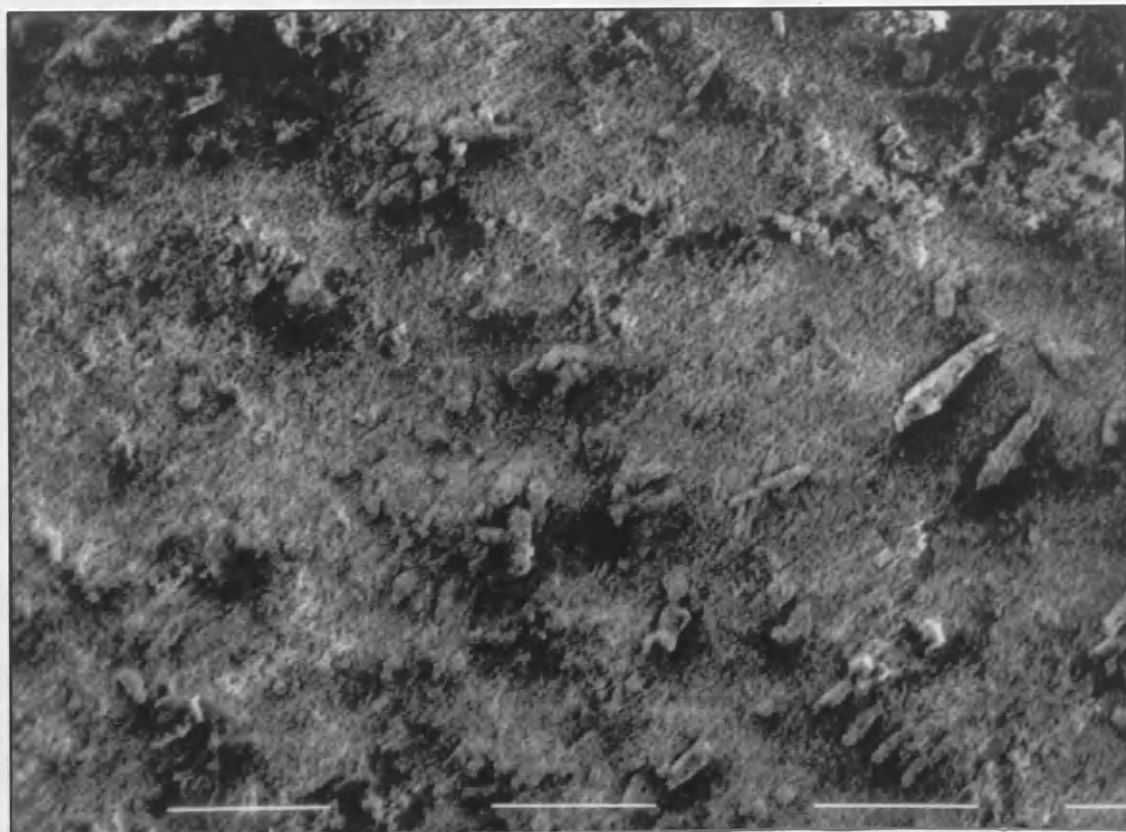


Figure 6.5: Scanning electron micrographs of a frosted microscope slide (a) before and (b) after coating with silver. Magnification x 1600.

(c) here to the surface



6.5 (c) after exposure of the silver-coated slide to a dilute solution of 2,2'-bipyridine. Magnification x 1600.

Figures 6.5 (a) and (b) clearly show that the regular, machined nature of the frosted slide surface morphology is not preserved after silver coating and that a randomly rough silver layer is deposited. The diameters of the silver surface features are in the range 40 to 150 nm and highly irregular. There is no evidence of surface rearrangement, after exposure to the adsorbate solution, from figure 6.5 (c).

(b) SERRS with  $\text{Ru}(\text{bipy})_3\text{I}_2$  and  $\text{Ru}(\text{bipy})_3\text{Cl}_2$ .

The SERR spectrum of a piece of silver coated slide immersed in an aqueous solution of  $\text{Ru}(\text{bipy})_3\text{Cl}_2$  is shown in figure 6.6. The corresponding resonance Raman spectrum is also displayed. Clearly, the SERR spectrum is highly enhanced and is almost identical to the spectrum of  $\text{Ru}(\text{bipy})_3\text{I}_2$  adsorbed on a silver colloid (figure 6.3). The SERR spectrum displays no obvious differences in relative intensities and band positions with respect to the RRS. The enhancement over the RRS is of the order of  $10^6$ .

It should be noted that the SERRS spectra, with silver slides, of solutions of  $\text{Ru}(\text{bipy})_3\text{I}_2$  and  $\text{Ru}(\text{bipy})_3\text{Cl}_2$  (of equal concentration) were identical in terms of relative intensities, band positions and enhancement. This indicates that the anion plays no significant role in the adsorption process. Such effects are more pronounced in electrochemical systems.

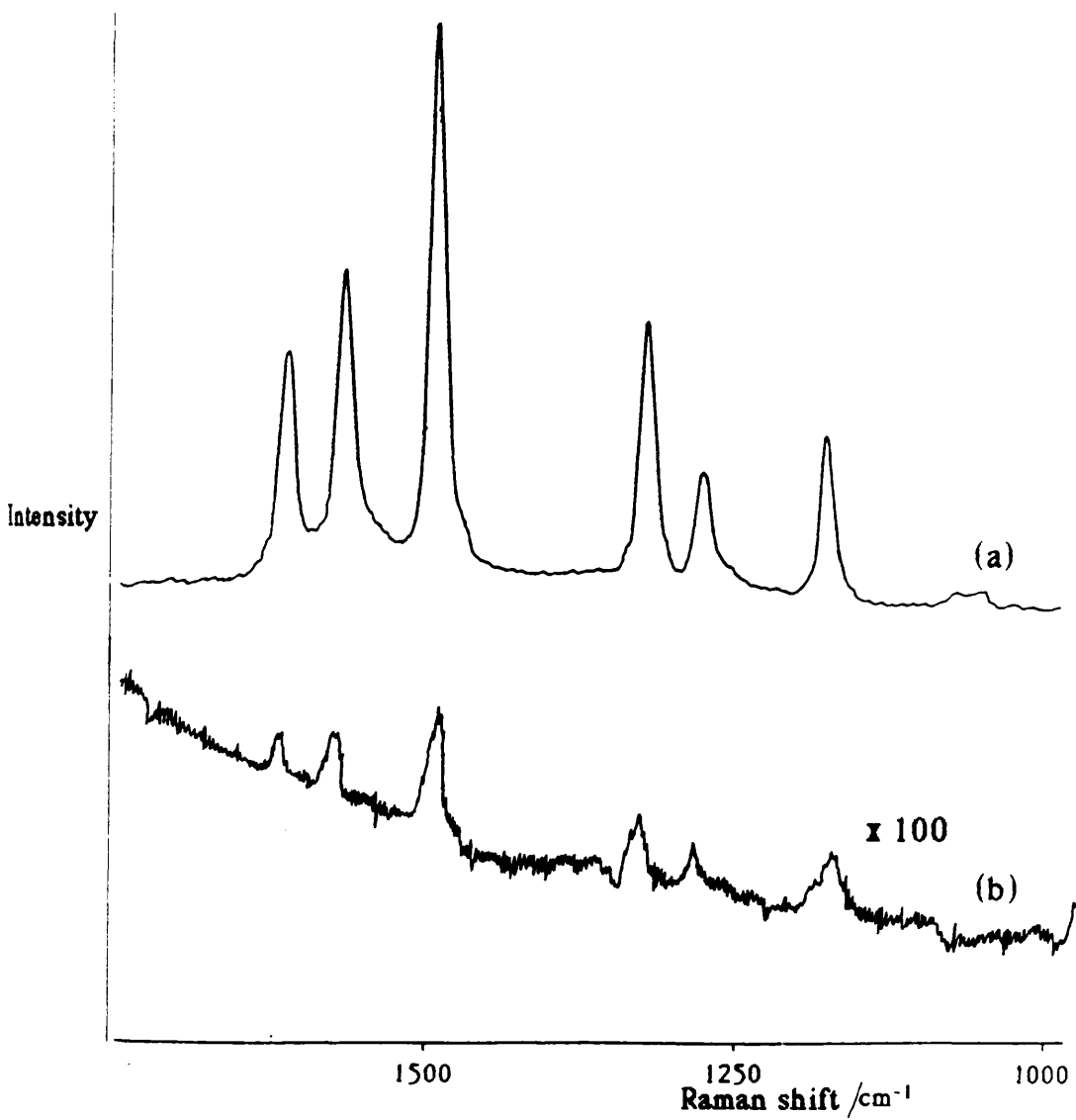


**Figure 6.6:** (a) SERR and (b) RR spectra of the silver slide/ $\text{Ru}(\text{bipy})_3\text{Cl}_2$  system ( $10^{-3} \text{ mol l}^{-1}$ ). [ $\text{Ar}^+$  laser, 488.0 nm excitation].

The SERR spectra of  $\text{Ru}(\text{bipy})_3\text{I}_2$  in contact with silver-coated frosted and flat microscope slides were also tested. Equal enhancement was observed. This is further evidence (along with SEM) that silver films coat onto substrates in a random fashion and that the morphology of the substrates before coating does not influence SERS enhancement. The roughness of the frosted slides may, however, help to physically stabilise the silver layer.

Another notable feature of the SERR spectrum of  $[\text{Ru}(\text{bipy})_3]^{2+}$  is the absence of fluorescence, which is so dominant in the RRS of  $\text{Ru}(\text{bipy})_3\text{Cl}_2$ . Fluorescence is a significant limitation of Raman spectroscopy. It is problematic for two main reasons. Firstly, both Stokes Raman and fluorescence bands occur at frequencies lower than that of the incident radiation. Both processes can occur in the same energy region and interfere. Secondly, the quantum yield of fluorescence processes is generally much higher than that of Raman scattering and weaker Raman signals can be lost under intense background fluorescence. The quenching mechanism at work in this case may involve the injection or withdrawal of electrons taking part in the fluorescence process.

#### (c) Optimisation of surface preparation procedures.

In order to maximise SERS enhancement and gauge the optimum practical procedure, SERR spectra were obtained from silver slides

which had been prepared with different concentrations of silver nitrate solution. In these experiments, all other factors were identical throughout: the concentrations and volumes of the other reactants used, heating times and sonication times. Table 6.1 summarises the results of these studies.

Table 6.1: Effect of variation in silver nitrate concentration.

<u>AgNO<sub>3</sub> concentration.</u> <u>(w/v %).</u>	<u>Description of</u> <u>resultant film.</u>	<u>Arbitrary indication</u> <u>of SERRS intensity</u> <u>with [Ru(bipy)<sub>3</sub>]<sup>2+</sup></u>
3	Very thick, white.	+
2	Even, yellow.	+++
1	Thin and uneven.	+
0.5	Not homogeneous.	(+)

More detailed study was clearly not required: the 2% solution of silver nitrate gives the most enhanced SERR spectrum. The use of a 3% solution of silver nitrate gives a silver surface which does not have adequate roughness features. The less concentrated silver nitrate solutions give patchy films with not enough active silver: these extremely thin films could be susceptible to burning in the laser beam.

Other variable factors include the time of heating. It was observed that if the slides were left for too long in the near-boiling silver

solution, thick white layers were produced.

In all subsequent preparations of silver-coated slides, 2% silver nitrate was used.

(d) Other aspects of the SERR spectrum of  $[\text{Ru}(\text{bipy})_3]^{2+}$  on silver slides.

(i) Dependence on time.

The SERR spectrum of  $\text{Ru}(\text{bipy})_3\text{Cl}_2$  ( $10^{-3}$  mol  $\text{l}^{-1}$  aqueous solution) was followed over a period of time. An initial spectrum was obtained immediately after the slide was immersed in the adsorbate solution and, thereafter, at ten minute intervals. Table 6.2 summarises the results obtained.

Table 6.2: Variance of the intensity of the  $1488 \text{ cm}^{-1}$  peak from the SERR spectrum of  $\text{Ru}(\text{bipy})_3\text{I}_2$  on a silver slide with time.

<u>Time (minutes).</u>	<u>Counts (arbitrary units: <math>1488 \text{ cm}^{-1}</math> signal, (peak height - baseline)).</u>
0	21
10	30
20	41
30	43
40	50
50	51
60	49

The graph plotted from this data (figure 6.7) shows that SERRS intensity reaches a maximum only after at least 30 to 40 minutes. This indicates that adequate time must be allowed, in SERS experiments,

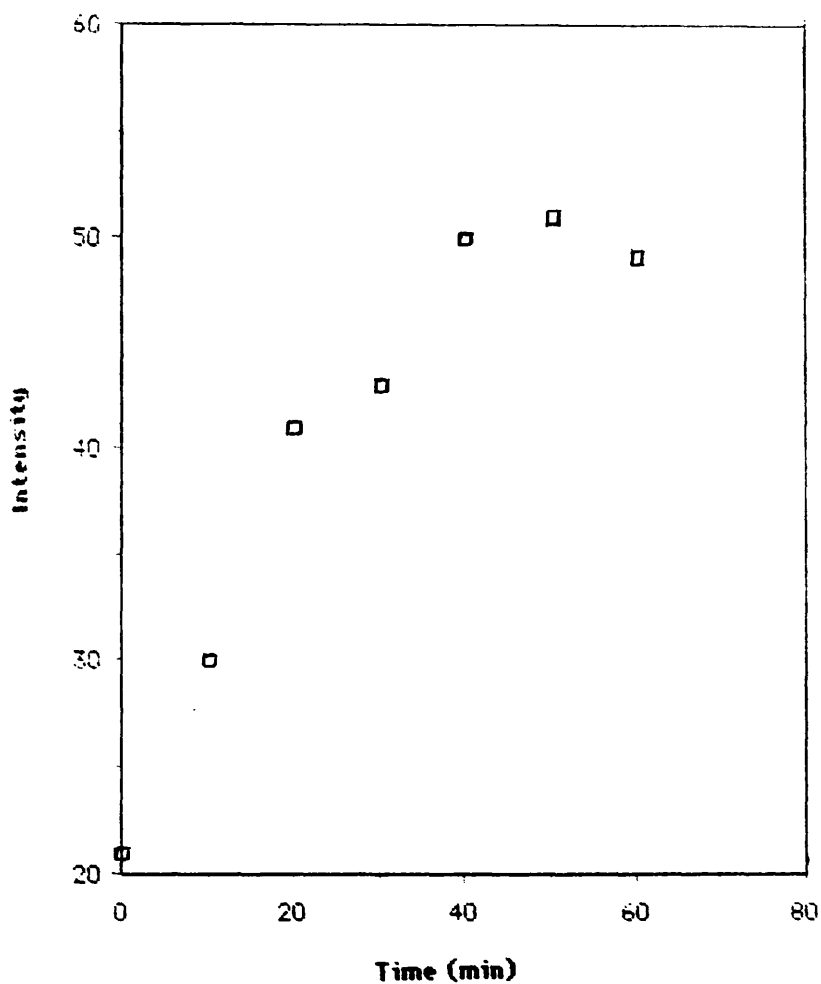


Figure 6.7: Plot of the intensity of the 1488 cm<sup>-1</sup> peak of the SERR spectrum of Ru(bipy)<sub>3</sub>I<sub>2</sub> on a silver slide versus time. Data from table 6.2.

between treatment of the slide with the adsorbate solution and the actual Raman experiment. Care was taken to ensure that all parameters were held constant throughout these studies. The petri-dish containing the adsorbate solution and the silver slide was not moved throughout the study and the incident laser beam was blocked between experiments.

(ii) Dependence on adsorbate concentration.

Successive dilutions were made to a  $10^{-2}$  mol l<sup>-1</sup> aqueous solution of Ru(bipy)<sub>3</sub>Cl<sub>2</sub> and small pieces of freshly-prepared silver slides were immersed in each dilution and the SERR spectra obtained. All other factors, such as the laser power, were held constant. The spectra showed a progressive decrease in SERRS enhancement with decrease in adsorbate solution concentration. Peaks, with acceptable signal-to-noise ratios, could still be detected at concentrations of  $10^{-9}$  mol l<sup>-1</sup> and lower.

This factor was re-examined quantitatively (table 6.3 and figure 6.8)

Table 6.3: Variance of the intensity of the 1488 cm<sup>-1</sup> peak of the SERR spectrum of Ru(bipy)<sub>3</sub>Cl<sub>2</sub> on silver slides with adsorbate concentration.

<u>Concentration of Ru(bipy)<sub>3</sub>Cl<sub>2</sub> (mol l<sup>-1</sup>)</u>	<u>Counts (arbitrary units: 1488 cm<sup>-1</sup> signal. (peak height - baseline))</u>
2 x 10 <sup>-4</sup>	984
4 x 10 <sup>-5</sup>	638
8 x 10 <sup>-6</sup>	525
1.6 x 10 <sup>-6</sup>	224
3.2 x 10 <sup>-7</sup>	180
6.4 x 10 <sup>-8</sup>	153
1.28 x 10 <sup>-8</sup>	120
2.56 x 10 <sup>-9</sup>	104
5.12 x 10 <sup>-10</sup>	81

These studies clearly demonstrate the remarkable sensitivity of silver slides in the detection of the [Ru(bipy)<sub>3</sub>]<sup>2+</sup> ion. The experiments, however, have a significant source of error. It was assumed that each of the silver slides used were identical and that the laser beam fell on an identical area of the slide in each case. Due to the randomly rough nature of the film and the variance in the dimensions of roughness features across the surface, this cannot be true. Although the general trend in this case is clear, with respect to individual SERS experiments and comparisons between experiments, the reproducibility of the practical method is probably not very high.

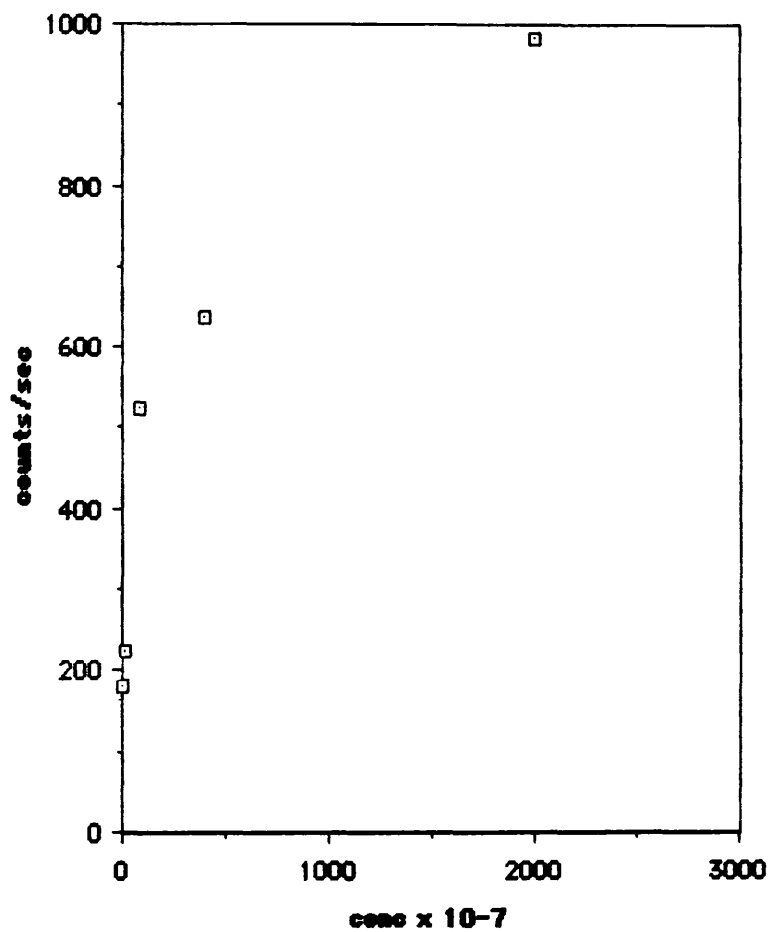


Figure 6.8: Plot of the intensity of the  $1488\text{ cm}^{-1}$  peak of the SERR spectrum of  $\text{Ru}(\text{bipy})_3\text{Cl}_2$  versus adsorbate concentration. Data from table 6.3.

(iii) Enhancement: effect of charge.

As discussed in section (b), the SERR spectrum of  $[\text{Ru}(\text{bipy})_3]^{2+}$  on silver slides shows no evidence of chemical bond formation between the adsorbate and the surface. It is known that colloidal silver particles are negatively charged and since silver slides are produced in an almost identical fashion, the silver layer may be negatively charged. The high degree of enhancement observed with  $[\text{Ru}(\text{bipy})_3]^{2+}$  could, therefore, be the result of some charge-mediated interaction. In order to test this hypothesis, SERR spectra were obtained from  $\text{Ru}(\text{bipy})_2\text{Cl}_2$  and  $\text{Ru}(\text{bipy})_2(\text{SCN})_2$  on silver slides. Both of these molecules are neutral. The observed enhancements, in each case, were only slightly lower than those obtained with the tris-2,2'-bipyridyl complex. The concentrations of each neutral complex solution were identical to the concentration of the solution of the tris-2,2'-bipyridyl complex used for the comparison. If, therefore, the enhancement of the Raman spectrum of  $[\text{Ru}(\text{bipy})_3]^{2+}$  is, indeed, charge-mediated, it is a very small effect.

(e) SERRS with other 2,2'-bipyridyl and 1,10-phenanthroline complexes.

Table 6.4 details the complexes studied.

All of the 2,2'-bipyridyl complexes, except  $\text{Mo}(\text{CO})_4(\text{bipy})$ , gave highly enhanced spectra. All the spectra displayed similar

characteristics in the 1000 to 1750  $\text{cm}^{-1}$  region. Clearly, these active vibrations are due to the ring modes of the 2,2'-bipyridyl ligands.

$\text{Ru}(\text{phen})_3\text{Cl}_2$  showed a high degree of SERRS enhancement (figure 6.9). Although the general pattern in the 1000 to 1750  $\text{cm}^{-1}$  region was similar to that of the 2,2'-bipyridyl complexes, the bands were at distinctly different positions. The question arises as to which ligand would predominate in the SERR spectra of a mixed-ligand complex. To resolve this question, the complex  $\text{Ru}(\text{bipy})_2(\text{phen})\text{Cl}_2$  was prepared. This complex displayed a broad absorption maximum at 450 nm. Figure 6.10 shows its SERR spectrum on a silver slide. Although this spectrum is dominated by fluorescence, bands are discernible above the rising baseline. Table 6.5 compares the band positions of this complex with those of  $[\text{Ru}(\text{bipy})_3]^{2+}$  and  $[\text{Ru}(\text{phen})_3]^{2+}$ . The band positions of the mixed ligand ruthenium(II) complex are assigned to one or other of the ligands involved.

From the spectrum of  $[\text{Ru}(\text{bipy})_2(\text{phen})]\text{Cl}_2$ , it is clear that the 2,2'-bipyridyl peaks are of higher intensity over the 1,10-phenanthroline peaks by a factor of approximately two. This is simply a consequence of the ratio of 'bipy' to 'phen' in the mixed-ligand complex. There is no evidence of competitive adsorption or the selective enhancement of one or other set of vibrational modes.

Table 6.4: 2,2'-bipyridyl and 1,10-phenanthroline complexes.

<u>Complex.</u>	<u>SERRS solvent.</u>	<u>Preparation.</u>
Mo(CO) <sub>4</sub> (bipy)	CH <sub>3</sub> CN	as received.
Ru(bipy) <sub>2</sub> (SCN) <sub>2</sub>	CH <sub>3</sub> CN	section 4.1.1(c).
Ru(bipy) <sub>2</sub> Cl <sub>2</sub>	CH <sub>3</sub> CN	section 4.1.1(d).
Ru(bipy) <sub>2</sub> (pn)I <sub>2</sub> *	CH <sub>3</sub> CN	as received.
Ru(phen) <sub>3</sub> Cl <sub>2</sub>	CH <sub>3</sub> CN	as received.
Ru(bipy) <sub>2</sub> (phen)Cl <sub>2</sub>	CH <sub>3</sub> CN	section 4.1.1(e).

\* pn = 1,2-propylenediamine.

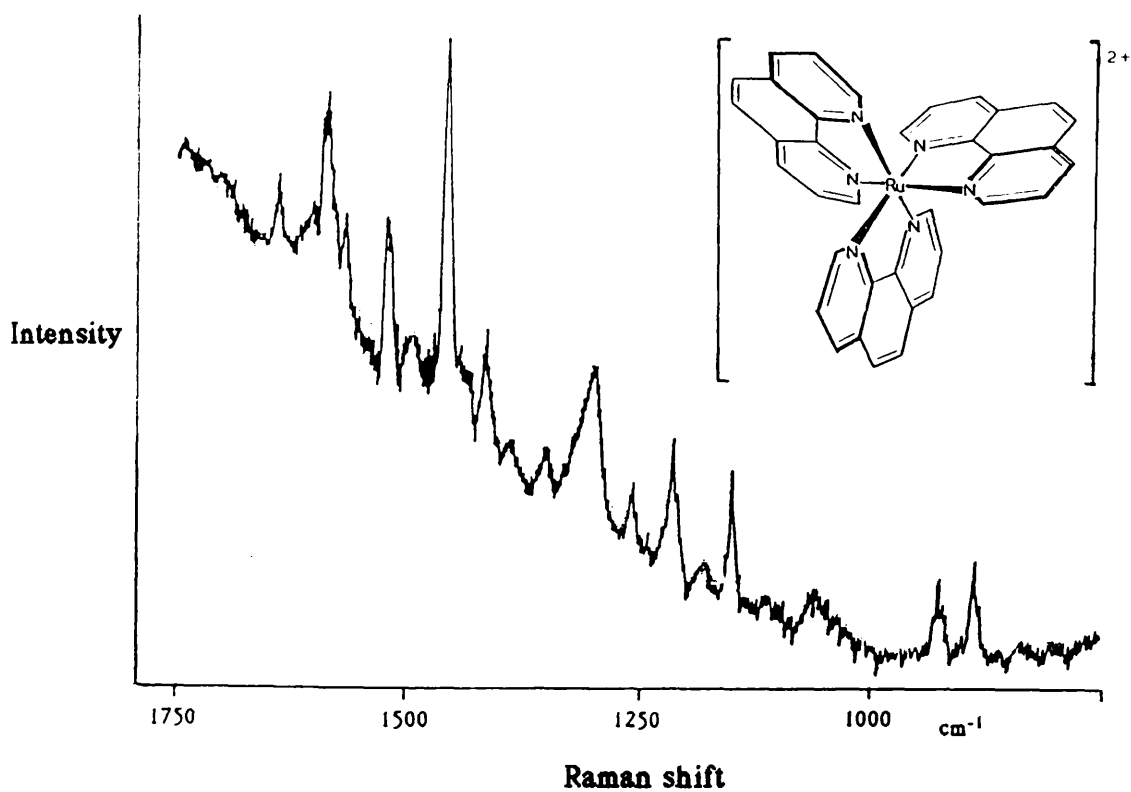


Figure 6.9: SERR spectrum of a  $10^{-3}$  mol  $\text{l}^{-1}$  acetonitrile solution of  $\text{Ru}(\text{phen})_3\text{Cl}_2$ /silver slide. [ $\text{Ar}^+$  laser, 488.0 nm excitation].

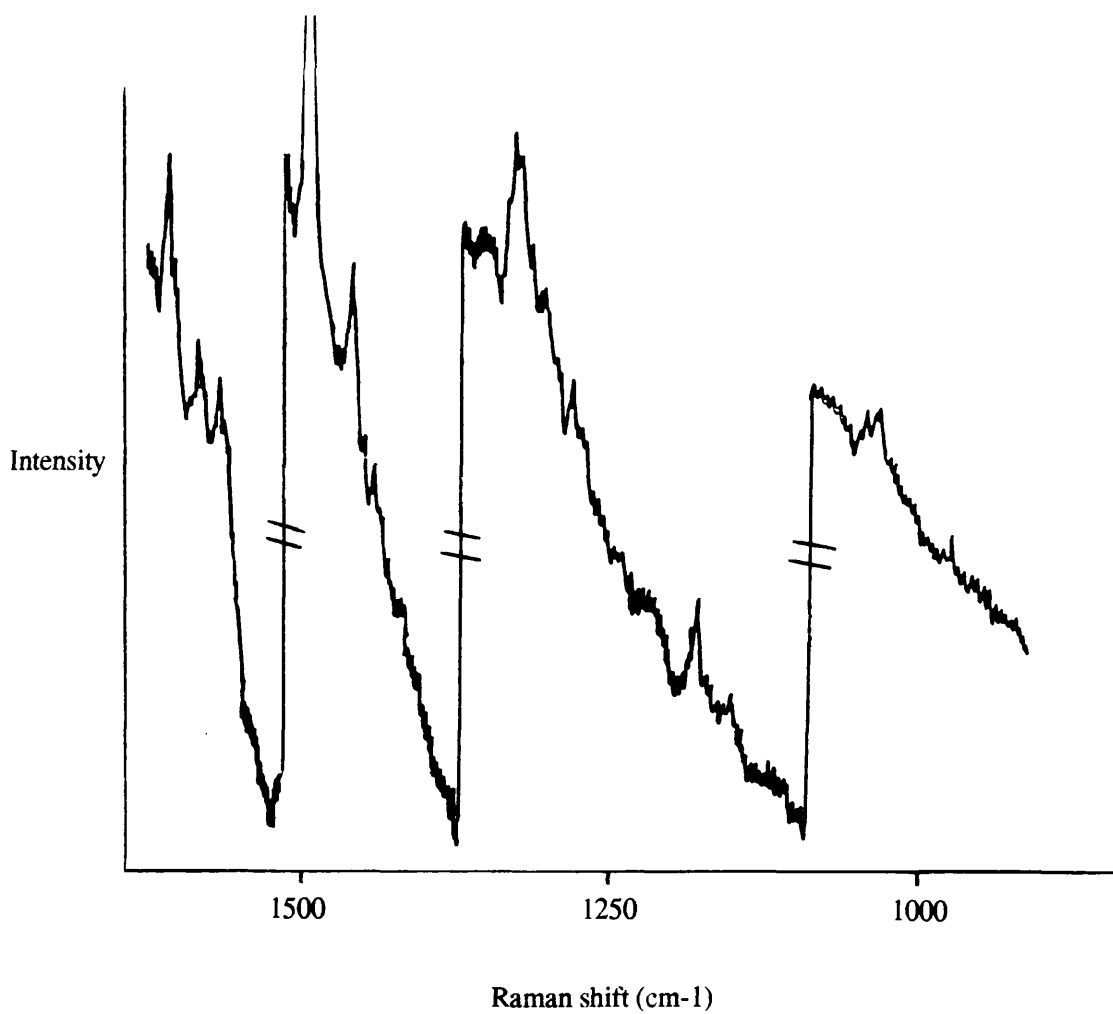


Figure 6.10: SERR spectrum of a  $10^{-3}$  mol  $l^{-1}$  acetonitrile solution of  $Ru(bipy)_2(phen)Cl_2$ /silver slide. [ $Ar^+$  laser, 488.0 nm excitation].

Table 6.5: Comparative band frequencies of  $[\text{Ru}(\text{bipy})_3]^{2+}$  ('bipy peaks'),  $[\text{Ru}(\text{phen})_3]^{2+}$  ('phen peaks') and  $[\text{Ru}(\text{bipy})_2(\text{phen})]\text{Cl}_2$  ('bipy-phen peaks'). (w = weak).

<u>(bipy) peaks.</u>	<u>(phen) peaks.</u>	<u>(bipy)(phen) peaks</u>	<u>corresponds to:</u>
	892		
1040		1041	bipy
	1060w		
	1155w		
1183		1182	bipy
	1217		
1285		1283	bipy
	1308	1308	phen
1329		1329	bipy
	1417		
	1460	1461	phen
1500		1500	bipy
	1520	1520	phen
1575		1573	bipy
	1583	1580	phen
1621		1620	bipy

(f) SERS-activity of silver-coated slides with organic and gaseous adsorbate species.

(i) 2,2'-bipyridine.

The SER spectrum of a  $1.8 \times 10^{-3} \text{ mol l}^{-1}$  aqueous solution of 2,2'-bipyridine adsorbed on a silver slide (figure 6.11) shows appreciable enhancement. With the same solution, the normal Raman spectrum (same figure) is lost beneath the noise. The SER spectrum compared to the Raman spectrum of bulk 2,2'-bipyridine (same figure) shows

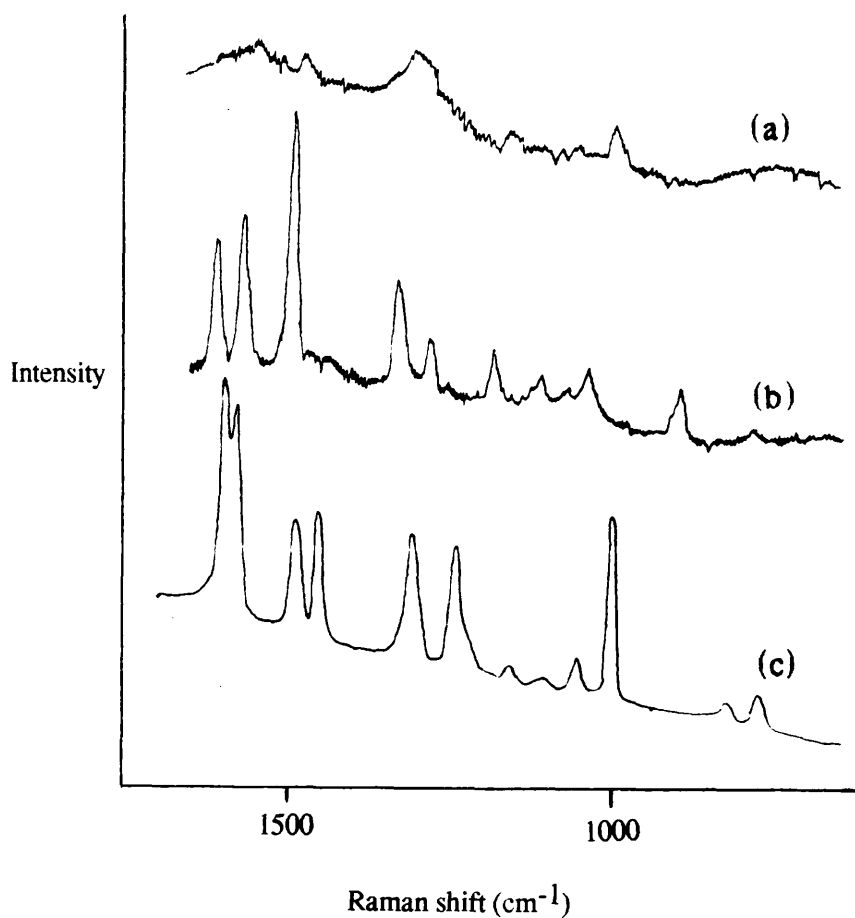


**Figure 6.11:** (a) normal Raman spectrum of an ethanolic solution of 2,2'-bipyridine.  
(b) SER spectrum of an ethanolic solution of 2,2'-bipyridine ( $1.8 \times 10^{-3} \text{ mol l}^{-1}$ )/silver slide.  
(c) normal (bulk) Raman spectrum of solid 2,2'-bipyridine. [Ar<sup>+</sup> laser, 488.0 nm excitation].

distinct differences. Table 6.6 details the bands present in each spectrum.

Table 6.6: Bands present in the SER spectrum of a  $1.8 \times 10^{-3} \text{ mol l}^{-1}$  solution of 2,2'-bipyridine and the NRS of the bulk adsorbate.

<u>NRS (<math>\text{cm}^{-1}</math>).</u>	<u>SERS (<math>\text{cm}^{-1}</math>).</u>
	884w
1004	
	1030
1056w	
	1068
	1175
1240	
	1278
1308	
	1324
1457	
1492	1490
	1564
1580	
1602	1600

The large differences between the SERS and NRS of 2,2'-bipyridine indicate chemical bonding between the molecule and the silver surface. This undoubtedly involves a Lewis acid/base interaction between one or both of the bipyridyl nitrogen atoms and the silver surface. Since rotation around the  $\text{C}_2\text{—C}_2'$  bond can occur, it is possible that only one nitrogen may be bound to the silver surface. The similarity of the SER spectrum to the RRS of  $[\text{Ru}(\text{bipy})_3]^{2+}$ , however, suggests bidentate

chelation, with ruthenium, in effect, replaced by silver as shown in figure 6.12.

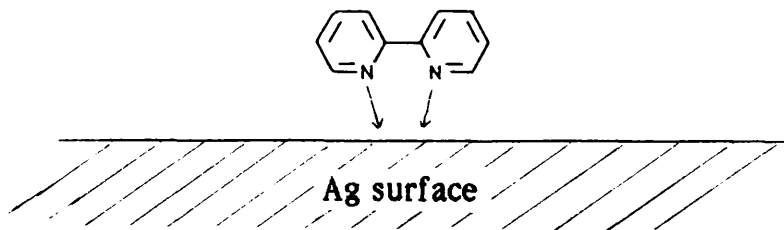
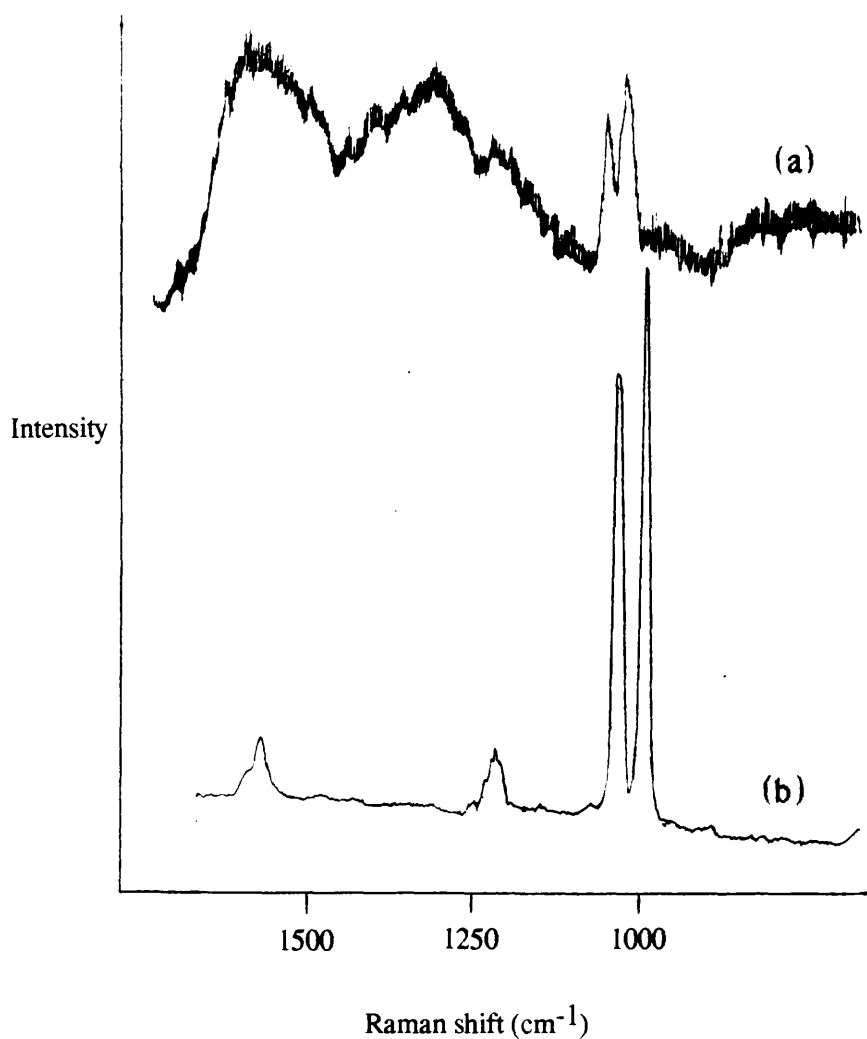


Figure 6.12: Interaction of 2,2'-bipyridine with a silver slide surface.

### (ii) Pyridine.

Figure 6.13 shows the SER spectrum of a solution of pyridine ( $0.1 \text{ mol l}^{-1}$ ) in contact with a silver-coated slide. The Raman spectrum of liquid pyridine is pictured for comparison, since the normal Raman spectrum of  $0.1 \text{ mol l}^{-1}$  pyridine, under the same conditions, was lost beneath background noise. There are significant differences between the spectra shown, as summarised in table 6.7.

Clearly, the differences indicate chemisorption of pyridine molecules through the nitrogen lone pairs, thus forming 'complexes' and altering the enhanced spectrum. The broad maxima in the SER spectrum may be associated with carbon deposition.



**Figure 6.13:** (a) SER spectrum of an aqueous solution of pyridine (0.1 mol l<sup>-1</sup>)/silver slide.  
(b) normal Raman spectrum of liquid pyridine.  
[Ar<sup>+</sup> laser, 488.0 nm excitation].

Table 6.7: SER spectrum of pyridine ( $0.1 \text{ mol l}^{-1}$  aqueous solution) and NRS of liquid pyridine (w = weak).

<u>NRS (<math>\text{cm}^{-1}</math>)</u>	<u>SERS (<math>\text{cm}^{-1}</math>)</u>
992	1009
1031	1036
1218w	1250 - 1350, broad
1596w	1510 - 1620, broad

(iii) Benzoic acid.

The SER spectrum of a  $10^{-3} \text{ mol l}^{-1}$  ethanolic solution of benzoic acid and the corresponding normal Raman spectrum were obtained. Figure 6.14 shows significant differences between the spectra. These differences may indicate the adsorption of benzoic acid through the carboxyl group and as the benzoate ion, evidenced by the lack of a clear carbonyl stretching mode.

(iv) Benzene.

Figure 6.15 shows the SER and NR spectra of a solution of benzene ( $0.1 \text{ mol l}^{-1}$ ). The system clearly exhibits no SERS enhancement, even with the high laser power output used.

Discussion.

These results show that, with organic adsorbates, silver slides

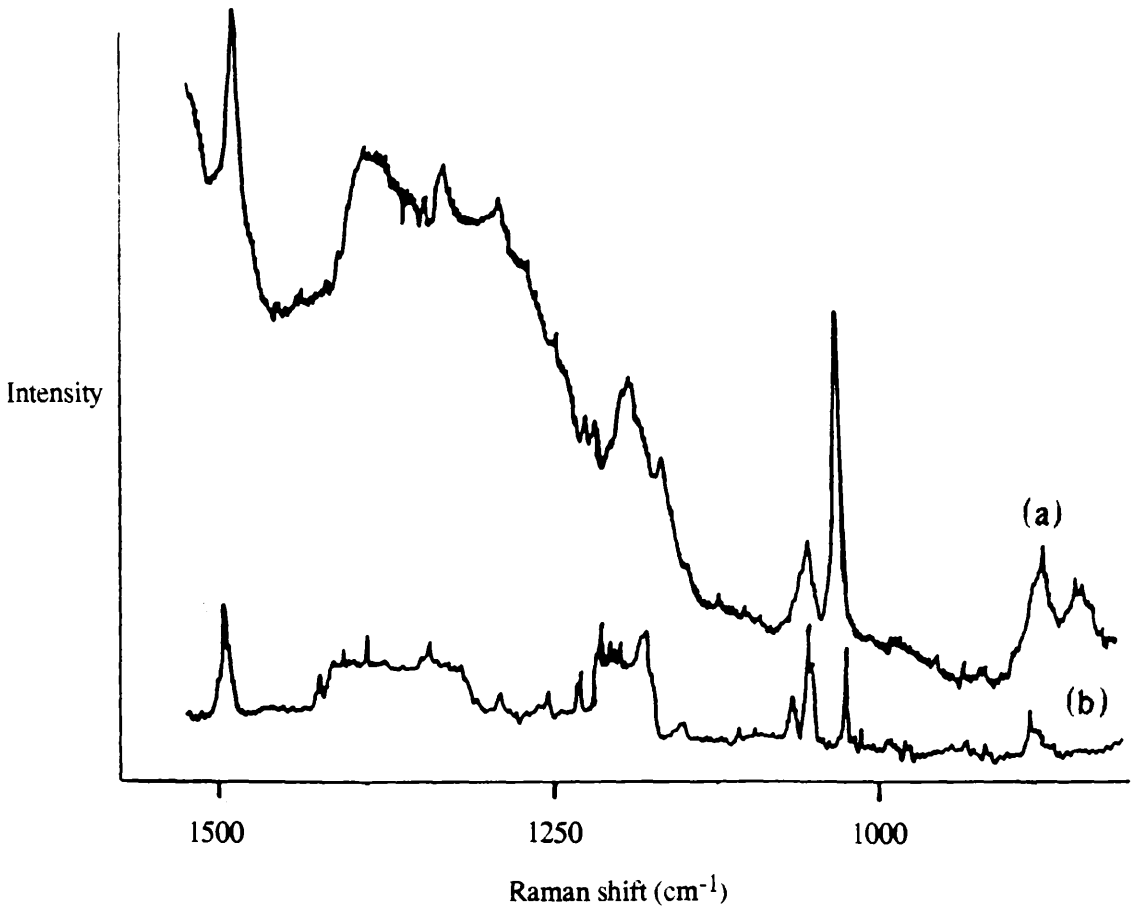


**Figure 6.14:** (a) SER spectrum of an ethanolic solution of benzoic acid ( $10^{-3} \text{ mol l}^{-1}$ )/silver slide.  
(b) normal Raman spectrum of the same solution.  
[Ar<sup>+</sup> laser, 488.0 nm excitation].

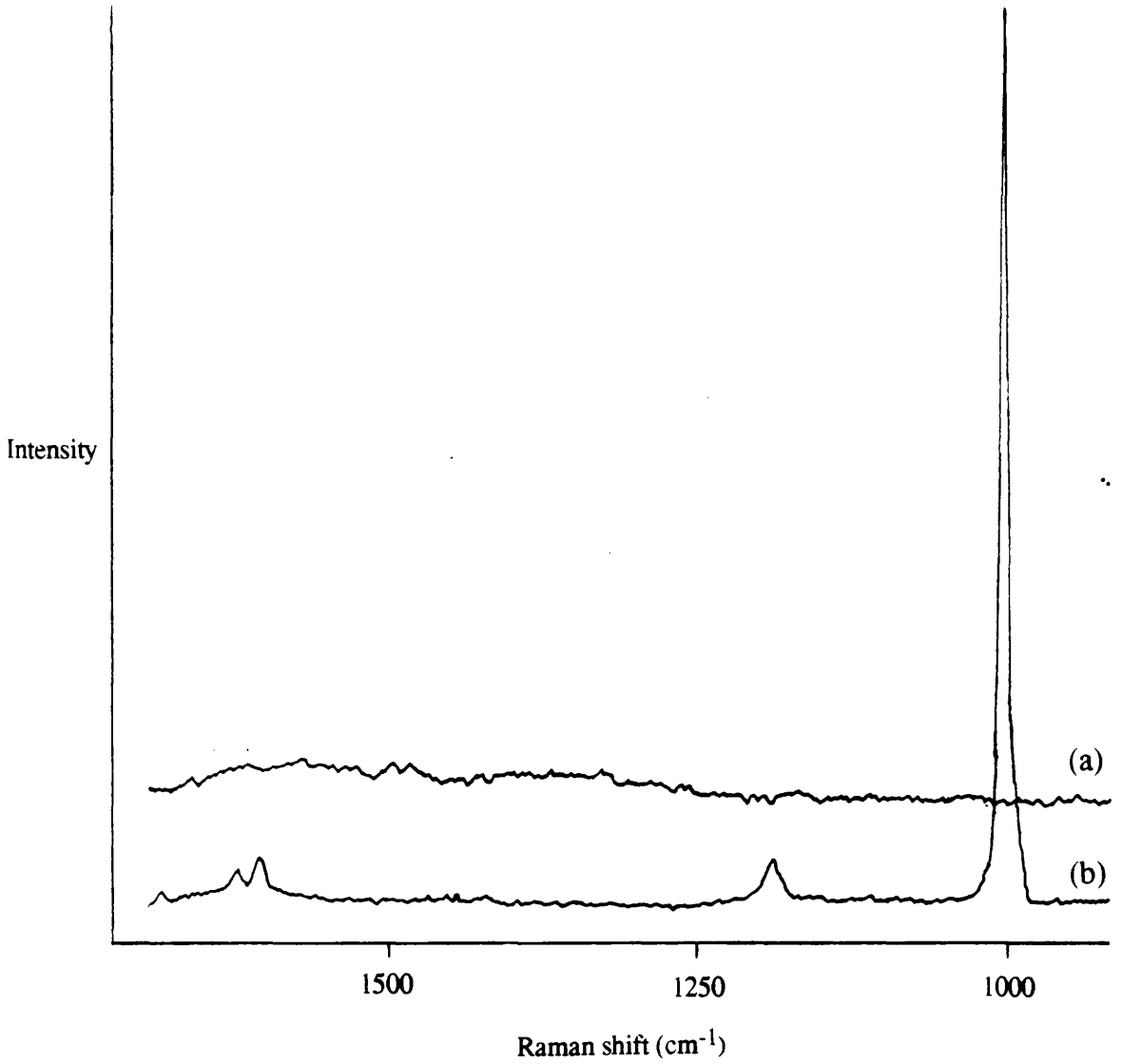


**Figure 6.15:** (a) SER spectrum of benzene ( $0.1 \text{ mol l}^{-1}$ )/silver slide.  
(b) normal Raman spectrum of the same solution.  
[Ar<sup>+</sup> laser, 488.0 nm excitation].

exhibit SER-activity only when exposed to molecules which have a strong site of co-ordination. The lack of SERS enhancement with benzene is a consequence of the inability of the molecule to bond strongly to the chemically-deposited silver surface. All the organic adsorbate species studied showed evidence of chemisorption and subsequent complexation with silver atoms. Whereas strong complexation seems to be necessary for high enhancement with organic adsorbates, it is not the case with inorganic complexes. The additional resonant enhancement factor associated with  $[\text{Ru}(\text{bipy})_3]^{2+}$  may be responsible for the inordinate enhancement.

#### (v) Gases.

The SERS of hydrogen sulphide gas and vapour-phase benzene and pyridine was studied. None showed any enhancement. It is thought that this may, in part, be due to the procedures used. In the case of hydrogen sulphide, the molecules may simply be desorbing from the metal surface at much lower than monolayer coverage.

It was observed that vapour-phase benzene and pyridine condensed on the sides of the vacuum cell. Clearly, in each case, the vapour pressure was not sufficient.

### 6.3.2 Gold and copper-coated microscope slides.

Attempts to prepare gold and copper films, by variations on the method used for silver-coated slides, proved unsuccessful. In each case, thin, patchy films were produced. SEM study (figure 6.16) confirmed this.

The absorption spectrum of a piece of gold-coated microscope slide showed a broad maximum at approximately 580 nm. Argon-ion excitation was, therefore, not suitable.

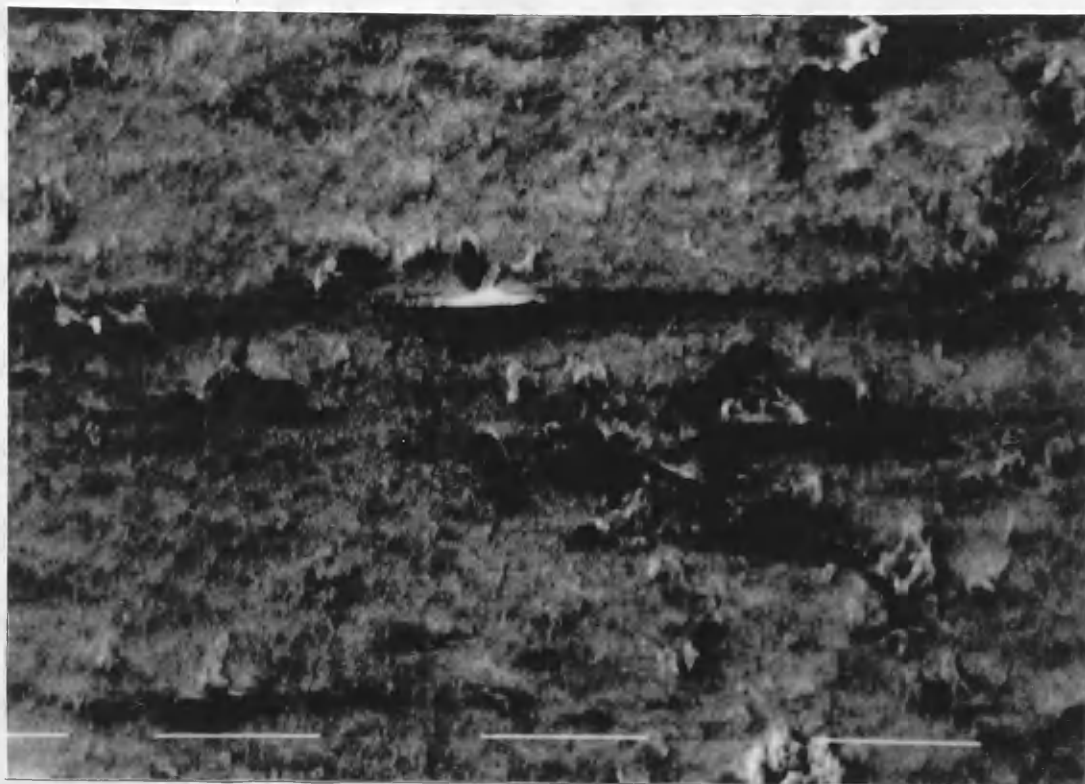
The SERS-activity of gold and copper films was tested with  $[\text{Ru}(\text{bipy})_3]^{2+}$  and various other adsorbates. The exciting line used was the 647.1 nm line of a krypton-ion laser. These spectra displayed no vibrational features. It is clear that slides produced through these preparative methods do not possess the required roughness features to support SERS enhancement.

### 6.3.3 General discussion.

The experiments outlined indicate that, for certain adsorbates, silver slides show a high degree of sensitivity with respect to SERS. When considered in relation to the relative ease and inexpense of production of the substrate, this indicates considerable potential in the field of SERS chemical sensing.

The substrate, however, has several notable drawbacks. Firstly, the

(a)



(b)

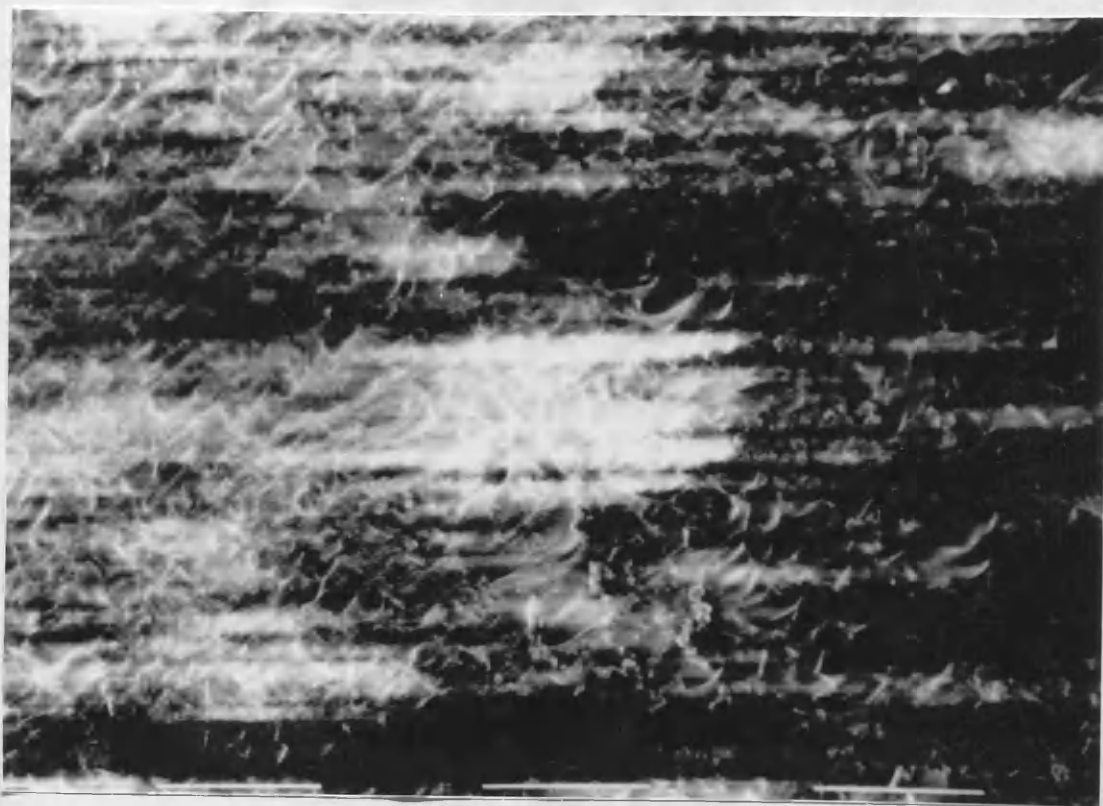


Figure 6.16: Scanning electron micrograph of (a) gold and (b) copper-coated microscope slides. Magnification  $\times 1600$ .

randomly rough morphology inevitably raises doubts about the reproducibility of the preparative procedure and the validity of comparing spectra obtained from different silver slides or even from different pieces or areas of the same silver slide. This problem has particular relevance to studies of concentration dependence and other precise, quantitative SERS investigations.

Secondly, as evidenced by SEM investigations, the size distribution of active silver particles is in the range 40 to 150 nm. Such a distribution randomly arrayed across a substrate inevitably leads to 'more active' and 'less active' areas on the silver surface. The effect may, however, be fairly small in practice but is extremely pertinent to the quantitative aspects of SERS analytical study.

The SERR and SER spectra obtained with silver-coated slides indicate that many different categories of molecules can be detected. Silver-coated slides, however, do not display the wide range of SERS-activity shown by colloids and electrode systems. Benzene, for example, can be detected in low concentrations through the use of other active systems, but not by silver slides.

The extraordinary sensitivity of the slides for the  $[\text{Ru}(\text{bipy})_3]^{2+}$  ion and other ruthenium-bipyridyl and phenanthroline complexes shows that they are suitable for the systematic investigation of  $[\text{Ru}(\text{bipy})_3]^{2+}$  and derivatives.

## 6.4 Supported silver colloids.

### 6.4.1 Filter paper-supported colloids.

This method of production of silver-coated filter paper was first reported in 1988 by Laserna *et al.* (107). Characterisation of the coated filter paper proved impossible due to the opaque nature of the substrate. Laserna *et al.*, however, carried out diffuse reflectance measurements on the surface. These results showed a broad reflectance minimum at 470 nm consistent with the formation of colloidal aggregates on the filter paper surface. They also studied the surface by SEM (section 2.2.3.8).

The SERS-activity of freshly-prepared silver-coated filter paper was tested with a range of adsorbates. Figure 6.17 shows the SERR spectrum of  $\text{Ru}(\text{bipy})_3\text{I}_2$  solution on a piece of coated filter paper. The vibrational features are identical to those obtained with colloids and silver slides. The degree of enhancement is almost comparable to that of the silver slide/complex system.

Organic adsorbates were also tested. The SER spectra of benzoic acid (figure 6.18) and pyridine in contact with the surface displayed appreciable enhancement. It can be seen that similar wavenumber shifts over the corresponding NRS are present in these spectra as were observed with silver slides. Benzoic acid is preferentially adsorbed through the carboxylate group and pyridine through the heteroaromatic

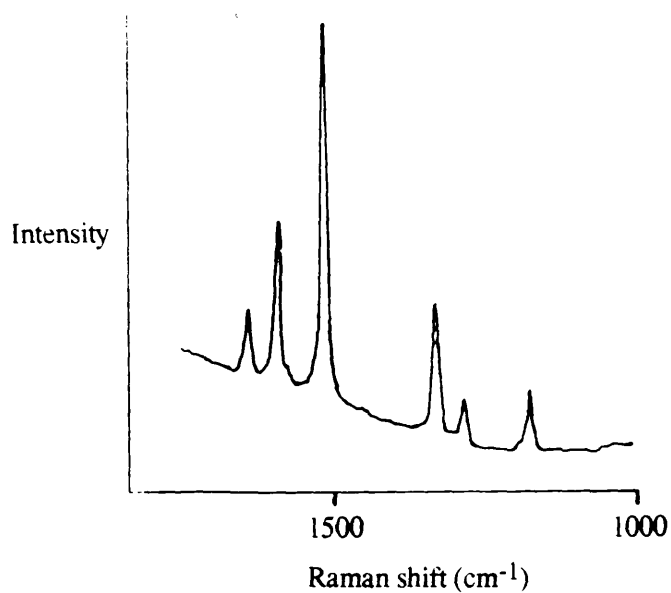


Figure 6.17: SERR spectrum of Ru(bipy)<sub>3</sub>I<sub>2</sub> ( $2 \times 10^{-3}$  mol l<sup>-1</sup>)/silver-coated filter paper. [Ar<sup>+</sup> laser, 488.0 nm excitation].

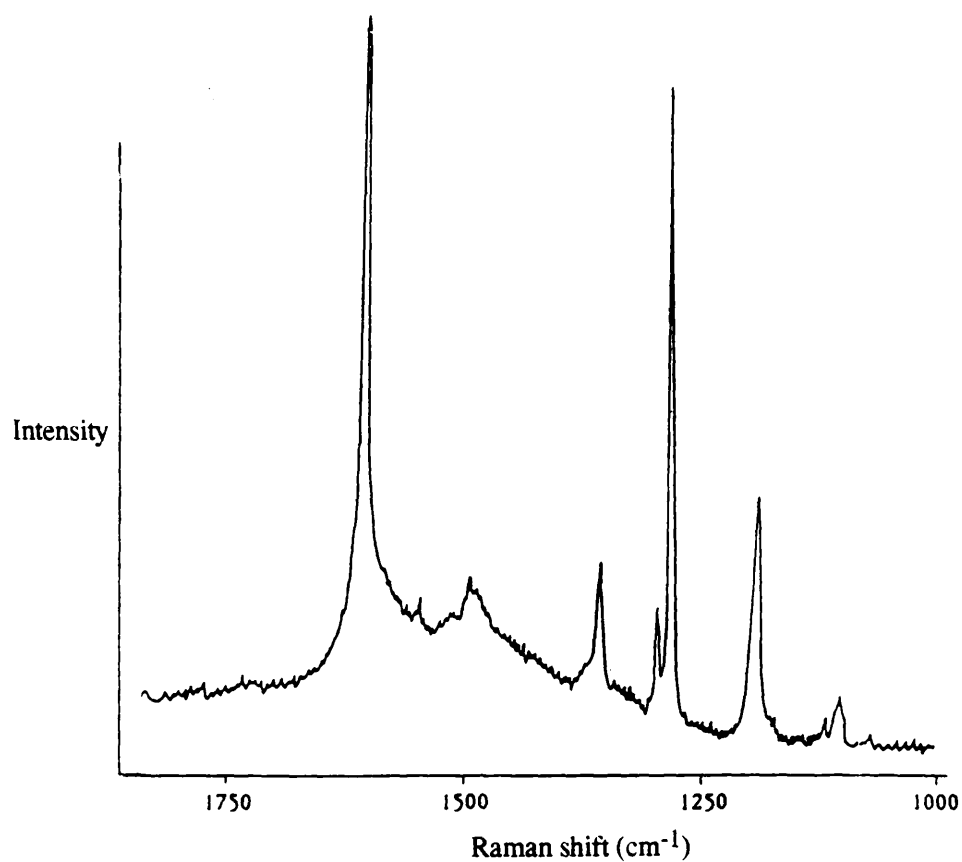


Figure 6.18: SERR spectrum of benzoic acid ( $10^{-4}$  mol l<sup>-1</sup>)/silver-coated filter paper. [Ar<sup>+</sup> laser, 488.0 nm excitation].

ring nitrogen. As with the silver slide system, benzene did not display any enhancement.

The coated filter paper substrate, as previously discussed, was green when freshly prepared, gradually becoming brown with slow oxidation. Laserna *et al.* stated that the half-life of the substrate, with 9-amino acridine as the adsorbate species, was approximately 15 to 20 minutes. In order to test this result, the activity of  $\text{Ru}(\text{bipy})_3\text{Cl}_2$  with a piece of silver-coated paper was tested when freshly prepared, at regular intervals immediately afterwards and after 24 hours. All other factors were held constant and the complex/surface system was kept enclosed during the 24 hour period. Table 6.8 and figure 6.19 summarise the results obtained.

Table 6.8: SERRS intensity (peak height - baseline, %) of the  $1488\text{ cm}^{-1}$  peak of  $\text{Ru}(\text{bipy})_3\text{Cl}_2$  with time (minutes).

<u>time (mins.)</u>	<u>SERRS intensity (%)</u>
0	62
5	60
10	55
15	56
20	50
25	51
30	50
40	47
60	48
90	43
3600	40

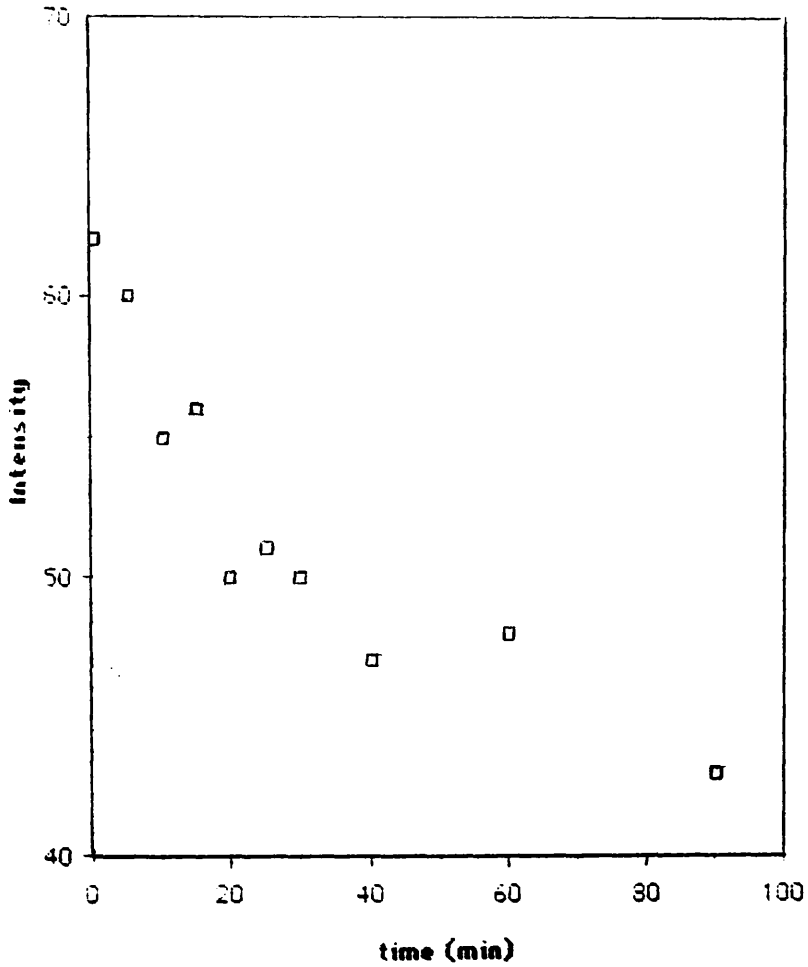


Figure 6.19: Plot of the intensity of the  $1488\text{ cm}^{-1}$  peak of the SERR spectrum of  $\text{Ru}(\text{bipy})_3\text{Cl}_2/\text{silver-coated filter paper}$  versus time.

The reading at time = 3600 minutes is subject to some uncertainty due to the error associated with obtaining the correct laser power output after it was switched back on. However, the general pattern of decreasing intensity with time after production is clear. The intensity, in this case, did not decrease at the same rapid rate as reported by Laserna *et al.*

#### 6.4.2 TLC plate-supported silver colloids.

This method, suggested by Séquaris and Koglin (110), is almost identical to the method for producing filter paper-supported colloids.

The substrate was found to be extremely unstable when placed in adsorbate solutions (the coated silica broke away from the plastic backing). In order to overcome this problem, in each case, a small volume of adsorbate solution was spotted carefully onto a small area of the surface and dried.

Figure 6.20 illustrates a SERR spectrum obtained using this surface. Clearly,  $\text{Ru}(\text{bipy})_3\text{I}_2$  displays a highly enhanced spectrum which is identical to those obtained with silver slides. Pyridine, benzoic acid and benzene, however, did not display any appreciable SERS enhancement.

#### 6.4.3 Discussion.

The analytical potential of both of these categories of surfaces has been discussed in a series of reports (107 - 109).

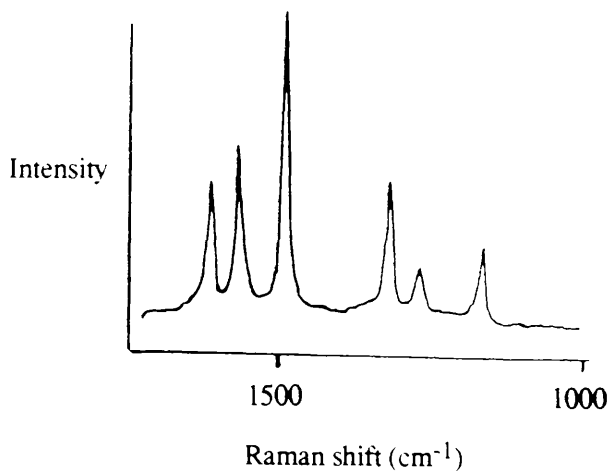


Figure 6.20: SERR spectrum of Ru(bipy)<sub>3</sub>I<sub>2</sub> ( $2 \times 10^{-3}$  mol l<sup>-1</sup>)/silver coated TLC plate [Ar<sup>+</sup> laser, 488.0 nm excitation].

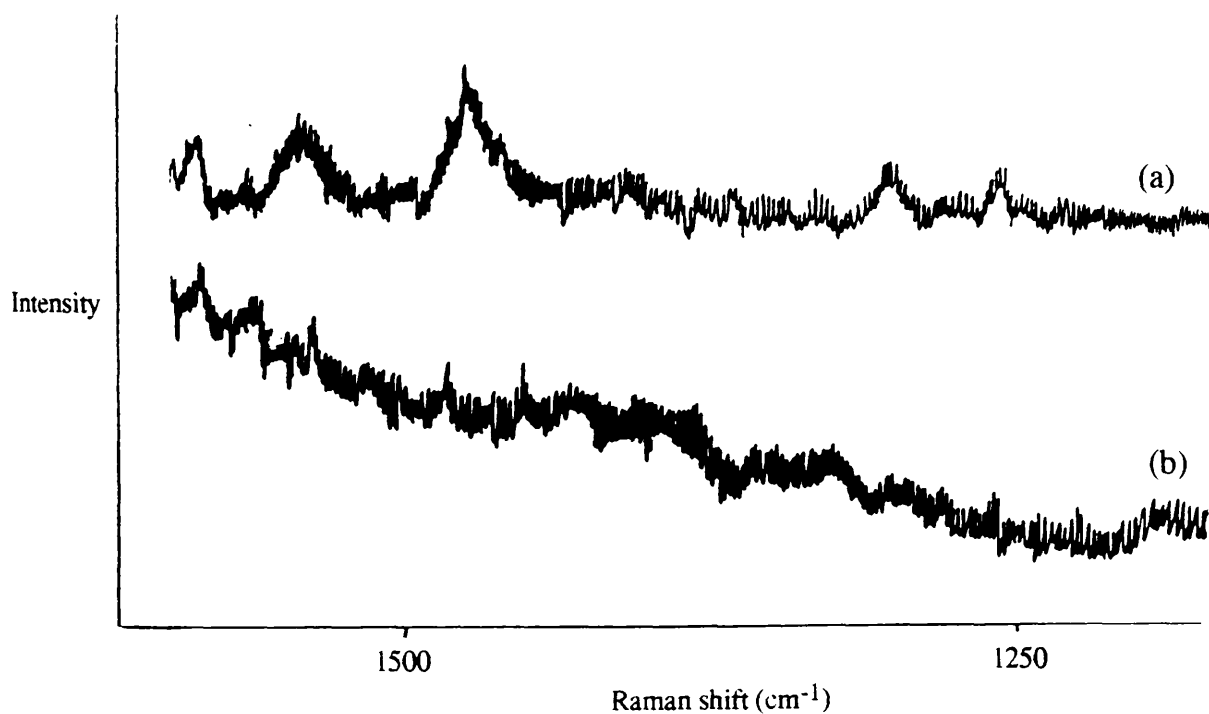


Figure 6.21: (a) SERR spectrum of Ru(bipy)<sub>3</sub>I<sub>2</sub> ( $2 \times 10^{-4}$  mol l<sup>-1</sup>)/silver-coated glass-supported silica spheres. (b) normal Raman spectrum of the adsorbate solution. [Ar<sup>+</sup> laser, 488.0 nm excitation].

The major advantage of supported colloids is that their use overcomes the problems encountered in colloidal experiments by providing active silver particles which are, in effect, already partially aggregated.

An important disadvantage of these substrates is the physical difficulty of manipulating the freshly-prepared wet surfaces and preparing them for SERS experiments. As has been demonstrated, unlike silver slides which are stable for long periods under distilled water, these surfaces have a short lifetime. The half-life of the Ru(bipy)<sub>3</sub>I<sub>2</sub>/silver-coated filter paper system, however, is longer than that previously reported by Laserna. This may be because the former system was kept totally enclosed, thus preventing rapid oxidation of the exposed silver surface. With relevance to this study, the SERRS spectra obtained from silver-coated filter paper showed no obvious differences or any additional vibrational information compared to the silver slide spectra. This is a manifestation of similar preparative procedures.

## 6.5 Silica spheres: chemical methods.

Three methods of production were used.

### 6.5.1 Filter paper-supported silica spheres.

This procedure simply involved a suspension of silica in distilled water being filtered, soaked in silver nitrate solution and sprayed with

sodium tetrahydroborate in a similar fashion to the method of Laserna *et al.*

As expected, the substrate was not stable in adsorbate solutions and, therefore, adsorbates were spotted carefully onto the surface. Ru(bipy)<sub>3</sub>I<sub>2</sub> showed slight enhancement over its normal Raman spectrum.

### 6.5.2 Glass-supported silica spheres.

Once a quantity of silica spheres had been coated onto glass and the adhesive had dried, silver coating was effected by the method of Laserna. The silver did not form homogeneously on the silica surface.

The SERS-activity of the surface was tested with Ru(bipy)<sub>3</sub>I<sub>2</sub> (figure 6.21). A noisy spectrum resulted which displayed slight enhancement over the normal Raman spectrum. It is obvious that a more satisfactory method of coating a surface such as this would be by vapour-deposition of an even silver film on the rough surface.

### 6.5.3 Modification of a method of production of silver-coated latex spheres (205).

The electronic absorption spectrum of the brown suspension produced from this reaction displayed a maximum at 441 nm.

SERRS with Ru(bipy)<sub>3</sub>I<sub>2</sub>, however, displayed no enhancement. This could be due to the formation of large silver aggregates since it was

observed that a small amount of brown precipitate had formed after the SERRS spectrum had been recorded.

#### 6.5.4 Discussion.

Clearly, chemical methods of coating silica spheres are unsuitable. With filter paper and TLC plates, aggregates of silver formed and, in the case of the filter paper method, stuck to the fibres of the paper substrate. With silica spheres, however, not enough active silver formed. Indeed, with the glass-supported silica spheres, it was observed that when the reducing agent was sprayed onto the saturated substrate, the resultant silver aggregate suspension appeared to run off the surface. This is certainly due to the inability of the silver aggregates to 'stick' to such a silica sphere template. Even if the silver produced had adhered to the silica spheres, the resultant morphology would have been one of aggregated silver formations and would not have reflected the morphology of the silica spheres.

The modified latex-coating method did not produce a SERS-active substrate. Clearly, the substitution of silica for latex is not feasible since the silver produced did not coat the particles but aggregated and eventually formed metal powder.

It is clear that the only other potentially successful method of coating silica is by vapour-deposition means.

## 6.6 Vapour-deposited surfaces.

### 6.6.1 Polycarbonate surface.

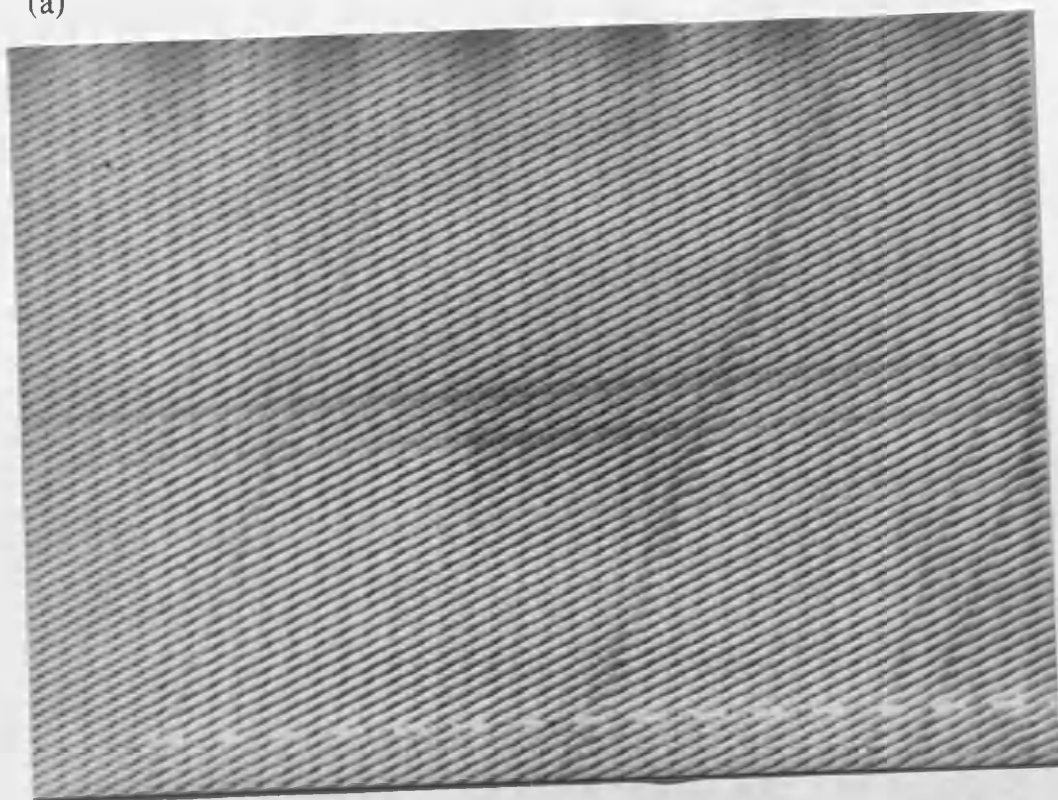
As received, this substrate was a transparent circular disc with a small hole in the centre. The disc could be cut into small pieces either by the use of a knife or scissors.

#### (a) Electron microscopy.

An initial scanning electron micrograph of a 1 cm<sup>2</sup> piece of polycarbonate, which had been cut from a disc and vapour-coated with a thin layer of gold, showed no surface features. This seemed surprising since it could plainly be seen, with the naked eye, that the polycarbonate surface diffracted visible light. The only other possibility was that the surface was rough on only one side. In order to investigate this, a piece of polycarbonate was vapour-coated with gold on both sides and studied by SEM. Three magnifications were obtained and are displayed in figure 6.22. These micrographs show that the polycarbonate surface consists of regularly spaced, undulating ridges approximately 340 nm apart. This is, of course, within the range of typical SERS-active roughness dimensions.

The discovery that the substrate is one-sided threw up experimental difficulties, associated with how the rough side would be recognisable for use in SERS experiments, since both sides appear identical to the naked eye. This problem was overcome by subjecting

(a)



(b)

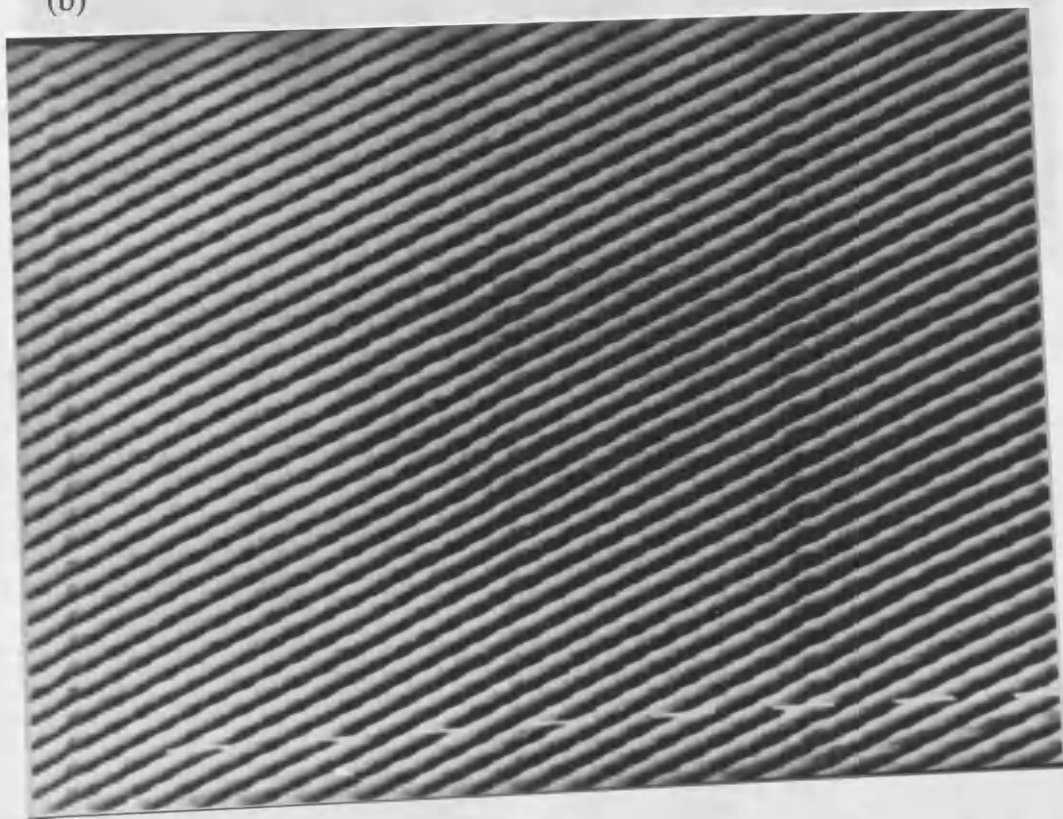
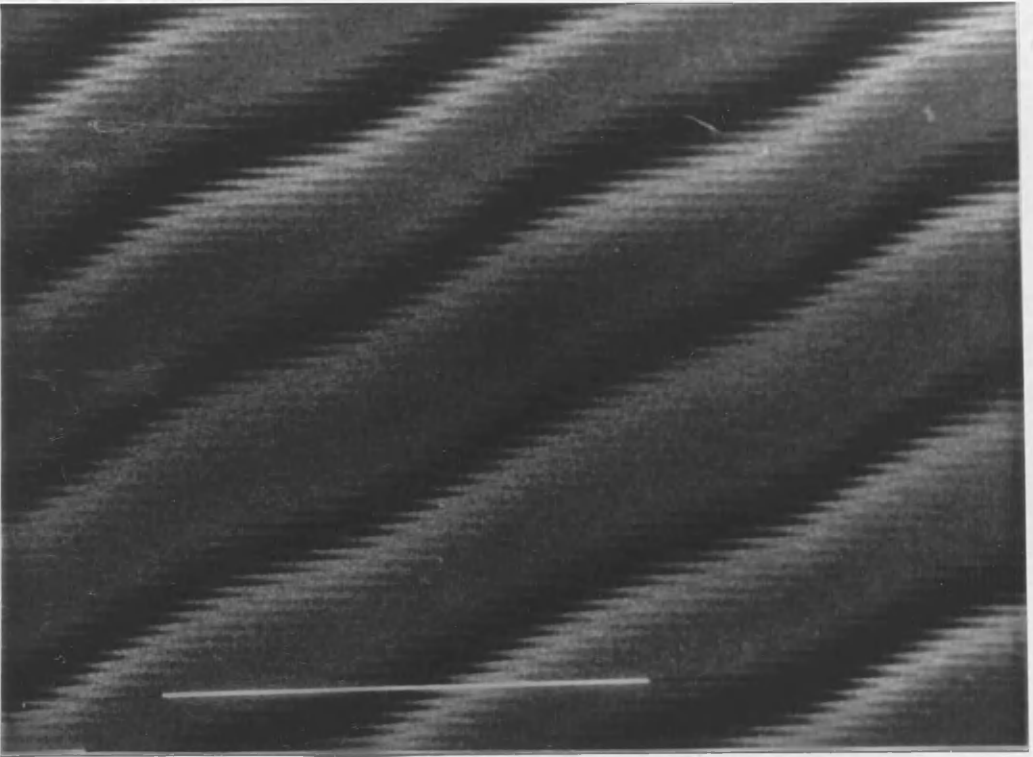


Figure 6.22: Scanning electron micrographs of the polycarbonate surface. Magnification (a) x 6,400, (b) x 12,800

(c)



(c) x 100,000.

both sides of the coated polycarbonate to adsorbate solutions. Due to the transparent nature of coated polycarbonate, the rough side was exposed to the incident laser beam whatever the orientation of the substrate on the sample stage.

One clear advantage of this category of substrate with respect to analytical SERS study is that it fulfils the requirement of reproducibility (if coated with an even layer of silver).

#### (b) Absorption spectroscopy.

The electronic absorption spectrum of a piece of silver-coated polycarbonate (50 nm thick) is pictured in figure 6.23. The spectrum has a broad maximum at 370 nm. After exposure to  $\text{Ru}(\text{bipy})_3\text{I}_2$  solution (figure 6.23), a maximum develops at 450 nm corresponding to the metal(d)  $\rightarrow$  ligand ( $\pi^*$ ) transition. There is, however, another peak present at 486 nm. It is possible that this is due to a charge-transfer interaction between adsorbate molecules and the metal surface. If this is the case, SERR spectra of  $[\text{Ru}(\text{bipy})_3]^{2+}$  on coated polycarbonate should show spectral changes due to surface/adsorbate molecule complex formation.

#### (c) SERRS of $\text{Ru}(\text{bipy})_3\text{I}_2$ .

The SERR spectrum of a solution of  $\text{Ru}(\text{bipy})_3\text{I}_2$  in contact with a piece of silver-coated polycarbonate (50 nm) is shown in figure 6.24.

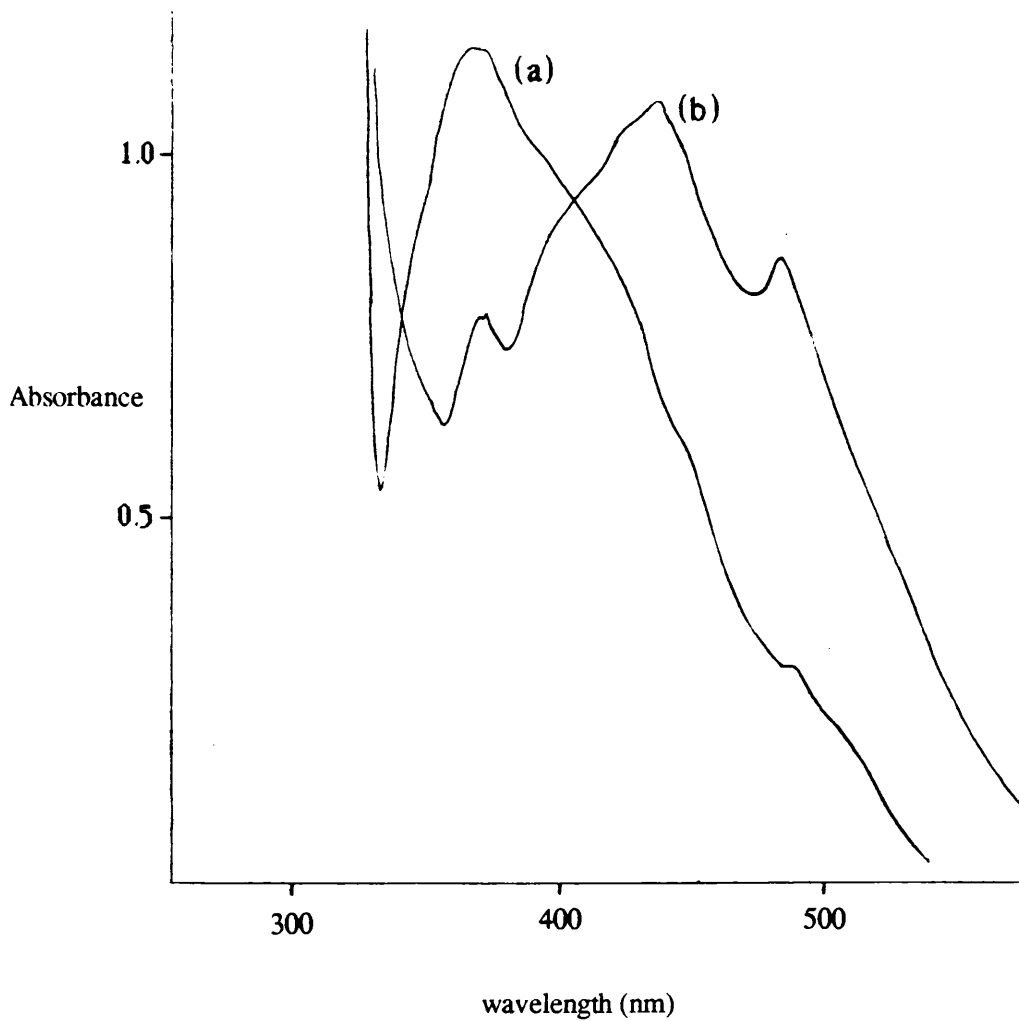


**Figure 6.23: Electronic absorption spectra of vapour silver-coated (50 nm) polycarbonate (a) before and (b) after exposure to a dilute solution of Ru(bipy)<sub>3</sub>I<sub>2</sub>.**

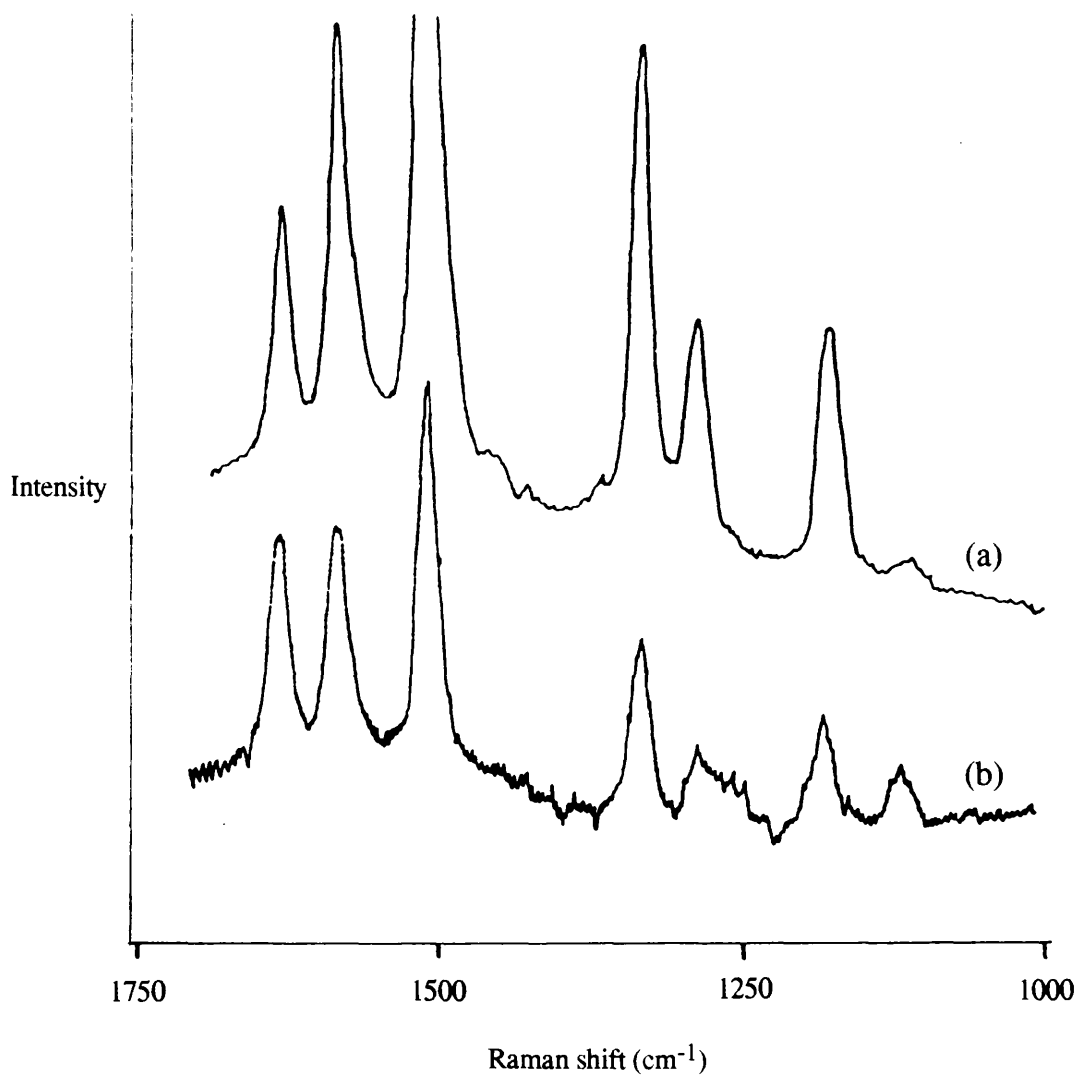


**Figure 6.24:** (a) SERR spectrum of Ru(bipy)<sub>3</sub>I<sub>2</sub> (2 × 10<sup>-4</sup> mol l<sup>-1</sup>)/chemically silver-coated slide.  
(b) SERR spectrum of the same solution in contact with vapour silver-coated (50 nm) polycarbonate.  
[Ar<sup>+</sup> laser, 488.0 nm excitation].

The SERR spectrum of a similar concentration of the complex in contact with a chemically coated silver slide is also shown. This SERRS spectrum effectively represents the RRS of  $\text{Ru}(\text{bipy})_3\text{I}_2$ , as shown in section 6.3.1(b). There are clearly subtle differences in wavenumber positions of bands and relative band intensities between the spectra. In addition, there is, what appears to be, a new peak in the polycarbonate spectrum at  $1115\text{ cm}^{-1}$ . The spectrum of a piece of polycarbonate, however, showed that this anomalous peak was due to the polycarbonate substrate itself. It is inevitable that SERR spectra of coated polycarbonate exhibit such bands as the surface is transparent to the laser beam.

Nevertheless, it is clear that these real changes in wavenumber and relative intensities may indicate chemisorption of the  $[\text{Ru}(\text{bipy})_3]^{2+}$  molecule. All of these aspects are discussed, in greater detail, in section 7.3.

One clear difference between the two spectra, however, is the degree of enhancement. With similar concentrations of adsorbate solutions, the enhancement with the silver coated polycarbonate is smaller by a factor of approximately ten compared to the enhancement shown by the silver slide.

#### Effect of excitation wavelength.

The question of whether or not a charge transfer complex forms was

probed by varying the excitation wavelength of laser radiation. If, indeed, the maximum at 486 nm in the absorption spectrum corresponds to charge transfer excitation, the excitation 'profile' should reach a maximum in this area. If the enhancement of the spectrum is purely associated with surface plasmon resonance, the maximum would be at 400 nm, assuming no surface rearrangement on contact with Ru(bipy)<sub>3</sub>I<sub>2</sub> solution.

As can be seen from table 6.9 and figure 6.25, the intensity of the 1483 cm<sup>-1</sup> peak of Ru(bipy)<sub>3</sub>I<sub>2</sub> reaches a maximum of intensity with exciting lines of 496.5 and 514.5 nm. This does not conclusively prove that a charge-transfer surface/adsorbate complex forms: more detailed study with a dye laser would be necessary in order to prove this fully. This area is considered further in section 7.3.

Table 6.9: Effect of changing the argon-ion excitation wavelength on the intensity of the 1483 cm<sup>-1</sup> peak of Ru(bipy)<sub>3</sub>I<sub>2</sub> adsorbed on silver-coated (50 nm) polycarbonate.

<u>Ar<sup>+</sup> excitation (nm)</u>	<u>Intensity (arbitrary: peak height - baseline)</u>
457.9	1140
476.5	1450
488.0	2070
496.5	2180
501.7	2200
514.5	2190

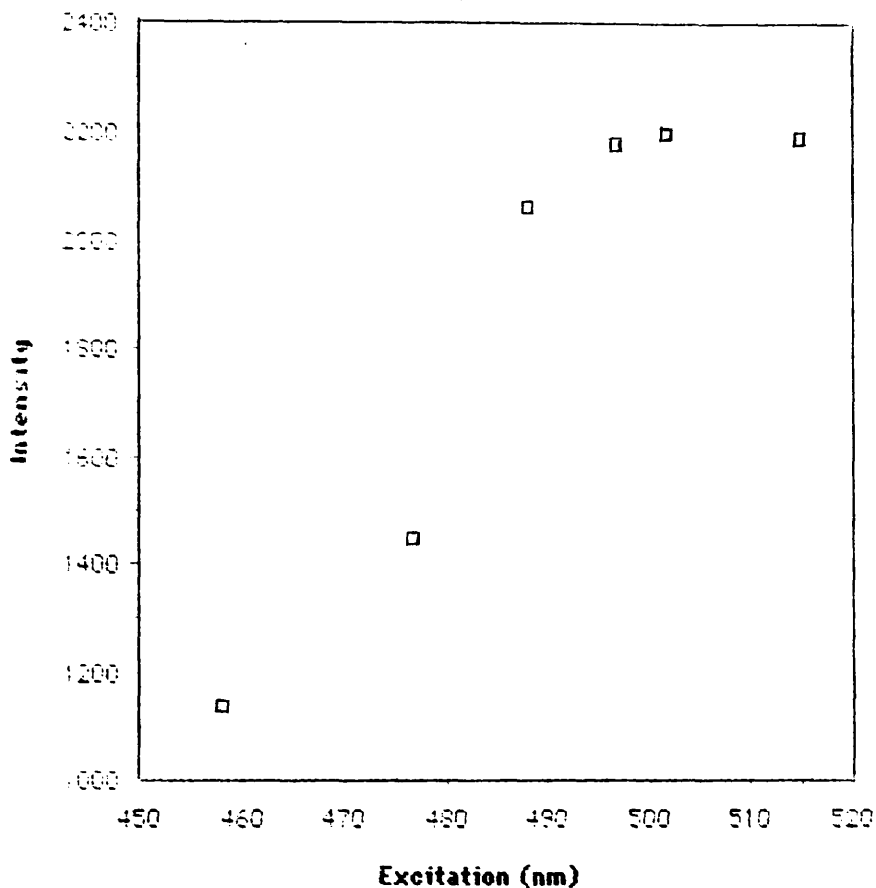


**Figure 6.25:** Plot of the intensity of the  $1483\text{ cm}^{-1}$  peak of the SERR spectrum of  $\text{Ru}(\text{bipy})_3\text{I}_2$ /vapour silver-coated (50 nm) polycarbonate versus excitation wavelength. Data from table 6.9.

Effect of variation in the vapour-coating procedure.

SERR spectra of  $\text{Ru}(\text{bipy})_3\text{I}_2$  in contact with pieces of polycarbonate coated with 25, 50 and 100 nm of silver are displayed in figure 6.26.

There are no obvious differences in terms of degree of enhancement between the three spectra. This finding is not surprising since the coating method used is unlikely to 'fill in' any of the surface features, even with thicker coatings. In most of the subsequent preparations of

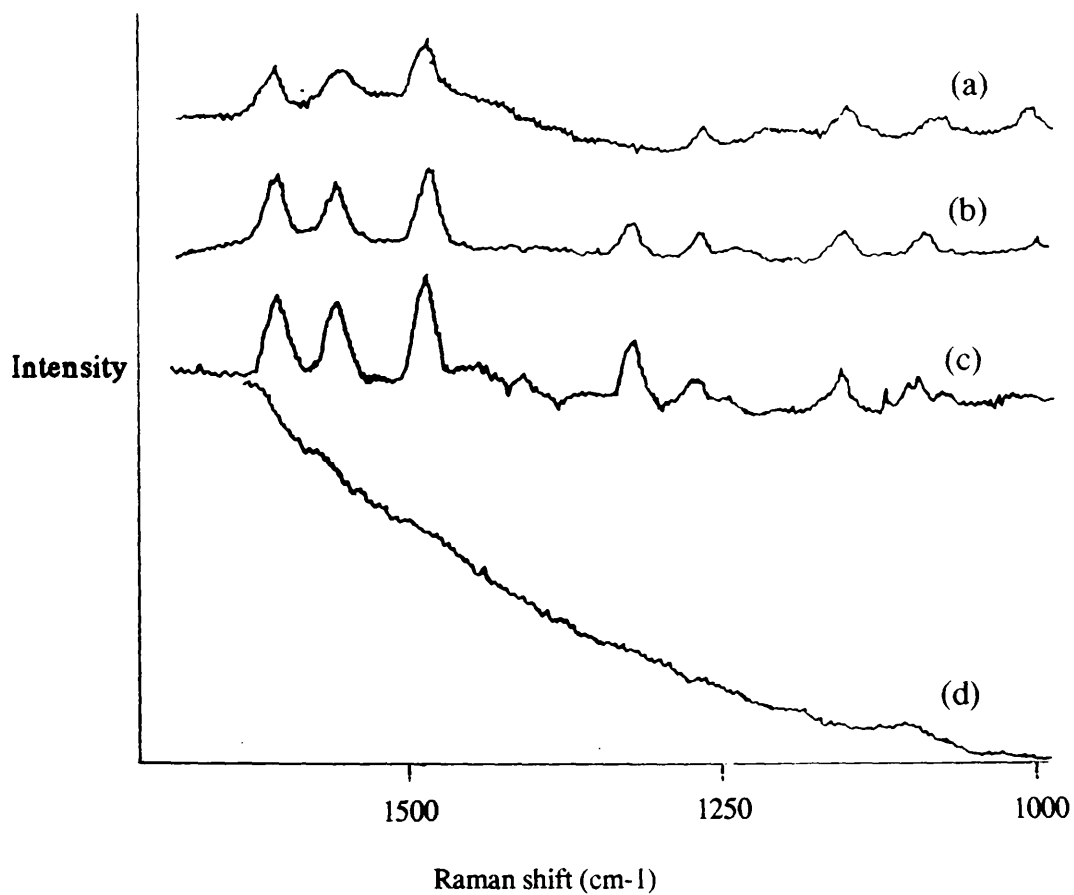


**Figure 6.26:** SERR spectra of Ru(bipy)<sub>3</sub>I<sub>2</sub> ( $2 \times 10^{-4}$  mol l<sup>-1</sup>) in contact with polycarbonate coated with (a) 25, (b) 50 and (c) 100 nm of silver. (d) normal Raman spectrum of the same solution. [Ar<sup>+</sup> laser, 488.0 nm excitation].

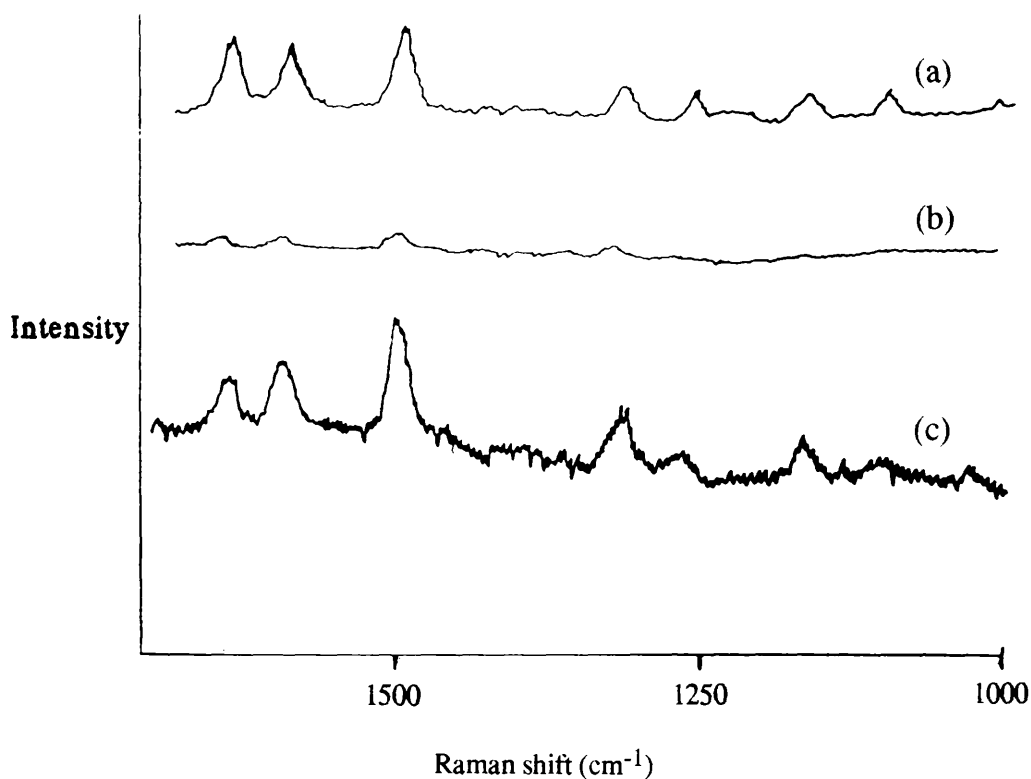


**Figure 6.27:** SERR spectra of  $\text{Ru}(\text{bipy})_3\text{I}_2$  ( $2 \times 10^{-4} \text{ mol l}^{-1}$ ) in contact with vapour 50 nm silver-coated (a) polycarbonate, (b) flat and (c) frosted microscope slides (counter sensitivity increased by a factor of 10). [ $\text{Ar}^+$  laser, 488.0 nm excitation].

silver-coated polycarbonate surfaces, 50 nm was chosen as the normal film thickness. This was a balance between economy and the possibility of a very thin layer of silver burning in the laser beam.

Figure 6.27 shows the SERR spectra of a solution of  $\text{Ru}(\text{bipy})_3\text{I}_2$  in contact with silver-coated (50 nm) polycarbonate and silver-coated (50 nm) flat and frosted microscope slides. The spectra of the flat and frosted microscope slides show considerably less enhancement compared to the spectrum of the polycarbonate. This demonstrates that the regular features on the polycarbonate surface cause enhancement, in addition to the silver mirror itself.

#### (d) Other adsorbates.

The SERS-activity of the polycarbonate surface with organic adsorbate species (pyridine, benzene, benzoic acid and p-amino benzoic acid) was tested. None of the spectra displayed any enhancement.

#### 6.6.2 Silica spheres.

Suspensions of silica spheres of varying dimensions, prepared *via* the method of Adams *et al* (204), were dried using two methods: rotary evaporation and slow evaporation in air to give semi-transparent plates.

Figure 6.28 shows the SERR spectrum of silver-coated (50 nm) silica spheres which had been dried by rotary evaporation immersed in a solution of  $\text{Ru}(\text{bipy})_3\text{I}_2$ . The spheres had been ground and stuck on a

glass substrate with 3M spray-glue and the resultant layer of spheres had been evened. The spectrum displays little enhancement over the RRS of the complex. The silica surface was opaque, thus rendering the measurement of its absorption spectrum impossible.

The electronic absorption spectrum of a vapour silver-coated evaporated silica plate, as shown in figure 6.29, exhibits a broad maximum at 408 nm. Figure 6.30 shows the SERR spectrum of  $\text{Ru}(\text{bipy})_3\text{I}_2$  in contact with this surface. Clearly, this spectrum is only slightly enhanced compared to the corresponding RRS.

Benzoic acid and pyridine showed no enhancement with this surface.

Both types of coated silica sphere surfaces were studied by SEM (figure 6.31). The rotary evaporated coated silica surface is highly disordered and randomly rough, whereas the slowly-evaporated surface has a more ordered morphology. The size distribution of the roughly spherical protrusions on the surface is between 300 and 1000 nm with the features spaced approximately 1000 nm apart. Since SERS-active substrates necessarily have coupled metal features, the large spacing of silver-coated spheres on the surface could explain the lack of enhancement.

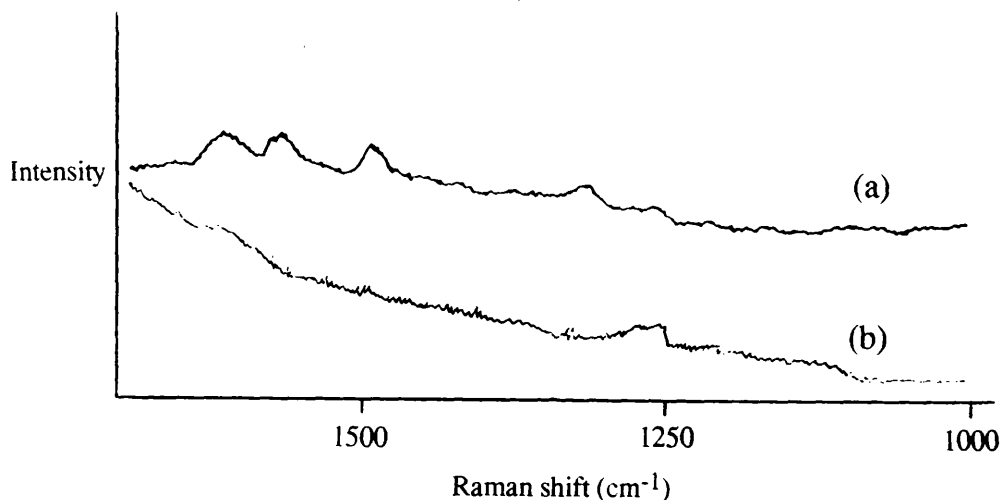


**Figure 6.28:** (a) SERR spectrum of Ru(bipy)<sub>3</sub>I<sub>2</sub> ( $2 \times 10^{-4}$  mol l<sup>-1</sup>)/vapour silver-coated (50 nm) silica spheres on glass. (b) normal Raman spectrum of the adsorbate solution. [Ar<sup>+</sup> laser, 488.0 nm excitation].

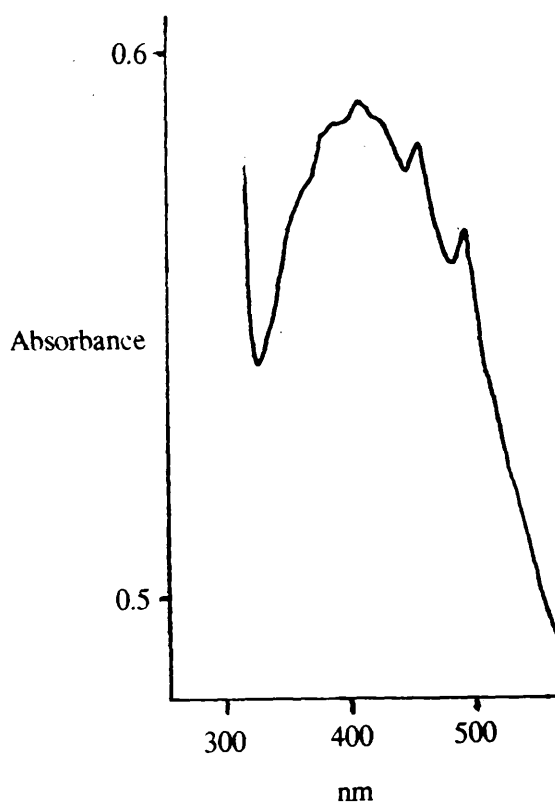


**Figure 6.29:** Electronic absorption spectrum of a vapour silver-coated (50 nm) slow-evaporated silica plate.

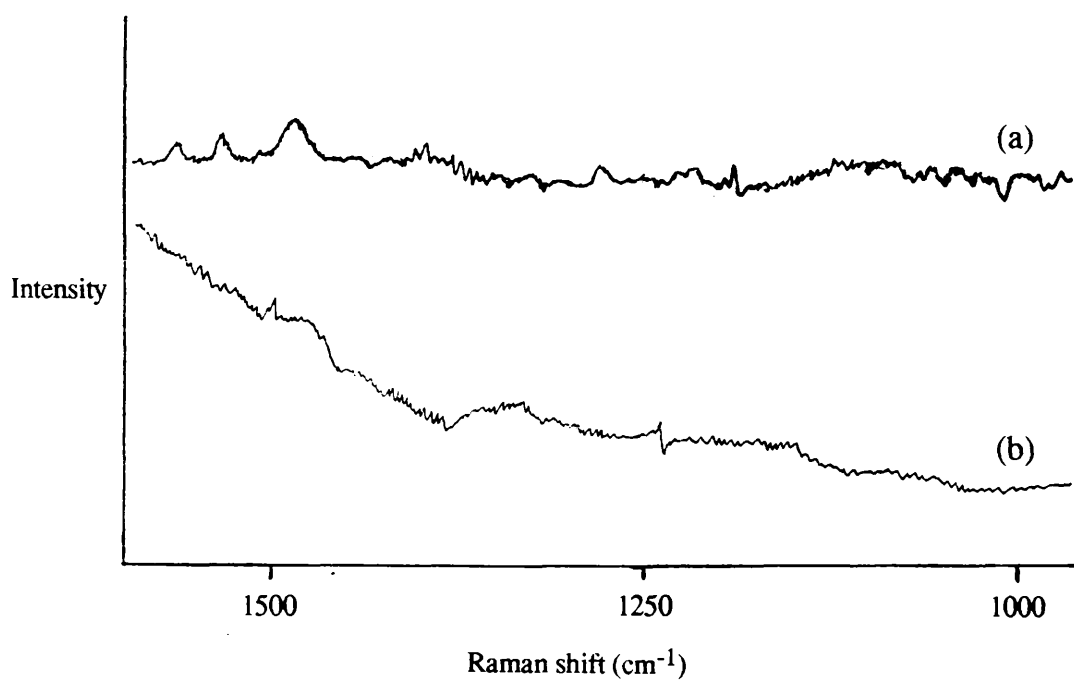


Figure 6.30: (a) SERR spectrum of Ru(bipy)<sub>3</sub>I<sub>2</sub> ( $2 \times 10^{-4}$  mol l<sup>-1</sup>)/ vapour silver-coated (50 nm) slow-evaporated silica plate. (b) normal Raman spectrum of the adsorbate solution. [Ar<sup>+</sup> laser, 488.0 nm excitation].

(a)



(b)

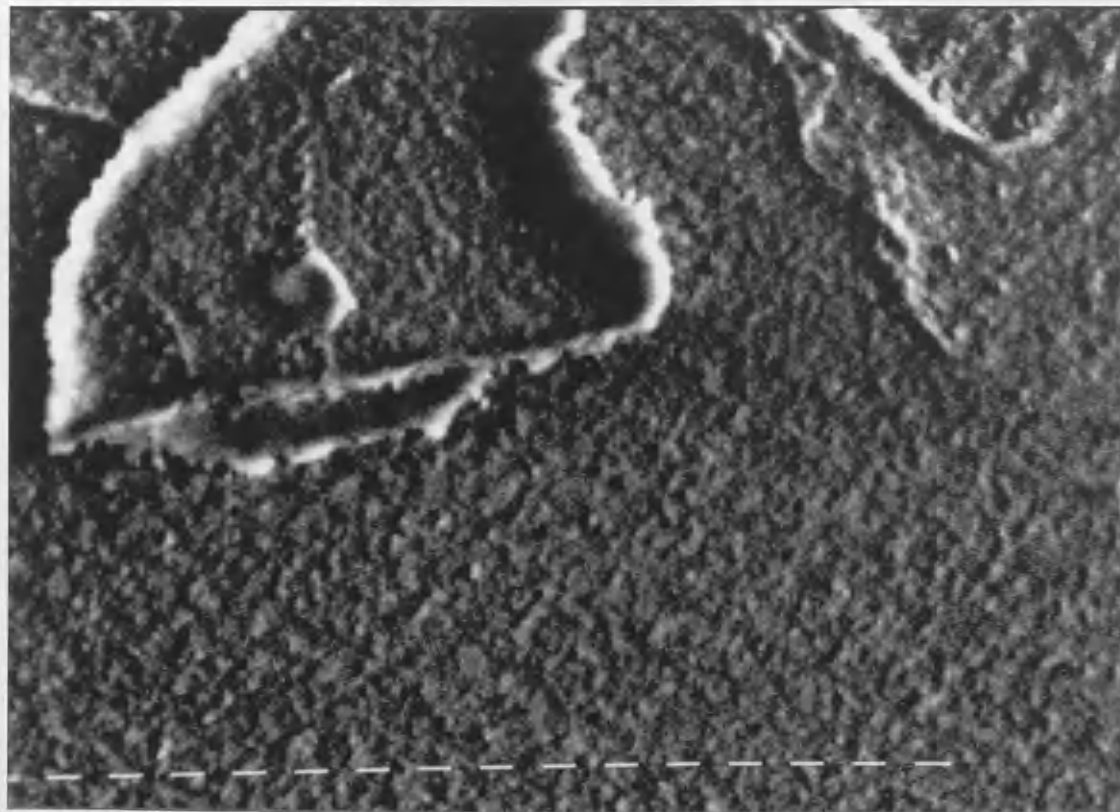


Figure 6.31: Scanning electron micrographs of (a) rotary-evaporated silica spheres and (b) slow-evaporated silica spheres. Magnification x 3200.

### 6.6.3 Discussion.

The inherent reproducibility of vapour silver-coated polycarbonate substrates renders them suitable for use in analytical SERS study. As the SEM study revealed, the variation of the roughness ridges across one piece of polycarbonate is extremely small. Hence, identical coated polycarbonate surfaces can be produced, provided the film thickness is carefully controlled. The preparative procedure, however, is necessarily time-consuming.

The SERR spectrum of  $\text{Ru}(\text{bipy})_3\text{I}_2$  shows clear differences with respect to the RRS and, consequently, the SERR spectrum of the molecule on silver slides. Although the existence of an adsorbate molecule/surface complex cannot be proved conclusively, the results obtained may be explained by considering the differences in preparative procedures used and the overall differences in the morphologies of the two types of surfaces. This is further discussed in section 7.3.

One limiting factor in the study of the SERRS of tris-2,2'-bipyridyl ruthenium(II) complexes is the enhancement obtained. Although it is evident that chemical bond formation occurs, to some extent, with the coated polycarbonate surface, the degree of enhancement is considerably smaller than that obtained with 'chemical' systems such as silver-coated slides. This may simply be a question of surface area. Although no accurate measurements were made, it is clear that the

regularly rough, homogeneous silver-coated polycarbonate surface has a much lower surface area than the randomly rough silver slide surface, leading to a decrease in the number of adsorbate molecules 'sampled' by the incident laser beam.

Another possible explanation for the lower enhancement concerns the dimensions of the polycarbonate roughness features. One of the basic tenets of the electromagnetic theory of enhancement states that, for a high degree of enhancement, the metal roughness features must be considerably smaller than the wavelength of the exciting radiation. The polycarbonate roughness features are 340 nm apart, compared to silver slide features of between 40 and 150 nm. With laser excitation of 488.0 nm, therefore, silver slides, having the smallest metal features, would be expected to produce the larger SERRS enhancement.

The ability of molecules such as  $\text{Ru}(\text{bipy})_3\text{I}_2$  to adsorb to the polycarbonate surface, but not organic species such as 2,2'-bipyridine and benzoic acid, may reflect the nature of the surface. The 2,2'-bipyridine molecule can rotate about the  $\text{C}_2-\text{C}_2'$  axis, whereas  $\text{Ru}(\text{bipy})_3\text{I}_2$  is essentially 'fixed'. It is possible that the highly ordered, smooth nature of the polycarbonate surface morphology may only allow such 'fixed' molecules, and not molecules which can bind in several ways, to adsorb. If this is the case, similar binding modes should be noted with other tris(2,2'-bipyridyl) and modified ruthenium(II)

complexes.

### 6.7 General comments.

The two surfaces which displayed the greatest potential with respect to the analytical applications of SERS were chemically prepared silver-coated slides and vapour-deposited silver-coated polycarbonate.

Silver-coated slides displayed intense enhancement with  $\text{Ru}(\text{bipy})_3\text{I}_2$  and also appreciable enhancement with simple organic molecules (2,2'-bipyridine, pyridine and benzoic acid). Molecules containing some type of co-ordinative atom or group seem to be necessary for the observation of SERS enhancement. In particular, the results obtained with silver slides indicate that molecules with heteroaromatic, nitrogen-containing rings should exhibit SERS activity.

The SERS and SERRS-activity of filter paper and TLC plate-supported silver colloids mirrored the activity of silver slides. The supported colloids, however, have several experimental drawbacks.

Silver-coated polycarbonate surfaces, although showing considerably less enhancement with  $[\text{Ru}(\text{bipy})_3]^{2+}$ , exhibited interesting adsorption effects. Clearly, the ordered nature of the surface morphology allows the chemisorption of the  $[\text{Ru}(\text{bipy})_3]^{2+}$  molecule.

This is reflected in the observation of new vibrational features in the resultant SERR spectra. The extent of chemisorption, however, is not clear.

CHAPTER SEVEN.

SERIES OF TRIS(2,2'-BIPYRIDINE) RUTHENIUM(II)

AND MODIFIED COMPLEXES ON CHEMICALLY-PREPARED

AND VAPOUR-DEPOSITED SURFACES.

## 7. SERRS OF TRIS(2,2-BIPYRIDINE) RUTHENIUM(II) AND MODIFIED COMPLEXES ON CHEMICALLY-PREPARED AND VAPOUR-DEPOSITED SURFACES.

### 7.1 Introduction.

The investigations described in chapter 6 revealed two interesting points in relation to SERS-active substrates and, particularly, the activity of  $[\text{Ru}(\text{bipy})_3]^{2+}$ .

(a) With silver slides and, indeed, all the chemically-produced surfaces tested,  $[\text{Ru}(\text{bipy})_3]^{2+}$  exhibited a high degree of enhancement which was dependent upon the concentration of adsorbate present. The SERR spectra were effectively enhanced duplicates of the corresponding resonance Raman spectra, indicating physisorption of the complex and subsequent enhancement through the electromagnetic mechanism.

The spectra showed high enhancement of ring breathing, hydrogen wagging, carbon-carbon and other ring modes of the 2,2'-bipyridyl ligand. This suggests that the small physisorptive interaction between the adsorbate molecule and the metal surface must occur *via* the 2,2-bipyridyl ring.

The equivalence of SERRS results with all the chemically-prepared substrates is a consequence of almost identical preparative routes.

(b) Vacuum-coated silver polycarbonate surfaces, as prepared, had

surface morphologies completely different from those of the chemically-prepared surfaces. As would be expected, the SERR spectra of the coated polycarbonate displayed subtle modifications with respect to the corresponding silver slide SERR spectra.

The rationale behind the following studies was to introduce and investigate the additional factor of the influence of co-ordinative substituents upon the adsorption behaviour of the parent  $[\text{Ru}(\text{bipy})_3]^{2+}$  molecule.

## **7.2 Chemically-prepared silver-coated slides.**

### **7.2.1 $\text{Ru}(\text{bipy})_3\text{I}_2$ : assignment of RRS and SERRS.**

The SERR spectrum of a solution of  $\text{Ru}(\text{bipy})_3\text{I}_2$  in contact with a silver slide and the RR spectrum of the complex are shown in figure 7.1.

Although the bands present in the SERR spectrum are intense and well-defined and simple to determine their positions accurately, the recording of the RRS of the molecule proved troublesome. As mentioned previously, the central problem is the dominance of fluorescence. A RRS with acceptable signal-to-noise ratios was obtained with high laser power output (500 mW at laser head) and high photon-counter sensitivity.

Presented in table 7.1 are spectral data from the SERR and RR spectra of  $\text{Ru}(\text{bipy})_3\text{I}_2$ . These data were based on several runs of each

spectrum. The variance of the band positions was commonly only 1 or 2  $\text{cm}^{-1}$ . Some peaks, however, were unable to be measured in the RRS.

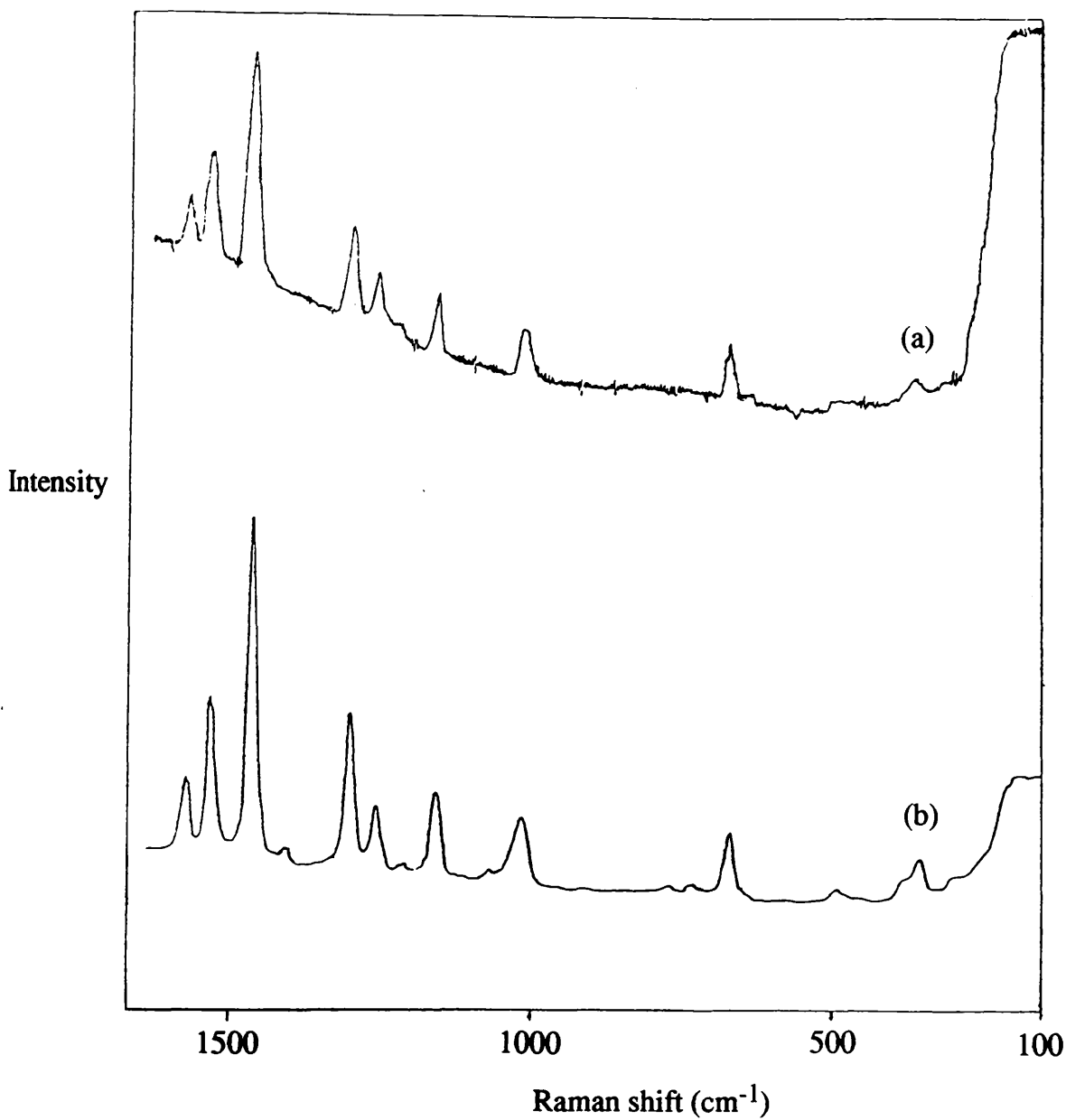
It is clear, from the tabulated data, that there are few differences, in terms of positions of bands, between the two spectra. There are also no obvious changes in relative intensities.

### Assignment.

The assignment of the vibrational modes of  $[\text{Ru}(\text{bipy})_3]^{2+}$ , as detailed in table 7.1, is from the studies of Mallick *et al.* (210). The assignment of the principle vibration of each mode is given. The full assignment of each mode is presented with the normal mode descriptions in figure 7.3. Mallick *et al.* assigned the spectrum on the basis of normal co-ordinate calculations, employing a modified valence force field procedure. The spectra were interpreted on the basis of effective  $C_{2v}$  symmetry (a single co-ordinated 2,2'-bipyridine ligand). The atom numbering and internal co-ordinate labelling scheme is indicated in figure 7.2.

Figure 7.3 shows the normal mode descriptions of the  $A_1$  Raman-active vibrations of the  $[\text{Ru}(\text{bipy})_3]^{2+}$  molecule. From the assignments, it can be seen that the normal modes are complex combinations of various stretching, wagging and breathing modes.

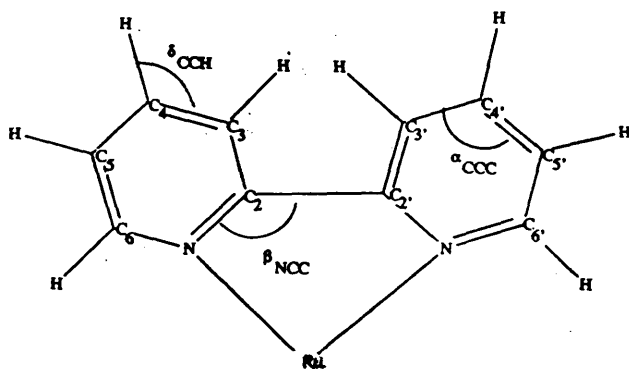
The low wavenumber region of the Raman spectrum of the complex



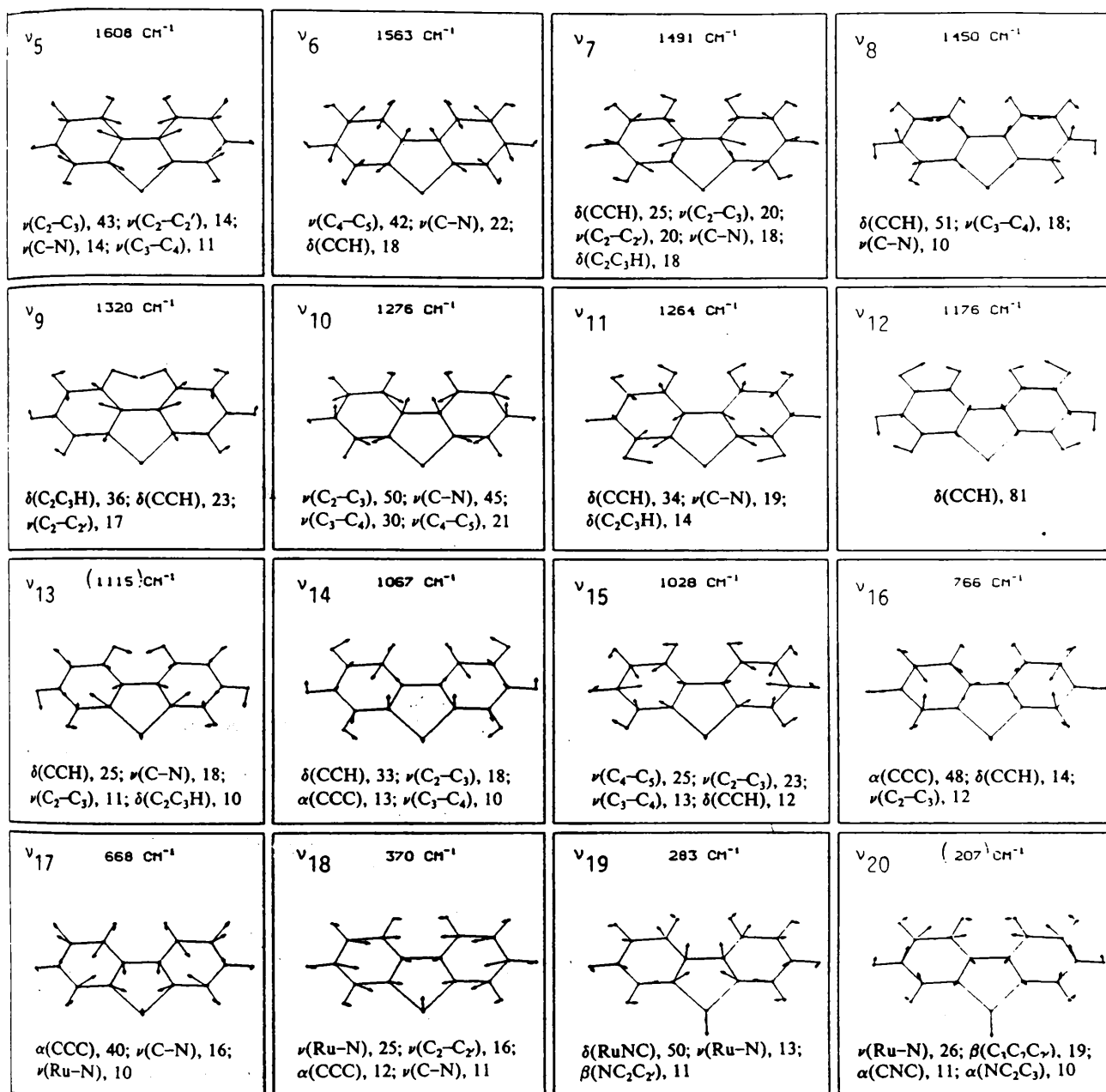
**Figure 7.1:** (a) Resonance Raman and (b) SERR spectra of  $\text{Ru}(\text{bipy})_3\text{I}_2$  ( $2 \times 10^{-3} \text{ mol l}^{-1}$  aqueous solution)/silver slide. [Ar<sup>+</sup> laser, 488.0 nm excitation].

Table 7.1: Data from resonance Raman and SERR spectra of  $2 \times 10^{-3}$  $\text{mol l}^{-1}$  Ru(bipy) $_3$ I $_2$  solution / silver-coated slide.

<u>RRS (cm<math>^{-1}</math>)</u>	<u>SERRS/Ag slide (cm<math>^{-1}</math>)</u>	<u>Assignment (210)</u>
	265	$\nu(\text{RuNC})$
339	335	
	372	$\nu(\text{RuN})$
435	435	
	467	
671	668	$\alpha(\text{CCC})$
	723	$\alpha(\text{CCC})$
	760	
1027	1025	$\nu(\text{C}_4-\text{C}_5)$
	1066	$\delta(\text{CCH})$
1176	1177	$\delta(\text{CCH})$
1264	1260	$\delta(\text{CCH})$
1276	1275	$\nu(\text{C}_2-\text{C}_3)$
1318	1318	$\delta(\text{C}_2\text{C}_3\text{H})$
	1451	$\delta(\text{CCH})$
1489	1488	$\delta(\text{CCH})$
1562	1560	$\nu(\text{C}_4-\text{C}_5)$
1604	1605	$\nu(\text{C}_2-\text{C}_3)$



**Figure 7.2: Atom numbering and internal co-ordinate labelling scheme of one co-ordinated 2,2'-bipyridine of the  $[\text{Ru}(\text{bipy})_3]^{2+}$  molecule. The  $\delta(\text{CCH})$  and  $\alpha(\text{CCC})$  modes are illustrated.**



**Figure 7.3: Normal mode descriptions of the  $A_1$  vibrations of  $[\text{Ru}(\text{bipy})_3]^{2+}$ . The band positions indicated are those calculated by Mallick *et al.* (210). The assignment of each mode is also given, along with potential energy distribution (PED, %).**

is dominated by Ru—N stretching and RuNC modes. In the region 600 to 1000  $\text{cm}^{-1}$ , ring-breathing (out of plane and in plane) is observed.

Between 1000 and 1650  $\text{cm}^{-1}$ , the spectrum shows mainly C=C stretching and in-plane hydrogen wagging modes. The C—H stretching modes between 3060 and 3075  $\text{cm}^{-1}$  were not examined.

### 7.2.2 RRS and SERRS with tris(diethyl-2,2'-bipyridine-4,4'-dicarboxylate) ruthenium(II), [Ru(diesbipy)<sub>3</sub>]<sup>2+</sup>.

Figure 7.4 shows the SERR spectrum of an aqueous solution of the diester complex in contact with a silver-coated slide, along with the corresponding RR spectrum. It should be noted that the two spectra shown are not under the same experimental conditions: they are displayed for the purposes of direct comparison. The power required to achieve acceptable signal-to-noise ratios in the RRS was orders of magnitude greater than the power needed to generate a strong SERR spectrum. Table 7.2 details all the band positions in the RR and SERR spectra of the diester complex. As with the parent complex, these figures are based on a series of identical spectra.

#### (a) Resonance Raman spectrum.

The RRS of the diester complex shows a broadly similar pattern, in the region displayed, compared to the RRS of the parent complex. There are, however, wavenumber shifts consistent with the modification of

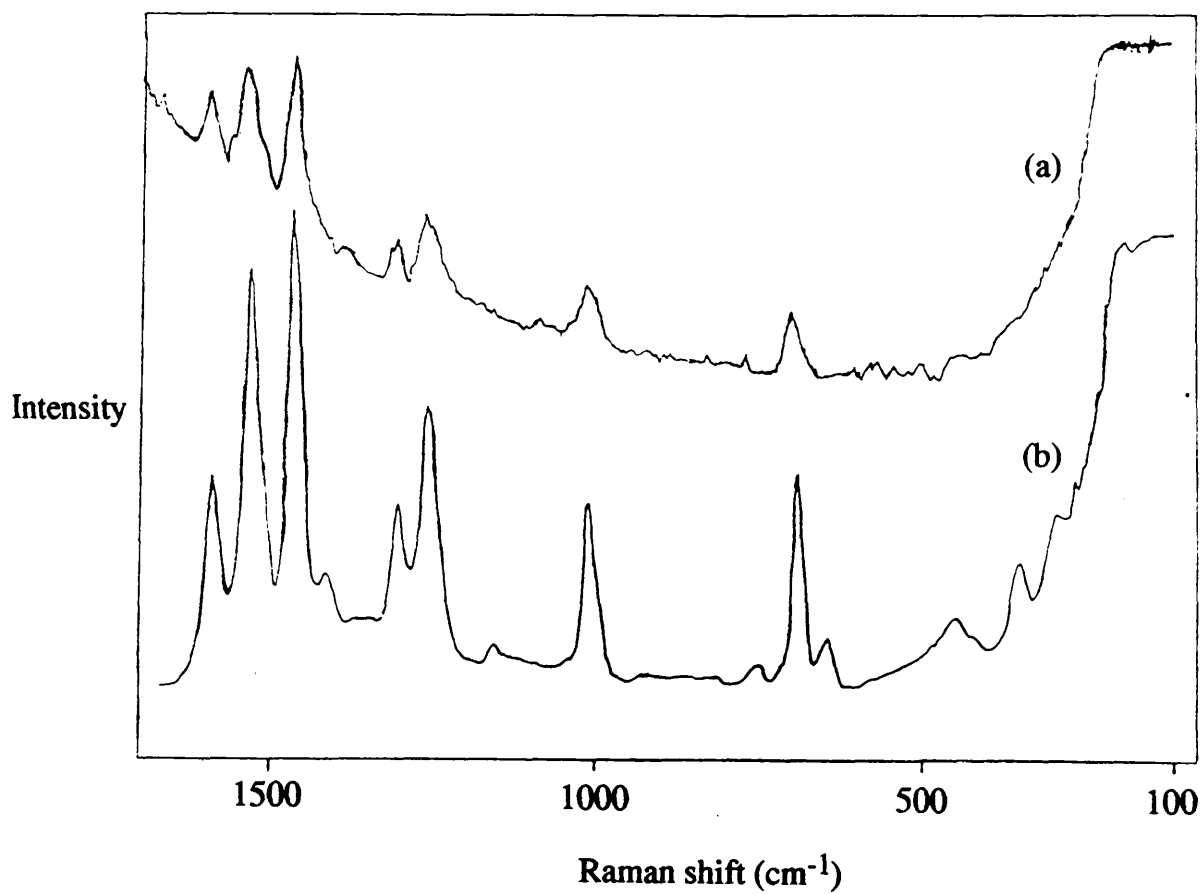


**Figure 7.4: (a) Resonance Raman and (b) SERR spectra of  $\text{Ru}(\text{diesbipy})_3[\text{BF}_4]_2$  (dilute aqueous solution)/silver slide. [ $\text{Ar}^+$  laser, 488.0 nm excitation].**

Table 7.2: Data from resonance Raman and SERR spectra of a dilute solution of Ru(diesbipy)<sub>3</sub>[BF<sub>4</sub>]<sub>2</sub> / silver-coated slide.

<u>RRS (cm<sup>-1</sup>)</u>	<u>SERRS/Ag slide (cm<sup>-1</sup>)</u>	<u>Assignment (210)</u>
	251	$\nu(\text{RuNC})$
	285	
	345	$\nu(\text{RuN})$
	459b	
	650	$\alpha(\text{CCC})$
693	690	$\alpha(\text{CCC})$
	763	
1025	1024	$\nu(\text{C}_4-\text{C}_5)$
	1182	$\delta(\text{CCH})$
1274	1274	$\nu(\text{C}_2-\text{C}_3)$
1319	1319	$\delta(\text{C}_2\text{C}_3\text{H})$
	1438	$\delta(\text{CCH})$
1482	1480	$\delta(\text{CCH})$
1557	1555	$\nu(\text{C}_4-\text{C}_5)$
1615	1615	$\nu(\text{C}_2-\text{C}_3)$

(b = broad)

the 2,2'-bipyridyl ligand in the  $C_4$  and  $C_{4'}$  positions. Two points are worthy of mention. Firstly, in the RRS of the parent complex, a peak was observed at  $1176\text{ cm}^{-1}$ , ascribed to an in plane hydrogen wagging mode (81% PED). In this region in the RRS of the diester complex a peak of comparable intensity is not present. A very small feature, however, can be observed. The diminution of this peak is not surprising, since the incorporation of carboxylic ester substituents in the ring, and the subsequent loss of two ring hydrogens, would have the effect of reducing the contribution of such hydrogen wagging modes.

Secondly, the peaks at  $1274$  and  $1319\text{ cm}^{-1}$  in the RRS of the diester have reversed their relative intensities with respect to the two corresponding peaks in the parent complex RRS (at  $1275$  and  $1318\text{ cm}^{-1}$ ). The peak at  $1319\text{ cm}^{-1}$  is assigned as hydrogen wagging ( $C_2C_3$ ), in-plane hydrogen wagging and  $C_2-C_{2'}$  stretching. The peak at  $1274\text{ cm}^{-1}$ , however, is not associated with any hydrogen wagging modes, being due to  $C=C$  and  $C=N$  vibrations, and, therefore, is stronger in the RRS of the diester complex.

No distinct modes associated with the carbonyl-ester groups are observed in the RRS. These vibrations will, in a similar fashion to the modes of the parent complex, be combined with the other ring modes resulting in shifts in the band positions.

(b) Comparison of the RRS and SERRS of the diester complex.

Clearly, there are no differences, in terms of band positions or relative intensities, between the two spectra, as displayed in figure 7.4. The SERR spectrum displays enhancement almost comparable to that observed with  $\text{Ru}(\text{bipy})_3\text{I}_2$ . The RRS shows evidence of fluorescence: the baseline begins to rise sharply from approximately  $1400\text{ cm}^{-1}$ . In the SERR spectrum the fluorescence is almost completely quenched.

These findings indicate that the presence of carboxylic ester substituents in the  $\text{C}_4$  and  $\text{C}_4'$  positions of each of the 2,2'-bipyridyl ligands incorporated in the complex does not influence the adsorption behaviour of the molecule on silver-coated slides. The complex does not chemically bind to the silver surface and, consequently, the enhancement, like that of  $[\text{Ru}(\text{bipy})_3]^{2+}$ , is caused exclusively by the electromagnetic (surface plasmon) effect.

No experiments were carried out to investigate the concentration dependence of the SERRS of the diester complex, but highly-enhanced spectra were obtained from solutions of  $10^{-5}\text{ mol l}^{-1}$  and lower concentrations.

7.2.3 Tris(4,4'-diamino-2,2'-bipyridine) ruthenium (II).



Figure 7.5 shows the SERR spectrum of a solution of the diamino

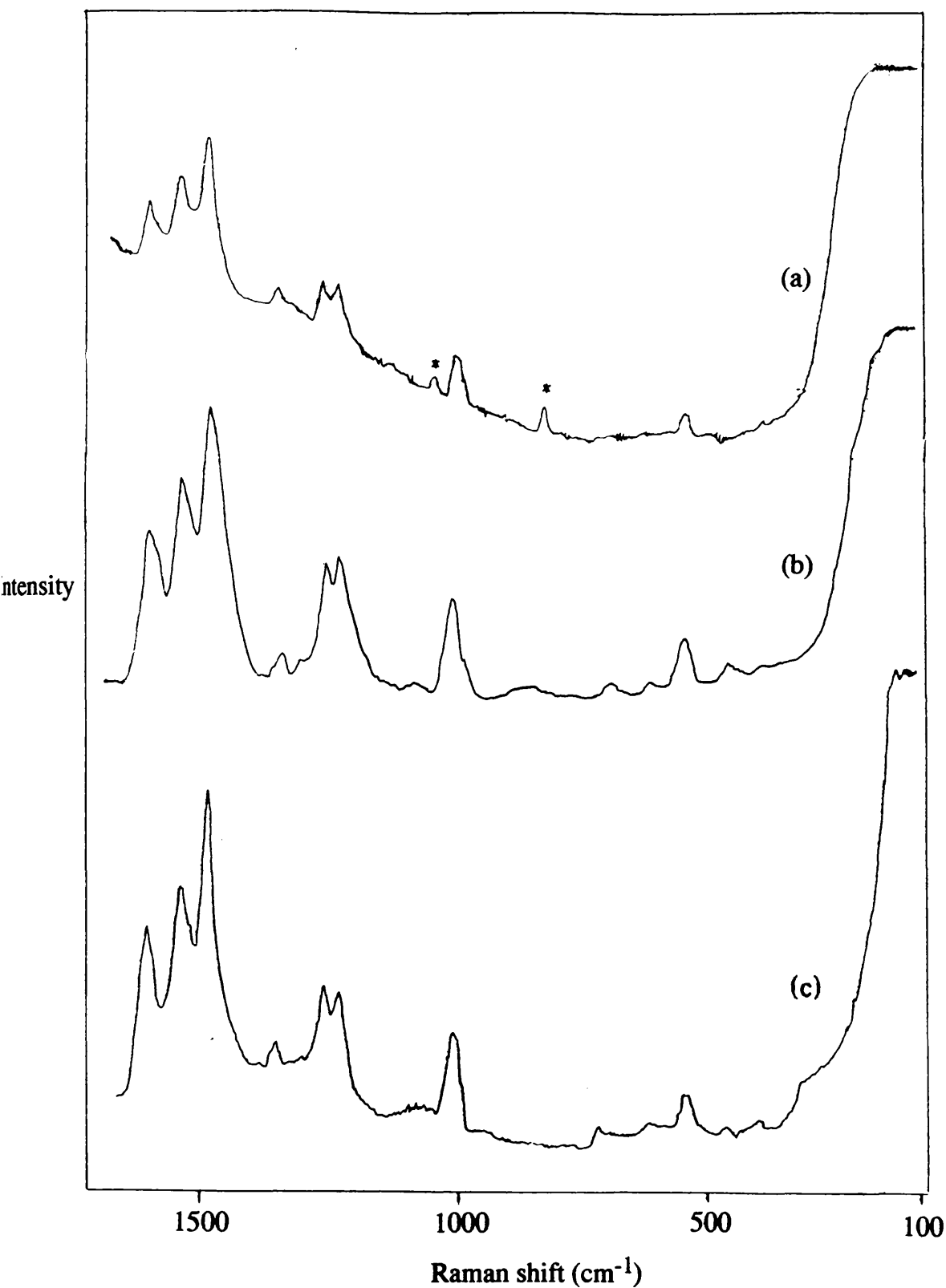


**Figure 7.5:** (a) Resonance Raman and (b) SERR spectra of  $\text{Ru}(\text{diambipy})_3\text{Cl}_2$  (dilute ethanolic solution)/silver slide. (c) SERR spectrum of the above solution after acidification/silver slide. [ $\text{Ar}^+$  laser, 488.0 nm excitation]. (\* - ethanol bands.)

Table 7.3: Data from resonance Raman and SERR spectra of a dilute ethanolic solution of Ru(diambipy)<sub>3</sub>Cl<sub>2</sub> / silver-coated slide.

<u>RRS (cm<sup>-1</sup>)</u>	<u>SERRS/Ag slide (cm<sup>-1</sup>)</u>	<u>Assignment (210)</u>
	420	
	491	
561	564	
	740	$\alpha(\text{CCC})$
1030	1028	$\nu(\text{C}_4\text{—C}_5)$
1246	1246	$\nu(\text{C}_2\text{—C}_3)$
1274	1274	$\delta(\text{C}_2\text{C}_3\text{H})$
1366	1365	$\delta(\text{CCH})$
1498	1496	$\delta(\text{CCH})$
1556	1557	$\nu(\text{C}_4\text{—C}_5)$
1616	1617	$\nu(\text{C}_2\text{—C}_3)$

complex in ethanol in contact with a freshly-prepared silver-coated slide. The RR spectrum of the complex is also presented. Spectral data, arising from several, reproducible runs of the RR and SERR spectra, are summarised in table 7.3.

(a) Resonance Raman spectrum.

The RR spectrum of the diamino complex proved particularly difficult to obtain. This was slightly surprising as there was no obvious high level of fluorescence to compete with the resonance Raman process. High incident laser power levels and high spectrometer sensitivity was necessary. Even with these levels, ethanolic vibrational modes are extremely strong in the spectrum obtained, as indicated.

The changes exhibited by the RRS of this complex, with respect to  $[\text{Ru}(\text{bipy})_3]^{2+}$ , are consistent with diamino substitution in the  $C_4$  and  $C_4'$ , 2,2'-bipyridyl ring positions.

The peak observed at  $1246\text{ cm}^{-1}$  may correspond to the  $1264\text{ cm}^{-1}$  peak of  $\text{Ru}(\text{bipy})_3\text{I}_2$ , assigned as hydrogen wagging and  $\text{C}=\text{N}$  stretching. The peak at  $1274\text{ cm}^{-1}$  in the spectrum of the diamino complex corresponds to the  $1276\text{ cm}^{-1}$  peak of  $[\text{Ru}(\text{bipy})_3]^{2+}$ , assigned as mainly  $\text{C}=\text{C}$  and  $\text{C}=\text{N}$  stretching. The strengthening of these two peaks and the disappearance of the peak at  $1318\text{ cm}^{-1}$  may be due to the presence of two new  $\text{C}=\text{N}$  bonds in each ligand and the subsequent mixing of these modes within existing modes associated with  $\text{C}=\text{N}$

stretching.

The other notable aspect of the RRS of this complex, in contrast to the RR spectra of both the parent and diester complexes, is the closeness of the three peaks in the region 1490 to 1620  $\text{cm}^{-1}$ .

(b) Comparison of the RR and SERR spectra of the diamino complex.

The SERR spectrum of the diamino complex displays no obvious band wavenumber shifts or relative intensity changes compared to the RRS of the complex. The enhancement of the SERR spectrum is, therefore, attributed to the electromagnetic mechanism. The presence of accessible amino groups in the 2,2'-bipyridyl ligands clearly does not induce adsorption of the complex. Nitrogen-mediated chemisorption on silver slides has already been observed with pyridine and 2,2'-bipyridine. The nitrogen atoms present in these molecules, however, have considerable Lewis base character and this is certainly the predominant type of chemisorption in these systems.

The highly enhanced SERR spectrum effectively 'filters out' the peaks attributed to ethanol in the RRS: only one such peak is just visible, at 875  $\text{cm}^{-1}$ , in the SERR spectrum.

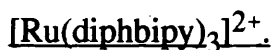
(c) Effect of protonation.

A solution of the diamino complex was treated with several drops of a 1 mol  $\text{l}^{-1}$  solution of hydrochloric acid in order to study the effect on SERRS of protonation of the complex. A small volume of dilute acid was

used in order that the changes in absorption characteristics noted with the addition of concentrated acid did not occur (section 5.2.3). Acid was added until the pH of the resultant solution was below 7. The solution did not change colour, even after several days.

Figure 7.5 shows the SERR spectrum of the ethanolic diamino solution after treatment with acid on a fresh silver-coated slide. Clearly, the features exhibited by this spectrum are identical to those in the SERR spectrum of the untreated solution. Protonation of the diamino-substituted 2,2'-bipyridyl ligands, therefore, does not affect enhancement or the adsorption behaviour of the complex.

#### 7.2.4 Tris(4,4'-diphenyl-2,2'-bipyridine) ruthenium(II),



Presented in figure 7.6 are the SERR and RR spectra of the diphenyl complex, in ethanol. Spectral data (from several runs) are recorded in table 7.4.

##### (a) Resonance Raman spectrum.

The RRS of this complex shows, ignoring the ethanolic bands, broadly the same pattern as the other complexes studied.

One interesting feature, however, is the strengthening of a peak at  $725\text{ cm}^{-1}$  which is, in the same region, present as a weak feature in the spectra of the other complexes. The strengthening of this peak,

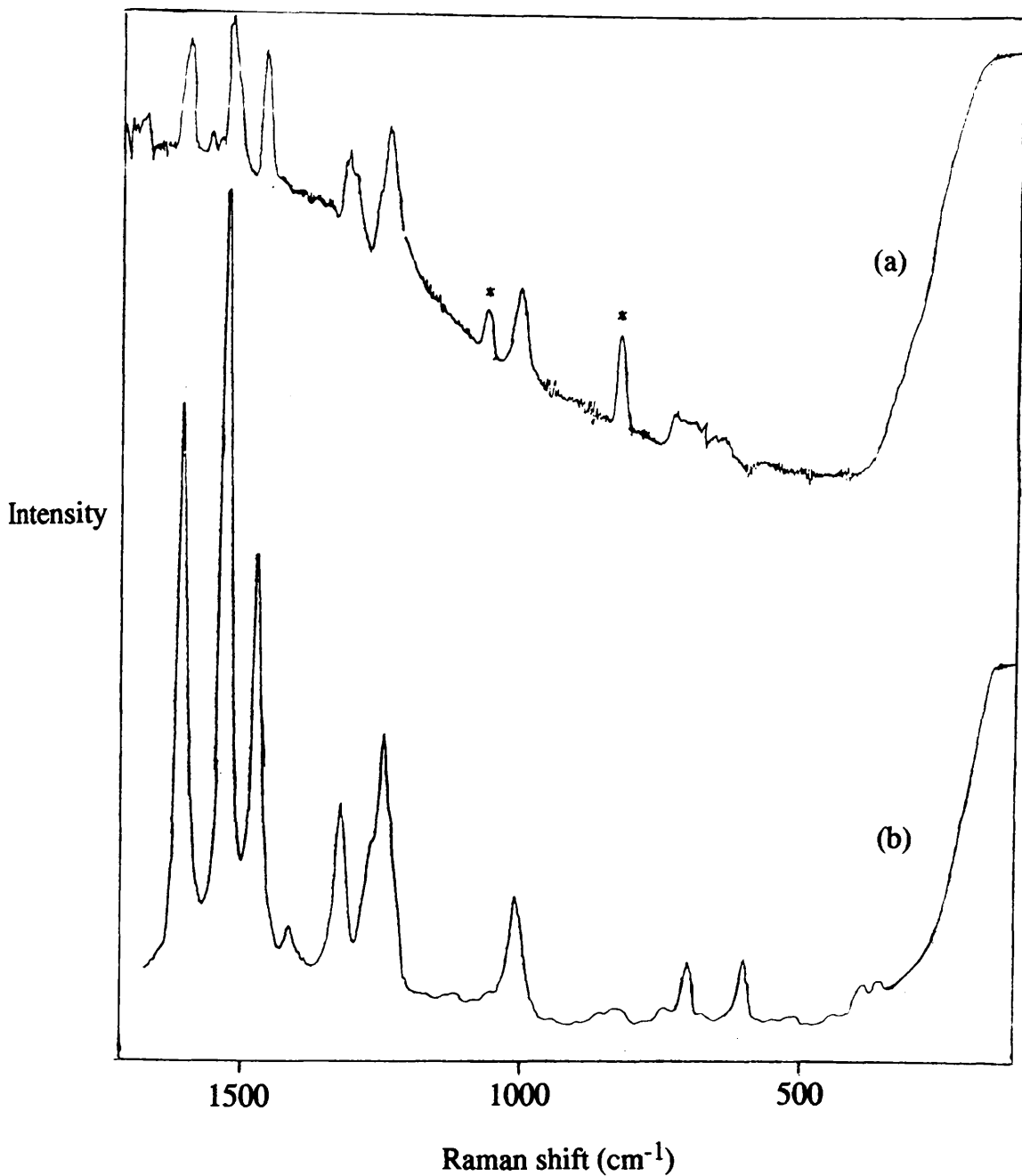


**Figure 7.6:** (a) Resonance Raman and (b) SERR spectra of Ru(diphbipy)<sub>3</sub>Cl<sub>2</sub> (dilute ethanolic solution)/silver slide. [Ar<sup>+</sup> laser, 488.0 nm excitation]. (\* - ethanol bands.)

**Table 7.4: Data from resonance Raman and SERR spectra of a dilute ethanolic solution of Ru(diphbipy)<sub>3</sub>I<sub>2</sub> / silver-coated slide.**

<u>RRS (cm<sup>-1</sup>)</u>	<u>SERRS/Ag slide (cm<sup>-1</sup>)</u>	<u>Assignment (210)</u>
	375	$\nu(\text{RuN})$
	410w	
	543w	
628b	628	$\alpha(\text{CCC})$
725b	725	$\alpha(\text{CCC})$
	767w	
	851w	
1025	1026	$\nu(\text{C}_4\text{—C}_5)$
	1060	$\delta(\text{CCH})$
1254	1254	$\nu(\text{C}_2\text{—C}_3)$
1332	1330	$\delta(\text{C}_2\text{C}_3\text{H})$
	1416w	$\delta(\text{CCH})$
1484	1483	$\delta(\text{CCH})$
1535	1534	$\nu(\text{C}_4\text{—C}_5)$
1610	1612	$\nu(\text{C}_2\text{—C}_3)$

(b = broad, w = weak)

assigned in the RRS of  $[\text{Ru}(\text{bipy})_3]^{2+}$  as a combination of  $\alpha(\text{CCC})$  and  $\text{C}=\text{C}$  stretching modes, is probably caused by the presence, in the substituted complex, of the new carbon frameworks in the ligands.

(b) Comparison of the RR and SERR spectra of the diphenyl complex.

As with the previous tris-ligand ruthenium(II) complexes, the SERR spectrum of the diphenyl complex exhibits effectively no changes in relative intensities or band wavenumber positions compared to its RR spectrum. Several bands which were hidden under the noisy baseline of the RRS are, however, clearly visible in the SERRS. Indeed, the two bands at  $628$  and  $725\text{ cm}^{-1}$  in the RRS are considerably more well-defined and distinct in the SERR spectrum. The intense fluorescence present in the RRS is clearly quenched in the SERRS.

Whereas with the diester and diamino complexes, where changes in the adsorption behaviour of the complex may have been expected due to the presence of co-ordinative groups in the ligands, the behaviour of the diphenyl complex is not surprising. Based on previous results with benzene on silver-coated slides, the presence of phenyl substituents on 2,2'-bipyridyl rings is hardly likely to induce chemisorption of the complex.

### 7.2.5 Tris(4,4'-dimethyl-2,2'-bipyridine) ruthenium(II),



Figure 7.7 shows the RR and SERR spectra of the dimethyl complex.

Spectral data (based on several identical spectra) are recorded in table

7.5.

#### (a) Resonance Raman spectrum.

The dimethyl complex can be considered to be, out of all the complexes studied, the one 'most similar' to the parent complex. This is reflected in the RR spectrum of the complex. A peak is present at  $1199 \text{ cm}^{-1}$  which, although shifted by some  $20 \text{ cm}^{-1}$ , corresponds to the peak at  $1177 \text{ cm}^{-1}$  in the spectrum of the parent complex. This peak is considerably reduced in intensity in the RR spectra of the other modified complexes. The intensities of the peaks at  $1270$  and  $1318 \text{ cm}^{-1}$  ( $1275$  and  $1318$  in the spectrum of  $[\text{Ru}(\text{bipy})_3]^{2+}$ ) have reverted to the relative intensities shown in the spectrum of  $[\text{Ru}(\text{bipy})_3]^{2+}$ . The relative intensity pattern of the three peaks of highest wavenumber ( $1484$ ,  $1545$  and  $1615 \text{ cm}^{-1}$ ) is considerably different to that of the corresponding bands of  $[\text{Ru}(\text{bipy})_3]^{2+}$ . The peak at  $1545 \text{ cm}^{-1}$ , assigned as C=C stretching, may be of the highest intensity because of the increase of carbons in the framework of the ligand due to the incorporation of two methyl substituents.

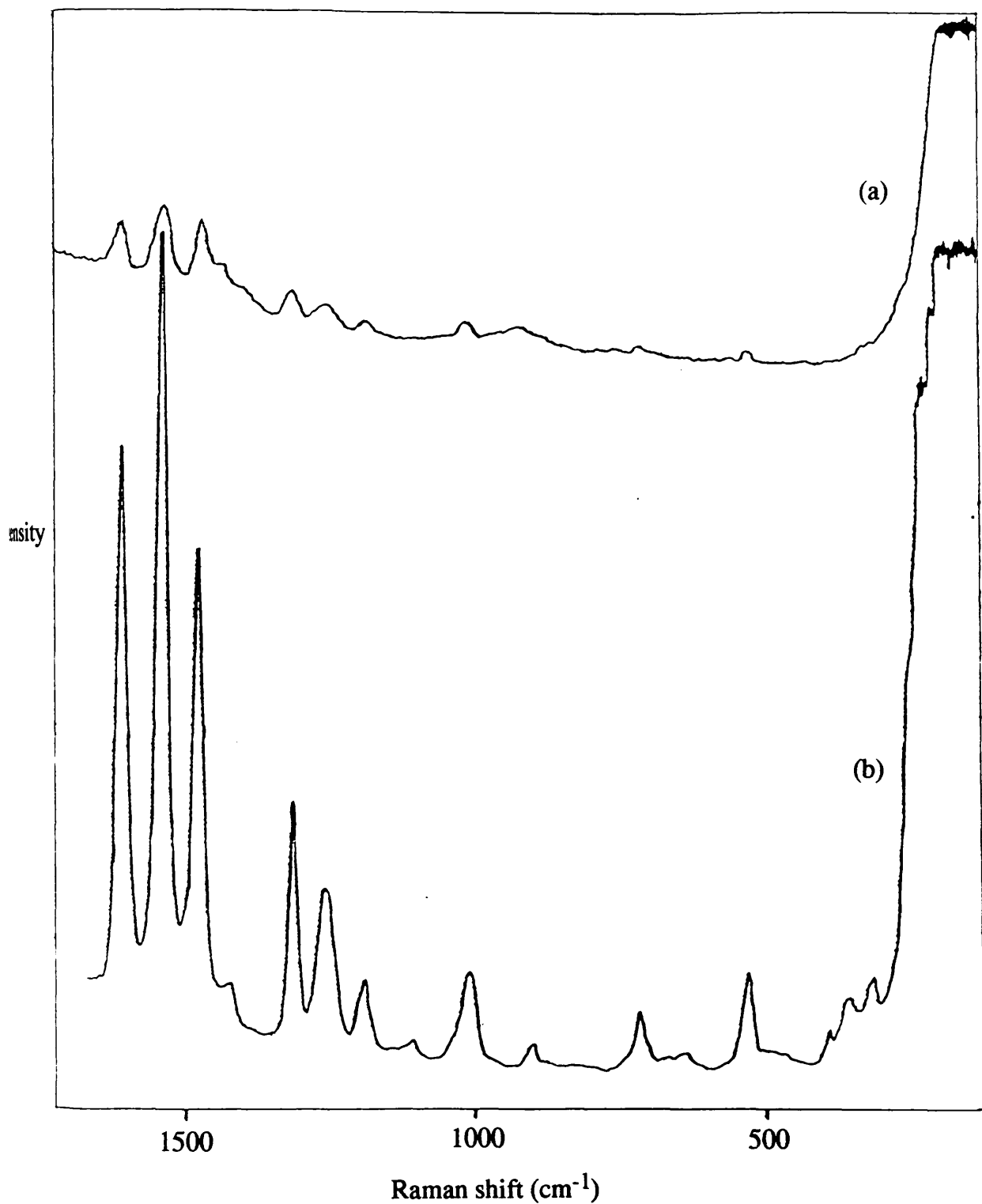


**Figure 7.7: (a) Resonance Raman and (b) SERR spectra of  $\text{Ru}(\text{dimebipy})_3\text{Cl}_2$  (dilute ethanolic solution)/silver slide. [ $\text{Ar}^+$  laser, 488.0 nm excitation].**

Table 7.5: Data from resonance Raman and SERR spectra of a dilute ethanolic solution of Ru(dimebipy)<sub>3</sub>Cl<sub>2</sub> / silver-coated slide.

<u>RRS (cm<sup>-1</sup>)</u>	<u>SERRS/Ag slide (cm<sup>-1</sup>)</u>	<u>Assignment (210)</u>
	335	
	400	
562	561	
	660w	α(CCC)
735	733	α(CCC)
	919w	
1030	1029	ν(C <sub>4</sub> —C <sub>5</sub> )
	1113	δ(CCH)
1199	1198	δ(CCH)
1270	1268	ν(C <sub>2</sub> —C <sub>3</sub> )
1318	1317	δ(C <sub>2</sub> C <sub>3</sub> H)
1430w	1427w	δ(CCH)
1484	1483	δ(CCH)
1545	1545	ν(C <sub>4</sub> —C <sub>5</sub> )
1615	1613	ν(C <sub>2</sub> —C <sub>3</sub> )

(b) Comparison of the RR and SERR spectra of the dimethyl complex.

The SERR spectrum of the complex clearly shows no significant changes in relative intensities or band positions with respect to the corresponding RR spectrum.

The SERR spectrum, however, shows many intense, distinct bands which are indistinguishable from background noise in the RRS. This illustrates the power of SERRS in obtaining new vibrational information on adsorbate species.

Once again, the fact that this complex displays no evidence of chemisorption on the silver surface is not surprising: methyl groups would not be expected to adsorb under these conditions or, indeed, influence any potential adsorption properties of the 2,2'-bipyridyl ring to any large extent.

7.2.6 Discussion.

The results obtained with silver-coated slides reveal several interesting points.

Firstly, it is clear that the substitution of the 2,2'-bipyridyl ligands in the tris-ligand ruthenium(II) complex does not, to any great extent, affect the magnitude of SERRS enhancement observed. Considered in relation to a purely electromagnetic surface and resonance Raman enhancement effect, this is not surprising. If the enhancement is

considered to arise from separate contributions from surface and resonance enhancement, the only factor which is likely to change, with changing substituents, is the resonance enhancement. Clearly, within experimental reproducibility, the surface enhancement factor is fairly constant from a qualitative viewpoint. The resonance enhancement factor will, of course, change with different complexes, having different metal(d)→ligand( $\pi^*$ ) charge-transfer absorptions. This, however, is not a large effect since the maxima of the five complexes studied are within a small wavelength range (table 5.1). The two enhancement factors combine to give a huge overall enhancement effect for all the complexes.

The effect of the presence of substituents in the C<sub>4</sub> and C<sub>4'</sub> positions of the 2,2'-bipyridyl molecule on the adsorption behaviour of the complexes at silver slide surfaces was studied. Potentially co-ordinative (diester, diamino) ligands were used in addition to modified ligands which, on the basis of earlier results, were highly unlikely to induce chemisorption. The results of these investigations show clearly that none of the modified ligands influence adsorption on the silver surface either through the substituents or through the 2,2'-bipyridyl ring itself.

From earlier results with 2,2'-bipyridine on chemically silver-coated slides, it is clear that the most likely route of co-ordination of the molecule to a chemically-produced substrate is through a Lewis

acid/base interaction involving the ring nitrogen atoms. This is clearly not possible due to the orientation of the 2,2'-bipyridyl segment in the molecule and the fact that it is already chelating to a ruthenium atom. Vanhecke *et al.* (100) argued that, with silver colloids, the  $[\text{Ru}(\text{bipy})_3]^{2+}$  ion adsorbs through the ring nitrogen whilst maintaining the Ru—N bond. This was suggested without evidence and, as discussed in section 2.2.3.5(b), is highly unlikely since none of the spectra of Vanhecke *et al.* displayed any indication of complex formation on the silver colloid surface. It is, therefore, unlikely that with silver slides as the active surface, the  $[\text{Ru}(\text{bipy})_3]^{2+}$  molecule can co-ordinate through the ring nitrogen. The presence of co-ordinative substituents does not influence adsorption either through the substituents themselves or in any other fashion.

The five categories of substituents on the 2,2'-bipyridyl ring include both electron-withdrawing and electron-releasing groups. Clearly, the effect of increased electron density in the ring (diamino and dialkyl substituents) and, therefore, on the ring nitrogen has no effect on the adsorption of either the ring or the nitrogen.

It is clear that the enhancement mechanism operating in these systems involves purely electromagnetic (surface plasmon) excitation. The roughness of the silver slide surface gives an extremely high surface area allowing the physisorption of a great number of adsorbate

molecules. The enhancement, in this case, is not confined to simply the first monolayer of physisorbed molecules.

This set of studies has also highlighted one of the most important aspects of the technique. The SERR spectra obtained, in each case, show vibrational features which were not observed easily or, indeed, at all in the respective RR spectra.

### 7.3 Vapour silver-coated polycarbonate.

#### 7.3.1 Tris(2,2'-bipyridyl) ruthenium(II).

##### (a) Note on the presentation of spectra.

Throughout this chapter, the SERR spectra of the complexes studied in contact with silver-coated polycarbonate are presented and compared with the corresponding SERR spectra of the complexes in contact with chemically-prepared silver slides. This comparison effectively equates to a comparison of polycarbonate SERR spectra with the respective resonance Raman spectra of the complexes since, as previously shown, all the silver slide SERR spectra of the ruthenium complexes are enhanced duplicates of their corresponding RR spectra.

##### (b) Raman spectrum of the polycarbonate substrate.

As discussed previously, the SERR spectrum of  $\text{Ru}(\text{bipy})_3\text{I}_2$  solution in contact with silver-coated polycarbonate shows some bands due to the polycarbonate substrate itself.

Several Raman spectra of a piece of uncoated polycarbonate were obtained in order to determine, more accurately, the positions of the polycarbonate bands. Figure 7.8 shows an example of such spectra. The spectrum displays peaks with appreciable signal-to-noise ratios at 700, 875, 1106, 1180, 1235 and 1629  $\text{cm}^{-1}$ . The peak at 875  $\text{cm}^{-1}$  is the most intense. Unfortunately, some of these peaks are in areas which would be expected to show modes of  $[\text{Ru}(\text{bipy})_3]^{2+}$  and modified complexes. This is, therefore, a considerable disadvantage of the polycarbonate surface. All polycarbonate bands are clearly indicated in subsequent spectra.

(c) SERR spectrum of  $\text{Ru}(\text{bipy})_3\text{I}_2$ .

Figure 7.9 shows the SERR spectrum of a piece of vacuum silver-coated (50 nm) polycarbonate exposed to a solution of  $\text{Ru}(\text{bipy})_3\text{I}_2$ . The corresponding spectrum with a silver slide is shown for reference. As can be deduced from the background noise, the spectra were obtained under different conditions. The sensitivity of the photon-counting system had to be increased by a factor of ten in order to achieve equal enhancement with the polycarbonate/complex system.

The positions of the SERRS bands present in each spectrum are detailed in table 7.6.

The only obvious differences between the two spectra, in terms of relative intensities, are the positions of the two peaks of highest

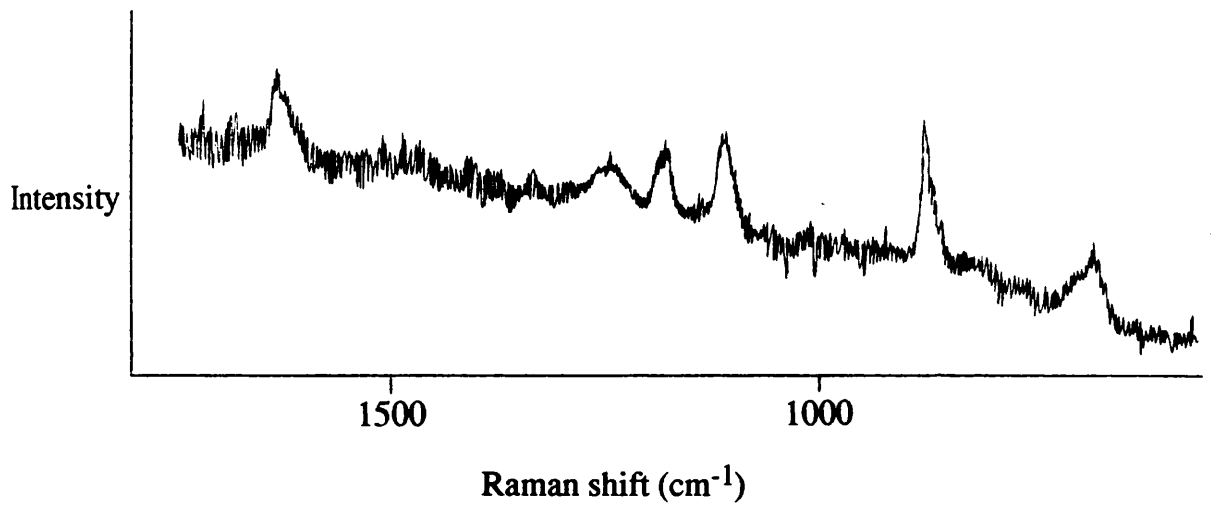
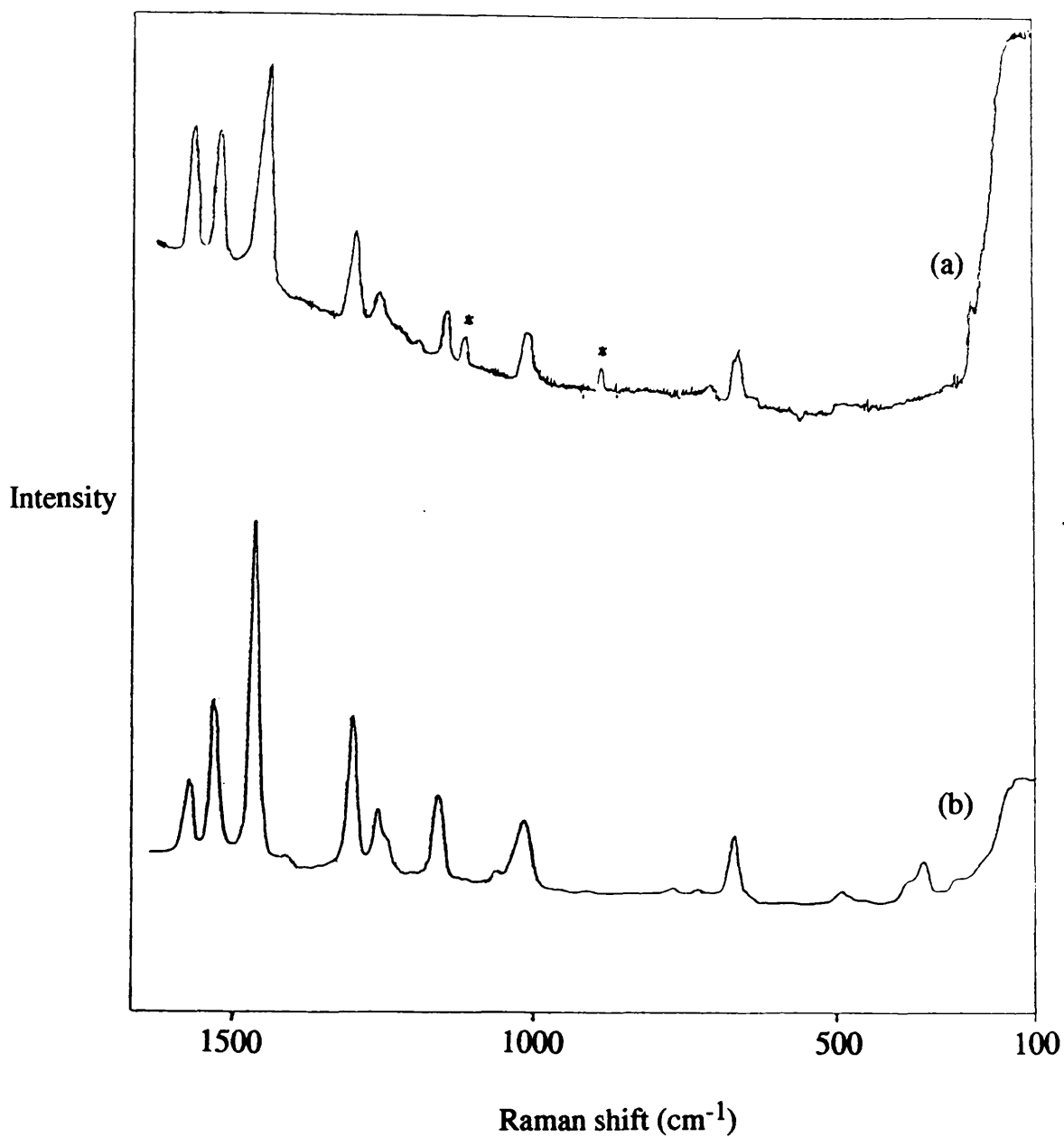


Figure 7.8: Raman spectrum of an uncoated piece of polycarbonate.  
[Ar<sup>+</sup> laser, 488.0 nm excitation].



**Figure 7.9:** (a) SERR spectrum/vacuum silver-coated polycarbonate and (b) SERR spectrum/silver slide of  $\text{Ru}(\text{bipy})_3\text{I}_2$  ( $2 \times 10^{-3}$   $\text{mol l}^{-1}$  aqueous solution) (photon counter sensitivity/10). [ $\text{Ar}^+$  laser, 488.0 nm excitation]. (\* = polycarbonate bands.)

Table 7.6: Data from SERR spectra of an aqueous solution of Ru(bipy)<sub>3</sub>I<sub>2</sub>(2 x 10<sup>-3</sup> mol l<sup>-1</sup>) on vapour silver-coated (50 nm)polycarbonate and a silver-coated slide.

<u>SERRS/Ag slide (cm<sup>-1</sup>)</u>	<u>SERRS/Ag pc (cm<sup>-1</sup>)</u>	<u>Assignment (210)</u>
	204	
265		$\nu(\text{RuNC})$
335		
372		$\nu(\text{RuN})$
435		
467		
668	664	$\alpha(\text{CCC})$
723	706	$\alpha(\text{CCC})$
760		
1025	1024	$\nu(\text{C}_4\text{—C}_5)$
1066		$\delta(\text{CCH})$
1177	1160	$\delta(\text{CCH})$
1260		$\delta(\text{CCH})$
1275	1276	$\nu(\text{C}_2\text{—C}_3)$
1318	1314	$\delta(\text{C}_2\text{C}_3\text{H})$
1451w		$\delta(\text{CCH})$
1488	1483	$\delta(\text{CCH})$
1560	1556	$\nu(\text{C}_4\text{—C}_5)$
1605	1602	$\nu(\text{C}_2\text{—C}_3)$

wavenumber. In the SERR spectrum of the silver slide, the peak at  $1560\text{ cm}^{-1}$  is over twice the intensity of the peak at  $1605\text{ cm}^{-1}$ . In the SERR spectrum of the polycarbonate, however, the two peaks are of approximately equal intensity.

In terms of vibrational band positions, the two spectra show several differences. All of the bands in the spectrum of the polycarbonate display a general shift to lower energy compared to the silver slide spectrum and, therefore, to the resonance Raman spectrum. This shift is not even, varying between  $1$  and  $17\text{ cm}^{-1}$ . Most of the wavenumber shifts in the spectrum, however, are of between  $4$  and  $7\text{ cm}^{-1}$ . There are no new bands present in the SERR spectrum of the polycarbonate except an extremely small feature at  $204\text{ cm}^{-1}$  which was not reproducible. Some bands observed in the SERR spectrum of the silver slide cannot be observed above background noise in the polycarbonate SERRS. This is simply a consequence of the lower enhancement obtained with the polycarbonate. The small wavenumber shifts of between  $4$  and  $7\text{ cm}^{-1}$  were observed time and again in a series of identical spectra. Clearly, these shifts are real and not a function of any inherent inaccuracy of the Raman spectrometer.

All of this evidence implies some degree of chemisorption of the  $[\text{Ru}(\text{bipy})_3]^{2+}$  molecule. The most likely adsorption mode is edge-on bonding through a 2,2-bipyridyl ring  $\text{C}=\text{C}$ . The enhancement of the

band at  $1605\text{ cm}^{-1}$ , ascribed to  $\nu(\text{C}=\text{C})$ , further evidences this. None of the ring modes in the polycarbonate SERR spectrum display any evidence of splitting or broadening and it is, therefore, likely that both pyridyls of the 2,2-bipyridyl ligand are attached to the silver surface. This situation, of course, leads to enhancement through the charge-transfer mechanism. It is likely, however, that the enhancement is a combination of both effects since the excitation wavelength (488.0 nm) is fairly close to both the surface plasmon (410 nm) and adsorbate/surface charge-transfer (beyond 514.5 nm) maxima, as indicated in section 6.6.1(c). Resonance Raman enhancement also plays a significant part in the enhancement process of this system.

### 7.3.2 [Ru(diesbipy)<sub>3</sub>]<sup>2+</sup>.

Figure 7.10 shows the SERR spectrum of a piece of silver-coated (50 nm) polycarbonate and of a chemically silver-coated slide exposed to an aqueous solution of the diester complex.

Compared to the spectrum of the polycarbonate exposed to [Ru(bipy)<sub>3</sub>]<sup>2+</sup>, the polycarbonate SERR spectrum of this complex was considerably easier to obtain and shows slightly greater enhancement.

Table 7.7 shows spectral data obtained from several runs of both spectra. The SERR spectra of the coated polycarbonate surface were highly reproducible.

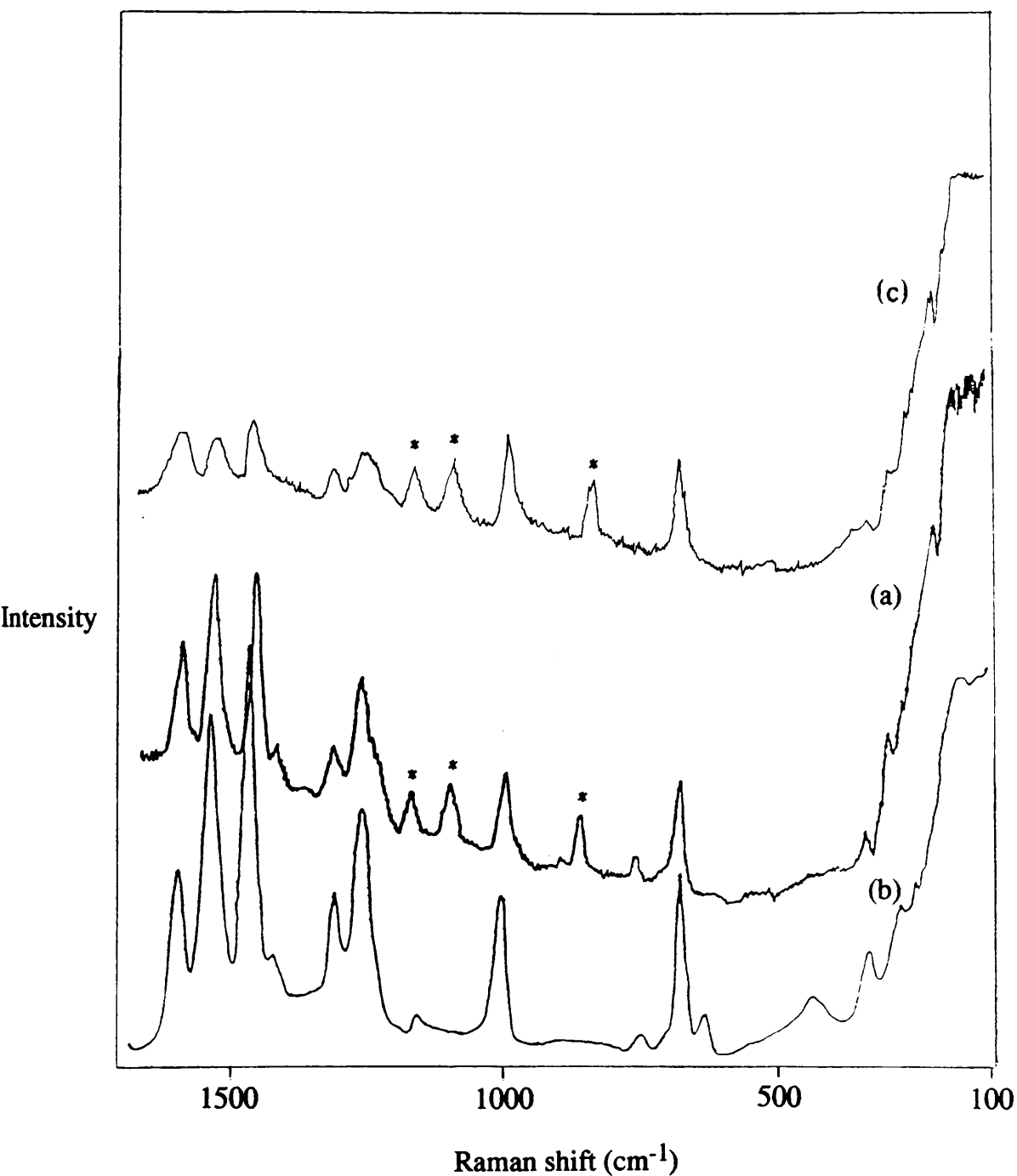


**Figure 7.10:** (a) SERR spectrum/vacuum silver-coated polycarbonate and (b) SERR spectrum/silver slide of  $\text{Ru}(\text{diesbipy})_3[\text{BF}_4]_2$  (dilute aqueous solution) (photon counter sensitivity/10). (c) SERR spectrum of the above silver polycarbonate surface after washing in water. [ $\text{Ar}^+$  laser, 488.0 nm excitation]. (\* = polycarbonate bands.)

Table 7.7: Data from SERR spectra of an aqueous solution ofRu(diesbipy)<sub>3</sub>[BF<sub>4</sub>]<sub>2</sub> on vapour silver-coated (50 nm)polycarbonate and a silver-coated slide.

<u>SERRS/Ag slide (cm<sup>-1</sup>)</u>	<u>SERRS/Ag pc (cm<sup>-1</sup>)</u>	<u>Assignment (210)</u>
	224	
251	246	
285	289	$\nu(\text{RuNC})$
345		$\nu(\text{RuN})$
459b		
650		$\alpha(\text{CCC})$
690	695	$\alpha(\text{CCC})$
763	787	
1024	1021	$\nu(\text{C}_4\text{—C}_5)$
1182		$\delta(\text{CCH})$
1274	1269	$\nu(\text{C}_2\text{—C}_3)$
1319	1316	$\delta(\text{C}_2\text{C}_3\text{H})$
1438w	1426w	$\delta(\text{CCH})$
1480	1472	$\delta(\text{CCH})$
1555	1546	$\nu(\text{C}_4\text{—C}_5)$
1615	1607	$\nu(\text{C}_2\text{—C}_3)$

The two spectra display clear differences in relative intensities and band positions. The main changes in relative intensity come within the the three peaks of highest wavenumber (at 1480, 1555 and 1615  $\text{cm}^{-1}$  in the silver slide spectrum). The peak at 1555  $\text{cm}^{-1}$  is slightly lower in intensity compared to the 1480  $\text{cm}^{-1}$  peak in the silver slide spectrum. In the polycarbonate spectrum, however, the two peaks are of approximately equal intensity. The peak at 1615  $\text{cm}^{-1}$  in the silver slide SERRS increases its intensity, relative to the other two peaks, in the polycarbonate spectrum.

The changes in band positions in the polycarbonate spectrum range between 3 and 24  $\text{cm}^{-1}$ , with most of the changes being of between 6 and 8  $\text{cm}^{-1}$ . In most cases, the shifts are to lower frequency. All of these shifts were duplicated in every run of the spectrum, with variance of approximately 1  $\text{cm}^{-1}$ .

Other notable changes include the absence of a peak in the polycarbonate spectrum which is present as a broad band in the silver slide SERRS. An additional peak is present, in the polycarbonate spectrum at 224  $\text{cm}^{-1}$  and with good reproducibility.

Figure 7.10 also shows the SERR spectrum of a sample of the same aqueous solution of the diester complex which had been in contact with a piece of silver-coated polycarbonate for over one hour and had then been washed with distilled water and dried. The resultant Raman

spectrum of the polycarbonate is very noisy but shows the strengthening of the peak of highest frequency and the possible splitting of the peak at  $1269\text{ cm}^{-1}$ .

As has been demonstrated for the parent complex, all of the findings outlined above indicate that chemisorption of the diester complex occurs to some degree.

The increase in relative intensity of the two peaks of highest frequency, assigned in the silver slide spectrum as  $\text{C}=\text{C}$  stretching modes, may indicate some role of the 2,2'-bipyridyl ring in the adsorption of the complex. However, it is likely that the carboxylate ( $\text{OCO}$ ) symmetric stretch is involved in these modes. The further evidence of the appearance, in the polycarbonate spectrum, of a new, reproducible mode at  $224\text{ cm}^{-1}$ , which could represent silver-carboxylate stretch, indicates that the molecule may adsorb on the silver surface through the substituent carboxylate ester group. The geometry of the overall diester complex ion entity effectively excludes the possibility of flat 2,2'-bipyridyl co-ordination to the metal surface and so the most likely bonding mode is a perpendicular carboxylate orientation.

The spectrum of the silver-coated polycarbonate surface after washing in water reveals an even greater increase in the relative

intensity of the peak of highest wavenumber. The process of washing may rid the surface of most of the weakly-bound physisorbed molecules and leave the chemically-bound adsorbate species attached. The splitting of the  $1269\text{ cm}^{-1}$  peak, which from the assignment of the parent complex involves  $\nu(\text{C}_3\text{—C}_4)$  and  $\nu(\text{C}_4\text{—C}_5)$  modes, could indicate that only one of the carboxylate ester substituents of the 2,2'-bipyridyl ring is co-ordinated to the silver surface.

### 7.3.3 [Ru(diambipy)<sub>3</sub>]<sup>2+</sup>.

Figure 7.11 shows the SERR spectrum of a solution of the diamino complex, in ethanol, in contact with a piece of silver-coated (50 nm) polycarbonate and the SERRS of the same solution in contact with a chemically silver-coated slide. Band position data are detailed in table 7.8.

The two spectra display obvious differences in relative intensities and band positions. Once again, the major changes in relative intensities occur within the three peaks of highest frequency. The relative strengthening of the peak at  $1610\text{ cm}^{-1}$  in the polycarbonate spectrum is accompanied by the possible splitting of the peak at  $1555\text{ cm}^{-1}$ . This peak is not as sharp as the corresponding peak appears in the silver slide SERRS.

Another obvious change involves the peak at  $1244\text{ cm}^{-1}$  in the

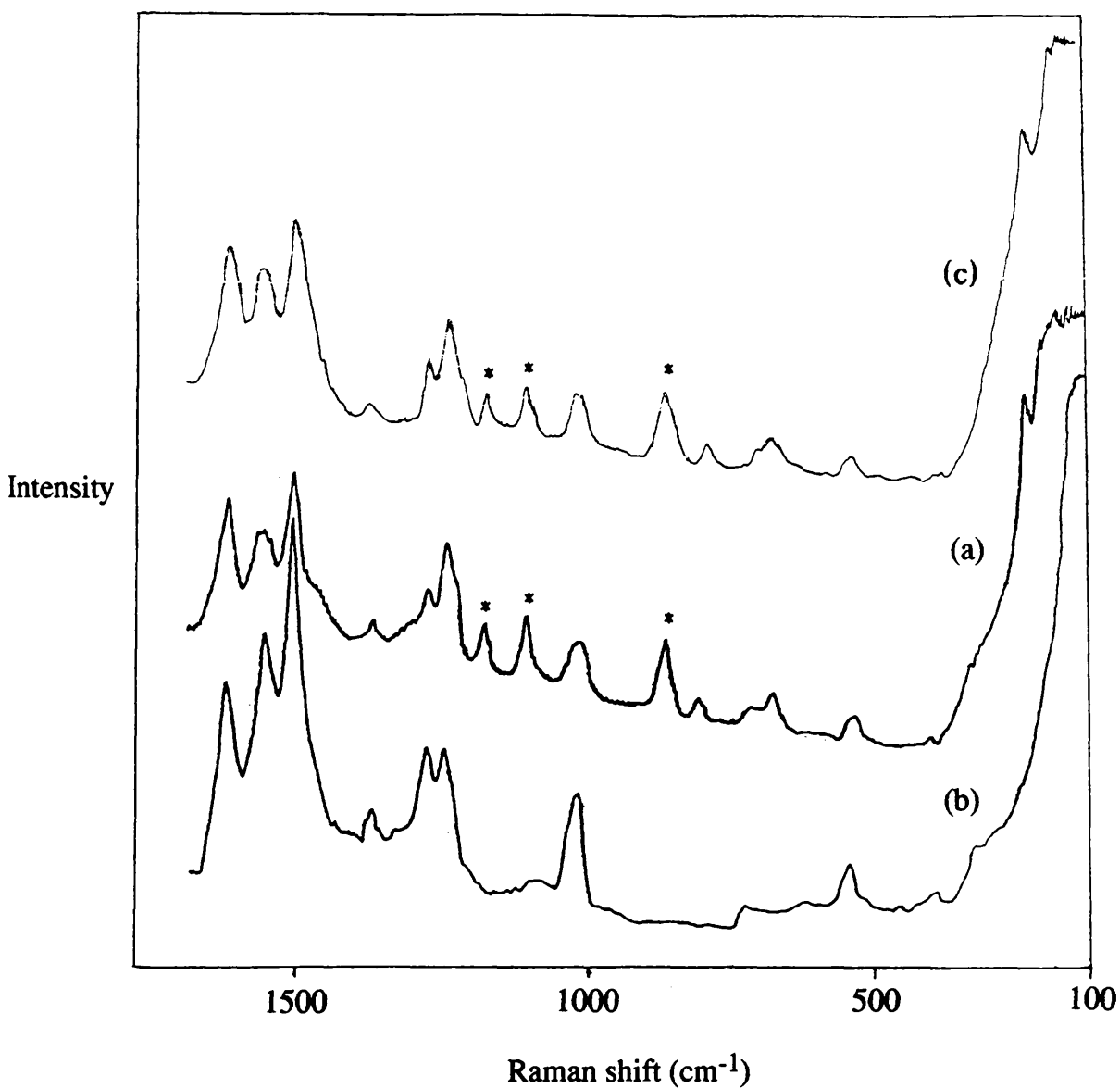


**Figure 7.11:** (a) SERR spectrum/vacuum silver-coated polycarbonate and (b) SERR spectrum/silver slide of  $\text{Ru}(\text{diambipy})_3\text{Cl}_2$  (dilute ethanolic solution) (photon counter sensitivity/10). (c) SERR spectrum/vacuum silver-coated polycarbonate of the same solution after acidification. [ $\text{Ar}^+$  laser, 488.0 nm excitation]. (\* - polycarbonate bands.)

Table 7.8: Data from SERR spectra of an ethanolic solution of

Ru(diambipy)<sub>3</sub>Cl<sub>2</sub> on vapour silver-coated (50 nm)

polycarbonate and a silver-coated slide.

<u>SERRS/Ag slide (cm<sup>-1</sup>)</u>	<u>SERRS/Ag pc (cm<sup>-1</sup>)</u>	<u>Assignment (210)</u>
	255	
	290	$\nu(\text{RuNC})$
420		$\nu(\text{RuN})$
491		
564	560	
	699	$\alpha(\text{CCC})$
740	797	
1028	1021	$\nu(\text{C}_4\text{—C}_5)$
1246	1244	$\nu(\text{C}_2\text{—C}_3)$
1274	1270	$\delta(\text{C}_2\text{C}_3\text{H})$
	1361	$\delta(\text{CCH})$
1496	1492	$\delta(\text{CCH})$
1557	1555	$\nu(\text{C}_4\text{—C}_5)$
1617	1610	$\nu(\text{C}_2\text{—C}_3)$

polycarbonate SERRS. This peak is of almost double the relative intensity of the corresponding peak in the silver slide spectrum.

The average change in band positions between the two spectra is approximately  $6$  to  $8\text{ cm}^{-1}$ , and in most cases to lower frequency.

These changes were found to be reproducible.

Another evident change in the polycarbonate SERRS is the appearance of a reproducible low energy peak at  $255\text{ cm}^{-1}$ .

These findings clearly indicate chemisorption of the diamino complex.

Once again, the selective enhancement of  $\nu(\text{C}_3\text{—C}_4)$  and  $\nu(\text{C}_4\text{—C}_5)$  modes ( $210$ ) indicates that the molecular adsorption site is in the region of the substituents. The low wavenumber band indicates attachment through the substituent amine group, the peak representing  $\nu(\text{Ag—N})$ . Such a feature in this region of the spectrum, however, could be ascribed to  $\nu(\text{Ru—N})$ . Since, however, no such band is observed in this area of the highly enhanced silver slide SERR spectrum, it is highly unlikely the feature would be observed in the spectrum of the polycarbonate.

Although the peak at  $1555\text{ cm}^{-1}$  is not cleanly split, there is considerable evidence of asymmetry. The splitting of this  $\nu(\text{C}_4\text{—C}_5)$  mode suggests that only one of the substituents on the 2,2'-bipyridyl ring is bound on the silver surface. The peak at  $1021\text{ cm}^{-1}$ , assigned as

$\nu(\text{C}_4\text{—C}_5)$ , also appears to be broader compared to the corresponding band in the silver slide SERRS.

#### Effect of protonation.

Figure 7.11 also shows the SERR spectrum of the diamino complex, after treatment with dilute hydrochloric acid, in contact with silver-coated polycarbonate. This spectrum is very similar to the spectrum of the original solution, indicating that the protonation of the complex has no obvious effect on the adsorption behaviour of the complex on the polycarbonate surface. The only difference between the spectra is that, with the same laser power and experimental conditions, the spectrum of the protonated diamino complex is less enhanced.

#### 7.3.4 $[\text{Ru}(\text{diphbipy})_3]^{2+}$ .

Figure 7.12 shows the SERR spectra of both silver-coated (50 nm) polycarbonate and a chemically silver-coated slide exposed to the same solution of the diphenyl complex. The spectral data obtained from these studies are shown in table 7.9.

The two spectra display subtle differences in band positions and relative intensities.

The most obvious change in band intensity is the relative strengthening of the peak at  $1254\text{ cm}^{-1}$ . There are no obvious wavenumber modifications within the three peaks of highest frequency

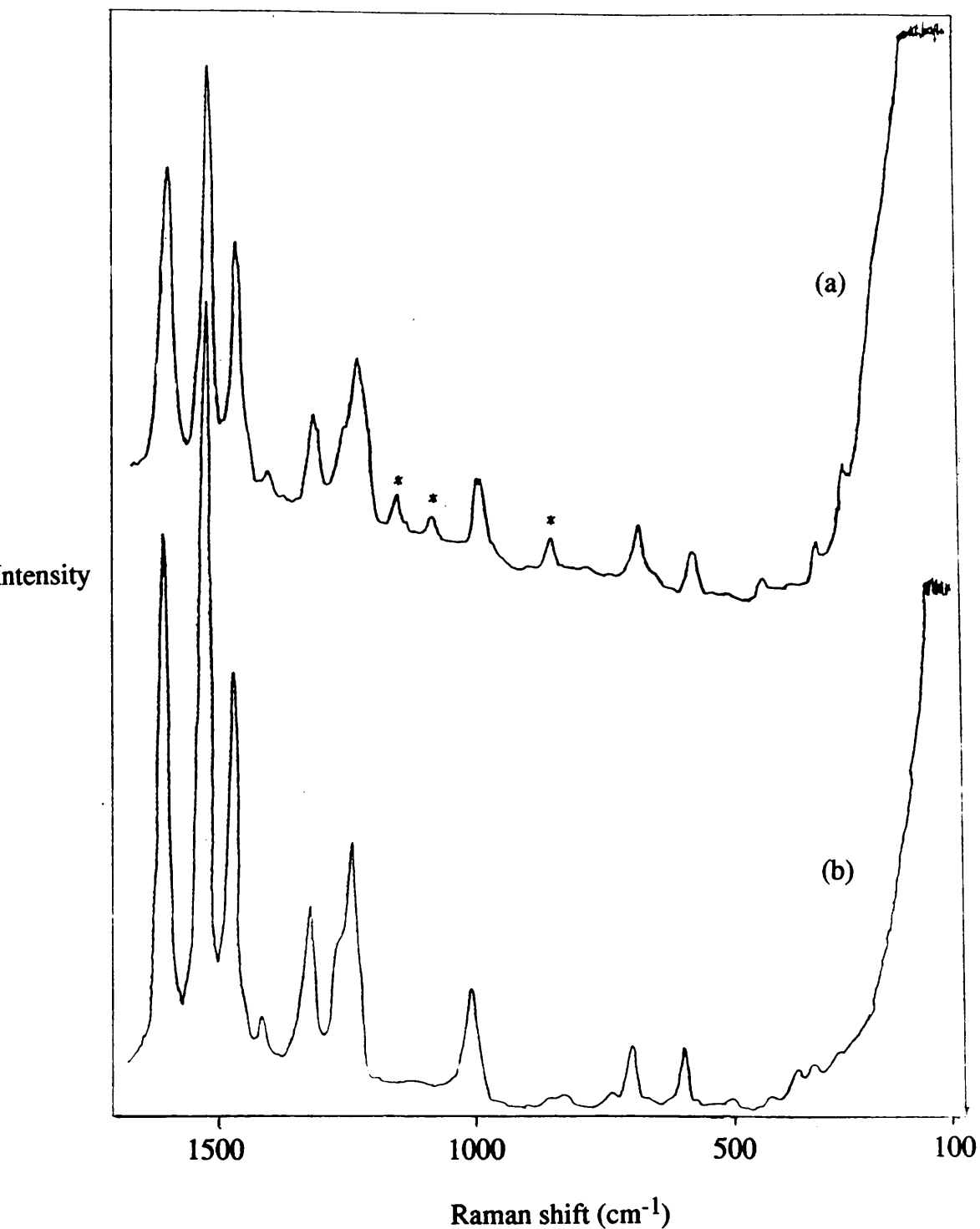


**Figure 7.12: (a) SERR spectrum/vacuum silver-coated polycarbonate and (b) SERR spectrum/silver slide of  $\text{Ru}(\text{diphbipy})_3\text{Cl}_2$  (dilute ethanolic solution) (photon counter sensitivity/10). [ $\text{Ar}^+$  laser, 488.0 nm excitation]. (\* - polycarbonate bands.)**

Table 7.9: Data from SERR spectra of an aqueous solution ofRu(diphbipy)<sub>3</sub>Cl<sub>2</sub> on vapour silver-coated (50 nm)polycarbonate and a silver-coated slide.

<u>SERRS/Ag slide (cm<sup>-1</sup>)</u>	<u>SERRS/Ag pc (cm<sup>-1</sup>)</u>	<u>Assignment (210)</u>
	330	$\nu(\text{RuNC})$
375w	382	$\nu(\text{RuN})$
410w		
543w		$\alpha(\text{CCC})$
628	627	$\alpha(\text{CCC})$
725	721	"
767w		
851w		
1026	1020	$\nu(\text{C}_4\text{—C}_5)$
1060w		$\delta(\text{CCH})$
1254	1254	$\nu(\text{C}_2\text{—C}_3)$
1330	1329	$\delta(\text{C}_2\text{C}_3\text{H})$
1416w	1418w	$\delta(\text{CCH})$
1483	1477	$\delta(\text{CCH})$
1534	1532	$\nu(\text{C}_4\text{—C}_5)$
1612	1609	$\nu(\text{C}_2\text{—C}_3)$

or, indeed, within any of the other bands in the spectrum.

The changes in band positions are smaller than the changes in the polycarbonate spectra of the other modified complexes. In this case, most of the peaks are shifted by 4 to 6  $\text{cm}^{-1}$  to lower frequency.

The only other noteworthy aspect of the polycarbonate SERRS of the diphenyl complex is the small degree of splitting of the peak at 1020  $\text{cm}^{-1}$ . No low frequency peaks were observed.

All this evidence indicates a small degree of chemisorption of the diphenyl complex occurs. The SERR spectrum of the complex on the polycarbonate surface is not modified, with respect to the corresponding silver slide SERRS, in the same way that the polycarbonate spectra of the other modified complexes exhibit change. Certainly, the general pattern of the spectrum, saving the splitting of the 1020  $\text{cm}^{-1}$  peak and a small change in relative intensity, is very similar to the silver slide SERR spectrum and, therefore, to the corresponding RR spectrum.

The extent of chemisorption of the complex is, therefore, very small. The fact that the peak at 1020  $\text{cm}^{-1}$  splits and the small increase in the intensity of the 1254  $\text{cm}^{-1}$  peak suggests that the complex adsorbs on the polycarbonate surface through one of the pyridyl ring  $\text{C}=\text{C}$  in the 2,2'-bipyridyl molecule.

The overall enhancement of the spectrum, therefore, has a small

chemical contribution with the bulk of the enhancement caused by the electromagnetic effect.

### 7.3.5 [Ru(dimebipy)<sub>3</sub>]<sup>2+</sup>.

Figure 7.13 shows the SERR spectra of a dilute solution of the dimethyl complex in contact with both silver-coated (50 nm) polycarbonate and a chemically silver-coated slide. Table 7.10 summarises the results of these studies.

In a similar manner to the spectra of the diphenyl complex, these spectra display only minor differences in relative intensities and band frequencies. The enhancement observed on the polycarbonate surface is high compared to the other complexes studied.

The main changes in relative intensities centre on the peaks at 1480 and 1607 cm<sup>-1</sup>. The relative intensities observed in the silver slide SERRS effectively 'swap round' in the polycarbonate SERRS, with the peak at 1607 cm<sup>-1</sup> increasing in relative intensity. This effect was reproducible.

The changes in band frequencies are relatively small. The average shift is between 3 and 5 cm<sup>-1</sup> to lower energy.

The only other notable spectral feature in the polycarbonate SERRS is the marked broadening of the peak at 1024 cm<sup>-1</sup>.

The polycarbonate SERR spectrum is complicated by the fact that

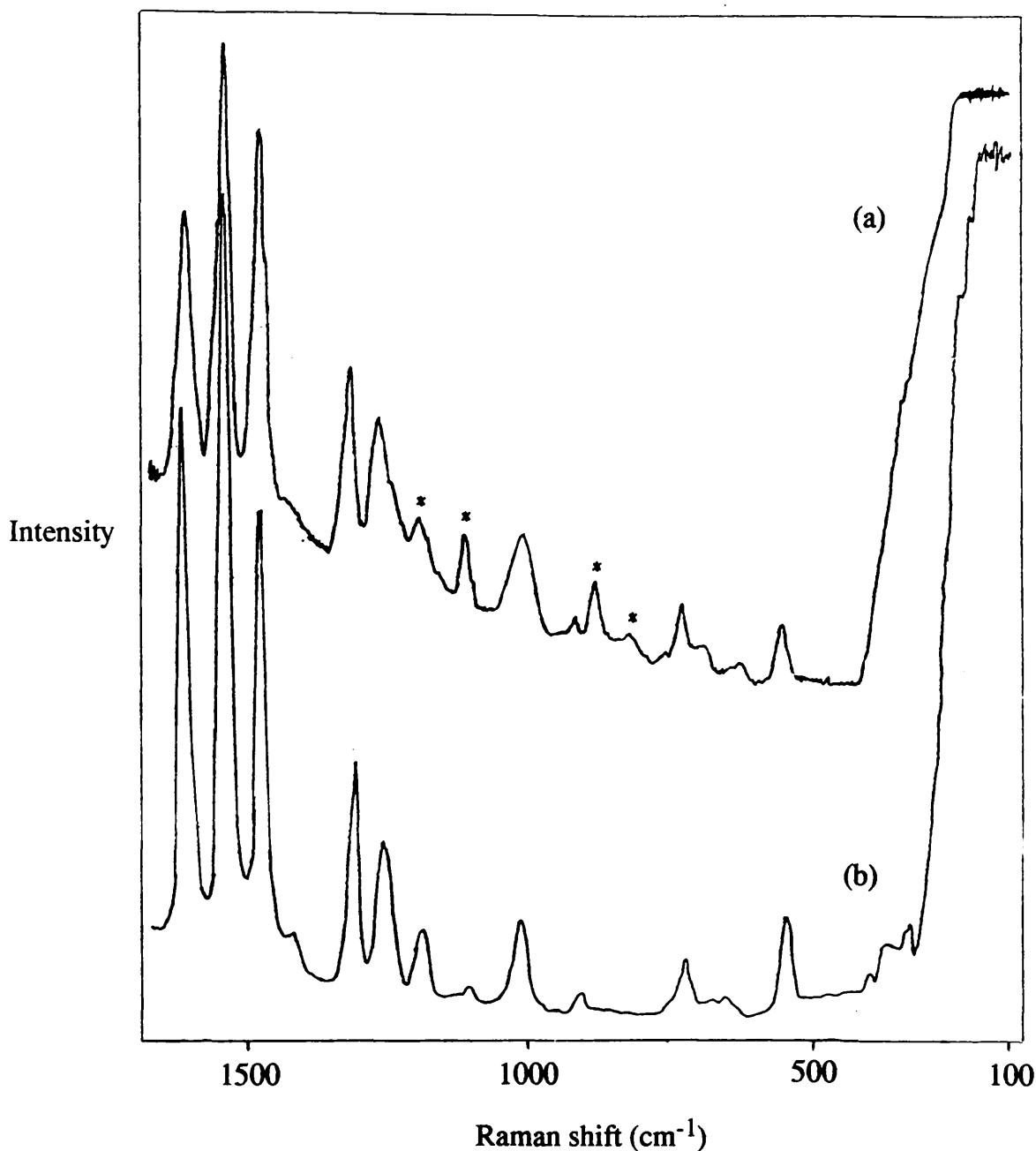


**Figure 7.13:** (a) SERR spectrum/vacuum silver-coated polycarbonate and (b) SERR spectrum/silver slide of Ru(dimebipy)<sub>3</sub>Cl<sub>2</sub> (dilute ethanolic solution) (photon counter sensitivity/10). [Ar<sup>+</sup> laser, 488.0 nm excitation]. (\* = polycarbonate bands.)

Table 7.10: Data from SERR spectra of an aqueous solution ofRu(dimebipy)<sub>3</sub>Cl<sub>2</sub> on vapour silver-coated (50 nm)polycarbonate and a silver-coated slide.

<u>SERRS/Ag slide (cm<sup>-1</sup>)</u>	<u>SERRS/Ag pc (cm<sup>-1</sup>)</u>	<u>Assignment (210)</u>
335		
400		
561	559	
660w		α(CCC)
733	731	α(CCC)
919w		
1029	1024	ν(C <sub>4</sub> —C <sub>5</sub> )
1113		δ(CCH)
1198	1199	δ(CCH)
1268	1272	ν(C <sub>2</sub> —C <sub>3</sub> )
1317	1314	δ(C <sub>2</sub> C <sub>3</sub> H)
1427w	1428	δ(CCH)
1483	1480	δ(CCH)
1545	1545	ν(C <sub>4</sub> —C <sub>5</sub> )
1613	1607	ν(C <sub>2</sub> —C <sub>3</sub> )

some of the polycarbonate modes are close to SERRS bands of the dimethyl complex.

All of the evidence outlined points to a similar bonding mode for this complex as was deduced for the parent complex. The 2,2'-bipyridyl molecule is, therefore, attached to the metal surface *via* one of the C=C bonds in the ring. The most likely attachment point is the C<sub>4</sub>—C<sub>5</sub> bond. The only difference is that, in this case, there is some evidence of asymmetry in the bonding orientation. It is possible that only one pyridyl ring of the 2,2'-bipyridyl ligand is attached to the metal surface with the other pyridyl extending out towards the bulk solution.

### 7.3.6 Discussion.

The enhancement and adsorption effects observed in the SERR spectra of these complexes on silver-coated polycarbonate substrates in many ways reflect the type of exciting radiation used. From section 6.6.1(c), it is clear that the substrate has a surface plasmon maximum at 410 nm. The subsequent determination of whether a feature observed at 486 nm in the absorption spectrum of a coated polycarbonate, which had been exposed to [Ru(bipy)<sub>3</sub>]<sup>2+</sup> solution, by 'excitation profile' measurement failed to realise any clear answers. The subsequent SERRS enhancement was observed to maximise around excitation of

514.5 nm (argon-ion). The investigation of whether the enhancement is, in fact, maximised at higher wavelength of laser radiation was not possible due to the unavailability of any laser lines other than those of the argon-ion system. If, as seems likely, the adsorbate/polycarbonate surface entity exhibits a charge-transfer maximum at some point in the spectrum beyond 514.5 nm, this would render the common excitation wavelength of 488.0 nm somewhere in the middle ground between the surface plasmon maximum and the charge-transfer maximum. If, indeed, the charge-transfer maximum is at 486 nm, with excitation of 488.0 nm, one would expect the enhancement to be extremely large and more obvious evidence of chemisorption would be expected to appear in the SERR spectrum. This is clearly not the case. The identity of the feature at 486 nm is, therefore, not clear.

On the basis of all this evidence, it is not surprising that all of the adsorbate/polycarbonate systems studied display both chemisorptive and physisorptive properties.

The adsorption behaviour exhibited by disubstituted tris-2,2'-bipyridyl ruthenium(II) complexes on silver-coated polycarbonate substrates confirms some of the earlier conclusions reached. As discussed previously, the large dimensions of roughness species on the polycarbonate surface are not conducive to high degrees of SERRS enhancement. The regular nature of the surface, however, is an

important factor governing the adsorption behaviour of the complexes.

The SERRS results show that with complexes having potentially co-ordinative substituents (diamino, diester complexes), the differences in relative intensities of bands and band frequencies over the corresponding RR spectra are quite marked. There is also considerable evidence for the attachment of the molecules *via* the substituent groups. With the other adsorbate complexes (diphenyl, dimethyl and parent complexes), the differences between the respective SERR and RR spectra are more subtle.

In some cases, the complexes adsorb through only one ligand substituent, giving effectively two non-equivalent pyridyl rings within the 2,2'-bipyridyl molecule.

The question of whether or not only one, two or all three ligands are involved in the adsorption of one complex ion has not been addressed. In each case, it seems unlikely that all three 2,2'-bipyridyl ligands are bound as, due to the geometry of the tris-ligand molecule, this would require the ion to be totally enclosed within the metal surface in a 'cage'-type structure. The attachment of two ligands is feasible, but the elucidation of the true adsorption mechanism would require further study.

CHAPTER EIGHT.

CONCLUSIONS.

## 8. CONCLUSIONS.

The overall objective of this body of work was to investigate fully certain aspects of the SERS-activity of tris(2,2'-bipyridyl) ruthenium(II) complexes and related species with particular relevance to the nature of the adsorbate/metal surface bond and to potential applications of SERS in chemical sensing. The results previously discussed indicate several broad conclusions.

(1) With common organic molecules as adsorbate species on chemically-produced surfaces such as silver slides, it is clear that the adsorbate must possess a co-ordinative site. Such sites include basic nitrogen atoms or carbonyl groups. Adsorbate species devoid of such molecular properties, such as benzene, display no SERS-activity with silver-coated slides. This, however, is not a universal rule as benzene and other molecules without any obvious co-ordinative site can exhibit SERS-activity under certain conditions (64). Benzene has displayed appreciable SERS enhancement with vapour-deposited surfaces and under vacuum conditions.

Chemisorption seems to be a necessary requirement for SERS-activity with common organics on chemically silver-coated slide surfaces. Surface plasmon resonance excitation is not sufficient to produce enhanced spectra coupled with the lack, in the case of most organic molecules, of a resonance Raman effect with excitation of

488.0 nm.

The spectra obtained from silver slides with, in turn, 2,2'-bipyridine, pyridine and benzoic acid as adsorbate species were not as highly enhanced as previous spectra reported in the literature (95) with silver colloid as the active surface.

(2) Chemically-produced silver slides exhibit SERS-activity with  $[\text{Ru}(\text{bipy})_3]^{2+}$  and modified analogues. The inherent resonance Raman effect, at 488.0 nm argon-ion excitation, and the surface plasmon enhancement mechanism combine to produce an extremely large degree of enhancement. In this case, however, chemisorption is not a necessary factor and the Raman spectra of the complexes are enhanced solely *via* the electromagnetic mechanism.

It is proposed that the main reasons for the inordinate enhancement produced, in this case, is the presence of the resonance Raman effect and the symmetry of the molecules.

The additional factor of resonance enhancement explains some of the additional enhancement beyond the levels obtained with simple organic molecules.  $\text{Ru}(\text{bipy})_3\text{I}_2$  and modified analogues are regular, almost 'spherical' molecules with no inherent fluxional motion. It is reasonable to envisage, with chemically-produced silver slides of high surface area, a high degree of non-chemisorptive surface coverage and,

consequently, a large number of adsorbate molecules sampled. This, therefore, leads to a high degree of enhancement.

Other possible reasons for the large enhancement, such as charge-induced adsorption, were ruled out.

The inordinate enhancement allows  $\text{Ru}(\text{bipy})_3\text{I}_2$  to be detected, on silver slides, at concentrations of lower than  $10^{-9}$  moles  $\text{l}^{-1}$ .

Superficially, this result indicates that silver slides have considerable analytical potential. This, however, must be measured against the fact that most analytical applications require the detection of complex organic molecules that, in the vast majority of cases, do not have any accessible absorption maximum. Developments in the field of laser technology and the vast range of laser excitation frequencies available may offset this disadvantage.

(3) The results of the comparative studies of the SERRS of  $\text{Ru}(\text{bipy})_3\text{I}_2$  and disubstituted analogues in contact with vapour silver-coated polycarbonate and chemically silver-coated slides proved interesting. Whereas none of the modified complexes chemisorbed on silver slides, there was evidence of chemisorption, in varying degrees, of the complexes on the vapour-deposited surface.

The additional factor of the substitution of the 2,2'-bipyridyl ligands was influential in the case of the polycarbonate, but the extent of the

effect was no greater than was originally predicted.

It is proposed that the ordered nature of the polycarbonate surface facilitates the adsorption of the highly symmetrical tris-ligand ruthenium(II) complexes. These molecules are rigid and, it is believed, incapable of any fluxional, rotational or substitution processes at metal surfaces.

The extent of the enhancement of the Raman spectrum of  $\text{Ru}(\text{bipy})_3\text{I}_2$  on the silver polycarbonate, which was considerably less than that obtained with silver slides, is critically dependent upon the dimensions of the surface roughness species. As previously indicated in section 6.6.3, the large dimensions of the roughness species and the proximity of the argon-ion laser exciting line do not favour high enhancement. The other critical factor is the effect of excitation wavelength and the distance of the surface plasmon absorption from the exciting line (488.0 nm). The surface plasmon maximum, due to the absence of any surface reorganisation effects, is unchanged with exposure to the adsorbate solution.

The only constant factor in the SERRS experiments with the tris-ligand ruthenium(II) complexes and the chemically-prepared silver slides and the vacuum silver-coated polycarbonate is the inherent resonance enhancement.

The lack of stronger spectral evidence for chemisorption of the

complexes on the polycarbonate surface is a manifestation of the exciting lines used: radically changed spectra may have been obtained through the use of krypton-ion exciting lines.

All of these studies show, what has become increasingly clear from SERS reports in the literature, that no general rules can be applied to a given SERS-active system.

The question of the nature of the adsorbate/surface bond cannot be answered simply since the nature of the bond changes with changing adsorbate species and SERS-active surfaces. Certainly, chemisorbed molecules are attached to the metal surface by real chemical bonds, causing radical changes in SER(R) spectra over normal and resonance Raman spectra. The other extreme is, of course, physisorption. The results with tris-ligand ruthenium(II) complexes on silver slides show that, although no more than simple Van der Waals' forces anchor the adsorbate to the metal surface, large enhancements are produced. The specific case of these complexes illustrates SERS perfectly as it is a combination of several factors that produce a huge enhancement: resonance enhancement close to the excitation wavelength, high surface area, regular adsorbate molecules and the proximity of the surface plasmon maximum and the excitation wavelength.

The results with silver-coated polycarbonate surfaces show that

$\text{Ru}(\text{bipy})_3\text{I}_2$ , although exhibiting large physisorptive enhancement with silver slides, can be induced to adsorb. These observations, however, have limited relevance to the analytical applications of SERS.

It is clear that each analytical SERS experiment must be judged in terms of all the factors influencing the enhancement. General predictions can, however, be made about certain molecular types. For example, an organic molecule containing a six-membered heterocyclic, nitrogen-containing ring would be expected to show SERS-activity, under argon-ion excitation, with silver colloids. The application of general rules, however, is generally not possible in SERS.

This, in part, is the reason why SERS has not become a widely applied analytical technique. Although SERS can be very powerful in some cases, the trace determination or analysis of a new compound is governed by the availability of appropriate active surfaces and laser systems.

Extensive theoretical study, which has almost run its course, over the last ten years has still not fully elucidated the nature of SERS enhancement. The application of SERS in chemical sensing has suffered from the lack of serious attempts to link the theoretical aspects with the analytical applications.

**REFERENCES.**

**REFERENCES.**

1. M. Fleischmann, P.J. Hendra and A.J. McQuillan, *Chem. Phys. Lett.*, 1974, **26**, 163.
2. M.G. Albrecht and J.A. Creighton, *J. Am. Chem. Soc.*, 1977, **99**, 5215.
3. D.L. Jeanmaire and R.P. Van Duyne, *J. Electroanal. Chem.*, 1977, **84**, 1.
4. T.E. Furtak and D. Roy, *AIP Conf. Proc.*, 1987, **160** (Adv. Laser Sci. 2), 452.
5. M. Fleischmann and I.R. Hill in "*Surface-Enhanced Raman Scattering*", R.K. Chang and T.E. Furtak eds., Plenum Press, New York, 1982.
6. V.V. Marinyuk, R.M. Lazarenko-Manevich and Ya.M. Kolotyrykin, *Elektrokhimya*, 1978, **14**, 1747.
7. D. Roy and T.E. Furtak, *J. Electroanal. Chem.*, 1987, **228**, 229.
8. D. Roy and T.E. Furtak, *Chem. Phys. Lett.*, 1986, **129**, 501.
9. D. Roy and T.E. Furtak, *Chem. Phys. Lett.*, 1986, **124**, 299.
10. T.E. Furtak and D. Roy, *Phys. Rev. Lett.*, 1983, **50**, 1301.
11. J. Giergel, S. Ushioda and J.C. Hemmiger, *Phys. Rev. B*, 1986, **33**, 5657.
12. M. Fleischmann, J. Robinson and R. Waser, *J. Electroanal. Chem.*, 1981, **117**, 257.

13. M. Fleischmann, P.J. Hendra, I.R. Hill and M.E. Pemble, *J. Electroanal. Chem.*, 1981, **117**, 243.
14. A. Regis and J. Corset, *Chem. Phys. Lett.*, 1980, **70**, 305.
15. R.L. Sobocinski and J.E. Pemberton, *Langmuir*, 1988, **4**, 836.
16. Y. Ikezawa, H. Saito, K. Matsui and G. Toda, *Surf. Science*, 1986, **176**, 603.
17. T.E. Furtak, *Solid State Commun.*, 1978, **28**, 903.
18. J. Billmann, G. Kovacs and A. Otto, *Surf. Science*, 1980, **92**, 153.
19. B. Pettinger and U. Wenning, *Chem. Phys. Lett.*, 1978, **56**, 253.
20. P. Gao, D. Gosztola, L. Leung and M. Weaver, *J. Electroanal. Chem.*, 1987, **233**, 211.
21. K.D. Beer, W. Tanner and R.L. Garrell, *J. Electroanal. Chem.*, 1989, **258**, 313.
22. J.E. Pemberton, A.L. Guy, R.L. Sobocinski, D.D. Tuschel and N.A. Cross, *Appl. Surf. Science*, 1988, **32**, 33.
23. A. Otto, J. Timper, J. Billmann, G. Kovacs and I. Pockrand, *Surf. Science*, 1980, **92**, L55.
24. J.F. Evans, M.G. Albrecht, D.M. Ullevig and R.M. Hexter, *J. Electroanal. Chem.*, 1980, **106**, 209.
25. S.G. Schultz, M. Janik-Czachor and R.P. Van Duyne, *Surf. Science*, 1981, **104**, 419.
26. D.D. Tuschel, J.E. Pemberton and J.E. Cook, *Langmuir*, 1986, **2**, 380.

27. J.E. Pemberton and M.M. Girard, *J. Electroanal. Chem.*, 1987, **217**, 79.
28. S.H. Macomber and T.E. Furtak, *Solid State Commun.*, 1983, **45**, 267.
29. H. Wetzel, H. Gerischer and B. Pettinger, *Chem. Phys. Lett.*, 1981, **78**, 392.
30. H. Wetzel, H. Gerischer and B. Pettinger, *Chem. Phys. Lett.*, 1981, **80**, 159.
31. B. Pettinger, U. Wenning and D.M. Kolb, *Ber. Bunsenges Phys. Chem.*, 1978, **82**, 1326.
32. H. Yamada, H. Nagata, K. Toba and Y. Nakao, *Surf. Science*, 1987, **182**, 269.
33. B.H. Loo, Y.G. Lee and D.O. Frazier, *Chem. Phys. Lett.*, 1985, **119**, 312.
34. P. Gao and M.J. Weaver, *Gov. Rep. Announce.*, 1986, **86**, Abstr. No. 602,688.
35. R. Holze, *J. Electroanal. Chem.*, 1988, **250**, 143.
36. J. Bukowska, K. Jackowska and K. Jaszczynski, *J. Electroanal. Chem.*, 1989, **260**, 373.
37. H. Sato, M. Kawasaki, K. Kasatani, E. Kawa and H. Suzuki, *Chem. Phys. Lett.*, 1986, **123**, 355.

38. J.R. Lombardi, R.L. Birke, L.A. Sanchez, I. Bernard and S.C. Sun, *Chem. Phys. Lett.*, 1984, **104**, 240.
39. T.E. Furtak and S.H. Macomber, *Chem. Phys. Lett.*, 1983, **95**, 328.
40. R.P. Van Duyne in "*Chemical and Biochemical Applications of Lasers*", **4**, C.B. Moore ed., Academic: New York, 1979.
41. J.L. Lippert and E.S. Brandt, *Langmuir*, 1988, **4**, 127.
42. M. Kerker, *Pure Appl. Chem.*, 1984, **56**, 1429.
43. R. Holze, *Electrochim. Acta*, 1987, **32**, 1527.
44. D.S Kellogg and J.E. Pemberton, *J. Phys. Chem.*, 1987, **91**, 1120.
45. L-W.H. Leung and M.J. Weaver, *J. Electroanal. Chem.*, 1987, **217**, 367.
46. L-W.H. Leung and M.J. Weaver, *J. Am. Chem. Soc.*, 1987, **109**, 5113.
47. M. Fleischmann and Z.Q. Tian, *J. Electroanal. Chem.*, 1987, **217**, 411.
48. A.L. Guy and J.E. Pemberton, *Langmuir*, 1987, **3**, 125.
49. M. Fleischmann, Z.Q. Tian and L.J. Li, *J. Electroanal. Chem.*, 1987, **217**, 397.
50. D.S. Kellogg and J.S. Pemberton, *J. Phys. Chem.*, 1987, **91**, 1126.
51. J. Desilvestro, D.A. Corrigan and M.J. Weaver, *J. Phys. Chem.*, 1986, **90**, 6408.
52. M.R. Mahoney, M.W. Howard and R.P. Cooney, *Chem. Phys. Lett.*, 1980, **71**, 59.

53. M.W. Howard, R.P. Cooney and A.J. McQuillan, *J. Raman Spectr.*, 1980, **9**, 273.
54. R.P. Cooney, M.R. Mahoney and M.W. Howard, *Chem. Phys. Lett.*, 1980, **76**, 448.
55. M. Moskovits, *Chem. Phys. Lett.*, 1983, **98**, 498.
56. P.F. Liao, J.G. Bergman, D.S. Chemla, A. Wokaun, J. Melngailis, A.M. Hawryluk and N.P. Economou, *Chem. Phys. Lett.*, 1981, **82**, 355.
57. J.P. Goudonnet, G.M. Begun and E.T. Arakawa, *Chem. Phys. Lett.*, 1982, **92**, 197.
58. R. Moody, T. Vo-Dinh and W.H. Fletcher, *Appl. Spectr.*, 1987, **41**, 966.
59. H. Yamada, K. Toba and Y. Nakao, *Indian J. Pure Appl. Phys.*, 1988, **26**, 72.
60. E.V. Albano, G. Andreasen and J. Heras, *Chem. Phys. Lett.*, 1986, **124**, 567.
61. E.V. Albano, S. Daiser, G. Ertl, R. Miranda, K. Wandelt and N. Garcia, *Phys. Rev. Lett.*, 1983, **51**, 2314.
62. E.V. Albano, S. Daiser, R. Miranda and K. Wandelt, *Surf. Science*, 1985, **150**, 367.
63. O. Erturk, D. Gherban and A. Otto, *Surf. Science*, 1988, **203**, 554.
64. A. Otto, *Indian J. Pure Appl. Phys.*, 1988, **26**, 141.

65. R.S. Venkatachalan, F.J. Boerio and P.G. Roth, *J. Raman Spectr.*, 1988, **19**, 281.
66. I. Pockrand, *Springer Tracts Mod. Phys.*, 1984, **104**.
67. D.P. DiLella and M. Moskovits, *J. Phys. Chem.*, 1981, **85**, 2042.
68. K. Itoh, M. Tsukada, T. Koyama and Y. Kobayashi, *J. Phys. Chem.*, 1986, **90**, 5286.
69. T.H. Wood, M.V. Klein and D.A. Zwemer, *Surf. Science*, 1981, **107**, 625.
70. T.H. Wood, D.A. Zwemer, C.V. Shank and J.E. Rowe, *Chem. Phys. Lett.*, 1981, **82**, 5.
71. Y.T. Wang and K.C. Lee, *Surf. Science*, 1988, **197**, 239.
72. M. Osawa, S. Yamamoto and W. Suetaka, *Appl. Surf. Science.*, 1988, **33**, 890.
73. I. Pockrand, *J. Electr. Spectr. Rel. Phenom.*, 1983, **29**, 357.
74. O. Erturk, C. Pettenkofer and A. Otto, *J. Electr. Spectr. Rel. Phenom.*, 1986, **38**, 113.
75. K. Otto, K.H. Frank and B. Reihl, *Surf. Science*, 1985, **162**, 891.
76. I. Pockrand, *Chem. Phys. Lett.*, 1982, **85**, 37.
77. Y. Gao and T. López-Ríos, *Surf. Science*, 1985, **162**, 976.
78. Y. Gao and T. López-Ríos, *J. Chem. Phys.*, 1987, **87**, 2327.
79. J.A. Creighton, C.G. Blatchford and M.G. Albrecht, *J. Chem. Soc. Faraday II*, 1979, **75**, 790.

80. G. Frens, *Nature Physical Science*, 1973, **241**, 20.
81. J.A. Creighton in "*Surface-Enhanced Raman Scattering*", R.K. Chang and T.E. Furtak eds., Plenum Press, New York, 1982.
82. O. Siiman, L.A. Bumm, R. Callaghan, C.G. Blatchford and M. Kerker, *J. Phys. Chem.*, 1983, **87**, 1014.
83. J. Notholt and K. Gottmann, *J. Phys. Chem.*, 1987, **91**, 2007.
84. O. Siiman and H. Feilchenfeld, *Proc. Int. Conf. Lasers*, 1987, 802.
85. H. Feilchenfeld and O Siiman, *J. Phys. Chem.*, 1986, **90**, 4590.
86. D.A. Weitz, M.Y. Lin and C.J. Sandroff, *Surf. Science*, 1985, **158**, 147.
87. M. Muniz-Miranda, N. Neto and G. Sbriana, *J. Phys. Chem.*, 1988 **92**, 954.
88. M. Moskovits and J.S. Suh, *J. Phys. Chem.*, 1988, **92**, 6327.
89. M. Moskovits, *J. Chem. Phys.*, 1982, **77**, 4408.
90. M. Moskovits and J.S. Suh, *J. Phys. Chem.*, 1984, **88**, 1293.
91. M. Kim and K. Itoh, *J. Phys. Chem.*, 1987, **91**, 126.
92. M. Kim and K. Itoh, *J. Electroanal. Chem.*, 1985, **188**, 137.
93. P. Hildebrandt and M. Stockburger, *J. Phys. Chem.*, 1984, **88**, 5935.
94. I.R. Nabiev, K.V. Sokolov and D.N. Voloshin, *J. Raman Spectr.*, 1990, **21**, 333.
95. M. Pagannone, B. Fornari and J. Mattei, *Spectrochim. Acta*, 1987, **43A**, 621.

96. C. Wan, K. Sun, G. Xu and Y. Tang, *Chem. Phys. Lett.*, 1988, **152**, 100.
97. S. Kai, W. Chaozhi and X. Guangzhi, *Spectrochim. Acta*, 1989, **45A**, 1029.
98. S.J. Greaves and W.P. Griffith, *J. Raman Spectr.*, 1988, **19**, 503.
99. T.J. Dines and R.D. Peacock, *J. Chem. Soc. Faraday II*, 1988, **84**, 3445.
100. F. Vanhecke, K. Heremans, A. Kirsch-De-Mesmaeker, L. Jaquet and A. Masschelein, *J. Raman Spectr.*, 1989, **20**, 617.
101. A. Kirsch-De-Mesmaeker, L. Jaquet, A. Masschelein, F. Vanhecke and K. Heremans, *Inorg. Chem.*, 1989, **28**, 2465.
102. J. de Groot, and R.E. Hester, *J. Phys. Chem.*, 1987, **91**, 1693.
103. M.A. Lippitsch, *Chem. Phys. Lett.*, 1981, **79**, 224.
104. M. Itabashi, K. Kato and K. Itoh, *Chem. Phys. Lett.*, 1983, **97**, 528.
105. C.G. Blatchford, J.R. Campbell and J.A. Creighton, *Surf. Science*, 1982, **120**, 435.
106. B. Pettinger, K. Krischet and G. Ertl, *Chem. Phys. Lett.*, 1988, **151**, 151.
107. J. J. Laserna, A.D. Campiglia and J.D. Winefordner, *Anal. Chim. Acta*, 1988, **208**, 21.
108. A. Berthod, and J.J. Laserna and J.D. Winefordner, *J. Pharm. and Biomed. Analysis*, 1988, **6**, 599.

109. J.J. Laserna, A.D. Campiglia and J.D. Winefordner, *Anal. Chem.*, 1989, **61**, 1697.
110. J.M. Séquaris and E. Koglin, *Fresenius' Z. Analyt. Chem.*, 1985, **321**, 758.
111. D. Yogev and S.J. Efrima, *J. Phys. Chem.*, 1988, **92**, 5754.
112. K.C. Gordon, J.J. McGarvey and K.P. Taylor, *J. Phys. Chem.*, 1989, **93**, 6814.
113. F. Ni and T.M. Cotton, *Anal. Chem.*, 1986, **58**, 3159.
114. P.B. Dorain, K.V. von Raben, R.K. Chang and B.L. Laube, *Chem. Phys. Lett.*, 1981, **84**, 405.
115. K.V. von Raben, P.B. Dorain, T.T. Chen and R.K. Chang, *Chem. Phys. Lett.*, 1983, **95**, 269.
116. H. Matsuta and K. Hirokawa, *Appl. Surf. Science*, 1987, **27**, 482.
117. P.B. Dorain and J.E. Boggio, *J. Chem. Phys.*, 1986, **84**, 135.
118. C.A. Murray, D.L. Allara and M. Rhinewine, *Phys. Rev. Lett.*, 1980, **46**, 57.
119. T.H. Wood and D.A. Zwemer, *J. Vac. Sci. Technol.*, 1981, **18**, 649.
120. J.E. Rowe, C.V. Shank, D.A. Zwemer and C.A. Murray, *Phys. Rev. Lett.*, 1980, **14**, 1770.
121. M. Moskovits, *Rev. Mod. Phys.*, 1985, **57**, 783.
122. H. Metiu in "*Surface-Enhanced Raman Scattering*", R.K. Chang and T.E. Furtak eds., Plenum Press, New York, 1982.

123. R.M. Hexter and M.G. Albrecht, *Spectrochim. Acta.*, 1979, **35A**, 233.
124. T.E. Furtak and J. Reyes, *Surf. Science*, 1980, **93**, 351.
125. F.W. King, R.P. Van Duyne and G.C. Schatz, *J. Chem. Phys.*, 1978, **69**, 4472.
126. S. Efrima and H. Metiu, *J. Chem. Phys.*, 1979, **70**, 1602.
127. W. H. Weber and G.W. Ford, *Surf. Science*, 1981, **109**, 451.
128. G.C. Schatz in "*Surface-Enhanced Raman Scattering*", R.K. Chang and T.E. Furtak eds., Plenum Press, New York, 1982.
129. P.J. Feibelman, *Phys. Rev. B*, 1980, **22**, 3654.
130. T.K. Lee and J.L. Birman, *Phys. Rev. B*, 1980, **22**, 5953.
131. M.R. Philpott, *J. Chem. Phys.*, 1975, **62**, 1812.
132. H. Metiu and P. Das, *Ann. Rev. Phys. Chem.*, 1984, **35**, 507.
133. M. Moskovits, *J. Chem. Phys.*, 1978, **69**, 4159.
134. M. Kerker, D.S. Wang and H. Chew, *Appl. Opt.*, 1980, **19**, 4159.
135. J.I. Gersten, *J. Chem. Phys.*, 1980, **72**, 5779.
136. D.S. Wang, H. Chew and M. Kerker, *Appl. Opt.*, 1980, **19**, 2256.
137. H.C. Van de Hulst, "*Light Scattering by Small Particles*", Wiley, New York, 1957.
138. S.L. McCall, P.M. Platzman and P.A. Wolff, *Phys. Lett.*, 1980, **77A**, 381.
139. D.S. Wang and M. Kerker, *Phys. Rev. B*, 1981, **24**, 1777.
140. J.I. Gersten and A. Nitzan, *J. Chem. Phys.*, 1980, **73**, 3023.

141. W. Krasser and A.J. Renouprez, *Solid State Commun.*, 1982, **41**, 231.
142. J.C. Maxwell-Garnett, *Philos. Trans. R. Soc. London*, 1904, **203**, 385.
143. P.K. Aravind, A. Nitzan and H. Metiu, *Surf. Science*, 1981, **110**, 189.
144. A. Wirgin and T. Lopez-Rios, *Opt. Commun.*, 1984, **48**, 416.
145. E.V. Albano, S. Daiser, G. Ertl, R. Mironda and K. Wandelt, *Phys. Rev. Lett.*, 1983, **51**, 2314.
146. H. Metiu, *Prog. Surf. Science*, 1984.
147. M. Moskovits and D.P. DiLella in "*Surface-Enhanced Raman Scattering*", R.K. Chang and T.E. Furtak eds., Plenum Press, New York, 1982.
148. M-Y. Kwon and J-T. Kim, *Chem. Phys. Lett.*, 1990, **169**, 337.
149. M. Mabuchi, T. Takenaka, Y. Fujiyoshi and N. Uyeda, *Surf. Science*, 1982, **119**, 150.
150. P.N. Sanda, J.M. Warlanmont, J.E. Demuth, J.C. Tsang, K. Cristmann and J. A. Bradley, *Phys. Rev. Lett.*, 1980, **45**, 1519.
151. R.R. Smardzewski, R.J. Colton and J.S. Murday, *Chem. Phys. Lett.*, 1979, **68**, 53.
152. P. Avouris and J.E. Demuth, *J. Chem. Phys.*, 1981, **75**, 4783.
153. K. Araya and R. Zeyher, *Phys. Rev. B*, 1981, **24**, 1852.
154. C.A. Murray and S. Bodoff, *Phys. Rev. Lett.*, 1984, **52**, 2273.
155. T.H. Wood, *Phys. Rev. B*, 1981, **24**, 2289.
156. A. Champion and D.R. Mullins, *Surf. Science*, 1985, **158**, 263.

157. J. Notholt and P.K. Ludwig, *Chem. Phys. Lett.*, 1988, **143**, 609.
158. S.L. McCall and P.M. Platzman, *Phys. Rev. B*, 1980, **22**, 1660.
159. H. Abe, K. Manzel and W. Schulze, *J. Chem. Phys.*, 1981, **74**, 792.
160. K-H. Li, *Surf. Science*, 1982, **115**, 513.
161. C-K. Hu and C-Y. Huang, *Opt. Commun.*, 1982, **43**, 395.
162. G.W. Robinson, *Chem. Phys. Lett.*, 1980, **76**, 191.
163. J.S. Suh and K.H. Michaelian, *J. Phys. Chem.*, 1987, **91**, 598.
164. M.J. Weaver, P. Gao, D. Gosztola, M.L. Patterson and M. Tadayyonii,  
*AC Symp. Ser.*, 1986, **307**, 135.
165. O. Siiman, R. Rivellini and R. Patel, *Inorg. Chem.*, 1988, **27**, 3940.
166. M.M. Carrabba, R.B. Edmonds and R.O. Rauh, *Anal. Chem.*, 1987, **59**,  
2559.
167. T. Vo-Dinh, M.Y.K. Hiromoto, G.M. Begun and R.L. Moody, *Anal.*  
*Chem.*, 1984, **56**, 1667.
168. A.M. Alak and T. Vo-Dinh, *Anal. Chem.*, 1987, **59**, 2149.
169. P.D. Enlow, M. Buncich, R.J. Warmack and T. Vo-Dinh, *Anal. Chem.*,  
1986, **58**, 1119.
170. T. Vo-Dinh in "*Chemical Analysis of Polycyclic Aromatic*  
*Compounds*", T. Vo-Dinh ed., Wiley, New York, 1988.
171. E. Koglin and J-M. Sequaris, *Top. Curr. Chem.*, 1986, **134**, 1.
172. K. Kniepp and J. Flemming, *J. Mol. Struct.*, 1986, **145**, 173.

173. S. Nie, C.G. Castillo, K.L. Bergbauer and I.R. Nabiev, *Appl. Spectr.*, 1990, **44**, 571.
174. B.N. Rospendowski, K. Kelly, C.R. Wolf and W.E. Smith, *J. Am. Chem. Soc.*, 1991, **113**, 1217.
175. G.D. Chimanov, R.G. Efremov and I.R. Nabiev, *J. Raman Spectr.*, 1990, **21**, 43.
176. I.R. Nabiev, G.D. Chimanov and R.G. Efremov, *J. Raman Spectr.*, 1990, **21**, 49.
177. E.L. Torres and J.D. Winefordner, *Anal. Chem.*, 1987, **59**, 1626.
178. K. Kniepp, *Exp. Tech. Phys.*, 1988, **36**, 161.
179. P. Hildebrandt and M. Stockburger, *J. Phys. Chem.*, 1984, **88**, 5935.
180. R. Aroca, C. Jennings, G.J. Kovacs, R.O. Loutfy and P.S. Vincett, *J. Phys. Chem.*, 1985, **89**, 4051.
181. R.A. Uphaus, T.M. Cotton and D. Mobius, *Thin Solid Films*, 1985, **132**, 173.
182. J.M. Bello and T. Vo-Dinh, *Appl. Spectr.*, 1990, **44**, 63.
183. A. Berthod, J.J. Laserna and J.D. Winefordner, *Appl. Spectr.*, 1987, **41**, 1137.
184. R.D. Freeman, R.M. Hammaker, C.E. Meloan and W.G. Fatel, *Appl. Spectr.*, 1988, **42**, 456.
185. G.T. Taylor, S.K. Sharma and K. Monahan, *Appl. Spectr.*, 1990, **44**, 635.

186. L.D. Ziegler, *J. Raman Spectr.*, 1990, **21**, 769.
187. R.W. Terhune, P.D. Maker and C.M. Savage, *Phys. Rev. Lett.*, 1965, **14**, 681.
188. J.T. Golab, J.R. Sprague, K.T. Carron, G.C. Schatz and R.P. Van Duyne, *J. Chem. Phys.*, 1988, **88**, 7942.
189. C.K. Johnson and S.A. Soper, *J. Phys. Chem.*, 1989, **93**, 7281.
190. N-T. Yu, S. Nie and L.A. Lipscomb, *J. Raman Spectr.*, 1990, **21**, 797.
191. R.A. Palmer and T.S. Piper, *Inorg. Chem.*, 1966, **5**, 864.
192. J.N. Braddock and T.J. Meyer, *J. Am. Chem. Soc.*, 1973, **95**, 3158.
193. S. Wajda and K. Rachlewicz, *Inorg. Chem. Acta*, 1978, **31**, 26.
194. T.J. Meyer, *Inorg. Synth.*, **24**, 292.
195. J. Crosby and C. Elfring, *J. Phys. Chem.*, 1976, **80**, 2206.
196. B. Bosnich, *Inorg. Chem.*, 1968, **7**, 2379.
197. F.H. Case, *J. Am. Chem. Soc.*, 1946, **68**, 2574.
198. G. Maerker and F.H. Case, *J. Am. Chem. Soc.*, 1958, **80**, 2745.
199. M.J. Cook, A.P. Lewis, G.S.G. McAuliffe, V. Skarda and A.J. Thomson, *J. Chem. Soc., Perkin Trans. 2*, 1984, 1293.
200. J. Haginiwa, *J. Pharm. Soc. Jap.*, 1955, **75**, 731.
201. U.C. Sarma, K.P. Sarma and R.K. Poddar, *Polyhedron*, 1988, **7**, 1727.
202. U.C. Sarma, S.C. Sarker, B.C. Paul and R.K. Poddar, *Inorg. Chim. Acta.*, 1990, **173**, 195.
203. W. Stober, A. Fink and E. Bonh, *J. Coll. Interf. Science*, 1968, **26**, 62.

204. J. Adams, T. Baird, P.S. Braterman, A. Cairns and J. Segal, *Mater. Res. Soc. Symp. Proc.*, 1988, **121**, 361.
205. P. Barnickel and A. Wokaun, *Mol. Phys.*, 1989, **67**, 1355.
206. E.A. Seddon and K.R. Seddon, *Top. Inorg. Gen. Chem.*, Monograph No. 19; "The Chemistry of Ruthenium", R.J.H. Clark, ed., Elsevier, Amsterdam, 1984.
207. F.H. Burstall, *J. Chem. Soc.*, **1936**, 173.
208. P. Belser, C. Daul and A. von Zelewsky, *Chem. Phys. Lett.*, 1981, **79**, 596.
209. P. Day and N. Sanders, *J. Chem. Soc. (A)*, **1967**, 1530.
210. P.K. Mallick, G.D. Danzer, D.P. Strommen and J.R. Kincaid, *J. Phys. Chem.*, 1988, **92**, 5628.